frontiers | Research Topics

Combining multiple non-invasive images and/or biochemical tests to predict prostate cancer aggressiveness

Edited by
Rulon Mayer and Steven Raman

Published in
Frontiers in Oncology

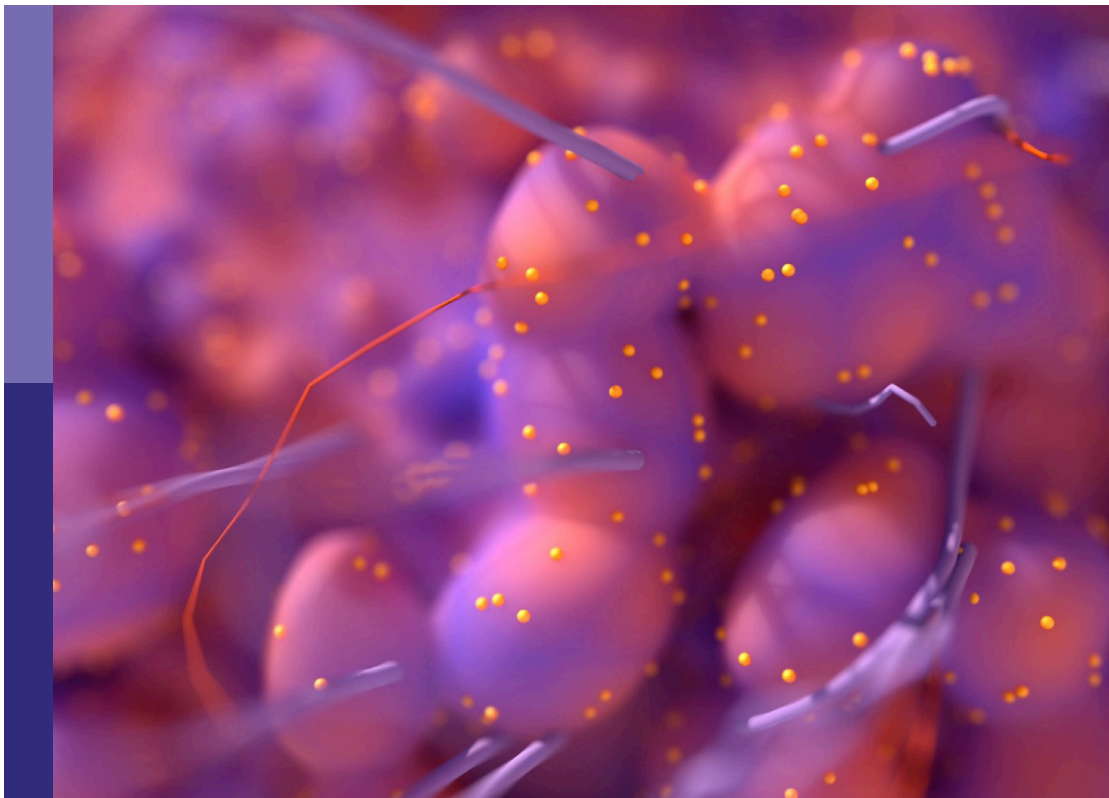

ISSN 1664-8714
ISBN 978-2-83251-822-9
DOI 10.3389/978-2-83251-822-9

About Frontiers

Frontiers is more than just an open access publisher of scholarly articles: it is a pioneering approach to the world of academia, radically improving the way scholarly research is managed. The grand vision of Frontiers is a world where all people have an equal opportunity to seek, share and generate knowledge. Frontiers provides immediate and permanent online open access to all its publications, but this alone is not enough to realize our grand goals.

Frontiers journal series

The Frontiers journal series is a multi-tier and interdisciplinary set of open-access, online journals, promising a paradigm shift from the current review, selection and dissemination processes in academic publishing. All Frontiers journals are driven by researchers for researchers; therefore, they constitute a service to the scholarly community. At the same time, the *Frontiers journal series* operates on a revolutionary invention, the tiered publishing system, initially addressing specific communities of scholars, and gradually climbing up to broader public understanding, thus serving the interests of the lay society, too.

Dedication to quality

Each Frontiers article is a landmark of the highest quality, thanks to genuinely collaborative interactions between authors and review editors, who include some of the world's best academicians. Research must be certified by peers before entering a stream of knowledge that may eventually reach the public - and shape society; therefore, Frontiers only applies the most rigorous and unbiased reviews. Frontiers revolutionizes research publishing by freely delivering the most outstanding research, evaluated with no bias from both the academic and social point of view. By applying the most advanced information technologies, Frontiers is catapulting scholarly publishing into a new generation.

What are Frontiers Research Topics?

Frontiers Research Topics are very popular trademarks of the *Frontiers journals series*: they are collections of at least ten articles, all centered on a particular subject. With their unique mix of varied contributions from Original Research to Review Articles, Frontiers Research Topics unify the most influential researchers, the latest key findings and historical advances in a hot research area.

Find out more on how to host your own Frontiers Research Topic or contribute to one as an author by contacting the Frontiers editorial office: frontiersin.org/about/contact

Combining multiple non-invasive images and/or biochemical tests to predict prostate cancer aggressiveness

Topic editors

Rulon Mayer — University of Pennsylvania, United States

Steven Raman — University of California, Los Angeles, United States

Citation

Mayer, R., Raman, S., eds. (2023). *Combining multiple non-invasive images and/or biochemical tests to predict prostate cancer aggressiveness*.

Lausanne: Frontiers Media SA. doi: 10.3389/978-2-83251-822-9

Table of contents

05 Editorial: Combining multiple non-invasive images and/or biochemical tests to predict prostate cancer aggressiveness
Rulon Mayer, Steven Raman and Charles B. Simone

09 Does Multiparametric Magnetic Resonance of Prostate Outperform Risk Calculators in Predicting Prostate Cancer in Biopsy Naïve Patients?
Ugo Giovanni Falagario, Giovanni Silecchia, Salvatore Mariano Bruno, Michele Di Nauta, Mario Auciello, Francesca Sanguedolce, Paola Milillo, Luca Macarini, Oscar Selvaggio, Giuseppe Carrieri and Luigi Cormio

16 IVIM Parameters on MRI Could Predict ISUP Risk Groups of Prostate Cancers on Radical Prostatectomy
Chun-Bi Chang, Yu-Chun Lin, Yon-Cheong Wong, Shin-Nan Lin, Chien-Yuan Lin, Yu-Han Lin, Ting-Wen Sheng, Chen-Chih Huang, Lan-Yan Yang and Li-Jen Wang

25 MRI-Based Nomogram of Prostate Maximum Sectional Area and Its Zone Area for Prediction of Prostate Cancer
Shaoqin Jiang, Zhangcheng Huang, Bingqiao Liu, Zhenlin Chen, Yue Xu, Wenzhong Zheng, Yaoan Wen and Mengqiang Li

37 Developing Strategy to Predict the Results of Prostate Multiparametric Magnetic Resonance Imaging and Reduce Unnecessary Multiparametric Magnetic Resonance Imaging Scan
Junxiao Liu, Shuanbao Yu, Biao Dong, Guodong Hong, Jin Tao, Yafeng Fan, Zhaowei Zhu, Zhiyu Wang and Xuepei Zhang

44 MRI radiomics predicts progression-free survival in prostate cancer
Yushan Jia, Shuai Quan, Jialiang Ren, Hui Wu, Aishi Liu, Yang Gao, Fene Hao, Zhenxing Yang, Tong Zhang and He Hu

56 Combining prostate-specific antigen density with prostate imaging reporting and data system score version 2.1 to improve detection of clinically significant prostate cancer: A retrospective study
Yin Lei, Tian Jie Li, Peng Gu, Yu kun Yang, Lei Zhao, Chao Gao, Juan Hu and Xiao Dong Liu

64 Combination of PI-RADS score and PSAD can improve the diagnostic accuracy of prostate cancer and reduce unnecessary prostate biopsies
Changming Wang, Lei Yuan, Deyun Shen, Bin Zhang, Baorui Wu, Panrui Zhang, Jun Xiao and Tao Tao

74 Development of a novel nomogram for predicting clinically significant prostate cancer with the prostate health index and multiparametric MRI
Li-Cai Mo, Xian-Jun Zhang, Hai-Hong Zheng, Xiao-peng Huang, Lin Zheng, Zhi-Rui Zhou and Jia-Jia Wang

83 Assessing and testing anomaly detection for finding prostate cancer in spatially registered multi-parametric MRI
Rulon Mayer, Baris Turkbey, Peter Choyke and Charles B. Simone

92 Pilot study for generating and assessing nomograms and decision curves analysis to predict clinically significant prostate cancer using only spatially registered multi-parametric MRI
Rulon Mayer, Baris Turkbey, Peter Choyke and Charles B. Simone

frontiers | Frontiers in Oncology

TYPE Editorial
PUBLISHED 14 February 2023
DOI 10.3389/fonc.2023.1156649

OPEN ACCESS

EDITED AND REVIEWED BY
Ronald M Bukowski,
Cleveland Clinic, United States

*CORRESPONDENCE
Rulon Mayer
mayerru@yahoo.com

SPECIALTY SECTION
This article was submitted to Genitourinary Oncology, a section of the journal Frontiers in Oncology

RECEIVED 01 February 2023
ACCEPTED 03 February 2023
PUBLISHED 14 February 2023

CITATION
Mayer R, Raman S and Simone CB 2nd (2023) Editorial: Combining multiple non-invasive images and/or biochemical tests to predict prostate cancer aggressiveness. *Front. Oncol.* 13:1156649. doi: 10.3389/fonc.2023.1156649

Editorial: Combining multiple non-invasive images and/or biochemical tests to predict prostate cancer aggressiveness

Rulon Mayer[1,2*], Steven Raman[3] and Charles B. Simone 2nd[4,5]

[1]Department of Radiation Oncology, Perelman School of Medicine, University of Pennsylvania, Philadelphia, PA, United States, [2]Oncoscore, Garrett Park, MD, United States, [3]Department of Radiology, University of California, Los Angeles Health System, Los Angeles, CA, United States, [4]Department of Radiation Oncology, New York Proton Center, New York, NY, United States, [5]Department of Radiation Oncology, Memorial Sloan Kettering Cancer Center, New York, NY, United States

KEYWORDS

multi-parametric MRI, prostate cancer, multivariable regression analyses, PI-RADS, prostate serum antigen, spatially registered images, nomogram

Editorial on the Research Topic
Combining multiple non-invasive images and/or biochemical tests to predict prostate cancer aggressiveness

Introduction

This Special Topics Issue in *Frontiers in Oncology*, Genitourinary Oncology compiles research articles that noninvasively assess prostate tumors through combining multiple disparate independent quantitative data. The contributions to the Special Topics discuss the performance of more common resources and methods that have been employed in the medical arena, such as biomarkers, clinical data, visual inspection of multi-parametric MRI (mpMRI), as well as adapting and applying novel approaches derived from other fields that quantitatively assess spatially registered multi-parametric MRI (SRMP-MRI).

Background

> "What's past is prologue," William Shakespeare, The Tempest
> "The past is a stepping stone, not a mill stone," Robert Plant

Quantifiable research endeavors can benefit from combining multiple independent pieces of information or variables (1–3) to describe or ascertain a given condition or predict an outcome. The sources of input information may be garnered from biomarkers, clinical factors, meta information, human intelligence, detectors and/or images. Having multiple input factors that supplement and/or complement each other without mere duplication improves the accuracy of the predicted outcome. To aid combining disparate data in the clinic, nomograms (4) have provided a graphical tool for computing the likelihood of an effect

due to a number of input variables. Standard measures can establish the significance of the input information for evaluating or achieving a desired goal.

Extracting information, however, may burden and harm the patient (5). For prostate cancer, a 6-12 core transrectal ultrasound-based needle biopsy supplemented by MRI has been the principal means of diagnosis and patient risk stratification. Aside from possible under sampling the prostate (6, 7), such an invasive procedure carries the risks of pain, hemorrhage, and infection for the patient (8). Although the widely implemented non-invasive PSA indicator has significantly reduced PCa mortality, its low specificity lead to under and overtreatment and loss quality of life for the patient (9).

To improve PCa diagnosis, grading, and alleviate patient suffering, non-invasive strategies have been developed, such as the Prostate Imaging Reporting and Data System (PI-RADS) (9). PI-RADS (10) is a protocol for radiologists to visually inspect multiple MRI sequences and combine the assessments to determine the prostate tumor's aggressiveness. However, such a qualitative approach depends on the training and experience of the radiologists.

Only one study (Jia et al.) in this compilation applies Artificial Intelligence (AI) methods to find image texture features and combine them to predict outcomes. AI harnesses the available image data and the growing computing power, is fashionable, and successful. However, there are drawbacks to the AI, such as overtraining of models lead to low accuracy, require fixed measurement conditions such as magnetic field, and textures are unconnected to physiology. The studies in this issue mostly avoid these pitfalls.

Discussion

Table 1 summarizes nine studies, including Chang et al., Falagario et al., Jia et al., Jiang et al., Lei et al., Liu et al., Mo et al., Wang et al., and Mayer et al. that examined the efficacy of combining various forms of PSA, prostate volume, and PI-RADS to non-invasively predict Clinically Significant Prostate Cancer (csPCa) or presence in MRI. There are a number of exceptions in this compilation. Chang et al. used two statistical metrics that characterize the diffusion, namely the mean and kurtosis to predict the International Society of Urological Pathology staging (ISUP). Falagario et al. added clinically based Risk Factors to mpMRI and improved the accuracy for detecting csPCa. Unlike other studies in this compilation, only Jia et al. applied AI and radiomics to predict the csPCa. Jiang et al. used geometric measures for the prostate to predict the presence of prostate cancer. Liu et al. departed from the others in examining input data that predicted the need for mpMRI. The summary cites the input variables, dependent variable, number of patients, an evaluation metric, specifically the Area Under the Curve (AUC) from Receiver Operator Characteristic and whether a nomogram was generated. All studies achieved high AUC and showed that adding mpMRI and using multiple variables relative to a single variable improved the accuracy. All studies need further verification with prospective studies and higher patient numbers.

Two articles in this Special Topics issue studied spatially registered hyperspectral mpMRI. The first (Mayer et al.) eschewed the familiar independent variables (PI-RADS, PSA, age, etc), but instead tapped variables associated with SRMP-MRI such as eccentricity, Signal to Clutter Ration and achieved high AUC. The second (Mayer et al.), not in Table 1, does not use multiple features to predict an outcome. Instead, Mayer et al. studied an anomaly detector that finds deviant voxels within the normal prostate through processing the SRMP-MRI and examines a variety of statistical methods to manipulate the covariance matrix in order to generate an optimized AUC. Further studies are warranted that compared the anomaly detection with a radiologist tumor contouring of the SRMP-MRI tumors.

TABLE 1 Retrospective, single center studies included in this Special Topics issue.

Author	Input Variables	Prediction	Number of Patients	Evaluation Metrics	Best or Range of AUC	Nomogram
Chang	D_{mean} ,$D_{kurtosis}$	ISUP	45	AUC	0.907	No
Faligario	mpMRI, RC	csPCa	221	AUC, DCA	0.8	No
Jia	Radiomics: T2, DWI, Clinical Data	PFS	191	AUC, DCA, Calibration Curve	0.917-0.926	No
Jiang	Age, PSA, transCGA, PA	PCa	691	AUC	0.918	Yes
Lei	PI-RADS, PSAD	csPCa	422	AUC	0.97	No
Liu	Total PSA, Free PSA, PSAD, Prostate Volume, Age	Tumor Presence in MRI	784	AUC, DCA	0.8	No
Mo	Prostate Health Index (Free PSA, Total PSA), PI-RADS, Prostate Volume	csPCa	315	AUC	0.882	Yes
Wang	PI-RADS, PSAD	csPCa	833	AUC	0.94	No
Mayer	Eccentricity, Signal to Clutter Ratio, Tumor Volume	csPCa	25	AUC, DCA	0.861-0.969	Yes

mpMRI, Multi-parametric MRI; PI-RADS, Prostate Imaging Reporting And Data system; AUC, Area Under the Curve; DCA, Decision Curve Analysis; RC, Risk Calculator; PSAD, Prostate Serum Antigen Density; PFS, Progression Free survival; ISUP, International Society of Urological Pathology; D_{mean}, Mean diffusion; $D_{kurtosis}$, Diffusion kurtosis; csPCa, Clinically Significant Prostate Cancer; PA, maximum prostate sectional area; transCGA, transverse central gland area.

Future research

> "The best way to predict the future is to create it." Abraham Lincoln
> "The past is in your head, the future is in your hands." Margaret Atwood

The works presented in this issue directly suggested future refinements, such as more patients, prospective studies, application to greater number of clinics, but hints at more ambitious projects such as:

New biomarkers.

A number of studies in Special Topics showed that adding PSA to mpMRI boosts sensitivity and specificity for reliably determining csPCa. New biomarkers, beyond PSA (11, 12), show promise in identifying the presence of prostate tumors with fewer false positives than PSA. Future studies might combine these novel biomarkers with PI-RADS or mpMRI for further improvement.

Directed proton therapy

Due to the increasing prevalence of proton beam therapy and its ability to more precisely deliver radiation therapy (13), imaging (14, 15) may reveal that certain patients benefit from exposing only a portion of the prostate, rather than the entire prostate, to irradiation, thus reducing possible side effects from unnecessarily exposing nearby normal tissues. To date, only treatment planning studies (13) suggest the feasibility of using mpMRI for this purpose.

Qualitative/quantitative color maps.

Currently radiologists (10) visually inspect individual greyscale images to discern and interpret lesions. An alternative coloring schemes assigns red, green, blue to components in SRMP-MRI and generate a composite color image that can be quantified (16–18). Color in this case codes for PCa and normal tissue physiology. This coloring is not equivalent to false or pseudo coloring applied to individual images to show relative intensities within a given image. Future research (18) may clinically test employing tumor color display for patient care management and possibly derive new quantitative metrics for assessing tumors.

Cross-clinic transformation

MRI scanning conditions (magnetic field strength, pulse sequences etc.), can vary among clinics which hinders AI-based techniques from generalization. Previously (19), "whitening-dewhitening" transformed target signatures for supervised target detections to handle the changes in conditions. Similarly (20), signatures based on Gleason score status were transformed. Future research may transform prostate tumor signatures across multiple clinics. A single library may hold multiple tumor signatures in the future.

mpMRI and genomics

Other research directions may combine multiple data input or images to infer tumor genomics. A meta-analysis (21) found that mpMRI-visible cancer related to genotype, phenotype, physiology (proliferative signaling, DNA damage, and inflammatory processes). Others (22, 23) correlated mpMRI visibility with aggressive genomic and proteomic features. Further research incorporating all mpMRI modalities may further discriminate among genomic metrics or find more markers.

Magnetic resonance spectroscopy

MRS uses many bands, similar to airborne hyperspectral imagers. However, MRS suffers from crude spatial resolution (MRS (24) is 0.25 cm^3 versus mpMRI is 0.006 cm^3) causing sampling issues. The limited MRS sample number precludes exploiting the statistical analysis due to background covariance matrix inversion non-singularity. Covariance matrix regularization can mitigate the insufficient sampling. Elevating the MRS spatial resolution by degrading the spectral resolution may enable MRS statistical analysis similar to remote sensing. Remote sensing proved the value of making the trade-offs and possibly help the clinic.

Author contributions

Conception and design: RM, CS. Administrative support: RM, CS. Collection and assembly of data: RM. Data analysis and interpretation: RM. Writing of manuscript: RM, SR, CS. All authors (RM, SR, CS) listed have made a substantial, direct, and intellectual contribution to the work and approved it for publication.

Acknowledgments

Dr. Huaiyu (Heather) Chen-Mayer for suggested modifications to the manuscript.

Conflict of interest

RM works for Oncoscore.

The remaining authors declare that the research was conducted in the absence of any commercial or financial relationships that could be construed as a potential conflict of interest.

Publisher's note

References

1. Hall DL, Llinas J. An Introduction to Multisensor Data Fusion. In: *Proceedings of the IEEE.* (1997) 85:6–23. doi: 10.1109/5.554205

2. Hay SI. An overview of remote sensing and geodesy for epidemiology and public health application. *Adv Parasitol* (2000) 47:1–35. doi: 10.1016/s0065-308x(00)47005-3

3. Schober P, Vetter TR. Linear regression in medical research. *Anesth Analg.* (2021) 132(1):108–9. doi: 10.1213/ANE.0000000000005206

4. Balachandran VP, Gonen M J, Smith JJ, DeMatteo RP. Nomograms in oncology – more than meets the eye. *Lancet Oncol* (2015) 16(4):e173–80. doi: 10.1016/S1470-2045(14)71116-7

5. Loeb S, Vellekoop A, Ahmed HU, Catto J, Emberton M, Nam R, et al. Systematic review of complications of prostate biopsy. *Eur Urol* (2013) 6):876–92. doi: 10.1016/j.eururo.2013.05.049

6. Epstein JI, Feng Z, Trock BJ, Pierorazio PM. Upgrading and downgrading of prostate cancer from biopsy to radical prostatectomy: Incidence and predictive factors using the modified Gleason grading system and factoring intertiary grades. *Eur Urol.* (2012) 61:1019–24. doi: 10.1016/j.eururo.2012.01.050

7. King CR. Long JP prostate biopsy grading errors: A sampling problem? *Int J Cancer* (2000) 90(6):326–30. doi: 10.1002/1097-0215(20001220)90:6<326::AID-IJC3>3.0.CO;2-J

8. Wu YP, Li XD, Ke ZB, Chen SH, Chen PZ, Wei Y, et al. Risk factors for infectious complications following transrectal ultrasound-guided prostate biopsy. *Infect Drug Resist* (2018) 11:1491–7. doi: 10.2147/IDR.S171162

9. Bernal-Soriano MC, Parker LA, López-Garrigos M, Hernández-Aguado I, Caballero-Romeu JP, Gómez-Pérez L, et al. Factors associated with false negative and false positive results of prostate-specific antigen (PSA) and the impact on patient health: Cohort study protocol. *Med (Baltimore).* (2019) 98(40):e17451. doi: 10.1097/MD.0000000000017451

10. Weinreb JC, Barentsz JO, Choyke PL, Cornud F, Haider MA, Macura KJ, et al. PI-RADS prostate imaging - reporting and data system: 2015, version 2. *Eur Urol* (2016) 69:16–40. doi: 10.1016/j.eururo.2015.08.052

11. Salciccia S, Capriotti AL, Laganà A, Fais S, Logozzi M, DeBerardinis E, et al. Biomarkers in prostate cancer diagnosis: From current knowledge to the role of metabolomics and exosomes. *Int J Mol Sci* (2021) 22:4367. doi: 10.3390/ijms22094367

12. Ferro M, Lucarelli G, de Cobelli O, Del Giudice F, Musi G, Mistretta FA, et al. The emerging landscape of tumor marker panels for the identification of aggressive prostate cancer: the perspective through bibliometric analysis of an Italian translational working group in uro-oncology. *Minerva Urol Nephrol* (2021) 73:442–51. doi: 10.23736/S2724-6051.21.04098-4

13. Kaiser A, Eley JG, Onyeuku NE, Rice SR, Wright CC, McGovern NE, et al. Proton therapy delivery and its clinical application in select solid tumor malignancies. *J Vis Exp* (2019) 144):10. doi: 10.3791/58372

14. Wang T, Zhou J, Tian S, Wang Y, Patel P, Jani AB, et al. A planning study of focal dose escalations to multiparametric MRI-defined dominant intraprostatic lesions in prostate proton radiation therapy. *Br J Radiol* (2020) 93(1107):20190845. doi: 10.1259/bjr.20190845

15. Wysock JS, Lepor H. Multi-parametric MRI imaging of the prostate–implications for focal therapy. *Transl Androl Urol* (2017) 6(3):453–63. doi: 10.21037/tau.2017.04.29

16. Mayer R, Simone CB2nd, Turkbey B, Choyke P. Algorithms applied to spatially registered multi-parametric MRI for prostate tumor volume measurement. *Quant Imaging Med Surg* (2021) 11:119–32. doi: 10.21037/qims-20-137a

17. Schanda J. *Colorimetry: Understanding the CIE System*. Hoboken, New Jersey: Wiley-Interscience (2007).

18. Kather JN, Weidner A, Attenberger U, Bukschat Y, Weis CA, Weis M, et al. Color-coded visualization of magnetic resonance imaging multiparametric maps. *Sci Rep* (2017) 7:41107. doi: 10.1038/srep41107

19. Mayer R, Bucholtz F, Scribner D. Object detection by using "Whitening/DeWhitening" to transform target signatures in multi-temporal hyper- and multi-spectral imagery. *IEEE Trans Geosci Remote Sensing.* (2003) 41:1136–42. doi: 10.1109/TGRS.2003.813553

20. Mayer R, Simone CB 2nd, Skinner W, Turkbey B, Choyke P. Pilot study for supervised target detection applied to spatially registered multiparametric MRI in order to non-invasively score prostate cancer. *Comput Biol Med* (2018) 94:65–73. doi: 10.1016/j.compbiomed.2018.01.003

21. Norris JM, Simpson BS, Parry MA, Allen C, Ball R, Freeman A, et al. Genetic landscape of prostate cancer conspicuity on multiparametric magnetic resonance imaging: A systematic review and bioinformatic analysis. *Eur Urol Open Sci* (2020) 20:37–47. doi: 10.1016/j.euros.2020.06.006

22. Houlahan KE, Salmasi A, Sadun TY, Pooli A, Felker ER, Livingstone J, et al. Molecular hallmarks of multiparametric magnetic resonance imaging visibility in prostate cancer. *Eur Urol.* (2019) 76(1):18–23. doi: 10.1016/j.eururo.2018.12.036

23. Khoo A, Liu LY, Sadun TY, Salmasi A, Pooli A, Felker E, et al. Prostate cancer multiparametric magnetic resonance imaging visibility is a tumor-intrinsic phenomena. *J Hematol Oncol* (2022) 15(1):48. doi: 10.1186/s13045-022-01268-6

24. Hu J, Feng W, Hua J, Jiang Q, Xuan Y, Li T, et al. A high spatial resolution *in vivo* 1H magnetic resonance spectroscopic imaging technique for the human breast at 3 T. *Med Phys* (2009) 36(11):4870–7. doi: 10.1118/1.3213087

frontiers in Oncology

ORIGINAL RESEARCH
published: 08 January 2021
doi: 10.3389/fonc.2020.603384

Does Multiparametric Magnetic Resonance of Prostate Outperform Risk Calculators in Predicting Prostate Cancer in Biopsy Naïve Patients?

Ugo Giovanni Falagario[1], Giovanni Silecchia[2], Salvatore Mariano Bruno[1], Michele Di Nauta[1], Mario Auciello[1,2], Francesca Sanguedolce[3], Paola Milillo[4], Luca Macarini[4], Oscar Selvaggio[1], Giuseppe Carrieri[1] and Luigi Cormio[1,2]*

[1] Department of Urology and Organ Transplantation, University of Foggia, Foggia, Italy, [2] Department of Urology, Bonomo Teaching Hospital, Andria, Italy, [3] Department of Pathology, University of Foggia, Foggia, Italy, [4] Department of Radiology, University of Foggia, Foggia, Italy

OPEN ACCESS

Edited by:
Izak Faiena, Columbia University, United States

Reviewed by:
Wayne Brisbane, University of California, Los Angeles, United States
Gopal Nand Gupta, Loyola University Medical Center, United States

***Correspondence:**
Ugo Giovanni Falagario
ugofalagario@gmail.com

Specialty section:
This article was submitted to Genitourinary Oncology, a section of the journal Frontiers in Oncology

Received: *06 September 2020*
Accepted: *24 November 2020*
Published: *08 January 2021*

Citation:
Falagario UG, Silecchia G, Bruno SM, Di Nauta M, Auciello M, Sanguedolce F, Milillo P, Macarini L, Selvaggio O, Carrieri G and Cormio L (2021) Does Multiparametric Magnetic Resonance of Prostate Outperform Risk Calculators in Predicting Prostate Cancer in Biopsy Naïve Patients? Front. Oncol. 10:603384. doi: 10.3389/fonc.2020.603384

Background: European Association of Urology (EAU) guidelines recommend using risk-calculators (RCs), imaging or additional biomarkers in asymptomatic men at risk of prostate cancer (PCa).

Objectives: To compare the performance of mpMRI, a RC we recently developed and two commonly used RC not including mpMRI in predicting the risk of PCa, as well as the added value of mpMRI to each RC.

Design, Setting, and Participants: Single-center retrospective study evaluating 221 biopsy-naïve patients who underwent prebiopsy mpMRI.

Outcome Measurements and Statistical Analysis: Patients' probabilities of any PCa and clinically significant PCa (csPC, defined as Gleason-Score ≥3 + 4) were computed according to mpMRI, European Randomized Study of Screening for Prostate Cancer RC (ERSPC-RC), the Prostate Biopsy Collaborative Group RC (PBCG-RC) and the Foggia Prostate Cancer RC (FPC-RC). Logistic regression, AUC, and Decision curve analysis (DCA) were used to assess the accuracy of tested models.

Results and Limitation: The FPC-RC outperformed mpMRI in diagnosing both any PCa (AUC 0.76 *vs* 0.69) and csPCa (AUC 0.80 *vs* 0.75). Conversely mpMRI showed a higher accuracy in predicting any PCa compared to the PBCG-RC and the ERSPC-RC but similar performances in predicting csPCa. At multivariable analysis predicting csPCa and any PCa, the addition of mpMRI findings improved the accuracy of each calculator. DCA showed that the FPC-RC provided a greater net benefit than mpMRI and the other RCs. The addition of mpMRI findings improved the net benefit provided by each calculator.

Conclusions: mpMRI was outperformed by the novel FPC-RC and showed similar performances compared to the PBCG and ERSPC RCs in predicting csPCa. The addition of mpMRI findings improved the diagnostic accuracy of each of these calculators

Keywords: prostate cancer, mpMRI, decision curve analysis, clinically significant prostate cancer, risk calculator

INTRODUCTION

In current clinical practice, the cancer detection rate (CDR) of a first extended prostate biopsy (PBx) prompted by an elevated serum prostate-specific antigen (PSA) level and/or an abnormal digital rectal examination (DRE) is around 40%, dropping to approximately 25% in the setting of screening programs, *i.e.* patients with serum PSA between 2.5 and 10 ng/ml (1, 2).

To reduce the risk of unnecessary PBxs, current European Association of Urology (EAU) guidelines (3) provide a strong recommendation to offer further risk-assessment to asymptomatic men with normal DRE but PSA levels between 2 and 10 ng/ml prior to performing PBx. Such "further risk assessment" should be done by one of following tools: i) risk-calculator (RC); ii) imaging; iii) an additional serum or urine-based test (3). Interestingly, while this recommendation has remained unchanged in 2018 and 2019 Guidelines, the 2020 Guidelines provide a weak recommendation to perform mpMRI in any patient with clinical suspicion for prostate cancer (PCa). If mpMRI demonstrates lesion(s) suspicious for PCa, systematic and target biopsy should be performed, whereas biopsy can be avoided when mpMRI is negative and the clinical suspicion of PCa is low. By doing so, the 2020 Guidelines somehow bind the decision to perform mpMRI to the clinical suspicion of PCa which is well determined by available RCs.

RCs are designed to determine the risk of an individual harboring PCa by entering into a statistical model his clinical parameters. To date, several calculators have been developed and externally validated; a few also include mpMRI findings and biomarkers but questions remain on the additional value provided by such tests. Indeed, a recent study aiming at comparing and externally validating prostate cancer RCs incorporating mpMRI demonstrated that the addition of mpMRI parameters to RCs based on standard clinical variables was limited (3). Overall, available information regarding the use of RCs, mpMRI or biomarkers as triage test and the utility of combining them remain scarce.

The present study therefore aimed to compare the performance of mpMRI with the performances of two commonly-used externally-validated calculators not including mpMRI (4, 5) and a novel externally-validated calculator we recently developed (6) in predicting the risk of harboring PCa, as well as the added value of mpMRI to each RC.

PATIENTS AND METHODS

Our Internal Review Board which approved the database on prostate biopsy was queried to identify patients who underwent mpMRI and trans-rectal prostate biopsy at our institution under the clinical suspicion of PCa. The patient population used for the development of our RC was not included in the present study.

Prostate mpMRI was triggered by PSA higher than 3.0 ng/ml and/or abnormal DRE and were interpreted by a single dedicated radiologist (PM) with 10 years of experience in prostate MRI, using the PIRADSv2.0 recommendations (7).

All patients underwent PSA measurement before DRE and transrectal ultrasound (TRUS). Uroflowmetry (UFM) was carried out before PBx, waiting for the patient to report a strong sensation to void.

MRI examinations were performed using a 1.5 T MR scanner (Achieva, Philips Healthcare, Best, The Netherlands) and surface array coils (SENSE Flex surface) or with endorectal coil (ERC) combined with 16-channel surface coil (TORSO-XL coil). The mpMRI protocol was compliant with PIRADs 2.0 recommendations (7) and consisted of: A. Turbo-Spin-Echo (TSE) T2-weighed imaging in axial, coronal and sagittal planes [repetition time (TR) 5,300, echo time (TE) 150 ms, slice thickness 3 mm, field of view (FOV) 180 × 180, number of signal averaged (NSA) 8]; B. TSE T1-weighed imaging in axial plane [TR/TE 400–650/12 ms, thickness 3 mm, FOV 180 × 180, NSA 3]; C. Diffusion-weighted imaging sequence (DWI) in the axial plane [TR/TE 3,481/92 ms, slice thickness 3 mm, FOV 180 × 220, NSA 4, b-values 0–500–1000–1,500/2,000 s/mm^2]; D. Dynamic contrast enhanced prostate MRI was performed using a T1-weighted high resolution isotropic volume examination (THRIVE) on the axial plane [TR/TE 4.5/2.2 ms, slice thickness 3 mm, FOV 184 × 220, NSA 1] following injection of 0.1 ml/kg of gadobutrol followed by 20 ml of saline solution using an automatic injector at a rate of 2 ml/s.

In accordance with the current EAU guidelines, patients with negative mpMRI (PIRADS 1 and 2 lesions were considered to be negative) received a standard ultrasound guided transrectal PBx using our 18-core template (8); those with a positive mpMRI received a transrectal electromagnetic-tracked MRI/US fusion guided biopsy (Navigo, UC-CARE, Yokneam, ISR). To avoid large differences in the number of cores, we attempted to include the two target cores from each mpMRI-suspicious lesions into our 18-core biopsy scheme (SBx). All procedures were carried out by two of us (OS, GS) under local non-infiltrative anesthesia (8, 9).

A single, dedicated uropathologist (FS) reviewed all biopsy specimens according to International Society of Urological Pathology; Gleason Grade Groups (GGG) were assigned to each patient (10). Contemporary diagnostic criteria for high-grade prostatic intraepithelial neoplasia (HGPIN), atypical small acinar proliferation (ASAP) of prostate (11), and PCa were followed.

Statistical Analysis

Outcomes of the present study were probabilities of any PCa (GGG≥1) and clinically significant PCa (csPC defined as GGG≥2) as assessed by mpMRI alone, or by one RC alone, namely the European Randomized Study of Screening for Prostate Cancer (ERSPC) (4), the Prostate Biopsy Collaborative Group (PBCG) (5) and the Foggia Prostate Cancer (FPC) RCs (6), or by adding mpMRI to each RC.

Our primary objective was to compare the accuracy of mpMRI and the FPC-RC. As a secondary objective we sought to compare the accuracy of mpMRI with two of the most used available RCs. Finally, we determined the added value of mpMRI to each of the tested models.

For descriptive statistics, continuous variables were reported as medians and interquartile ranges, whereas categorical variables were reported as rates. Patients' probabilities of any PCa as well as csPCa were computed applying the coefficients (available upon request to the authors of the original publications) to the logit functions for the ERSPC-RC and the FPC-RC. Conversely, individual probability of i. No cancer, ii. Low grade cancer, and iii. High grade cancer for the PBCG-RC was computed using the coefficients and formulas provided by the authors as supplementary materials (5).

Univariable logistic regression was carried out in order to compare each RC against mpMRI as predictors of the outcomes of interest.

Three models predicting any PCa and three models predicting csPCa were created adding mpMRI to the individual risk computed for each calculator, in a multivariable model. Since the PBCG-RC was developed using multinomial regression (*i.e.* it provides risk of no cancer, low-grade cancer, high-grade cancer), the risk prediction for any cancer was computed as 1-risk of no cancer and was identical to the risk of low-grade cancer + risk of high-grade cancer.

The corresponding area under receiver operating characteristic (ROC) curve (AUC) and decision curve analysis (DCA) were used to assess the predictive accuracy and clinical benefit of tested models.

Statistical analyses were performed according to the latest guidelines (12) using STATA 15 (StataCorp LP, College Station, TX, USA). Significance was set at $\alpha = 0.05$.

RESULTS

Between January 2017 and October 2019, a total of 415 patients underwent mpMRI and PBx at our Institution. Men receiving five alfa-reductase inhibitors (N = 50), or who had previously undergone PBx (N = 174), or invasive treatment for benign prostatic hyperplasia (n = 11), or with dwelling urethral catheters (N = 5), or with a voided volume of less than 150 ml (N = 7) were excluded from the present study. Patients with PSA >20 ng/ml (N = 18) were also excluded as we found them to have a too high risk (>75%) of harboring PCa.

After the exclusion criteria, the final population included 221 biopsy naïve patients with complete data. Patients characteristics are summarized in **Table 1**; 43 patients (19.5%) had a negative mpMRI (PIRADS 1–2), thus underwent 18-core US guided transrectal PBx, whereas the remaining 168 underwent mpMRI/US guided fusion PBx. Their PIRADS score was 3, 4, and 5 in 35 (15.8%), 120 (54.3%) and 23 (10.4%), respectively.

Any PCa and csPCa detection rates were 53.8% (n = 119) and 27.1% (n = 60), respectively. The negative predictive value of mpMRI (PIRADS 1–2) in predicting any PCa and csPCa was 76.7 and 97.7% respectively. The positive predictive value of mpMRI (PIRADS 3–4–5) was 61.2% for any PCa and 33.1% for csPCa.

Univariable analysis predicting the outcomes of interest is shown in **Table 2**. RCs and mpMRI PIRADS score were all significant predictors of any PCa and csPCa ($p < 0.05$).

The FPC-RC outperformed mpMRI in diagnosing both any PCa (AUC 0.76 *vs* 0.69) and csPCa (AUC 0.80 *vs* 0.75). Conversely mpMRI showed a higher accuracy in predicting any PCa compared to the PBCG-RC and the ERSPC-RC but similar performances in predicting csPCa (**Table 2**, **Figures 1A–C**).

Multivariable analysis showed that the addition of mpMRI findings improved the diagnostic accuracy of each calculator in predicting both csPCa and any PCa. The model derived from the addition of mpMRI to the FPC-Rc showed the highest accuracy in diagnosing both any PCa (AUC 0.78) and csPCa (AUC 0.87) (**Table 3**, **Figures 1B, D**).

Finally, DCA showed that the FPC-RC provided greater net benefit than mpMRI in predicting any PCa and csPCa. Conversely mpMRI had a higher net benefit compared to the other RCs. Again, the addition of mpMRI findings improved the net benefit provided by each calculator benefit (**Figure 2**).

DISCUSSION

Over the last years, mpMRI has gained popularity as a reliable tool in localizing specific regions of the prostate highly suspicious

TABLE 1 | Descriptive characteristics of the study population.

	Overall population N = 221
Age	66.0 (60.0, 71.0)
DRE, n (%)	
Negative	123 (55.7%)
Suspicious	98 (44.3%)
Family History	
Negative	108 (76.1%)
Positive	34 (23.9%)
PSA, ng/ml	5.5 (4.1, 7.4)
PSA density	0.11 (0.07, 0.15)
Prostate volume, cc	52.0 (39.0, 69.0)
PIRADS	
1-2	43 (19.5%)
3	35 (15.8%)
4	120 (54.3%)
5	23 (10.4%)
Any Cancer	119 (53.8%)
Cs Cancer	60 (27.1%)
NPV of PIRADS 1-2	97.8% (42/43)
PPV of PIRADS 3-4-5	33.1% (59/178)

TABLE 2 | Univariable analysis predicting any cancer and csPCa using risk calculators and mpMRI.

	OUTCOME: ANY PCa				OUTCOME: csPCa			
	O.R.	**95% CI**	**P>|z|**	**AUC**	**O.R.**	**95% CI**	**P>|z|**	**AUC**
FPC-RC, per unit	1.05	1.03,1.07	<0.001	0.760	1.06	1.04,1.08	<0.001	0.801
PBCG-RC, per unit	1.03	1.01,1.05	0.001	0.615	1.05	1.03,1.07	<0.001	0.733
ERSPC-RC, per unit	1.00	1.00,1.00	0.001	0.614	1.09	1.06,1.13	<0.001	0.749
MRI highest PIRADS								
1-2	Ref.			0.690	Ref.			0.754
3	2.20	0.83,5.85	0.114		1.24	0.07,20.49	0.883	
4	5.91	2.66,13.15	<0.001		24.32	3.23,182.86	0.002	
5	11.88	3.52,40.14	<0.001		65.33	7.59,562.40	<0.001	

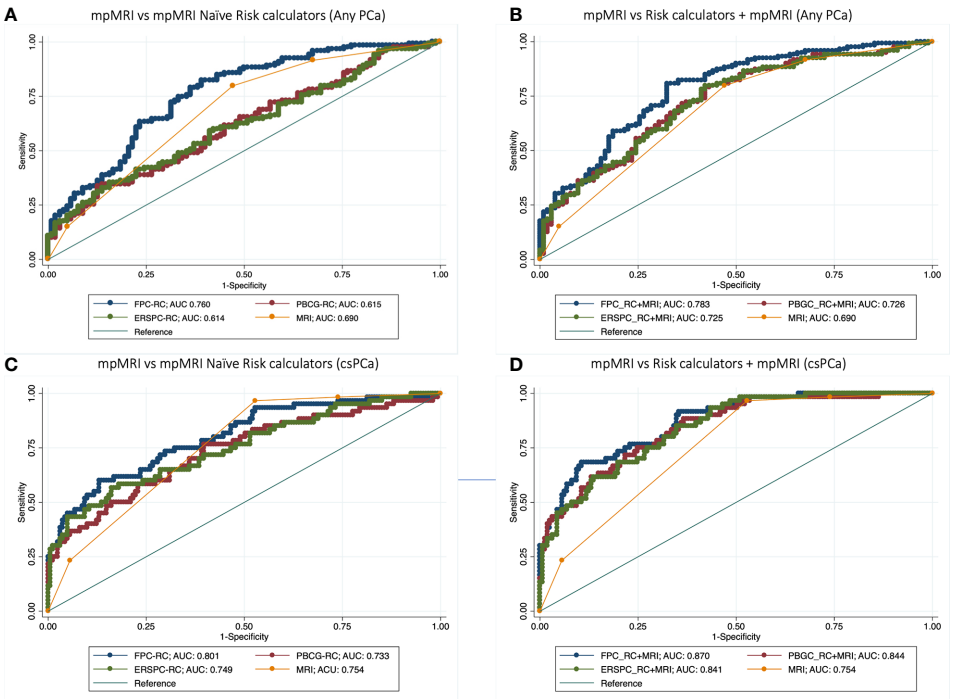

FIGURE 1 | Receiver operator curve (ROC) analysis comparing accuracy of mpMRI *vs* mpMRI naïve Risk calculators (RCs) **(A–C)**, and model based on mpMRI + RCs **(B–D)** for detecting any PCa **(A, B)** and clinically significant prostate cancer **(C, D)**.

for csPCa; therefore, there is a trend to recommend it as the most efficient tool in predicting PCa at PBx (13). Such recommendation is however based on prospective studies in high volume tertiary cancer centers that do not reflect everyday practice in less experienced centers (14–16). Indeed, mpMRI suffers a great inter-reader and inter-center variability (13, 17, 18); moreover, it is expensive. and not all institutions may afford to test every patient at risk for PCa. Conversely, RCs are freely available online and have been proved to be effective in several external validation cohorts.

The first interesting finding of our study was that the FPC-RC, which has recently been externally validated in a cohort of 1,377 biopsy naïve patients from 11 institutions (19), outperformed mpMRI in predicting PBx outcomes. This finding somehow further supports the clinical value of benign prostatic obstruction parameters in the evaluation of patients with PCa suspicion (20–22). Differently from mpMRI, the FPC-RC is a freely available and almost inexpensive tool that can be easily used during any medical consultation. Should our findings be replicated in further external cohorts, the FPC-RC may become an essential tool for patients requiring "further risk assessment" prior to performing PBx.

When compared to other RCs, mpMRI outperformed the ERSPC-RC and the PBCG-RC in predicting any PCa but showed similar performances in predicting csPCa.

Our study also aimed to answer the relevant question whether combining diagnostic tools may improve their diagnostic accuracy. Overall, the addition of mpMRI findings improved the diagnostic accuracy of each calculator in predicting both csPCa and any PCa. Our findings are in line with those from a single center study whereby the diagnostic accuracy of 4 RCs incorporating mpMRI

TABLE 3 | Multivariable analysis predicting any PCa and csPCa.

	OUTCOME: ANY PCa				OUTCOME: csPCa			
	O.R.	**95% CI**	**P>|z|**	**AUC**	**O.R.**	**95% CI**	**P>|z|**	**AUC**
MODEL-1								
FPC-RC, per unit	1.04	1.03,1.06	<0.001	0.783	1.06	1.04,1.08	<0.001	0.870
MRI highest Pirads								
1-2	Ref.				Ref.			
3	1.91	0.67,5.47	0.226		1.67	0.08,33.59	0.738	
4	3.51	1.47,8.40	0.005		25.74	2.67,247.97	0.005	
5	6.42	1.73,23.89	0.006		60.17	5.18,698.68	0.001	
MODEL-2								
PBCG-RC, per unit	1.03	1.00,1.05	0.015	0.726	1.05	1.03,1.07	<0.001	0.844
MRI highest Pirads								
1-2	Ref.				Ref.			
3	2.28	0.85,6.14	0.104		1.30	0.08,22.33	0.855	
4	5.59	2.49,12.55	<0.001		23.75	3.06,184.34	0.002	
5	9.78	2.84,33.63	<0.001		51.87	5.73,469.84	<0.001	
MODEL-3								
ERSPC-RC, per unit	1.00	1.00,1.00	0.012	0.725	1.08	1.04,1.12	<0.001	0.841
MRI highest Pirads								
1-2	Ref.				Ref.			
3	2.29	0.85,6.17	0.102		1.66	0.09,30.08	0.731	
4	5.58	2.48,12.54	<0.001		24.23	2.87,204.38	0.003	
5	9.66	2.80,33.28	<0.001		45.37	4.62,445.97	0.001	

Three models were created adding mpMRI to each risk calculator.

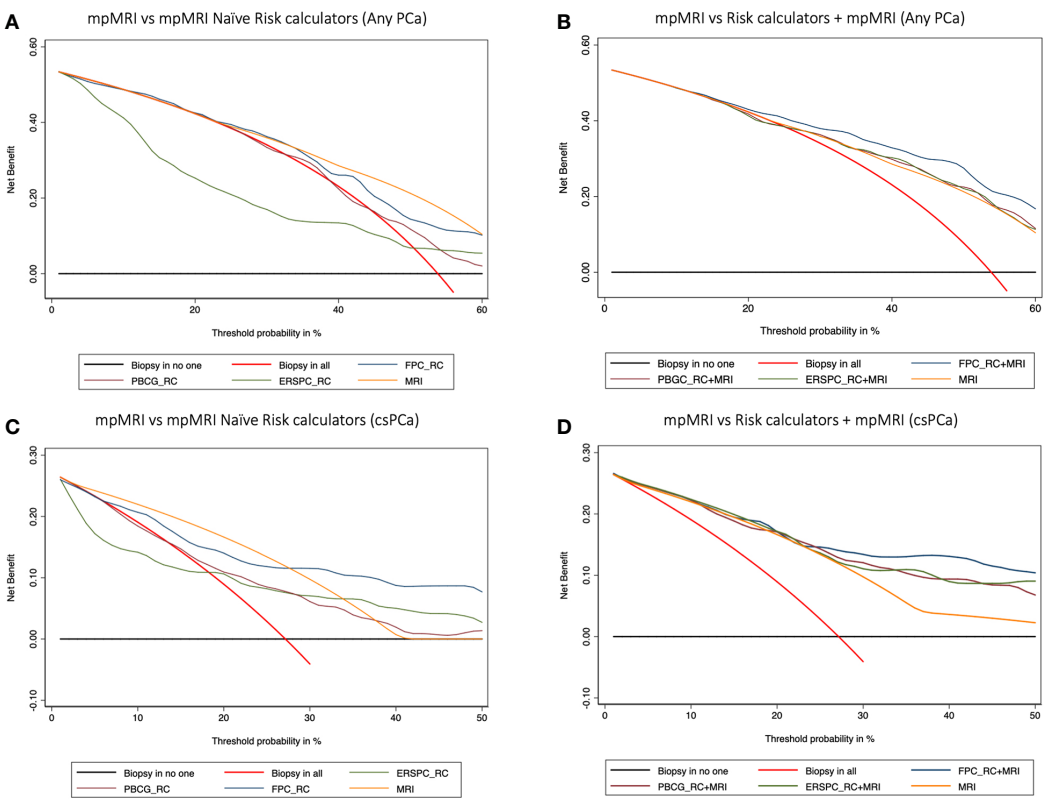

FIGURE 2 | Decision curve analysis (DCA) comparing the clinical utility of mpMRI *vs* mpMRI naïve risk calculators (RCs) **(A–C)**, and model-based on mpMRI + RCs **(B–D)** for detecting any PCa **(A, B)** and clinically significant prostate cancer **(C, D)**. The DCA simulates two scenarios: one in which all patients would receive biopsy (biopsy in all) and one in which none undergoes biopsy (biopsy in no one). Clinically useful models lie above these scenarios. Models including mpMRI +RCs showed a higher net benefit at each threshold probability and thus outperformed mpMRI alone in determining the need for a prostate biopsy.

(23–26) was compared with that of the ERSPC-RC (4) and PBCG-RC (5) in a population of 468 patients. The four RCs incorporating mpMRI parameters provided better discrimination, calibration, and clinical usefulness; however, none of the six calculators demonstrated clinical benefit against a "biopsy all" strategy at thresholds of less than 15% (27). This finding underlines a potentially relevant limitation of RCs; specifically, a model that shows benefit at high thresholds of probability is clinically useless in a screening setting since the decision to perform a biopsy is especially difficult in patients with borderline risk.

In the present study, DCA showed that the combination of mpMRI and RCs provided a greater benefit than the "biopsy all" strategy at low thresholds. Having said this, additional external validation studies in different biopsy settings are warranted since the clinical utility of these models could be cohort dependent. It is also worth mentioning that calculators including mpMRI, though outperforming the mpMRI naïve ones, involve obtaining mpMRI in all patients and this may not be afforded in centers with limited resources (28). Conversely, mpMRI naïve RCs offer the unique opportunity to potentially tailor further testing, such as mpMRI and PBx itself, on an individual basis. Indeed, it has been pointed out that RCs and biomarkers may help in selecting patients who could benefit from mpMRI and PBx and patients with a very low risk of csPCa in whom the positive predictive value of mpMRI is low and mpMRI and PBx should be avoided (29–31).

The findings of this study have to be seen in light of some limitations. First, the FPC-RC was developed at our institution, and this can explain its better performance compared to the other tested RCs. Even if the patient population used for the development of the RC was not included in the present study, this cannot be considered an external validation study. Other potential study limitations include its relatively small sample size and its retrospective nature; however, we elected to use strict inclusion criteria and data were prospectively collected. Finally, we did not test novel and promising tools such as bi-parametric MRI (32) and novel biomarkers (33), but this would have been beyond the aim of a study comparing currently available tests.

CONCLUSIONS

The present study pointed out that mpMRI was outperformed by the novel FPC-RC and showed similar performances compared to the PBCG and ERSPC risk calculators in predicting csPCa. The addition of mpMRI findings improved the diagnostic accuracy of each of these calculators. Further studies are needed to assess how these findings can be used to safely avoid unnecessary biopsies.

DATA AVAILABILITY STATEMENT

The raw data supporting the conclusions of this article will be made available by the authors, without undue reservation.

ETHICS STATEMENT

The studies involving human participants were reviewed and approved by the University of Foggia Ethics committee. The patients/participants provided their written informed consent to participate in this study.

AUTHOR CONTRIBUTIONS

LC, UF, GC, LM, and OS conceived and designed the study. GS, MB, MN, MA, and PM acquired the data. LC, UF, and PM analyzed and interpreted the data. LC, UF, GS, and MB drafted the manuscript. LC, GC, OS, and LM made critical revisions of the manuscript for important intellectual content. LC and UF conducted the statistical analysis. LC, GC, OS, and LM supervised the study. All authors contributed to the article and approved the submitted version.

REFERENCES

1. Louie KS, Seigneurin A, Cathcart P, Sasieni P. Do prostate cancer risk models improve the predictive accuracy of PSA screening? A meta-analysis. *Ann Oncol* (2015) 26(5):848–64. doi: 10.1093/annonc/mdu525
2. Lughezzani G, Lazzeri M, Larcher A, Lista G, Scattoni V, Cestari A, et al. Development and internal validation of a Prostate Health Index based nomogram for predicting prostate cancer at extended biopsy. *J Urol* (2012) 188(4):1144–50. doi: 10.1016/j.juro.2012.06.025
3. Mottet N, van den Bergh RCN, Briers E, Cornford P, De Santis M, Fanti S, et al. EAU - ESTRO - ESUR - SIOG Guidelines on Prostate Cancer 2020. In: . *European Association of Urology Guidelines. 2020 Edition*. Arnhem, The Netherlands: European Association of Urology Guidelines Office (2020).
4. Roobol MJ, Verbeek JFM, van der Kwast T, Kummerlin IP, Kweldam CF, van Leenders G. Improving the Rotterdam European Randomized Study of Screening for Prostate Cancer Risk Calculator for Initial Prostate Biopsy by Incorporating the 2014 International Society of Urological Pathology Gleason Grading and Cribriform growth. *Eur Urol* (2017) 72(1):45–51. doi: 10.1016/j.eururo.2017.01.033
5. Ankerst DP, Straubinger J, Selig K, Guerrios L, De Hoedt A, Hernandez J, et al. A Contemporary Prostate Biopsy Risk Calculator Based on Multiple Heterogeneous Cohorts. *Eur Urol* (2018) 74(2):197–203. doi: 10.1016/j.eururo.2018.05.003
6. Cormio L, Cindolo L, Troiano F, Marchioni M, Di Fino G, Mancini V, et al. Development and Internal Validation of Novel Nomograms Based on Benign Prostatic Obstruction-Related Parameters to Predict the Risk of Prostate Cancer at First Prostate Biopsy. *Front Oncol* (2018) 8:438:438. doi: 10.3389/fonc.2018.00438
7. Muller BG, Shih JH, Sankineni S, Marko J, Rais-Bahrami S, George AK, et al. Prostate Cancer: Interobserver Agreement and Accuracy with the Revised Prostate Imaging Reporting and Data System at Multiparametric MR Imaging. *Radiology* (2015) 277(3):741–50. doi: 10.1148/radiol.2015142818
8. Cormio L, Lorusso F, Selvaggio O, Perrone A, Sanguedolce F, Pagliarulo V, et al. Noninfiltrative anesthesia for transrectal prostate biopsy: a randomized prospective study comparing lidocaine-prilocaine cream and lidocaine-ketorolac gel. *Urol Oncol* (2013) 31(1):68–73. doi: 10.1016/j.urolonc.2010.09.004
9. Cormio L, Pagliarulo V, Lorusso F, Selvaggio O, Perrone A, Sanguedolce F, et al. Combined perianal-intrarectal (PI) lidocaine-prilocaine (LP) cream and lidocaine-ketorolac gel provide better pain relief than combined PI LP cream and periprostatic nerve block during transrectal prostate biopsy. *BJU Int* (2012) 109(12):1776–80. doi: 10.1111/j.1464-410X.2011.10622.x
10. Epstein JII, Egevad L, Amin MB, Delahunt B, Srigley JR, Humphrey PA, et al. The 2014 International Society of Urological Pathology (ISUP) Consensus Conference on Gleason Grading of Prostatic Carcinoma: Definition of

Grading Patterns and Proposal for a New Grading System. *Am J Surg Pathol* (2016) 40(2):244–52. doi: 10.1097/PAS.0000000000000530
11. Sanguedolce F, Cormio A, Musci G, Troiano F, Carrieri G, Bufo P, et al. Typing the atypical: Diagnostic issues and predictive markers in suspicious prostate lesions. *Crit Rev Clin Lab Sci* (2017) 54(5):309–25. doi: 10.1080/10408363.2017.1363155
12. Assel M, Sjoberg D, Elders A, Wang X, Huo D, Botchway A, et al. Guidelines for reporting of statistics for clinical research in urology. *BJU Int* (2019) 123 (3):401–10. doi: 10.1111/bju.14640
13. Wajswol E, Winoker JS, Anastos H, Falagario U, Okhawere K, Martini A, et al. A cohort of transperineal electromagnetically tracked magnetic resonance imaging/ultrasonography fusion-guided biopsy: assessing the impact of inter-reader variability on cancer detection. *BJU Int* (2019) 125(4):531–40. doi: 10.1111/bju.14957
14. Ahmed HU, El-Shater Bosaily A, Brown LC, Gabe R, Kaplan R, Parmar MK, et al. Diagnostic accuracy of multi-parametric MRI and TRUS biopsy in prostate cancer (PROMIS): a paired validating confirmatory study. *Lancet* (2017) 389(10071):815–22. doi: 10.1016/S0140-6736(16)32401-1
15. Kasivisvanathan V, Rannikko AS, Borghi M, Panebianco V, Mynderse LA, Vaarala MH, et al. MRI-Targeted or Standard Biopsy for Prostate-Cancer Diagnosis. *N Engl J Med* (2018) 378(19):1767–77. doi: 10.1056/NEJMoa1801993
16. Rouviere O, Puech P, Renard-Penna R, Claudon M, Roy C, Mege-Lechevallier F, et al. Use of prostate systematic and targeted biopsy on the basis of multiparametric MRI in biopsy-naive patients (MRI-FIRST): a prospective, multicentre, paired diagnostic study. *Lancet Oncol* (2019) 20(1):100–9. doi: 10.1016/S1470-2045(18)30569-2
17. Rosenkrantz AB, Ginocchio LA, Cornfeld D, Froemming AT, Gupta RT, Turkbey B, et al. Interobserver Reproducibility of the PI-RADS Version 2 Lexicon: A Multicenter Study of Six Experienced Prostate Radiologists. *Radiology* (2016) 280(3):793–804. doi: 10.1148/radiol.2016152542
18. Smith CP, Harmon SA, Barrett T, Bittencourt LK, Law YM, Shebel H, et al. Intra- and interreader reproducibility of PI-RADSv2: A multireader study. *J Magn Reson Imaging* (2019) 49(6):1694–703. doi: 10.1002/jmri.26555
19. Cindolo L, Bertolo R, Minervini A, Sessa F, Muto G, Bove P, et al. External validation of Cormio nomogram for predicting all prostate cancers and clinically significant prostate cancers. *World J Urol* (2020) 38(10):2555–61. doi: 10.1007/s00345-019-03058-1
20. Cormio L, Lucarelli G, Netti GS, Stallone G, Selvaggio O, Troiano F, et al. Post-void residual urinary volume is an independent predictor of biopsy results in men at risk for prostate cancer. *Anticancer Res* (2015) 35(4):2175–82.
21. Cormio L, Lucarelli G, Selvaggio O, Di Fino G, Mancini V, Massenio P, et al. Absence of Bladder Outlet Obstruction Is an Independent Risk Factor for Prostate Cancer in Men Undergoing Prostate Biopsy. *Medicine (Baltimore)* (2016) 95(7):e2551. doi: 10.1097/MD.0000000000002551
22. Cicione A, Cormio L, Cantiello F, Palumbo IM, De Nunzio D, Lima E, et al. Presence and severity of lower urinary tract symptoms are inversely correlated with the risk of prostate cancer on prostate biopsy. *Minerva Urol Nefrol* (2017) 69(5):486–92. doi: 10.23736/S0393-2249.17.02737-0
23. Radtke JP, Wiesenfarth M, Kesch C, Freitag MT, Alt CD, Celik K, et al. Combined Clinical Parameters and Multiparametric Magnetic Resonance Imaging for Advanced Risk Modeling of Prostate Cancer-Patient-tailored Risk Stratification Can Reduce Unnecessary Biopsies. *Eur Urol* (2017) 72 (6):888–96. doi: 10.1016/j.eururo.2017.03.039
24. van Leeuwen PJ, Hayen A, Thompson JE, Moses D, Shnier R, Bohm M, et al. A multiparametric magnetic resonance imaging-based risk model to determine the risk of significant prostate cancer prior to biopsy. *BJU Int* (2017) 120 (6):774–81. doi: 10.1111/bju.13814
25. Mehralivand S, Shih JH, Rais-Bahrami S, Oto A, Bednarova S, Nix JW, et al. A Magnetic Resonance Imaging-Based Prediction Model for Prostate Biopsy Risk Stratification. *JAMA Oncol* (2018) 4(5):678–85. doi: 10.1001/jamaoncol.2017.5667
26. Alberts AR, Roobol MJ, Verbeek JFM, Schoots IG, Chiu PK, Osses DF, et al. Prediction of High-grade Prostate Cancer Following Multiparametric Magnetic Resonance Imaging: Improving the Rotterdam European Randomized Study of Screening for Prostate Cancer Risk Calculators. *Eur Urol* (2019) 75(2):310–8. doi: 10.1016/j.eururo.2018.07.031
27. Saba K, Wettstein MS, Lieger L, Hotker AM, Donati OF, Moch H, et al. External Validation and Comparison of Prostate Cancer Risk Calculators Incorporating Multiparametric Magnetic Resonance Imaging for Prediction of Clinically Significant Prostate Cancer. *J Urol* (2019) 203(4):719–26. doi: 10.1097/JU.0000000000000622. 101097JU0000000000000622.
28. Perez IM, Jambor I, Kauko T, Verho J, Ettala O, Falagario U, et al. Qualitative and Quantitative Reporting of a Unique Biparametric MRI: Towards Biparametric MRI-Based Nomograms for Prediction of Prostate Biopsy Outcome in Men With a Clinical Suspicion of Prostate Cancer (IMPROD and MULTI-IMPROD Trials). *J Magn Reson Imaging* (2020) 51(5):1556–67. doi: 10.1002/jmri.26975
29. Falagario UG, Martini A, Wajswol E, Treacy PJ, Ratnani P, Jambor I, et al. Avoiding Unnecessary Magnetic Resonance Imaging (MRI) and Biopsies: Negative and Positive Predictive Value of MRI According to Prostate-specific Antigen Density, 4Kscore and Risk Calculators. *Eur Urol Oncol* (2019) 3 (5):700–4. doi: 10.1016/j.euo.2019.08.015
30. Beksac AT, Cumarasamy S, Falagario U, Xu P, Takhar M, Alshalalfa M, et al. Multiparametric Magnetic Resonance Imaging Features Identify Aggressive Prostate Cancer at the Phenotypic and Transcriptomic Level. *J Urol* (2018) 200(6):1241–9. doi: 10.1016/j.juro.2018.06.041
31. Falagario UG, Jambor I, Lantz A, Ettala O, Stabile A, Taimen P, et al. Combined Use of Prostate-specific Antigen Density and Magnetic Resonance Imaging for Prostate Biopsy Decision Planning: A Retrospective Multi-institutional Study Using the Prostate Magnetic Resonance Imaging Outcome Database (PROMOD). *Eur Urol Oncol* (2020). doi: 10.1016/j.euo.2020.08.014
32. Perez IM, Jambor I, Kauko T, Verho J, Ettala O, Falagario U, et al. Qualitative and Quantitative Reporting of a Unique Biparametric MRI: Towards Biparametric MRI-Based Nomograms for Prediction of Prostate Biopsy Outcome in Men With a Clinical Suspicion of Prostate Cancer (IMPROD and MULTI-IMPROD Trials). *J Magn Reson Imaging* (2019) 51(5):1556–67. doi: 10.1002/jmri.26975
33. Stallone G, Cormio L, Netti GS, Infante B, Selvaggio O, Fino GD, et al. Pentraxin 3: a novel biomarker for predicting progression from prostatic inflammation to prostate cancer. *Cancer Res* (2014) 74(16):4230–8. doi: 10.1158/0008-5472.CAN-14-0369

Conflict of Interest: The authors declare that the research was conducted in the absence of any commercial or financial relationships that could be construed as a potential conflict of interest.

frontiers in Oncology

ORIGINAL RESEARCH
published: 01 July 2021
doi: 10.3389/fonc.2021.659014

IVIM Parameters on MRI Could Predict ISUP Risk Groups of Prostate Cancers on Radical Prostatectomy

Chun-Bi Chang[1,2†], Yu-Chun Lin[2,3], Yon-Cheong Wong[1,2], Shin-Nan Lin[1,2], Chien-Yuan Lin[4], Yu-Han Lin[3†], Ting-Wen Sheng[2,5], Chen-Chih Huang[2,5], Lan-Yan Yang[6‡] and Li-Jen Wang[2,5*‡]*

[1] Department of Medical Imaging and Intervention, Chang Gung Memorial Hospital, College of Medicine, Chang Gung University, Taoyuan, Taiwan, [2] Department of Medical Imaging and Radiological Sciences, Chang Gung University, Taoyuan, Taiwan, [3] Department of Medical Imaging and Intervention, Chang Gung Memorial Hospital, Taoyuan, Taiwan, [4] Department of Clinical Science, General Electric (GE) Healthcare, Taipei, Taiwan, [5] Department of Medical Imaging and Intervention, New Taipei Municipal TuCheng Hospital, Chang Gung Memorial Hospital and Chang Gung University, Taoyuan, Taiwan, [6] Biostatistics Unit of Clinical Trial Center, Chang Gung Memorial Hospital, Taoyuan, Taiwan

OPEN ACCESS

Edited by:
Sanja Štifter,
Skejby Sygehus, Denmark

Reviewed by:
Alessandro Tafuri,
University of Verona, Italy
Joshua Cabral,
Howard University, United States

***Correspondence:**
Li-Jen Wang
lijenwang0918@gmail.com
Lan-Yan Yang
lyyang0111@gmail.com

†These authors have contributed equally to this work and share first authorship

‡These authors have contributed equally to this work

Specialty section:
This article was submitted to Genitourinary Oncology, a section of the journal Frontiers in Oncology

Received: 26 January 2021
Accepted: 11 June 2021
Published: 01 July 2021

Citation:
Chang C-B, Lin Y-C, Wong Y-C, Lin S-N, Lin C-Y, Lin Y-H, Sheng T-W, Huang C-C, Yang L-Y and Wang L-J (2021) IVIM Parameters on MRI Could Predict ISUP Risk Groups of Prostate Cancers on Radical Prostatectomy. Front. Oncol. 11:659014. doi: 10.3389/fonc.2021.659014

Purpose: To elucidate the usefulness of intravoxel incoherent motion (IVIM)/apparent diffusion coefficient (ADC) parameters in preoperative risk stratification using International Society of Urological Pathology (ISUP) grades.

Materials and Methods: Forty-five prostate cancer (PCa) patients undergoing radical prostatectomy (RP) after prostate multiparametric magnetic resonance imaging (mpMRI) were included. The ISUP grades were categorized into low-risk (I-II) and high-risk (III-V) groups, and the concordance between the preoperative and postoperative grades was analyzed. The largest region of interest (ROI) of the dominant tumor on each IVIM/ADC image was delineated to obtain its histogram values (i.e., minimum, mean, and kurtosis) of diffusivity (D), pseudodiffusivity (D*), perfusion fraction (PF), and ADC. Multivariable logistic regression analysis of the IVIM/ADC parameters without and with preoperative ISUP grades were performed to identify predictors for the postoperative high-risk group.

Results: Thirty-two (71.1%) of 45 patients had concordant preoperative and postoperative ISUP grades. D_{mean}, $D^*_{kurtosis}$, $PF_{kurtosis}$, ADC_{min}, and ADC_{mean} were significantly associated with the postoperative ISUP risk group (all $p < 0.05$). D_{mean} and $D^*_{kurtosis}$ (model I, both $p < 0.05$) could predict the postoperative ISUP high-risk group with an area under the curve (AUC) of 0.842 and a 95% confidence interval (CI) of 0.726–0.958. The addition of $D^*_{kurtosis}$ to the preoperative ISUP grade (model II) may enhance prediction performance, with an AUC of 0.907 (95% CI 0.822–0.992).

Conclusions: The postoperative ISUP risk group could be predicted by D_{mean} and $D^*_{kurtosis}$ from mpMRI, especially $D^*_{kurtosis}$. Obtaining the biexponential IVIM parameters is important for better risk stratification for PCa.

Keywords: prostate cancer, IVIM, ISUP grade, diffusivity, pseudodiffusivity, perfusion fraction, kurtosis

INTRODUCTION

The Gleason scores (GSs) obtained from prostate biopsies or transurethral resection of the prostate (TURP) before radical prostatectomy (RP) are used as treatment guidance for prostate cancers (PCas) by stratifying them into low-risk (GS 6), intermediate-risk (GS 7) and high-risk (GS 8-10) groups. For example, low-risk patients may undergo active surveillance or brachytherapy as monotherapy (1, 2). However, the concordance of the GS on prostate biopsy and the GS according to RP are limited, ranging from 31% to 60% (3–5), which implies possibly inappropriate treatment selection for some patients when relying on the GS obtained from prostate biopsies (4, 5). Recently, the International Society of Urological Pathology (ISUP) adopted a new grading system for PCas using GSs 6, 3 + 4, 4 + 3, 8, and 9-10 as grades I, II, III, IV, and V, respectively, to replace the old risk stratification groups (i.e., GS 6, 7, 8-10) (6). The intermediate-risk group (GS 7) in the old risk stratification system is divided into GS 3 + 4 (grade II) and 4 + 3 (grade III) in the new ISUP grade system because there is a significant difference in recurrence between patients in the two new grades (6). The hazard ratios of biochemical recurrence relative to ISUP grade I were 1.9, 5.1, 8.0, and 11.7 for ISUP grades II, III, IV, and V, respectively. Thus, the accurate prediction of the postoperative ISUP grade according to the RP specimen is important for risk stratification and treatment selection for PCas.

Diffusion weighted imaging (DWI) is currently considered a key component of prostate multiparametric magnetic resonance imaging (mpMRI) examinations (7, 8). There are statistically significant correlations between the apparent diffusion coefficients (ADCs) and the GSs of PCas (9–11). The ADC values representing water diffusion are usually calculated from DWI using monoexponential fitting (12), which, however, does not consider the influence of intravoxel incoherent motion (IVIM) (13, 14). Thus, Le Bihan et al. (15). proposed an IVIM model using biexponential fitting, which allows the extraction of IVIM parameters, including diffusivity (D), pseudodiffusivity (D*), and perfusion fraction (PF). Two studies have shown that both ADC and IVIM parameters are associated with low risk (GS 6) and intermediate/high risk (GS 7-10) *via* biopsy or RP (16, 17). Nonetheless, it remains unclear whether the ADC/IVIM parameters are associated with the postoperative ISUP grades and thus may be useful for their prediction. In addition, for patients with preoperative ISUP grades obtained *via* biopsy or TURP, do the addition of the ADC/IVIM parameters have incremental value for risk stratification? Thus, the purpose of the current study was to elucidate whether ADC and IVIM parameters alone or in combination with preoperative ISUP grades could predict the postoperative ISUP grade.

Abbreviations: GS, Gleason score; TURP, transurethral resection of the prostate; RP, radical prostatectomy; PCa, prostate cancer; ISUP, International Society of Urological Pathology; DWI, Diffusion weighted imaging; mpMRI, multiparametric magnetic resonance imaging; ADC, apparent diffusion coefficient; IVIM, intravoxel incoherent motion; D, diffusivity; D*, pseudodiffusivity; PF, perfusion fraction; DCE, dynamic contrast enhancement; FOV, field of view; PSA, prostate-specific antigen; TRUS, transrectal ultrasound.

MATERIALS AND METHODS

Patients

The institutional review board approved this retrospective study and provided a waiver for obtaining informed consent from the enrolled patients. From June 2016 to December 2017, 247 patients underwent prostate mpMRI, including DWI, IVIM, and dynamic contrast enhancement (DCE) pulse sequences. The patients who met all inclusion criteria and did not fit any of the exclusion criteria were enrolled for final analysis. The inclusion criteria were (1) a histological diagnosis of PCa by prostate biopsy or TURP, (2) no treatments for PCa before mpMRI, and (3) RP after mpMRI. At this stage, 195 patients were excluded due to violation of inclusion criteria, including ten without a histological diagnosis, 20 with records of treating PCa (such as prior RP, anti-hormone therapy, radiation therapy, etc.), and 165 without receiving RP. Of 52 patients who met all inclusion criteria, seven patients were excluded because of fitting the exclusion criteria. The exclusion criteria were (1) no PCa found in RP specimens (n = 1), (2) concurrent malignancy other than PCa in RP specimens (n = 1), (3) a time interval of more than 90 days between mpMRI and RP (n = 5) (16, 18), (4) poor diagnostic quality due to artifact of hip prostheses on mpMRI (n = 0), and (5) no detectable PCa on mpMRI (n = 0). Forty-five patients were eligible for this study and were used to construct the database (**Figure 1**).

MRI Technique and IVIM/ADC Parameters on MRI

All MRI acquisitions were performed on a 3T clinical scanner (Discovery MR750, GE Healthcare, Milwaukee, USA). The mpMRI pulse sequences included conventional T2-weighted imaging (T2WI) in the sagittal, coronal and axial planes and T1-weighted imaging (T1WI) in the axial plane as well as functional imaging such as DWI, IVIM and DCE. T2WI was performed using a fast spin echo (FSE) sequence with repetition time (TR) = 5800-6100 ms; echo time (TE) = 92 - 103 ms; slice thickness = 4 mm; matrix = 384 × 320; and field of view (FOV) = 180 × 180 - 240 × 240 mm^2. T1WI was performed using an FSE sequence with TR = 660 ms; TE = 15 ms; slice thickness = 4 mm; matrix = 256 × 224; and FOV = 180 × 180 mm^2. IVIM imaging was performed using 8 b values (i.e., 0, 10, 30, 50, 80, 100, 400, 1000 s/mm^2) with a reduced FOV (rFOV) = 20 × 10 cm^2; matrix = 80 × 40; and TE = 53.4 ms. After IVIM DWI, DCE using a three-dimensional (3D) T1-weighted spoiled gradient-echo sequence in the axial plane (TR = 2.6 ms; TE = 1.1 ms; flip angle = 13°; number of excitations (NEX) = 1; matrix = 140 × 140; FOV = 280 × 280 mm^2; and slice thickness = 4 mm) was acquired using a standard dose (0.1 mmol/kg body weight) of gadopentetate dimeglumine (Gd-DTPA; Magnevist; Bayer-Schering, Burgess Hill, UK) administered at a rate of 3 mL/s with a temporal resolution of 5.4 seconds and a total acquisition time of 324 seconds (60 phases). A uroradiologist with over 20 years of experience reviewed the ADC and IVIM images using homemade software written in MATLAB (R2015b; MathWorks,

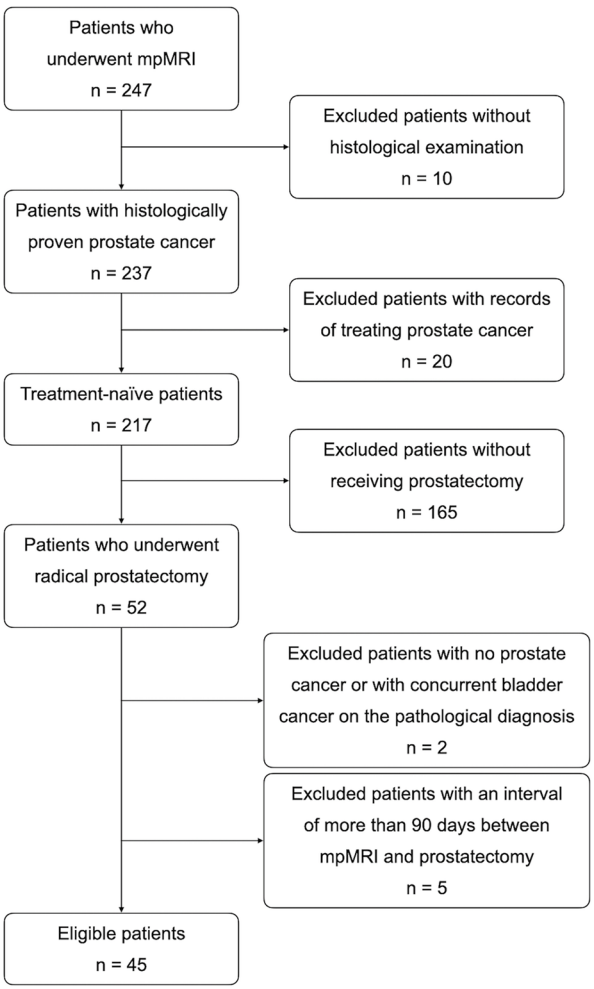

FIGURE 1 | Flow diagram of the enrollment of the 45 patients selected by applying inclusion and exclusion criteria.

Inc., Natick, MA, USA) and delineated the largest region of interest (ROI) of the dominant tumor nodule on each image (**Figures 2**–**4**). Histogram values (i.e., minimum, mean, and kurtosis) of the IVIM parameters (D, D*, and PF) were then calculated and obtained using a biexponential model (15). Histogram values (i.e., minimum, mean, and kurtosis) of the ADCs generated from DWI using a standard monoexponential model (19) were recorded.

Clinical Variables and Risk Groups Based on Preoperative and Postoperative Gleason Grading

For each patient, we recorded his age and prostate-specific antigen (PSA) titer at diagnosis. The preoperative ISUP grades of PCas (6, 20) were recorded using the histological results from transrectal ultrasound (TRUS) biopsy or TURP specimens and categorized into low-risk (grade I-II) and high-risk (grade III-V) groups. The percentage of positive TRUS biopsy specimen cores was recorded. The final pathological results based on RP specimens were then used for recording postoperative ISUP grades and similarly categorized into the two risk groups. The preoperative and postoperative ISUP grades and their corresponding risk groups of all patients were compared and recorded as same, upgraded or downgraded.

Statistical Analysis

Descriptive statistics for continuous variables are expressed as the median and interquartile range (IQR) because of the small sample size and skewed distributions. Categorical variables are expressed as counts and proportions. The kappa statistic was calculated to analyze the agreement between the preoperative and postoperative ISUP grades. The associations of clinical characteristics and the IVIM/ADC parameters with the final risk groups (high/low) based on the postoperative ISUP grades were analyzed using the Mann-Whitney U test for continuous variables. Furthermore, multivariable logistic regression with forward selection procedure was performed to identify the predictors of a high-risk stratification for the RP specimens. First, all clinical characteristics (including age, PSA at diagnosis, positive biopsy specimen cores) and all IVIM/ADC parameters were initially entered in a logistic regression to identify the significant predictors of the postoperative ISUP risk group based on forward selection (Model I). Afterward, we added a factor of risk groups based on the preoperative ISUP grade combining with the model of forward procedure to investigate its adding effect (Model II). The ROC curves were plotted to show the predictive performance of the models. A similar multivariable logistic regression with forward selection procedure was also performed to identify the key predictors of postoperative ISUP grade or risk group upgrading. All statistical analyses were performed using SPSS Statistics version 25 (IBM, Armonk, New York). A two-tailed p-value of less than 0.05 was considered statistically significant.

RESULTS

The descriptive statistics of the clinical characteristics and the IVIM/ADC parameters of the 45 patients are summarized in **Table 1**. Before RP, the median PSA titer at diagnosis was 14.2 ng/mL, and 10 patients (22.2%) had PSA titer less than 9 ng/mL at diagnosis, ranging from 2.0 ng/mL to 8.3 ng/mL. Of these 10 patients, two patients (4.0%) had a PSA titer less than 4 ng/mL at diagnosis: 2.0 ng/mL and 3.2 ng/mL. Of the 45 patients, 41 (91.1%) underwent TRUS biopsy, and 4 (8.9%) underwent TURP to obtain the GS. Among ADC, D, and D*, D* had the lowest mean, and ADC had the highest. In contrast, D* had the highest kurtosis, and ADC had the lowest.

Table 2 shows the distributions of the preoperative and postoperative ISUP grades of the 45 patients. For the preoperative TRUS biopsies and TURP specimens, ISUP grades I and III were the most common. However, grade III was the most common for the postoperative RP specimens. Fifteen of 45 (33.3%) patients had the same preoperative and postoperative ISUP grades. Thirty-two (71.1%) patients were categorized into the same preoperative and postoperative ISUP risk groups (16 low-risk and 16 high-risk). Overall, 7 (15.6%) patients upgraded from low risk to high risk (i.e., grade I to III for 2, and II to III

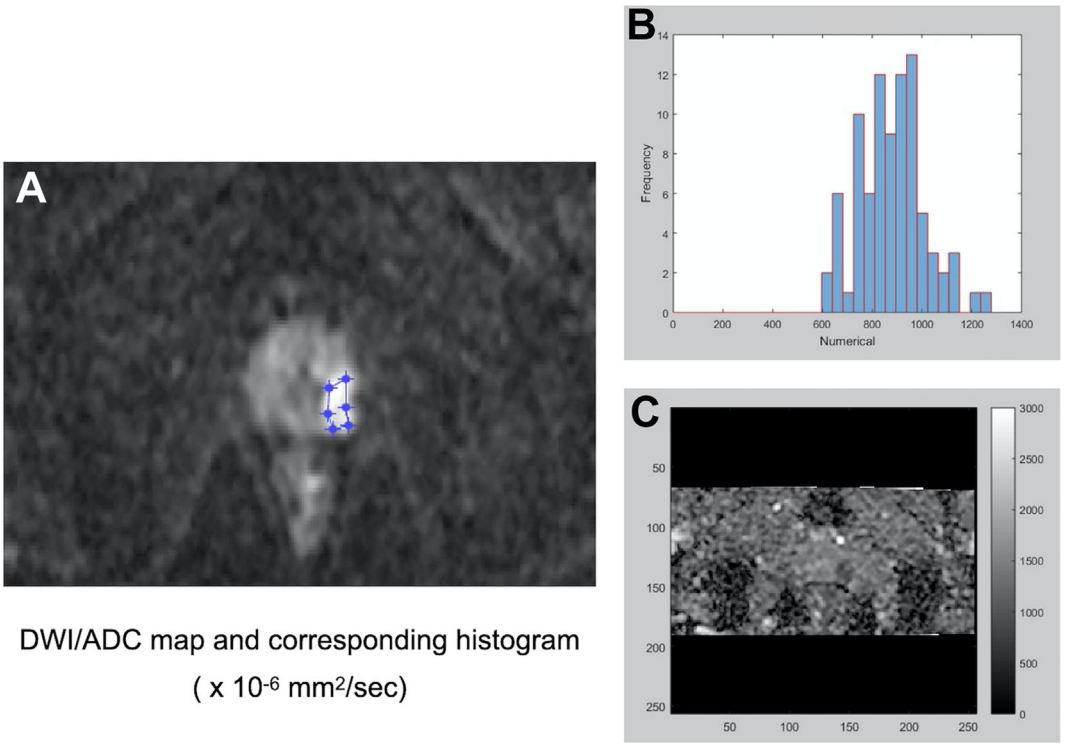

FIGURE 2 | A representative PCa with a preoperative Gleason score of 3 + 3 for the histogram analysis of DW imaging measures. After identifying the dominant tumor nodule in the prostate gland, a region of interest (ROI) was delineated manually on a conventional DWI image (b = 1500 s/mm^2) **(A)** to obtain an ADC map and the corresponding histogram **(B)** of the ADC map **(C)**.

TABLE 1 | Clinical characteristics and IVIM/ADC parameters obtained on MRI of 45 prostate cancer patients before radical prostatectomy.

Variables	Median (IQR)
Clinical characteristics	
Age at diagnosis (years)	66.0 (63.0–71.0)
PSA at diagnosis (ng/mL)	14.2 (9.1–20.4)
Positive biopsy specimen cores (%)	33.3 (8.3–50.0)
IVIM and ADC parameters	
D_{min} (×10^{-6} mm^2/s)	481.0 (363.0–644.0)
D_{mean} (×10^{-6} mm^2/s)	934.7 (832.7–1024.9)
$D_{kurtosis}$	3.2 (2.6–3.8)
D^*_{min} (×10^{-6} mm^2/s)	0.0 (0.0–0.0)
D^*_{mean} (×10^{-6} mm^2/s)	376.6 (253.3–490.8)
$D^*_{kurtosis}$	44.4 (17.9–70.0)
PF_{min} (%)	0.02 (0.01–0.22)
PF_{mean} (%)	60.7 (54.6–72.1)
$PF_{kurtosis}$	1.5 (1.3–2.4)
ADC_{min} (×10^{-6} mm^2/s)	580.0 (445.0–852.0)
ADC_{mean} (×10^{-6} mm^2/s)	1181.7 (1022.4–1281.1)
$ADC_{kurtosis}$	3.0 (2.4–3.7)

All the statistics for the variables are expressed as the median (IQR).
IVIM, intravoxel incoherent motion; ADC, apparent diffusion coefficient; MRI, magnetic resonance imaging; PSA, prostate-specific antigen; D, diffusivity; min, minimum; D, pseudodiffusivity; PF, perfusion fraction.*

TABLE 2 | ISUP grades of prostate cancers obtained before radical prostatectomy (RP) and using histological results of the RP specimens of the 45 patients.

Preoperative ISUP grades	ISUP grades from RP specimens				
	I	II	III	IV	V
I, n (%)	2 (15.4)	9 (69.2)	2 (15.4)	0 (0)	0 (0)
II, n (%)	1 (10.0)	4 (40.0)	5 (50.0)	0 (0)	0 (0)
III, n (%)	1 (7.7)	5 (38.5)	7 (53.8)	0 (0)	0 (0)
IV, n (%)	0 (0)	0 (0)	4 (66.7)	0 (0)	2 (33.3)
V, n (%)	0 (0)	0 (0)	1 (33.3)	0 (0)	2 (66.7)

Row percentages shown in parentheses.
ISUP, International Society of Urological Pathology.

for 5) and 6 (13.3%) patients downgraded from high risk to low risk (i.e., grade III to I for 1 and III to II for 5) postoperatively. There was moderate agreement between the preoperative and postoperative ISUP risk groups (kappa = 0.423, p=0.005). There were significant associations of preoperative and postoperative ISUP risk group, as 16 of 22 (72.7%) postoperative ISUP low-risk patients and 7 of 23 (30.4%) postoperative ISUP high-risk patients were regarded to have preoperative ISUP low-risk grades (p=0.005).

The clinical characteristics (i.e., age and PSA at diagnosis and percentage of positive cores from TRUS biopsy) had no associations with both the postoperative ISUP high-risk group and postoperative ISUP risk group upgrading (**Table 3**; **Table S1** and **S2**). However, multiple IVIM and ADC parameters, including D_{mean}, $D^*_{kurtosis}$, $PF_{kurtosis}$, ADC_{min}, and ADC_{mean}, were significantly associated with postoperative ISUP risk group

(all $p < 0.05$, **Table 3**). Besides, D_{mean}, $PF_{kurtosis}$, and ADC_{mean}, were associated with postoperative ISUP risk group upgrading (all $p \leq 0.05$, **Table S2**). Further multivariable logistic regression analysis showed that D_{mean} and $D^*_{kurtosis}$ were significant predictors for the postoperative ISUP high-risk group (both $p < 0.05$, model I, **Table 4**). D_{mean} was the only significant predictor for the postoperative ISUP risk group upgrading, with a negative relationship ($p < 0.0001$, **Table S3**). Significant predictors for the postoperative ISUP grade upgrading were not identified. By using the preoperative ISUP grade as an adjustment variable, the additive effect of $D^*_{kurtosis}$ and Dmean could improve the performance of the prediction models ($p < 0.05$, model II, **Table 4**). **Figure 5** shows that the areas under the ROC curves for model I and model II were 0.842 (95% CI 0.726–0.958) and 0.907 (95% CI 0.822–0.992), respectively.

TABLE 4 | Multivariable analysis of significant predictors of high-risk group according to radical prostatectomy specimens using logistic regression analysis.

Predictor	Estimate (S.E.)	OR (95% CI)	*p*
Model I			
D_{mean} ($\times 10^{-6}$ mm^2/s)	-0.002 (0.001)	0.998 (0.996–0.999)	0.003
$D^*_{kurtosis}$	0.045 (0.014)	1.046 (1.018–1.075)	0.001
Model II			
D_{mean} ($\times 10^{-6}$ mm^2/s)	-0.005 (0.001)	0.995 (0.993–0.998)	0.002
$D^*_{kurtosis}$	0.052 (0.018)	1.053 (1.016–1.092)	0.005
Preoperative ISUP grades			
I	*Reference*		
II	2.785 (1.249)	16.193 (1.399–187.381)	0.026
III, IV, V	2.575 (1.111)	13.126 (1.489–115.733)	0.020

S.E., standard error; OR, odds ratio; CI, confidence interval; D, diffusivity; D, pseudodiffusivity; ISUP, the International Society of Urological Pathology.*

DISCUSSION

This study shows that there is only moderate agreement in the preoperative and postoperative ISUP risk groups, with a final concordance of 71.1%. Two major factors may account for this limited concordance: (1) bias in the pathological evaluation and (2) sampling error from an underrepresented area (21). Previous studies have also reported similar but lower concordances for GS risk groups ranging from 31% to 60% (3–5). Although the higher concordance achieved in this study could be explained by the use of more biopsy cores (12, 13) than in previous studies (10 or fewer), 29% of patients who upgraded or downgraded postoperatively remained misclassified in the risk stratification and could have been potentially misled in the treatment selection if it had been based on the preoperative ISUP risk group alone.

There were significant associations of the postoperative ISUP risk groups with ADC_{min}, ADC_{mean}, D_{mean}, $PF_{kurtosis}$ and $D^*_{kurtosis}$ (all $p < 0.05$) but not with the clinical characteristics in this study. Previous studies have also reported that ADC_{mean} and D_{mean} are associated with the GS risk group but not with clinical characteristics (16–18, 22–24). Since there is an inverse correlation between ADC_{mean} and GS 6-10 obtained from biopsies (19), the significant differences in ADC_{mean} using the monoexponential model and D_{mean} using the biexponential model between GS risk groups are reasonable and could be expected. However, the new ISUP grades differ from GS, as GS 7 is now categorized into two grades, ISUP grade II for GS 3 + 4 and ISUP grade III for GS 4 + 3, because of their substantial differences in recurrence. Shan et al. (18). showed that ADC_{mean}, PF_{mean}, and D_{mean} could differentiate GS 3 + 4 from GS > 3 + 4 according to RP with AUCs of 0.744, 0.726 and 0.732, respectively (all $p < 0.05$), which is similar to our results except for PF_{mean}. In IVIM models, PF represents the proportion of water flowing in capillaries of the total water in a voxel, and D* represents water movement in the randomly oriented capillary network mimicking

TABLE 3 | Associations of clinical characteristics and IVIM/ADC parameters obtained before radical prostatectomy with final risk groups of 45 prostate cancer patients.

Variables	ISUP grade groups*		*p*
	Low risk (N = 22)	High risk (N = 23)	
Age (years)	65.5 (63.0–71.0)	66.0 (61.0–71.0)	0.849
PSA at diagnosis (ng/mL)	11.8 (8.3–17.4)	14.5 (9.1–21.4)	0.586
Positive biopsy cores (%)	25.0 (8.3–50.0)	33.3 (12.5–50.0)	0.741
D_{min} ($\times 10^{-6}$ mm^2/s)	494.0 (350.0–692.0)	455.0 (363.0–563.0)	0.247
D_{mean} ($\times 10^{-6}$ mm^2/s)	971.7 (901.4–1113.6)	881.6 (800.3–995.7)	0.035
$D_{kurtosis}$	2.8 (2.2–4.0)	3.5 (3.0–3.8)	0.073
D^*_{min} ($\times 10^{-6}$ mm^2/s)	0.0 (0.0–0.0)	0.0 (0.0–0.0)	0.282
D^*_{mean} ($\times 10^{-6}$ mm^2/s)	423.5 (251.4–603.5)	369.6 (298.0–420.8)	0.555
$D^*_{kurtosis}$	19.3 (4.8–49.4)	59.7 (34.2–84.8)	< 0.001
PF_{min} (%)	0.06 (0.01–2.2)	0.02 (0.01–0.13)	0.219
PF_{mean} (%)	58.1 (42.8–73.2)	62.0 (57.6–71.2)	0.376
$PF_{kurtosis}$	2.3 (1.6–3.9)	1.3 (1.3–1.5)	0.001
ADC_{min} ($\times 10^{-6}$ mm^2/s)	705.5 (535.0–927.0)	535.0 (434.0–682.0)	0.044
ADC_{mean} ($\times 10^{-6}$ mm^2/s)	1274.7 (1084.8–1304.4)	1094.6 (1016.8–1231.4)	0.035
$ADC_{kurtosis}$	2.7 (2.2–3.7)	3.4 (2.8–4.0)	0.077

All the statistics for the variables are expressed as the median (IQR).

All compared with the Mann-Whitney U test.

**Final ISUP grade groups using results of histological examinations of radical prostatectomies.*

IVIM, intravoxel incoherent motion; ADC, apparent diffusion coefficient; ISUP, the International Society of Urological Pathology; PSA, prostate-specific antigen; D, diffusivity; min, minimum; D, pseudodiffusivity; PF, perfusion fraction.*

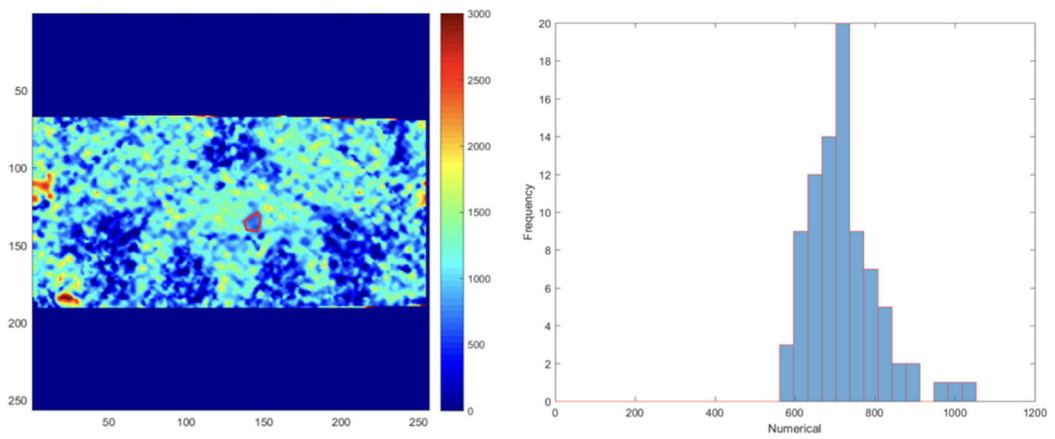

D map and corresponding histogram (x 10^{-6} mm^2/sec)

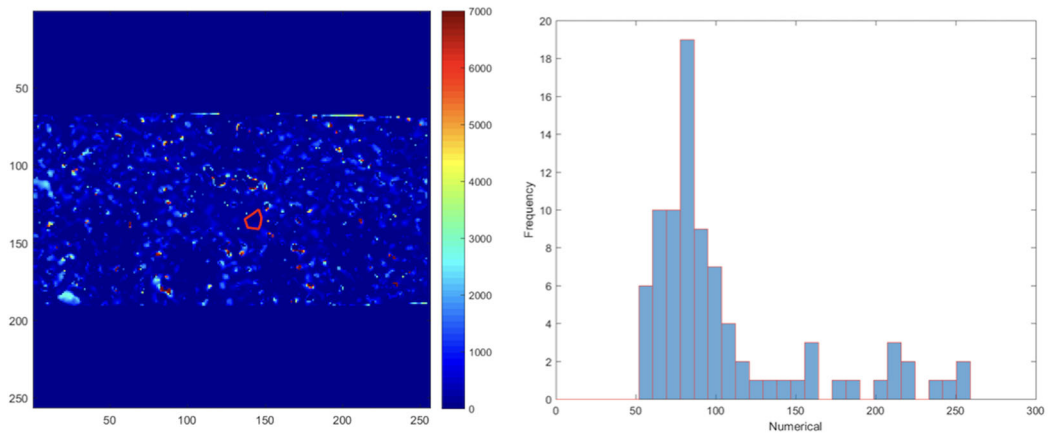

D* map and corresponding histogram (x 10^{-6} mm^2/sec)

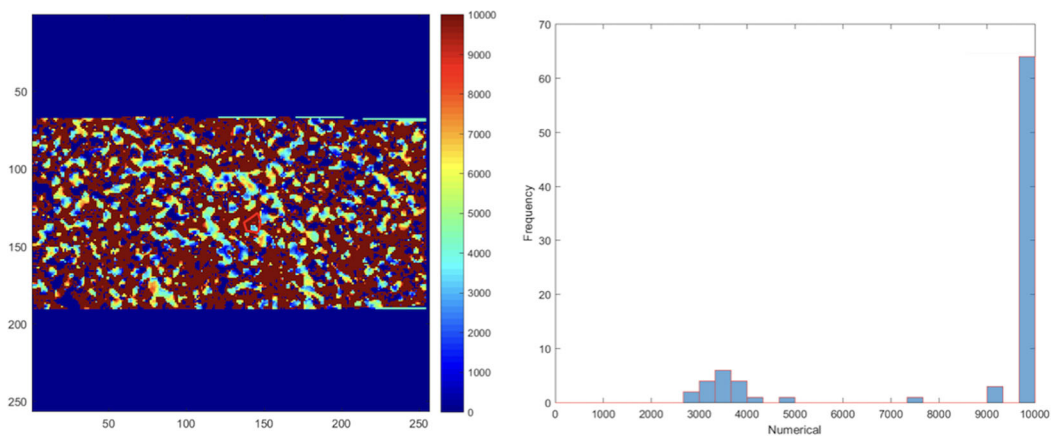

PF map and corresponding histogram (x 10^{-2} %)

FIGURE 3 | Another ROI was delineated manually on the IVIM D map. The ROI on the D map was automatically copied to the D* and PF maps by our homemade software. Then, the corresponding histograms of the D, D*, and PF maps were obtained. The process was repeated for each DWI image and IVIM map containing the dominant tumor nodule.

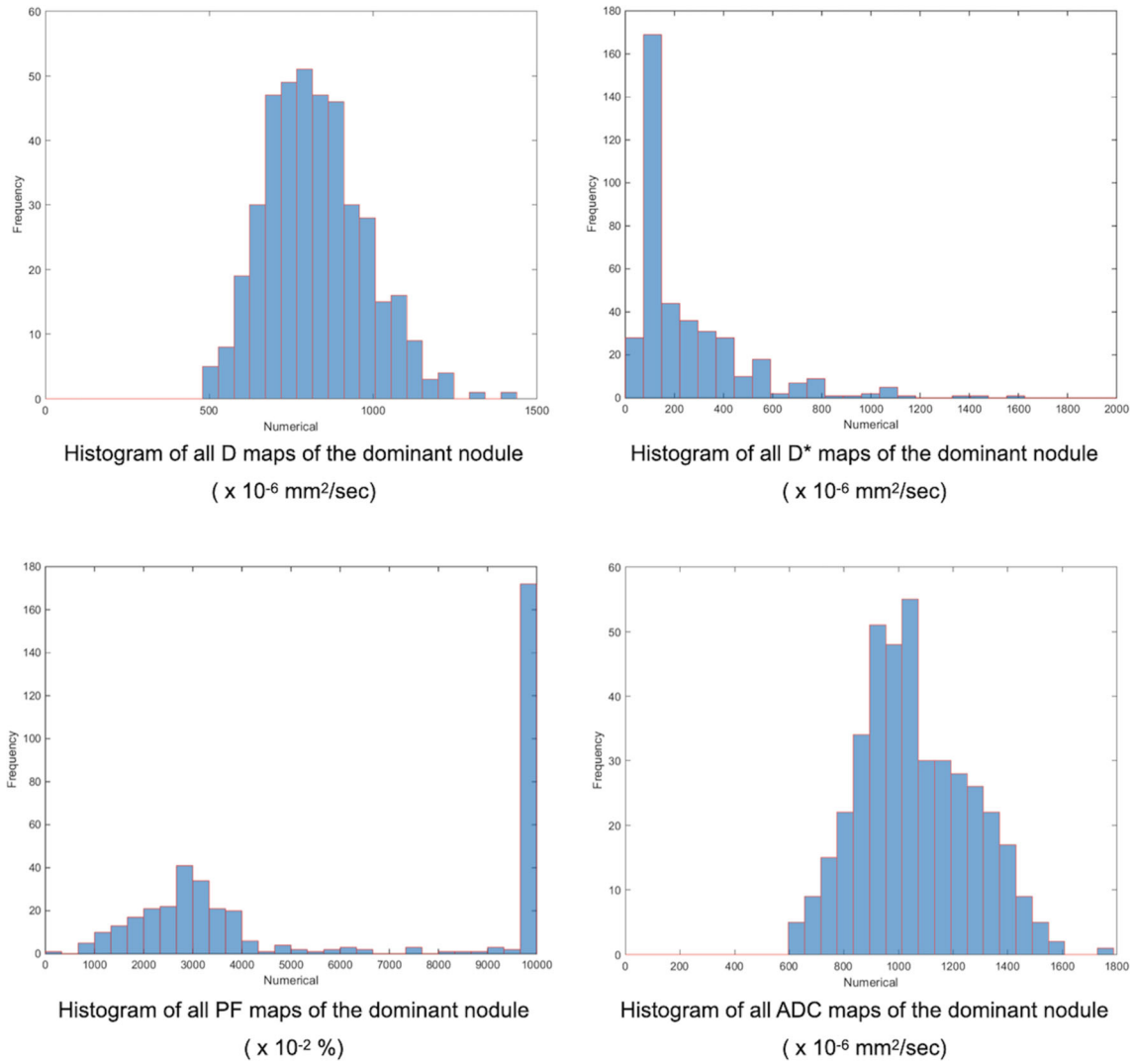

FIGURE 4 | Finally, our homemade software constructed the whole dominant nodule histograms for D, D*, PF, and ADC by combining the different histograms from each image. The minimum, mean, and kurtosis of the IVIM/ADC parameters were extracted from the whole dominant nodule histogram and used for further analysis.

diffusion (15). This study showed that the postoperative ISUP high-risk group had significantly higher $D^*_{kurtosis}$ and lower $PF_{kurtosis}$ than the low-risk group, which means that there are more outliers of the D* distribution and fewer outliers of the PF distribution (25). Thus, the postoperative ISUP high-risk grades tend to have markedly more heterogeneous water movement in the capillary network in voxels and a relatively more restricted range of PF than the low-risk group. The associations of these ADC and IVIM parameters with the postoperative ISUP risk group implies their potential usefulness in preoperative risk stratification and prediction for the postoperative ISUP grades, which have replaced the old GS system worldwide.

From a practical point of view, it is necessary to address whether the ADC/IVIM parameters could predict the final postoperative ISUP risk groups, and multivariate analysis with controlling variables showed that D_{mean} and $D^*_{kurtosis}$, rather than $PF_{kurtosis}$ and ADC_{mean}, were significant predictors for the postoperative ISUP risk group in this study. This means that lower D_{mean} and higher $D^*_{kurtosis}$ values predict the postoperative ISUP high-risk group with an expected high accuracy (0.842), as shown by the AUC, which is higher than the concordance (0.71) of the preoperative and postoperative ISUP risk group. The limited concordance between the preoperative and postoperative ISUP grades or GSs might result in the inappropriate selection of treatment. Thus, are the ADC and IVIM parameters helpful in filling this gap? This study shows that the addition of $D^*_{kurtosis}$ into the model using the preoperative ISUP grades has incremental value, achieving a high AUC of 0.907, which accounts for a 67.8% decrease in upgrading/downgrading the postoperative ISUP risk group with respect to the preoperative ISUP risk group. Thus, it is worth obtaining IVIM parameters using a biexponential model

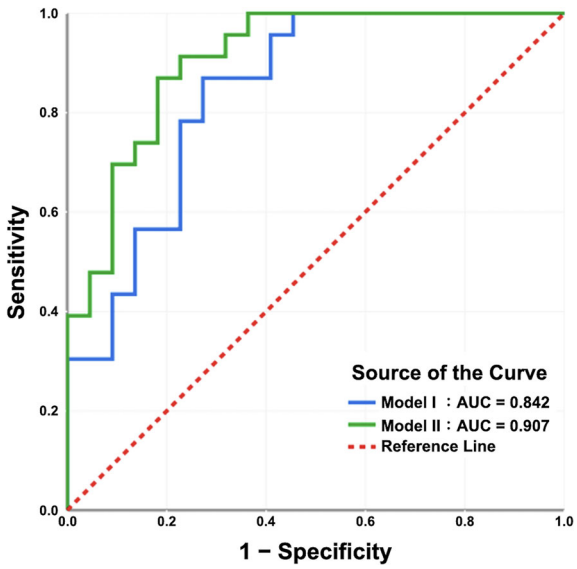

FIGURE 5 | The receiver operating characteristic curves of the prediction models. The areas under the curves of model I and model II are 0.842 and 0.907, respectively. In model I, the IVIM/ADC parameters D_{mean} and $D^*_{kurtosis}$ were significant predictors for the ISUP high-risk group according to radical prostatectomy (RP) specimens. In model II, the use of the preoperative ISUP grade as an adjustment variable, in addition to D_{mean} and $D^*_{kurtosis}$, may enhance the predictive performance of the model.

because unlike the ADC parameters, they are significant predictors of postoperative ISUP grade, both without and with biopsy/TURP information.

Le Bihan et al. (15). proposed the IVIM model by assuming a 2-compartment scenario and characterized the diffusion signals with a biexponential decay function. Since IVIM is an expanded form of DWI, it can be used for PCa detection in peripheral and transition zones of the prostate, just like monoexponential-fitted ADC. Previous studies had shown that the IVIM parameters were not superior to ADC in evaluating PCa in the transition zone (22) but might increase the diagnostic performance in detecting PCa in the peripheral zone (24). For tumor detection in the whole prostate, IVIM parameters and ADC might have comparable diagnostic performance (18). Overall, the biexponential-fitted IVIM did not add more information in tumor detection than traditional ADC. However, the IVIM parameters, as shown in the present study, would be beneficial to predict GS, aggressiveness, and postoperative ISUP risk group of PCa. The IVIM diffusion might, therefore, potentially influence the treatment selection of PCa.

There are limitations in the present work. First, this is a retrospective study of PCa patients undergoing RP with possible selection bias resulting from the recruitment of operable patients undergoing active surveillance, radiation therapy or hormone therapy by using the GS from biopsies/TURP as a reference for treatment selection. Another limitation is the small number of patients included in the present study due to the strict inclusion and exclusion criteria used, which, however, were implemented to ensure comparability between mpMRI and the RP specimens (e.g., patients with a delay of more than 90 days between mpMRI and RP were excluded). Future studies with prospective designs and large patient cohorts should be performed to confirm our results.

In conclusion, predicting the postoperative ISUP risk group with the use of histological information from biopsies/TURP could be unsatisfactory and sometimes misleading. It might be feasible and helpful to use the IVIM parameters Dmean and D*kurtosis from mpMRI alone to predict the postoperative ISUP risk group. The addition of $D^*_{kurtosis}$ to the preoperative ISUP grades has incremental value in the prediction of postoperative ISUP grades. Therefore, it is important to obtain IVIM parameters using a biexponential model for better risk stratification for PCa before surgery or other treatments.

DATA AVAILABILITY STATEMENT

The raw data supporting the conclusions of this article will be made available by the authors, without undue reservation.

ETHICS STATEMENT

The studies involving human participants were reviewed and approved by the Institutional Review Board of Chang Gung Medical Foundation (IRB number, 202000712B0). The IRB approved a waiver for obtaining informed consent from patients/participants in this study.

AUTHOR CONTRIBUTIONS

Study concept and design: L-JW and L-YY. Acquisition, analysis, or interpretation of data: all authors. Drafting of the manuscript: C-BC, Y-HL, and Y-CL. Critical revision of manuscript: L-JW and L-YY. Statistical analysis: L-JW, L-YY, C-BC, and Y-CW.

Administrative, technical, and material support: Y-HL, Y-CL, Y-CW, S-NL, C-YL, T-WS, and C-CH. Study supervision: L-JW and L-YY. All authors contributed to the article and approved the submitted version.

ACKNOWLEDGMENTS

The authors acknowledge the statistical assistance provided by the Clinical Trial Center, Chang Gung Memorial Hospital, Linkou, Taiwan, which was founded by the Ministry of Health and Welfare of Taiwan; MOHW109-TDU-B-212-114005.

SUPPLEMENTARY MATERIAL

The Supplementary Material for this article can be found online at: https://www.frontiersin.org/articles/10.3389/fonc.2021.659014/full#supplementary-material

REFERENCES

1. Klotz L. Active Surveillance for Favorable-Risk Prostate Cancer: Who, How and Why? *Nat Clin Pract Oncol* (2007) 4:692. doi: 10.1038/ncponc0966
2. Salembier C, Lavagnini P, Nickers P, Mangili P, Rijnders A, Polo A, et al. Tumour and Target Volumes in Permanent Prostate Brachytherapy: A Supplement to the ESTRO/EAU/EORTC Recommendations on Prostate Brachytherapy. *Radiother Oncol* (2007) 83:3. doi: 10.1016/j.radonc.2007.01.014
3. Hsieh TF, Chang CH, Chen WC, Chou CL, Chen CC, Wu HC. Correlation of Gleason Scores Between Needle-Core Biopsy and Radical Prostatectomy Specimens in Patients With Prostate Cancer. *J Chin Med Assoc* (2005) 68:167. doi: 10.1016/S1726-4901(09)70243-6
4. Suer E, Gokce MI, Gulpinar O, Guclu AG, Haciyev P, Gogus C, et al. How Significant is Upgrade in Gleason Score Between Prostate Biopsy and Radical Prostatectomy Pathology While Discussing Less Invasive Treatment Options? *Scand J Urol* (2014) 48:177. doi: 10.3109/21681805.2013.829519
5. Colleselli D, Pelzer AE, Steiner E, Ongarello S, Schaefer G, Bartsch G, et al. Upgrading of Gleason Score 6 Prostate Cancers on Biopsy After Prostatectomy in the Low and Intermediate tPSA Range. *Prostate Cancer Prostatic Dis* (2010) 13:182. doi: 10.1038/pcan.2009.54
6. Epstein JI, Zelefsky MJ, Sjoberg DD, Nelson JB, Egevad L, Magi-Galluzzi C, et al. A Contemporary Prostate Cancer Grading System: A Validated Alternative to the Gleason Score. *Eur Urol* (2016) 69:428. doi: 10.1016/j.eururo.2015.06.046
7. Tamada T, Sone T, Jo Y, Toshimitsu S, Yamashita T, Yamamoto A, et al. Apparent Diffusion Coefficient Values in Peripheral and Transition Zones of the Prostate: Comparison Between Normal and Malignant Prostatic Tissues and Correlation With Histologic Grade. *J Magn Reson Imaging* (2008) 28:720. doi: 10.1002/jmri.21503
8. Hambrock T, Somford DM, Huisman HJ, van Oort IM, Witjes JA, Hulsbergen-van de Kaa CA, et al. Relationship Between Apparent Diffusion Coefficients at 3.0-T MR Imaging and Gleason Grade in Peripheral Zone Prostate Cancer. *Radiology* (2011) 259:453. doi: 10.1148/radiol.11091409
9. Turkbey B, Shah VP, Pang Y, Bernardo M, Xu S, Kruecker J, et al. Is Apparent Diffusion Coefficient Associated With Clinical Risk Scores for Prostate Cancers That are Visible on 3-T MR Images? *Radiology* (2011) 258:488. doi: 10.1148/radiol.10100667
10. Barbieri S, Bronnimann M, Boxler S, Vermathen P, Thoeny HC. Differentiation of Prostate Cancer Lesions With High and With Low Gleason Score by Diffusion-Weighted MRI. *Eur Radiol* (2017) 27:1547. doi: 10.1007/s00330-016-4449-5
11. Peng Y, Jiang Y, Yang C, Kruecker J, Kadoury S, Merino MJ, et al. Quantitative Analysis of Multiparametric Prostate MR Images: Differentiation Between Prostate Cancer and Normal Tissue and Correlation With Gleason Score–a Computer-Aided Diagnosis Development Study. *Radiology* (2013) 267:787. doi: 10.1148/radiol.13121454
12. Gibbs P, Liney GP, Pickles MD, Zelhof B, Rodrigues G, Turnbull LW, et al. Correlation of ADC and T2 Measurements With Cell Density in Prostate Cancer at 3.0 Tesla. *Invest Radiol* (2009) 44:572. doi: 10.1097/RLI.0b013e3181b4c10e
13. Quentin M, Blondin D, Klasen J, Lanzman RS, Miese FR, Arsov C, et al. Comparison of Different Mathematical Models of Diffusion-Weighted Prostate MR Imaging. *Magn Reson Imaging* (2012) 30:1468. doi: 10.1016/j.mri.2012.04.025
14. Pang Y, Turkbey B, Bernardo M, Kruecker J, Kadoury S, Merino MJ, et al. Intravoxel Incoherent Motion MR Imaging for Prostate Cancer: An Evaluation of Perfusion Fraction and Diffusion Coefficient Derived From Different B-Value Combinations. *Magn Reson Med* (2013) 69:553. doi: 10.1002/mrm.24277
15. Le Bihan D, Breton E, Lallemand D, Aubin ML, Vignaud J, Laval-Jeantet M. Separation of Diffusion and Perfusion in Intravoxel Incoherent Motion MR Imaging. *Radiology* (1988) 168:497. doi: 10.1148/radiology.168.2.3393671
16. Yang DM, Kim HC, Kim SW, Jahng GH, Won KY, Lim SJ, et al. Prostate Cancer: Correlation of Intravoxel Incoherent Motion MR Parameters With Gleason Score. *Clin Imaging* (2016) 40:445. doi: 10.1016/j.clinimag.2016.01.001
17. Zhang YD, Wang Q, Wu CJ, Wang X-N, Zhang J, Liu H, et al. The Histogram Analysis of Diffusion-Weighted Intravoxel Incoherent Motion (IVIM) Imaging for Differentiating the Gleason Grade of Prostate Cancer. *Eur Radiol* (2015) 25:994. doi: 10.1007/s00330-014-3511-4
18. Shan Y, Chen X, Liu K, Zeng M, Zhou J. Prostate Cancer Aggressive Prediction: Preponderant Diagnostic Performances of Intravoxel Incoherent Motion (IVIM) Imaging and Diffusion Kurtosis Imaging (DKI) Beyond ADC at 3.0 T Scanner With Gleason Score at Final Pathology. *Abdom Radiol (NY)* (2019) 44:3441. doi: 10.1007/s00261-019-02075-3
19. Le Bihan D, Mangin JF, Poupon C, Clark D, Pappata S, Molko N, et al. Diffusion Tensor Imaging: Concepts and Applications. *J Magn Reson Imaging* (2001) 13:534. doi: 10.1002/jmri.1076
20. Epstein JI, Egevad L, Amin MB, Delahunt B, Srigley JR, Humphrey PA. The 2014 International Society of Urological Pathology (ISUP) Consensus Conference on Gleason Grading of Prostatic Carcinoma: Definition of Grading Patterns and Proposal for a New Grading System. *Am J Surg Pathol* (2016) 40:244. doi: 10.1097/PAS.0000000000000530
21. King CR, Long J P. Prostate Biopsy Grading Errors: A Sampling Problem? *Int J Cancer* (2000) 90:326. doi: 10.1002/1097-0215(20001220)90:6<326::AID-IJC3>3.0.CO;2-J
22. Bao J, Wang X, Hu C, Hou J, Dong F, Guo L. Differentiation of Prostate Cancer Lesions in the Transition Zone by Diffusion-Weighted MRI. *Eur J Radiol Open* (2017) 4:123. doi: 10.1016/j.ejro.2017.08.003
23. Shinmoto H, Tamura C, Soga S, Shiomi E, Yoshihara N, Kaji T, et al. An Intravoxel Incoherent Motion Diffusion-Weighted Imaging Study of Prostate Cancer. *AJR Am J Roentgenol* (2012) 199:W496. doi: 10.2214/AJR.11.8347
24. Valerio M, Zini C, Fierro D, Giura F, Colarieti A, Giuliani A, et al. 3T Multiparametric MRI of the Prostate: Does Intravoxel Incoherent Motion Diffusion Imaging Have a Role in the Detection and Stratification of Prostate Cancer in the Peripheral Zone? *Eur J Radiol* (2016) 85:790. doi: 10.1016/j.ejrad.2016.01.006
25. Westfall PH. Kurtosis as Peakedness, 1905 - 2014. R.I.P. *Am Stat* (2014) 68:191. doi: 10.1080/00031305.2014.917055

Conflict of Interest: Author C-YL was employed by General Electric (GE) Healthcare.

The remaining authors declare that the research was conducted in the absence of any commercial or financial relationships that could be construed as a potential conflict of interest.

frontiers in Oncology

ORIGINAL RESEARCH
published: 09 September 2021
doi: 10.3389/fonc.2021.708730

MRI-Based Nomogram of Prostate Maximum Sectional Area and Its Zone Area for Prediction of Prostate Cancer

Shaoqin Jiang[1,2†], Zhangcheng Huang[2†], Bingqiao Liu[2†], Zhenlin Chen[2], Yue Xu[2], Wenzhong Zheng[2], Yaoan Wen[2] and Mengqiang Li[2]*

[1] Department of Urology, Changhai Hospital, Second Military University, Shanghai, China, [2] Laboratory of Urology, Department of Urology, Fujian Union Hospital, Fujian Medical University, Fuzhou, China

OPEN ACCESS

Edited by:
Riccardo Schiavina, University of Bologna, Italy

Reviewed by:
Caterina Gaudiano, Policlinico Sant'Orsola-Malpighi, Italy
Gian Maria Busetto, University of Foggia, Italy

****Correspondence:***
Mengqiang Li
limengqiang1976@163.com

[†]These authors have contributed equally to this work and share first authorship

Specialty section:
This article was submitted to Genitourinary Oncology, a section of the journal Frontiers in Oncology

Received: *12 May 2021*
Accepted: *19 August 2021*
Published: *09 September 2021*

Citation:
Jiang S, Huang Z, Liu B, Chen Z, Xu Y, Zheng W, Wen Y and Li M (2021) MRI-Based Nomogram of Prostate Maximum Sectional Area and Its Zone Area for Prediction of Prostate Cancer. Front. Oncol. 11:708730. doi: 10.3389/fonc.2021.708730

Objective: To reduce unnecessary prostate biopsies, we designed a magnetic resonance imaging (MRI)-based nomogram prediction model of prostate maximum sectional area (PA) and investigated its zone area for diagnosing prostate cancer (PCa).

Methods: MRI was administered to 691 consecutive patients before prostate biopsies from January 2012 to January 2020. PA, central gland sectional area (CGA), and peripheral zone sectional area (PZA) were measured on axial T2-weighted prostate MRI. Multivariate logistic regression analysis and area under the receiver operating characteristic (ROC) curve were performed to evaluate and integrate the predictors of PCa. Based on multivariate logistic regression coefficients after excluding combinations of collinear variables, three models and nomograms were generated and intercompared by Delong test, calibration curve, and decision curve analysis (DCA).

Results: The positive rate of PCa was 46.74% (323/691). Multivariate analysis revealed that age, PSA, MRI, transCGA, coroPZA, transPA, and transPAI (transverse PZA-to-CGA ratio) were independent predictors of PCa. Compared with no PCa patients, transCGA (AUC = 0.801) was significantly lower and transPAI (AUC = 0.749) was significantly higher in PCa patients. Both of them have a significantly higher AUC than PSA (AUC = 0.714) and PV (AUC = 0.725). Our best predictive model included the factors age, PSA, MRI, transCGA, and coroPZA with the AUC of 0.918 for predicting PCa status. Based on this predictive model, a novel nomogram for predicting PCa was conducted and internally validated (C-index = 0.913).

Conclusions: We found the potential clinical utility of transCGA and transPAI in predicting PCa. Then, we firstly built the nomogram based on PA and its zone area to evaluate its diagnostic efficacy for PCa, which could reduce unnecessary prostate biopsies.

Keywords: nomogram, prostate maximum sectional area, prostate zone area, prostate cancer, prostate biopsy

INTRODUCTION

Prostate cancer (PCa) is the most common cancer among men in the Western world, and it has an increasing prevalence (1). There is an international consensus that early detection and treatment of PCa can improve the survival rate of PCa patients. Prostate-specific antigen (PSA) is the most widely used screening marker to detect PCa at an early stage. The larger clinical trial found that patients having undergone PSA screening had 25% lower PCa death rates than those who did not (2). After tests reveal an elevated serum PSA level, most patients require puncture biopsy of the prostate, because the prostate biopsy remains the gold standard method for diagnosing PCa. However, we have to face a clinical problem that the prostate biopsy is an invasive operation. It not only brings pain and fear to the patients, but also may cause medical complications such as infection and hemorrhage (3). Because prostate biopsy always has the probability of missing tumor tissue, it is not able to make a 100% diagnosis of PCa. The rate of negative prostate biopsies was substantially high (58.51%–69.30%) especially in cases with only elevated PSA levels, thus greatly affecting patients' quality of life (4, 5). Therefore, it is rational to avoid the biopsy on patients who are ultimately proved to be negative cases.

In order to overcome the limitations of PSA test, Benson et al. proposed the concept of PSA density (PSAD, PSA value divided by prostate volume), which was considered to increase the accuracy of PSA test for diagnosing the PCa (6). The main principle is that PCa tissues can release more PSA per unit volume to blood serum than enlarged or normal prostate tissues do. Recent research had also shown that PSA density could overweigh PSA in distinguishing clinically significant PCa and intraprostatic inflammation before prostate biopsy (7). However, it has been reported that the prostate volume was frequently roughly calculated using the prolate ellipsoid formula before operation, in which there is 10%–20% error compared with prostatectomy specimens in the clinical situation (8, 9). So, this kind of prostate volume should be further improved for assessing the exact risk of PCa. Therefore, we considered finding new MRI-based predictors to enhance the role of roughly calculated prostate volume for predicting PCa.

In MRI images of prostate zonal anatomy, the prostate comprises the peripheral zone, transition zone, central zone, and anterior fibromuscular stroma (10). A related study showed that approximately 75%–85% of PCa cases are located in the peripheral zone, rather than the central gland. The central gland is the typical site of BPH, which includes the transition zone, central zone, and anterior fibromuscular stroma (11). MRI images can clearly identify different anatomical areas of the prostate, which is beneficial to improve the detection rate of PCa. We first propose the concept of the prostate maximum sectional area (PA) for predicting PCa by MRI images, which includes both central gland sectional area (CGA) and peripheral zone sectional area (PZA). Comparatively, MRI is regarded as the most precise noninvasive method, as it can assess PA with high reproducibility and accuracy compared with rough prostate volume calculated by the common formula (12).

Nomogram is a simple intuitive graph of a complex mathematical formula (13). It is widely used for cancer prediction, primarily because of their ability to use biologic and clinical variables building a graphically depictive statistical predictive model that is tailored to an individual patient (14). User-friendly graphical interfaces for generating these estimates facilitate the use of nomograms to aid in clinical decision-making.

The purpose of the current study was to establish a new nomogram about PA and its associated zone area such as CGA and PZA on axial T2 fat-saturated MRI for diagnosing PCa. To the best of our knowledge, no previous literature has employed MRI-based PA and the associated zone area for the prediction of PCa before prostate biopsy among Chinese population.

METHODS

Study Population

The study was designed as a retrospective cohort study that was conducted in the Laboratory of Urology and the Department of Urology of Fujian Medical University Union Hospital (Fuzhou, China). We enrolled 691 consecutive patients who underwent multiparametric magnetic resonance image (mp-MRI) before initial transrectal ultrasound (TRUS)-guided prostate biopsy from January 2012 to January 2020, followed by data anonymization. Eligible patients who matched the selection criteria were identified by the following criteria: elevated PSA levels (≥10 $ng{\cdot}ml^{-1}$), suspected cancer on digital rectal examination (DRE), hyperechoic or hypoechoic TRUS, or abnormal MRI findings. For PSA values between 4 and 10 $ng{\cdot}ml^{-1}$, the biopsy criterion was ratio of free to total PSA < 16%. The exclusion criteria were as follows: previous prostate biopsy, history of prostate surgery, pathological examination revealing tumors other than adenocarcinoma, and incomplete mp-MRI information or imaging artifacts (**Figure 1**). The study was ethically approved by the Institutional Review Board of Fujian Medical University Union Hospital with an approval number of 2020KY059. Written informed consent was obtained from patients before the study commenced. Details of patients' identity had to be omitted. Our work complies with the Code of Ethics of the World Medical Association (Declaration of Helsinki, revised in 2013).

Clinical Data and Variable Definitions

Clinical characteristics including age, body mass index (BMI), PSA, free PSA (FPSA), free-to-total PSA (FTPSA), prostate volume (PV), PSA density (PSAD), MRI, transverse prostate maximum sectional

Abbreviations: BMI, body mass index; FPSA, free PSA; PSA, prostate-specific antigen; FTPSA, $\frac{\text{free PSA}}{\text{PSA}}$; PV, prostate volume; sagiPSAPA, $\frac{\text{PSA}}{\text{sagi PA}}$; PSAD, PSA density; sagiPSACGA, $\frac{\text{PSA}}{\text{sagi CGA}}$; PA, prostate maximum sectional area; sagiPSAPZA, $\frac{\text{PSA}}{\text{sagi PZA}}$; CGA, central gland sectional area; transPSAPA, $\frac{\text{PSA}}{\text{trans PA}}$; PZA, peripheral zone sectional area; transPSACGA, $\frac{\text{PSA}}{\text{trans CGA}}$; sagiPA, sagittal prostate maximum sectional area; transPSAPZA, $\frac{\text{PSA}}{\text{trans PZA}}$; sagiCGA, sagittal central gland sectional area; coroPSAPA, $\frac{\text{PSA}}{\text{coro PA}}$; sagiPZA, sagittal peripheral zone sectional area; coroPSACGA, $\frac{\text{PSA}}{\text{coro CGA}}$; transPA, transverse prostate maximum sectional area; coroPSAPZA, $\frac{\text{PSA}}{\text{coro PZA}}$; transCGA, transverse central gland sectional area; sagiPAI, $\frac{\text{sagiPZA}}{\text{sagi CGA}}$; transPZA, transverse peripheral zone sectional area; transPAI, $\frac{\text{transPZA}}{\text{trans CGA}}$; coroPA, coronal prostate maximum sectional area; coroPAI, $\frac{\text{coroPZA}}{\text{coro CGA}}$; coroCGA, coronal central gland sectional area; ALP, alkaline phosphatase; coroPZA, coronal peripheral zone sectional area; LDH, lactate dehydrogenase

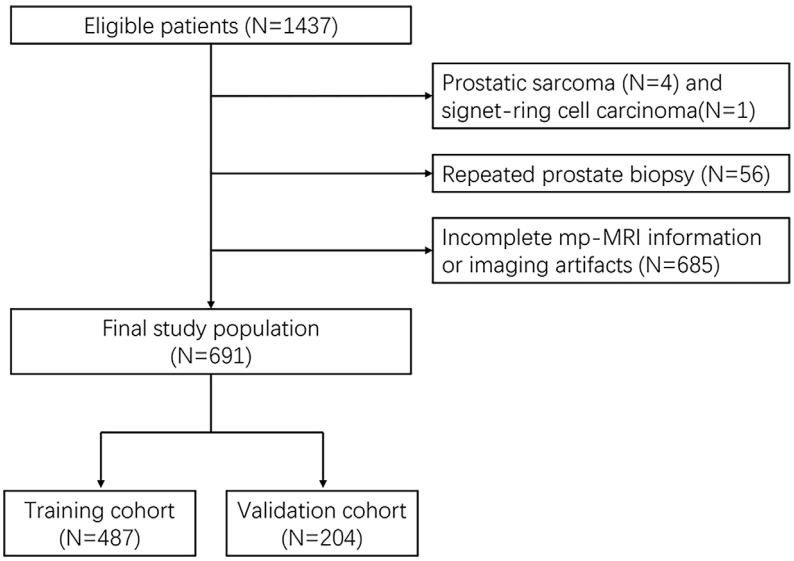

FIGURE 1 | Flow chart of patient selection.

area (transPA), coronal prostate maximum sectional area (coroPA), sagittal prostate maximum sectional area (sagiPA), transverse peripheral zone sectional area (transPZA), coronal peripheral zone sectional area (coroPZA), sagittal peripheral zone sectional area (sagiPZA), transverse central gland sectional area (transCGA), coronal central gland sectional area (coroCGA), sagittal central gland sectional area (sagiCGA), alkaline phosphatase (ALP), and lactate dehydrogenase (LDH) were collected before prostate biopsy. Subsequently, transverse PSA-to-PA ratio (transPSAPA), coronal PSA-to-PA ratio (coroPSAPA), sagittal PSA-to-PA ratio (sagiPSAPA), transverse PSA-to-PZA ratio (transPSAPZA), coronal PSA-to-PZA ratio (coroPSAPZA), sagittal PSA-to-PZA ratio (sagiPSAPZA), transverse PSA-to-CGA ratio (transPSACGA), coronal PSA-to-CGA ratio (coroPSACGA), sagittal PSA-to-CGA ratio (sagiPSACGA), transverse PZA-to-CGA ratio (transverse prostate area index, transPAI), coronal PZA-to-CGA ratio (coronal prostate area index, coroPAI), and sagittal PZA-to-CGA ratio (sagittal prostate area index, sagiPAI) were calculated. The prostate maximum sectional area on prostate T2WI MRI had the following definition: In the transverse plane, when the bilateral prostate lobes are basically symmetrical, and the quasi-circular internal urethral sphincter can be seen in the middle of the prostate, the maximum section is the one for which the sectional area becomes smaller when scanning upward or downward. In the coronal plane, when the bilateral prostate lobes are basically symmetrical, and the strip-type internal urethral sphincter can be seen in the middle of the prostate, the maximum section is the one for which the sectional area becomes smaller when scanning upward or downward. In the sagittal plane, when the strip-type internal urethral sphincter can be seen in the middle of the prostate, the maximum section is the one for which the sectional area becomes smaller when scanning upward or downward.

Image Acquisition and Interpretation

A Siemens Magnetom Trio Tim 3.0-T superconducting MRI scanner with an 18-channel phased-array torso coil was used to create all magnetic resonance images [repetition time (TR) 400 ms, echo time (TE) 80 ms, slice thickness = 3 mm, interslice gap = 30%, acquisition four times with fat-suppression technique]. T2-weighted images in the sagittal, coronal, and transverse planes, diffusion-weighted images, apparent diffusion coefficient in the transverse plane, and dynamic contrast-enhanced images were acquired according to the international prostate MRI guidelines (15). Interpretation of the MRI findings was performed by a radiologist and a urologist (with 5 or more years of experience in prostate imaging),who measured PA and CGA on fat-saturated T2WI MRI (**Figure S1**).

Prostate Biopsy Method

Following local non-infiltrative anesthesia, all prostate biopsies were performed transrectally under TRUS guidance (BK Medical, USA). A standard 13-core systematic prostate biopsy was obtained including transitional, peripheral, and anterior zone from base to apex by an 18-gauge/25-cm biopsy needle (Bard Peripheral Vascular, Inc). All patients underwent standard prostate biopsies, which were performed by an experienced urologist (more than 5 years of experience in prostate biopsy). All biopsy specimens were examined and recorded by two experienced pathologists.

Statistical Analysis

Distributions of variables were compared by the chi-squared test for categorical variables and the Mann–Whitney *U* test for continuous variables, which was not normally distributed. The values of all continuous variables (age, BMI, PSA, FPSA, FTPSA, transPA, coroPA, sagiPA, transPZA, coroPZA, sagiPZA, transCGA, coroCGA, sagiCGA, transPSAPA, coroPSAPA, sagiPSAPA,

transPSAPZA, coroPSAPZA, sagiPSAPZA, transPSACGA, coroPSACGA, sagiPSACGA, ALP, and LDH) were not normally distributed. Variables including BMI, FPSA, FTPSA, transPZA, and ALP were excluded due to lack of statistical significance in univariate logistic regression analysis. We integrated variables with great clinical significance including age, PSA, and MRI into the base model. The remaining variables were reassembled into all kinds of possible combinations through enumeration algorithm. Then, we combined base model and each different combinations together to form our predict models. Correlation analysis was used to detect the multicollinearity between every two variables (**Figure S2**). Any model that contained two or more multicollinearity variables will be eliminated before the next step. Then, multivariate logistic regression analysis was performed on the rest of these models to identify the independence of each predictor for diagnosing PCa and calculate its variance inflation factor (VIF). Models will also be eliminated when their VIF ≥ 2. The diagnostic efficacy of these models was evaluated by the area under the curve (**Figure 2**). The first three combinations with the highest AUC were chosen as our final models. The statistical differences among three models and each single predictor were compared by Delong test, respectively. The cutoff value, sensitivity, specificity, and positive and negative likelihood ratios were computed for these variables and prediction models. Nomograms were generated to predict the

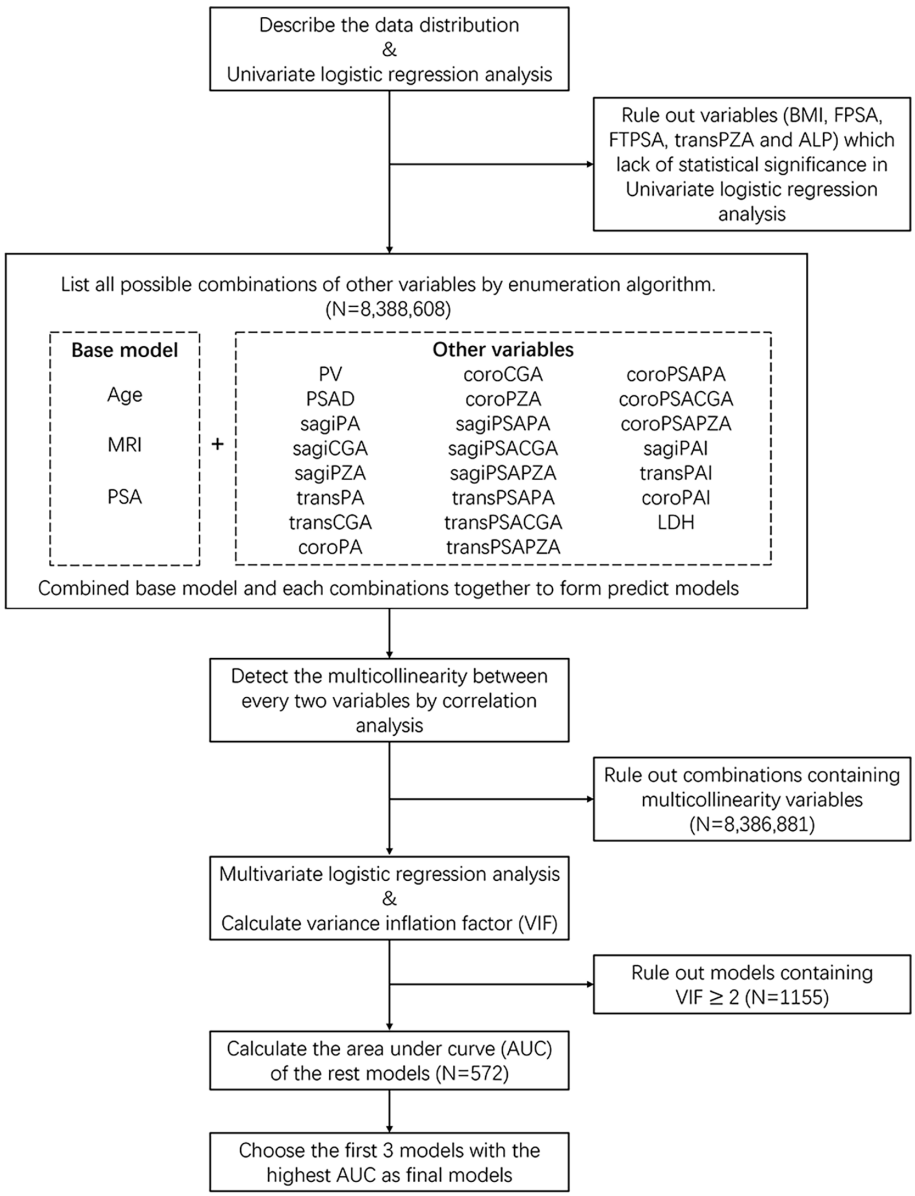

FIGURE 2 | Flow chart of statistical analysis.

probability of PCa, based on the multivariate regression coefficients in three models. These models were recalibrated both in the training cohort and the validation cohort to evaluate the nomogram's discrimination capacity by 1,000 random bootstrap samples with replacement. Calibration slope less than 1 reflects proper fit of the model. The clinical utility of three models was quantified by decision curve analysis (DCA) through summing the benefits (true positives) and subtracting the harms (false positives). Statistical significance was defined as p-value < 0.05. Statistical analysis, nomogram, and calibration plot were generated using R studio (version 4.0.3).

RESULTS

Clinical Characteristics

A total of 230 (47.23%) of 487 patients in the training cohort and 93 (45.59%) of 204 patients in the validation cohort were diagnosed with PCa (**Table 1**). Univariate logistic regression analysis showed that all variables were statistically significant predictors of PCa detection except for BMI, FPSA, FTPSA, transPZA, and ALP in the training cohort. No significance was found in variables between the training cohort and validation cohort except for age (**Table 2**).

Multivariate Logistic Regression Models

To evaluate the synergistic ability of every single predictor for predicting PCa, we created different models that did not contain multicollinearity. The first three models with the highest AUC were chosen as our final models, which were model 1, model 2, and model 3. Model 1 consists of age, PSA, MRI, transCGA, and coroPZA after excluding sagiPAI, PV, and PSAD. Model 2 consists of age, PSA, MRI, transPAI, coroPZA, and transPA after excluding PV and PSAD. Model 3 consists of age, PSA, MRI, transPAI, and PV after excluding sagiPAI, coroPAI, and PSAD (**Table 3**). Age, MRI, and PSA were independent

TABLE 1 | Clinical characteristics of patients before the prostate biopsy.

	Training cohort				Validation cohort			
	No PCa	PCa	OR (95% CI)	p-value	No PCa	PCa	OR (95% CI)	p-value
	(n = 257)	(n = 230)			(n = 111)	(n = 93)		
Age*	67 (62;73)	70 (64;76)	1.05 (1.02;1.07)	<0.001	69 (64;74)	72 (66;77)	1.03 (1.00;1.07)	0.023
BMI*	23.00 (21.50;24.91)	23.88 (21.35;25.99)	1.04 (0.98;1.10)	0.082	23.90 (22.50;25.43)	22.70 (20.52;25.50)	0.92 (0.84;1.01)	0.031
MRI:				<0.001				<0.001
Abnormal	92 (35.8%)	186 (80.9%)	Ref.		43 (38.7%)	76 (81.7%)	Ref.	
Normal	165 (64.2%)	44 (19.1%)	0.13 (0.09;0.20)		68 (61.3%)	17 (18.3%)	0.14 (0.07;0.27)	
FPSA*	1.53 (0.92;2.50)	1.68 (0.69;7.27)	1.11 (1.06;1.17)	0.101	1.49 (0.98;2.42)	1.33 (0.18;3.51)	1.09 (1.02;1.16)	0.411
PSA*	11.13 (7.44;17.91)	26.09 (9.54;97.90)	1.04 (1.03;1.05)	<0.001	11.42 (7.07;16.74)	29.38 (13.22;86.47)	1.05 (1.03;1.07)	<0.001
FTPSA*	0.14 (0.10;0.18)	0.12 (0.08;0.20)	12.7 (2.26;71.0)	0.292	0.14 (0.11;0.20)	0.11 (0.07;0.18)	1.24 (0.11;13.7)	0.008
PV*	72.9 (49.6;105)	45.7 (33.5;64.8)	0.98 (0.97;0.98)	<0.001	69.3 (44.5;98.9)	41.7 (29.1;56.7)	0.97 (0.96;0.98)	<0.001
PSAD*	0.15 (0.10;0.23)	0.56 (0.25;1.46)	14.7 (7.56;28.8)	<0.001	0.16 (0.11;0.26)	0.65 (0.33;1.83)	109 (21.6;552)	<0.001
sagiPA*	20.1 (16.2;24.7)	15.5 (12.2;19.5)	0.89 (0.86;0.92)	<0.001	20.1 (16.3;24.8)	15.1 (12.1;18.0)	0.87 (0.82;0.92)	<0.001
sagiCGA*	12.8 (9.06;17.1)	8.09 (5.77;11.1)	0.83 (0.80;0.87)	<0.001	12.8 (9.62;17.1)	6.98 (5.16;9.99)	0.80 (0.74;0.86)	<0.001
sagiPZA*	6.49 (4.79;8.50)	7.11 (5.15;9.45)	1.06 (0.99;1.12)	0.041	6.23 (4.78;8.55)	6.80 (4.72;9.98)	1.08 (0.99;1.18)	0.187
transPA*	21.9 (17.5;28.0)	16.9 (13.0;20.4)	0.89 (0.86;0.91)	<0.001	21.0 (17.2;27.1)	16.1 (12.8;19.3)	0.86 (0.82;0.91)	<0.001
transCGA*	13.5 (9.76;18.2)	7.61 (5.77;10.6)	0.79 (0.75;0.83)	<0.001	13.9 (10.0;17.0)	7.06 (4.95;9.82)	0.78 (0.72;0.84)	<0.001
transPZA*	8.30 (5.91;10.3)	8.55 (5.96;10.9)	1.03 (0.98;1.07)	0.398	7.58 (5.89;9.77)	7.99 (6.30;10.5)	1.04 (0.96;1.13)	0.242
coroPA*	21.3 (17.1;27.9)	16.8 (13.1;20.2)	0.89 (0.86;0.91)	<0.001	22.2 (15.3;26.9)	15.5 (12.7;19.7)	0.88 (0.84;0.92)	<0.001
coroCGA*	16.2 (11.5;21.5)	8.91 (6.67;12.3)	0.83 (0.80;0.87)	<0.001	16.3 (10.7;21.3)	7.95 (5.58;11.4)	0.82 (0.77;0.87)	<0.001
coroPZA*	5.77 (4.23;7.21)	6.84 (5.31;8.79)	1.19 (1.11;1.28)	<0.001	5.45 (4.29;6.36)	6.76 (5.35;9.17)	1.33 (1.17;1.51)	<0.001
sagiPSAPA*	0.56 (0.39;0.88)	1.81 (0.73;4.44)	2.24 (1.84;2.73)	<0.001	0.56 (0.36;0.93)	2.02 (1.00;4.99)	3.13 (2.06;4.75)	<0.001
sagiPSACGA*	0.91 (0.62;1.37)	3.54 (1.46;8.17)	1.73 (1.51;1.97)	<0.001	0.82 (0.53;1.43)	4.10 (1.94;10.8)	2.30 (1.72;3.07)	<0.001
sagiPSAPZA*	1.78 (1.15;3.29)	4.18 (1.54;10.2)	1.19 (1.13;1.26)	<0.001	1.69 (0.99;2.95)	4.60 (2.30;10.0)	1.18 (1.09;1.27)	<0.001
transPSAPA*	0.51 (0.35;0.75)	1.55 (0.65;4.28)	2.48 (1.97;3.12)	<0.001	0.53 (0.34;0.81)	1.75 (0.84;4.81)	3.57 (2.22;5.76)	<0.001
transPSACGA*	0.81 (0.57;1.30)	3.43 (1.39;9.06)	1.75 (1.52;2.01)	<0.001	0.84 (0.54;1.40)	4.44 (1.78;11.9)	2.21 (1.67;2.93)	<0.001
transPSAPZA*	1.40 (0.89;2.36)	3.22 (1.29;8.44)	1.25 (1.17;1.34)	<0.001	1.44 (0.92;2.24)	3.85 (1.61;9.03)	1.32 (1.18;1.47)	<0.001
coroPSAPA*	0.52 (0.35;0.77)	1.47 (0.69;4.26)	2.51 (1.99;3.17)	<0.001	0.50 (0.34;0.82)	1.77 (0.88;4.44)	3.50 (2.21;5.53)	<0.001
coroPSACGA*	0.74 (0.47;1.09)	3.10 (1.29;7.36)	1.84 (1.58;2.14)	<0.001	0.66 (0.49;1.20)	4.08 (1.52;9.36)	2.39 (1.76;3.23)	<0.001
coroPSAPZA*	2.11 (1.21;3.57)	3.98 (1.72;9.83)	1.19 (1.13;1.25)	<0.001	2.08 (1.29;3.60)	4.80 (2.08;9.27)	1.23 (1.12;1.34)	<0.001
sagiPAI*	0.49 (0.34;0.74)	0.82 (0.51;1.26)	3.80 (2.51;5.75)	<0.001	0.47 (0.32;0.71)	0.85 (0.56;1.66)	4.22 (2.28;7.81)	<0.001
transPAI*	0.58 (0.41;0.87)	1.10 (0.62;1.61)	5.60 (3.71;8.46)	<0.001	0.54 (0.41;0.87)	1.27 (0.70;1.79)	7.70 (3.90;15.2)	<0.001
coroPAI*	0.36 (0.23;0.53)	0.74 (0.49;1.24)	9.21 (5.34;15.9)	<0.001	0.35 (0.23;0.48)	0.81 (0.55;1.32)	31.3 (10.7;92.0)	<0.001
ALP*	72.0 (60.0;85.0)	71.0 (59.0;88.3)	1.00 (1.00;1.01)	0.773	75.0 (60.5;85.0)	76.0 (61.0;89.0)	1.01 (1.00;1.01)	0.354
LDH*	176 (155;204)	182 (159;210)	1.01 (1.00;1.01)	0.034	179 (159;201)	184 (165;209)	1.01 (1.00;1.01)	0.125

PCa, prostate cancer; OR, odds ratio; FTPSA, free-to-total PSA; PA, prostate maximum sectional area; CGA, central gland sectional area; PZA, peripheral zone sectional area; PAI, PZA-to-CGA ratio; trans, transverse; coro, coronal; sagi, sagittal; PV, prostate volume; PSAD, PSA density.

**Continuous variables are shown as the median value and interquartile range.*

All variables were not normally distributed.

TABLE 2 | Clinical characteristics of patients in training cohort and validation cohort.

	All (*n* = 691)	Training cohort (*n* = 487)	Validation cohort (*n* = 204)	*p*-value
Age*	69 (63;75)	69 (63;74)	70 (65;76)	0.047
BMI*	23.44 (21.50;25.51)	23.44 (21.50;25.56)	23.45 (21.51;25.50)	0.882
MRI:				0.827
Abnormal	397 (57.5%)	278 (57.1%)	119 (58.3%)	
Normal	294 (42.5%)	209 (42.9%)	85 (41.7%)	
FPSA*	1.53 (0.85;3.08)	1.59 (0.86;3.24)	1.46 (0.85;2.72)	0.244
PSA*	14.02 (8.70;35.09)	13.76 (8.56;34.65)	14.64 (9.63;35.76)	0.460
FTPSA*	0.13 (0.09;0.19)	0.13 (0.09;0.19)	0.13 (0.09;0.19)	0.742
PV*	57.1 (39.4;85.1)	58.3 (40.5;86.7)	55.0 (36.2;82.5)	0.192
PSAD*	0.24 (0.13;0.65)	0.23 (0.13;0.65)	0.26 (0.14;0.65)	0.285
sagiPA*	17.9 (13.9;22.3)	18.0 (13.9;22.5)	17.5 (13.6;22.2)	0.533
sagiCGA*	10.4 (6.86;14.8)	10.4 (6.92;15.0)	10.4 (6.69;14.4)	0.548
sagiPZA*	6.71 (4.84;9.04)	6.74 (4.88;9.05)	6.59 (4.72;8.86)	0.532
transPA*	19.0 (15.0;24.2)	19.3 (15.3;24.3)	18.6 (14.9;23.7)	0.304
transCGA*	10.3 (7.05;15.2)	10.5 (7.21;15.2)	10.2 (6.62;15.1)	0.424
transPZA*	8.20 (5.95;10.7)	8.37 (5.94;10.8)	7.82 (6.01;10.3)	0.386
coroPA*	18.8 (14.5;24.6)	18.9 (14.7;24.6)	18.0 (14.2;24.4)	0.298
coroCGA*	12.0 (7.91;17.8)	12.1 (8.11;17.7)	11.4 (7.68;17.9)	0.481
coroPZA*	6.13 (4.58;7.92)	6.30 (4.54;7.97)	5.88 (4.64;7.65)	0.187
sagiPSAPA*	0.83 (0.48;2.07)	0.81 (0.47;1.99)	0.93 (0.49;2.19)	0.525
sagiPSAPZA*	2.34 (1.28;6.03)	2.29 (1.26;6.02)	2.47 (1.32;6.04)	0.635
sagiPSACGA*	1.43 (0.76;3.96)	1.37 (0.77;3.70)	1.53 (0.72;4.04)	0.560
transPSAPA*	0.70 (0.43;1.80)	0.69 (0.43;1.79)	0.75 (0.44;1.83)	0.367
transPSAPZA*	1.90 (1.07;4.27)	1.86 (1.02;4.20)	1.99 (1.19;4.40)	0.365
transPSACGA*	1.35 (0.73;4.04)	1.28 (0.73;3.77)	1.41 (0.75;4.10)	0.479
coroPSAPA*	0.73 (0.43;1.82)	0.72 (0.43;1.74)	0.78 (0.44;2.00)	0.386
coroPSAPZA*	2.57 (1.44;5.79)	2.57 (1.35;5.65)	2.54 (1.62;6.06)	0.371
coroPSACGA*	1.13 (0.62;3.52)	1.10 (0.62;3.38)	1.20 (0.62;3.69)	0.563
coroPAI*	0.50 (0.31;0.86)	0.50 (0.32;0.85)	0.48 (0.29;0.88)	0.779
transPAI*	0.75 (0.48;1.28)	0.75 (0.49;1.28)	0.76 (0.45;1.30)	0.983
sagiPAI*	0.60 (0.41;1.00)	0.60 (0.42;0.99)	0.57 (0.38;1.07)	0.812
ALP*	73.0 (60.0;86.3)	71.7 (59.0;86.0)	76.0 (60.8;87.0)	0.287
LDH*	179 (157;206)	178 (156;207)	181 (162;205)	0.490

PCa, prostate cancer; OR, odds ratio; FTPSA, free-to-total PSA; PA, prostate maximum sectional area; CGA, central gland sectional area; PZA, peripheral zone sectional area; PAI, PZA-to-CGA ratio; trans, transverse; coro, coronal; sagi, sagittal; PV, prostate volume; PSAD, PSA density.

**Continuous variables are shown as the median value and interquartile range.*

All variables were not normally distributed.

predictors of PCa in three models. The statistical significance of PV was not detected in both model 1 and model 2. The statistical significance of PSAD was not detected in all models.

Comparison of Predictive Accuracy

Furthermore, predictive accuracy of each predictor alone and models were assessed separately with ROC curve analysis. The AUC of model 1 (base model + coroPZA + transCGA) for predicting PCa was the highest among the models of any single predictor alone and the base model combined with any other predictors (**Figure 3** and **Table 4**). Delong test was used to compare the statistical difference of the AUC among three models and single predictors. Compared with model 3 (AUC = 0.907), the AUC of model 1 (AUC = 0.918) and model 2 (AUC = 0.916) had the same higher statistical advantages in the training cohort, while no statistical difference was found among the three models in the validation cohort (**Table 5**). The AUC of transCGA (0.801) was significantly higher than other single predictors. The AUC of coroPZA (0.635) was lower than other predictors, while there was no significant difference of AUC among transPAI, transPA, PV, and PSA in the training cohort (**Table 6**).

Nomograms, Calibration Plots, and DCA Curves

Based on the multivariate regression coefficients, the predictive models were visually presented as nomograms (**Figure 4** and **Figure S3**). The nomogram's discrimination of three models in the training cohort and validation cohort was shown in the calibration plot (**Figure 5**, **Figures S4** and **S5**). The C-index of model 1 for predicting PCa was 0.918 in the training cohort. The performance of model 2 (0.916) and model 3(0.907) in the calibration plot was not as good as that of model 1 in the training cohort, which demonstrates the superior fit of model 1. DCA curves showed that the nomogram based on model 1 has better net benefit gains in all range of threshold probabilities in the training cohort, while net benefit gains only improved when threshold probabilities are >8% in the validation cohort (**Figure 6**).

DISCUSSION

PCa is a malignant form of cancer whose diagnosis depends on the histopathological verification of adenocarcinoma in a

TABLE 3 | Multivariate logistic regression analysis of predictors associated with PCa before the prostate biopsy.

	Model 1				Model 2				Model 3		
Parameters	**Coefficient**	**OR (95% CI)**	***p*-value**	**Parameters**	**Coefficient**	**OR (95% CI)**	***p*-value**	**Parameters**	**Coefficient**	**OR (95% CI)**	***p*-value**
Age	0.070	1.073 (1.037–1.112)	0.0001	Age	0.071	1.073 (1.038–1.113)	0.0001	Age	0.071	1.074 (1.039–1.112)	<0.0001
MRI	−1.396	0.248 (0.144–0.419)	<0.0001	MRI	−1.400	0.247 (0.144–0.417)	<0.0001	MRI	−1.304	0.271 (0.160–0.455)	<0.0001
PSA	0.045	1.046 (1.021–1.072)	0.0002	PSA	0.044	1.045 (1.021–1.069)	0.0002	PSA	0.045	1.046 (1.023–1.070)	0.0001
sagiPAI	0.419	1.521 (0.884–2.682)	0.1403	transPAI	1.511	4.533 (2.587–8.246)	<0.0001	sagiPAI	0.339	1.404 (0.794–2.482)	0.2404
coroPZA	0.149	1.161 (1.040–1.298)	0.0063	coroPZA	0.150	1.162 (1.043–1.312)	0.0093	transPAI	1.198	3.313 (1.878–6.034)	0.0001
transCGA	−0.306	0.736 (0.655–0.822)	<0.0001	transPA	−0.168	0.845 (0.771–0.923)	0.0003	coroPAI	0.321	1.378 (0.918–2.377)	0.1223
PV	0.007	1.007 (0.990–1.023)	0.4148	PV	0.002	1.002 (0.984–1.020)	0.7963	PV	−0.022	0.978 (0.967–0.988)	<0.0001
PSAD	−0.321	0.726 (0.326–2.169)	0.4816	PSAD	−0.323	0.724 (0.329–2.082)	0.4663	PSAD	−0.29	0.748 (0.345–2.114)	0.5057

PCa, prostate cancer; OR, odds ratio; PA, prostate maximum sectional area; CGA, central gland sectional area; PZA, peripheral zone sectional area; PAI, PZA-to-CGA ratio; trans, transverse; coro, coronal; sagi, sagittal; PV, prostate volume; PSAD, PSA density.

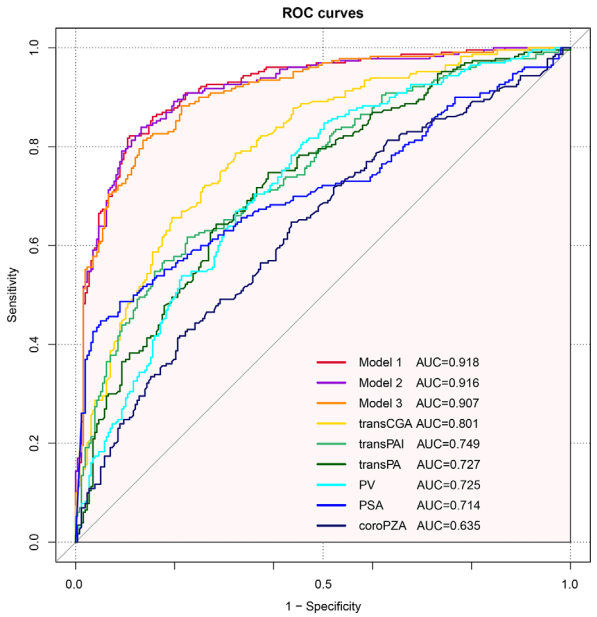

FIGURE 3 | Receiver operating characteristic curves depicting the accuracy of predictors of PCa before the initial biopsy. Base model: age + PSA + MRI. Model 1: Base model + coroPZA + transCGA. Model 2: Base model + transPAI + coroPZA + transPA. Model 3: Base model + transPAI + PV.

prostate biopsy. However, excess of prostate biopsy has led to increased side effects such as bleeding and infection. It also caused the inferior positive rate of 30%–40% (3, 5). A retrospective study including 1,203 patients who underwent prostate biopsy demonstrated that the overall rates of infectious and hemorrhagic complications after prostate biopsy were 8.23% and 15.71%, respectively (16). So, it needs to establish a method to carefully select patients who need prostate biopsy.

Numerous studies have reported the predictive value of prostate volume (PV) and prostate volume-adjusted PSA (i.e., PSAD) for PCa. For example, one study that measured 235 patients' prostate volume and PSA levels demonstrated that the AUC values of PSAD (0.712) and prostate volume (0.710) were higher than that of PSA (0.517) for diagnosing PCa (17). Our previous research found that the utility of PSAD for performing surveillance in patients at risk of PCa was higher than that of standard variables such as PSA (18). However, a retrospective study found that PSAD and PSA (AUC = 0.620 and 0.530, respectively) failed to outperform prostate volume (AUC = 0.680) for preoperative prediction of PCa (19). The current study confirmed that both PV and PSAD were good predictors of PCa in univariate logistic analysis. However, none of them showed statistical significance in model 1 and model 2. The reason is possibly that the prostate is not a regular geometric solid especially in the malignant growth mode of the tumor. Furthermore, prostate volume is usually estimated by an elliptical sphere formula (PV = 0.52 × length × width × height). Any error on the length, width, or height of prostate may be magnified through the multiplication (20). Previous

TABLE 4 | The AUC and cutoff values for predicting biopsy outcome and their sensitivity, specificity, and positive and negative likelihood ratios for PCa.

Parameters	AUC	Cutoff value	Sensitivity (%)	Specificity (%)	Positive likelihood ratio	Negative likelihood ratio
coroPZA	0.635	6.055	64.8%	56.4%	1.49	0.62
PSA	0.714	28.775	48.7%	91.1%	5.47	0.56
PV	0.725	69.562	80.9%	54.1%	1.76	0.35
transPA	0.727	18.505	64.3%	71.6%	2.26	0.50
transPAI	0.749	0.906	61.7%	77.4%	2.73	0.49
transCGA	0.801	11.045	78.7%	67.7%	2.44	0.31
Model 1	0.918	0.525	82.2%	89.1%	6.36	0.19
Model 2	0.916	0.471	83.9%	86.8%	7.75	0.27
Model 3	0.907	0.480	81.3%	86.4%	5.98	0.22

PCa, prostate cancer; AUC, area under the curve; PA, prostate maximum sectional area; CGA, central gland sectional area; PZA, peripheral zone sectional area; PAI, PZA-to-CGA ratio; trans, transverse; coro, coronal; PV, prostate volume; Base model, Age + PSA + MRI; Model 1, Base model + coroPZA + transCGA; Model 2, Base model + transPAI + coroPZA + transPA; Model 3, Base model + transPAI + PV.

TABLE 5 | The statistical difference in AUC of predicting PCa among three models.

Comparison (*p*-value)by Delong test	Model 1 *vs.* Model 2	Model 1 *vs.* Model 3	Model 2 *vs.* Model 3
Training cohort	0.300	0.019	0.042
Validation cohort	0.706	0.293	0.150

PCa, prostate cancer; Base model, Age + PSA + MRI; Model 1, Base model + coroPZA + transCGA; Model 2, Base model + transPAI + coroPZA + transPA; Model 3, Base model + transPAI + PV.

TABLE 6 | The statistical difference in AUC of predicting PCa among single predictors in the training cohort.

Comparison (*p*-value) by Delong test	transCGA	transPAI	transPA	PV	PSA	coroPZA
transCGA	—					
transPAI	0.002	—				
transPA	<0.001	0.442	—			
PV	<0.001	0.359	0.843	—		
PSA	0.01	0.307	0.718	0.762	—	
coroPZA	<0.001	<0.001	0.017	0.02	0.018	—

PCa, prostate cancer; PA, prostate maximum sectional area; CGA, central gland sectional area; PZA, peripheral zone sectional area; PAI, PZA-to-CGA ratio; trans, transverse; coro, coronal; PV, prostate volume.

studies had shown a high magnitude of bias between the calculation of prostate volume by the prolate ellipsoid formula and the actual prostate volume, which casts doubt on the diagnostic efficacy of PV and PSAD in PCa (21). Some studies had confirmed that the bias of calculated prostate volume fluctuates between 10% and 20% (8, 9). As we mentioned above, the increase of PSA level caused by any other reason, except for PCa, may lead to the error of PSAD and reduce its specificity for predicting PCa. Therefore, we do not think that PV and PSAD have the leading advantage of predicting PCa.

In order to overcome the difficulties mentioned above, we sought to replace the role of prostate volume with the incorporation of more accurate, simple prostatic imaging parameters. We found that PA (prostate maximum sectional area) is a good prostatic imaging parameter for predicting PCa by MRI test in line with the above requirements. MRI has higher spatial resolution and better soft tissue contrast than TRUS, and MRI can provide more accurate PA. So, it can reflect the actual size of the prostate (19). Thus, we used MRI-based PA as an alternative predictor of prostate volume for predicting PCa. As far as we know, we are the first to use prostate maximum sectional areas in sagittal, transverse, and coronal directions to predict PCa. The data of prostate sectional area from three different directions may help to improve its representativeness for irregular prostate. It can possibly find out the shape characteristics of the prostate in different directions. On the other hand, the area and its zone area of prostate were actually measured in MRI segments, which will decrease the systematic error to a great extent compared with the calculated prostate volume by formula. In our research, all sectional area predictors have statistical differences between PCa and no PCa patients in univariate analysis, except for transPZA. It proved that they had great potential in predicting PCa. We found that BPH patients had larger PA and CGA but smaller PZA in three directions compared with those who had PCa. It might result from the fact that BPH contributes to mechanical stress fields by pathological enlargement of the prostate central gland, hence further restraining PCa growth, as PCa mostly originates in the peripheral zone of the prostate (22). Through Delong test among single predictors, we find out the transCGA has the significantly highest AUC (0.801) among all predictors. Compared with no PCa, transCGA is significantly smaller in patients with PCa ($p < 0.001$). We speculated that this is due to the special behavior pattern of PCa growth on the transverse section. So far, we have not seen any relevant report that needs to be confirmed by further pathological or anatomical studies.

To further explore the potential of prostate sectional area related predictors to predict PCa, we built new predictors like PAI, PSAPA, PSACGA, and PSAPZA (calculated by PZA/CGA, PSA/PA, PSA/CGA, and PSA/PZA) based on the sectional area from three different directions in MRI segments. Each of these predictors had the potential ability to distinguish PCa from no PCa in univariate logistic analysis. Unfortunately, we found that PSAPA, PSACGA, and PSAPZA failed to outperform any predictors when we discovered the different models. So, we did not include these predictors in multivariate logistic analysis. However, PAI (prostate area index) showed favorable predictability in our final model, especially transPAI, which had an AUC (0.749) second only to transCGA. In both model

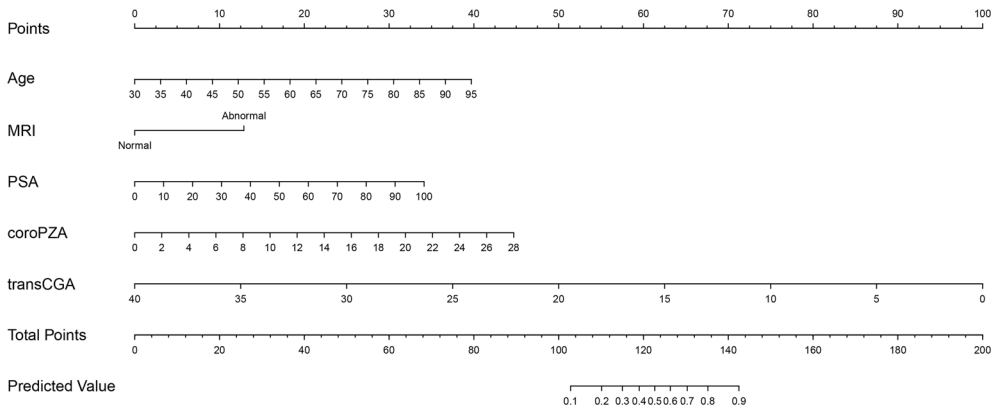

FIGURE 4 | Nomogram predicting the probability of PCa at the initial biopsy based on model 1.

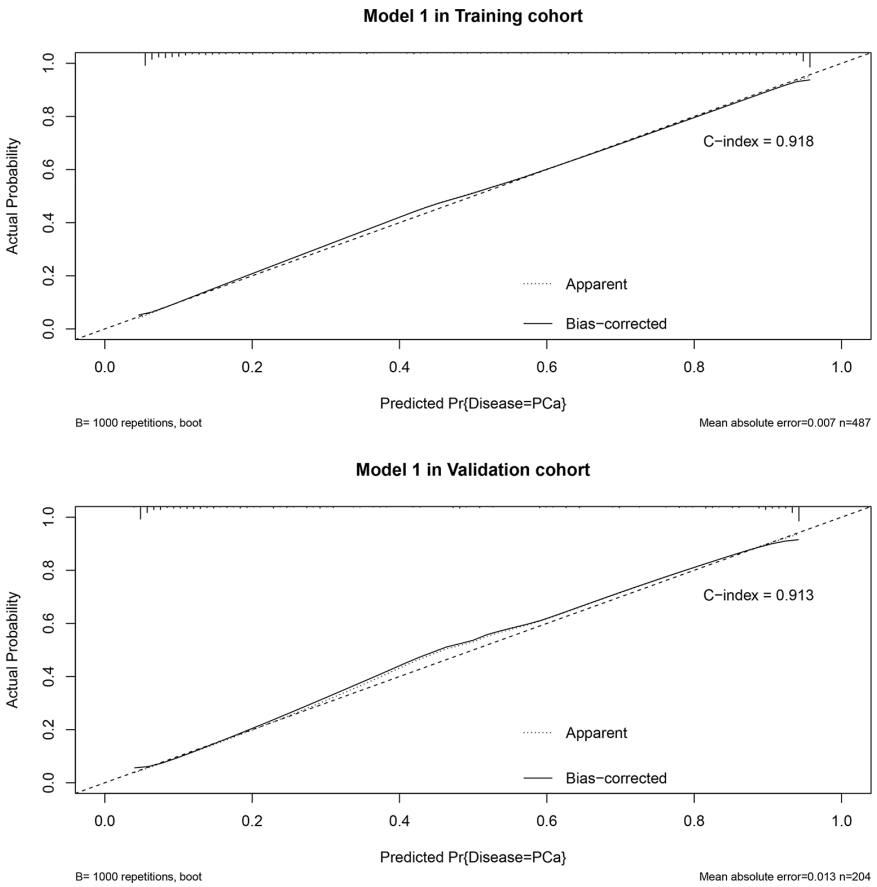

FIGURE 5 | Calibration plot in training cohort and validation cohort and predictive accuracy for PCa at initial biopsy based on model 1.

2 and model 3, transPAI had a certain contribution to the diagnosis of PCa compared with coroPAI and sagiPAI. This also confirms our previous hypothesis about the special behavior pattern of PCa growth on the transverse section. Patients with PCa have higher transPAI. It may be due to PCa often originating in the peripheral zone, which causes the enlargement of PZA. Then, it leads to an increase in PAI (PZA-to-CGA ratio) in turn.

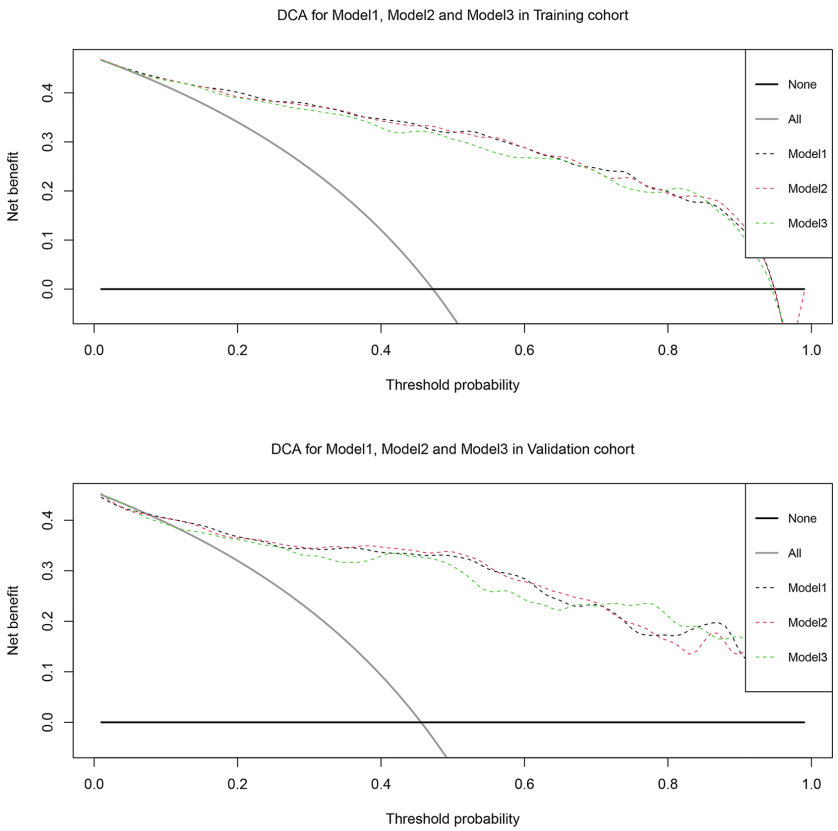

FIGURE 6 | Decision curve analysis of the effect of the nomogram based on model 1 for predicting prostate cancer in training cohort and validation cohort. Net benefit of nomogram is plotted with threshold probabilities for prostate cancer compared with the strategies of treating all patients or no one. The decision curve illustrated net benefit was improved when threshold probability > 8%.

With the changes to people's living habits, and the progression of population aging, the prevalence of PCa is increasing annually, especially among adults aged over 70 years. This situation has seriously affected the health of older adults (23). Our results also confirm this conclusion. The median age of men with PCa was 75 years, compared with 69 years for men without PCa ($p < 0.001$). Thus, age can be used as a reference for prostate biopsy.

To reduce unnecessary prostate biopsy and improve the diagnostic accuracy of PCa in clinical practice, nomograms integrating many independent predictors of PCa have been developed and validated. A previous study reported that nomograms could provide more individualized risk estimations of a certain disease, which could help clinicians to make management-related decisions for patients with PCa (24). For example, a nomogram developed on the basis of 1,144 men who underwent TRUS found that the C-index (0.876) was associated with their best model that integrates age, PSA, percentage free PSA, DRE, prostate transition zone volume, and TRUS for predicting PCa (25). Another study integrated age, prostate volume, PSA, FTPSA, TRUS, and DRE as its best model to develop a nomogram for the probability of detecting PCa in all patients, achieving a C-index of 0.853 (26). In the current study, we chose the best prediction model of the base model + transCGA + coroPZA to construct a new nomogram that could provide the risk of PCa for individual Chinese patients. Internal validation showed a predictive accuracy (C-index = 0.913) for PCa, which gained an advantage over some previous nomograms developed by Chinese researchers.

Our study has certain limitations. As with any retrospective study, there was the risk of selection bias in assessing the value of the prostate maximum sectional area on mp-MRI. In addition to the issues surrounding the small sample size, our models were calibrated using internal validation only, with no external validation conducted to ensure their utility. Therefore, further clinical studies that employ long-term follow-up to evaluate our model's practical applicability are required before it is prospectively applied to patients.

We first found that MRI-based CGA, PZA, and PA in the sagittal, transverse, and coronal section have potential predictive value for diagnosing PCa, especially transCGA. We put forward a new predictor named transPAI. We found that it was significantly higher in PCa patients. Our nomogram model based on age + MRI + PSA + transCGA + coroPZA had great predictive accuracy for PCa. The application of this nomogram model may further decrease the rate of unnecessary biopsies.

DATA AVAILABILITY STATEMENT

Publicly available datasets were analyzed in this study. These data can be found here: https://www.wolai.com/nYw7M5iJDyxn91RDWTmoPj?theme=light.

AUTHOR CONTRIBUTIONS

SJ conceived the study and carried out the investigation, methodology, and original draft preparation. ZH and BL carried out the investigation, methodology, and formal analysis, and participated in the conceptualization of the manuscript. ZC carried out the data curation, investigation, and methodology. YX, WZ, and YW participated in the formal analysis. ML conceived the study; carried out the supervision, review, and editing of the manuscript; and took responsibility for the integrity of the work as corresponding author. All authors contributed to the article and approved the submitted version.

FUNDING

This work was supported by the Startup Fund for Scientific Research, Fujian Medical University (Grant number: 2018QH1044) and Joint Funds for the Innovation of Science and Technology, Fujian province (Grant number: 2017Y9023).

ACKNOWLEDGMENTS

We thank Richard Lipkin, PhD, from Liwen Bianji, Edanz Group China (www.liwenbianji.cn/ac), for editing the English text of a draft of this manuscript.

SUPPLEMENTARY MATERIAL

The Supplementary Material for this article can be found online at: https://www.frontiersin.org/articles/10.3389/fonc.2021.708730/full#supplementary-material

Supplementary Figure 1 | Prostate location and MR imagine in transverse **(A)**, sagittal **(B)** and coronal **(C)** plane. Red: Central gland sectional area, CGA; Blue: Peripheral zone sectional area, PZA.

Supplementary Figure 2 | Correlation analysis among each predictor used to eliminate combinations including collinear predictors.

Supplementary Figure 3 | Nomogram predicting the probability of PCa at the initial biopsy based on model 2 **(A)** and model 3 **(B)**.

Supplementary Figure 4 | Calibration plot in training cohort and validation cohort and predictive accuracy for PCa at initial biopsy based on model 2.

Supplementary Figure 5 | Calibration plot in training cohort and validation cohort and predictive accuracy for PCa at initial biopsy based on model 3.

REFERENCES

1. Henley SJ, Ward EM, Scott S, Ma J, Anderson RN, Firth AU, et al. Annual Report to the Nation on the Status of Cancer, Part I: National Cancer Statistics. *Cancer* (2020) 126(10):2225–49. doi: 10.1002/cncr.32802
2. Cuzick J, Thorat M, Andriole G, Brawley O, Brown P, Culig Z, et al. Prevention and Early Detection of Prostate Cancer. *Lancet Oncol* (2014) 15 (11):e484–92. doi: 10.1016/s1470-2045(14)70211-6
3. Smith RA, Andrews KS, Brooks D, Fedewa SA, Manassaram-Baptiste D, Saslow D, et al. Cancer Screening in the United States, 2019: A Review of Current American Cancer Society Guidelines and Current Issues in Cancer Screening. *CA: Cancer J Clin* (2019) 69(3):184–210. doi: 10.3322/caac.21557
4. Mottet N, Bellmunt J, Bolla M, Briers E, Cumberbatch M, De Santis M, et al. EAU-ESTRO-SIOG Guidelines on Prostate Cancer. Part 1: Screening, Diagnosis, and Local Treatment With Curative Intent. *Eur Urol* (2017) 71 (4):618–29. doi: 10.1016/j.eururo.2016.08.003
5. Shen P, Zhao J, Sun G, Chen N, Zhang X, Gui H, et al. The Roles of Prostate-Specific Antigen (PSA) Density, Prostate Volume, and Their Zone-Adjusted Derivatives in Predicting Prostate Cancer in Patients With PSA Less Than 20.0 Ng/mL. *Andrology* (2017) 5(3):548–55. doi: 10.1111/andr.12322
6. Benson MC, Whang IS, Olsson CA, McMahon DJ, Cooner WH. The Use of Prostate Specific Antigen Density to Enhance the Predictive Value of Intermediate Levels of Serum Prostate Specific Antigen. *J Urol* (1992) 147:817–21. doi: 10.1016/s0022-5347(17)37394-9
7. Bruno SM, Falagario UG, d'Altilia N, Recchia M, Mancini V, Selvaggio O, et al. PSA Density Help to Identify Patients With Elevated PSA Due to Prostate Cancer Rather Than Intraprostatic Inflammation: A Prospective Single Center Study. *Front Oncol* (2021) 11:693684. doi: 10.3389/fonc.2021.693684
8. Zlotta A, Djavan B, Marberger M, Schulman C. Prostate Specific Antigen Density of the Transition Zone: A New Effective Parameter for Prostate Cancer Prediction. *J Urol* (1997) 157(4):1315–21. doi: 10.1097/00005392-199704000-00041
9. Choi YJ, Kim JK, Kim HJ, Cho KS. Interobserver Variability of Transrectal Ultrasound for Prostate Volume Measurement According to Volume and Observer Experience. *AJR Am J Roentgenology* (2009) 192(2):444–9. doi: 10.2214/ajr.07.3617
10. Yacoub JH, Oto A. MR Imaging of Prostate Zonal Anatomy. *Radiol Clinics N Am* (2018) 56(2):197–209. doi: 10.1016/j.rcl.2017.10.003
11. Augustin H, Erbersdobler A, Hammerer PG, Graefen M, Huland H. Prostate Cancers in the Transition Zone: Part 2; Clinical Aspects. *BJU Int* (2004) 94 (9):1226–9. doi: 10.1111/j.1464-410X.2004.05147.x
12. Rahmouni A, Yang A, Tempany CM, Frenkel T, Epstein J, Walsh P, et al. Accuracy of *in-Vivo* Assessment of Prostatic Volume by MRI and Transrectal Ultrasonography. *J Comput Assisted Tomography* (1992) 16(6):935–40. doi: 10.1097/00004728-199211000-00020
13. Balachandran V, Gonen M, Smith J, DeMatteo R. Nomograms in Oncology: More Than Meets the Eye. *Lancet Oncol* (2015) 16(4):e173–80. doi: 10.1016/s1470-2045(14)71116-7
14. Iasonos A, Schrag D, Raj G, Panageas K. How to Build and Interpret a Nomogram for Cancer Prognosis. *J Clin Oncol* (2008) 26(8):1364–70. doi: 10.1200/jco.2007.12.9791
15. Weinreb J, Barentsz J, Choyke P, Cornud F, Haider M, Macura K, et al. PI-RADS Prostate Imaging - Reporting and Data System: 2015, Version 2. *Eur Urol* (2016) 69(1):16–40. doi: 10.1016/j.eururo.2015.08.052
16. Wu YP, Li XD, Ke ZB, Chen SH, Chen PZ, Wei Y, et al. Risk Factors for Infectious Complications Following Transrectal Ultrasound-Guided Prostate Biopsy. *Infect Drug Resist* (2018) 11:1491–7. doi: 10.2147/idr.S171162
17. Tanaka N, Fujimoto K, Chihara Y, Torimoto M, Hirao Y, Konishi N, et al. Prostatic Volume and Volume-Adjusted Prostate-Specific Antigen as Predictive Parameters for Prostate Cancer Patients With Intermediate PSA Levels. *Prostate Cancer Prostatic Dis* (2007) 10(3):274–8. doi: 10.1038/sj.pcan.4500957
18. Zheng S, Jiang S, Chen Z, Huang Z, Shi W, Liu B, et al. The Roles of MRI-Based Prostate Volume and Associated Zone-Adjusted Prostate-Specific Antigen Concentrations in Predicting Prostate Cancer and High-Risk Prostate Cancer. *PLoS One* (2019) 14(11):e0218645. doi: 10.1371/journal.pone.0218645
19. Peng Y, Shen D, Liao S, Turkbey B, Rais-Bahrami S, Wood B, et al. MRI-Based Prostate Volume-Adjusted Prostate-Specific Antigen in the Diagnosis of

Prostate Cancer. *J Magn Reson Imaging JMRI* (2015) 42(6):1733–9. doi: 10.1002/jmri.24944
20. Tang P, Chen H, Uhlman M, Lin Y, Deng X, Wang B, et al. A Nomogram Based on Age, Prostate-Specific Antigen Level, Prostate Volume and Digital Rectal Examination for Predicting Risk of Prostate Cancer. *Asian J Androl* (2013) 15(1):129–33. doi: 10.1038/aja.2012.111
21. Murray NP, Reyes E, Orellana N, Fuentealba C, Duenas R. A Comparative Performance Analysis of Total PSA, Percentage Free PSA, PSA Velocity, and PSA Density Versus the Detection of Primary Circulating Prostate Cells in Predicting Initial Prostate Biopsy Findings in Chilean Men. *BioMed Res Int* (2014) 2014:676572. doi: 10.1155/2014/676572
22. Lorenzo G, Hughes TJR, Dominguez-Frojan P, Reali A, Gomez H. Computer Simulations Suggest That Prostate Enlargement Due to Benign Prostatic Hyperplasia Mechanically Impedes Prostate Cancer Growth. *Proc Natl Acad Sci* (2019) 116(4):1152–61. doi: 10.1073/pnas.1815735116
23. Zhang S, Zhao S, Fu X. Intensity Modulated Radiotherapy in Combination With Endocrinotherapy in the Treatment of Middle and Advanced Prostatic Cancer. *Pakistan J Med Sci* (2019) 35(5):1264–9. doi: 10.12669/pjms.35.5.591
24. Shariat SF, Karakiewicz PI, Suardi N, Kattan MW. Comparison of Nomograms With Other Methods for Predicting Outcomes in Prostate Cancer: A Critical Analysis of the Literature. *Clin Cancer Res* (2008) 14 (14):4400–7. doi: 10.1158/1078-0432.Ccr-07-4713
25. Wang Y, Xie S, Shangguan X, Pan J, Zhu Y, Xin Z, et al. Prostate Transitional Zone Volume-Based Nomogram for Predicting Prostate Cancer and High Progression Prostate Cancer in a Real-World Population. *J Cancer Res Clin Oncol* (2017) 143(7):1157–66. doi: 10.1007/s00432-017-2389-3
26. Huang Y, Cheng G, Liu B, Shao P, Qin C, Li J, et al. A Prostate Biopsy Strategy Based on a New Clinical Nomogram Reduces the Number of Biopsy Cores Required in High-Risk Patients. *BMC Urol* (2014) 14:8. doi: 10.1186/1471-2490-14-8

Conflict of Interest: The authors declare that the research was conducted in the absence of any commercial or financial relationships that could be construed as a potential conflict of interest.

frontiers in Oncology

ORIGINAL RESEARCH
published: 14 September 2021
doi: 10.3389/fonc.2021.732027

Developing Strategy to Predict the Results of Prostate Multiparametric Magnetic Resonance Imaging and Reduce Unnecessary Multiparametric Magnetic Resonance Imaging Scan

Junxiao Liu[1†], Shuanbao Yu[1†], Biao Dong[1†], Guodong Hong[1†], Jin Tao[1], Yafeng Fan[1], Zhaowei Zhu[1], Zhiyu Wang[1] and Xuepei Zhang[1,2]*

[1] Department of Urology, The First Affiliated Hospital of Zhengzhou University, Zhengzhou, China, [2] Key Laboratory of Precision Diagnosis and Treatment for Chronic Kidney Disease in Henan Province, Zhengzhou, China

Purpose: The clinical utility of multiparametric magnetic resonance imaging (mpMRI) for the detection and localization of prostate cancer (PCa) has been evaluated and validated. However, the implementation of mpMRI into the clinical practice remains some burden of cost and availability for patients and society. We aimed to predict the results of prostate mpMRI using the clinical parameters and multivariable model to reduce unnecessary mpMRI scans.

Methods: We retrospectively identified 784 men who underwent mpMRI scans and subsequent prostate biopsy between 2016 and 2020 according to the inclusion criterion. The cohort was split into a training cohort of 548 (70%) patients and a validation cohort of 236 (30%) patients. Clinical parameters including age, prostate-specific antigen (PSA) derivates, and prostate volume (PV) were assessed as the predictors of mpMRI results. The mpMRI results were divided into groups according to the reports: "negative", "equivocal", and "suspicious" for the presence of PCa.

Results: Univariate analysis showed that the total PSA (tPSA), free PSA (fPSA), PV, and PSA density (PSAD) were significant predictors for suspicious mpMRI ($P < 0.05$). The PSAD (AUC = 0.77) and tPSA (AUC = 0.74) outperformed fPSA (AUC = 0.68) and PV (AUC = 0.62) in the prediction of the mpMRI results. The multivariate model (AUC = 0.80) had a similar diagnostic accuracy with PSAD ($P = 0.108$), while higher than tPSA ($P = 0.024$) in predicting

OPEN ACCESS

Edited by:
Benyi Li,
University of Kansas Medical Center, United States

Reviewed by:
Liping Xie,
Zhejiang University, China
Nicolò Maria Buffi,
Humanitas University, Italy

****Correspondence:***
Xuepei Zhang
zhangxuepei@263.net

[†]These authors have contributed equally to this work

Specialty section:
This article was submitted to Genitourinary Oncology, a section of the journal Frontiers in Oncology

Received: *28 June 2021*
Accepted: *23 August 2021*
Published: *14 September 2021*

Citation:
Liu J, Yu S, Dong B, Hong G, Tao J, Fan Y, Zhu Z, Wang Z and Zhang X (2021) Developing Strategy to Predict the Results of Prostate Multiparametric Magnetic Resonance Imaging and Reduce Unnecessary Multiparametric Magnetic Resonance Imaging Scan. Front. Oncol. 11:732027. doi: 10.3389/fonc.2021.732027

the mpMRI results. The multivariate model illustrated a better calibration and substantial improvement in the decision curve analysis (DCA) at a threshold above 20%. Using the PSAD with a 0.13 ng/ml^2 cut-off could spare the number of mpMRI scans by 20%, keeping a 90% sensitivity in the prediction of suspicious MRI-PCa and missing three (3/73, 4%) clinically significant PCa cases. At the same sensitivity level, the multivariate model with a 32% cut-off could spare the number of mpMRI scans by 27%, missing only one (1/73, 1%) clinically significant PCa case.

Conclusion: Our multivariate model could reduce the number of unnecessary mpMRI scans without comprising the diagnostic ability of clinically significant PCa. Further prospective validation is required.

Keywords: prostate cancer, magnetic resonance imaging, prostate-specific antigen, prostate-specific antigen density, multivariate model

INTRODUCTION

Prostate cancer (PCa) is the second most common malignancy in men, with over 1 million new cases and 375,304 deaths in 2020 (1). The diagnostic tools of PCa mainly includes digital rectal examination (DRE), prostate-specific antigen (PSA) test, multiparametric magnetic resonance imaging (mpMRI), and prostate biopsy (2). DRE requires extensive experience, and has a limited value in decision-making (3). PSA is a better predictor of PCa than DRE, and is the gold standard for PCa screening (4). The mpMRI has a good sensitivity for the detection and localization of clinically significant PCa (CSPCa, defined as Gleason score ≥ 3 + 4) (5, 6). Prostate biopsy is the gold standard for PCa diagnosis, but is invasive.

While these risk stratification tools have an additional value in the diagnostic pathway of PCa, it is controversial to perform mpMRI and prostate biopsy in every man with an elevated serum tPSA level and/or other clinical suspicion, in consideration of the costs for patients, the burden, and availability for society. Performing mpMRI and/or prostate biopsy among men with a high risk of CSPCa could be an acceptable option (7). A dozen of risk calculators incorporating clinical variables and/or novel biomarkers have been developed to predict the results of prostate biopsy and to reduce unnecessary biopsy by 36%–66% (8–12). However, the knowledge about developing a strategy to predict the results of mpMRI and select patients who could benefit from mpMRI is limited (13, 14).

Our prior study, consistent with other studies, found that clinical parameters such as age, PSA derivates [total PSA (tPSA), free/total PSA (f/tPSA), and PSA density (PSAD)], and prostate volume (PV) were significant predictors for PCa and CSPCa (8, 15). Therefore, we question whether the negative and equivocal mpMRI scans could be limited using a model based on these clinical parameters among men with an elevated PSA level. Our study aimed to predict the results of mpMRI using the inexpensive, inexperience, and readily available clinical parameters and multivariable model, and to assess the impact of potentially avoidable mpMRI scans. Overall, this study will be helpful for optimizing the diagnostic pathway, implementing a precision treatment strategy, and reducing the burden for patients and health care providers.

MATERIALS AND METHODS

Study Populations

This retrospective study was approved by the institutional review board. We identified 903 consecutive patients who underwent PSA test, mpMRI scans, and subsequent prostate biopsy between April 2016 and March 2020 at our medical center (**Supplementary Figure 1**). Patients were excluded due to incomplete data (94 cases) or being diagnosed with other types of tumor/cancer (25 cases), leaving 784 (87%) patients available for analysis (**Supplementary Figure 1**). The 70% and 30% of the study population were randomly divided into a training cohort (548 cases) and a validation cohort (236 cases), respectively (**Supplementary Figure 1**).

Clinical, Imaging, and Pathological Parameters Collection

The clinical parameters including age at prostate biopsy, serum tPSA and fPSA values, PV, and reports of mpMRI examination were extracted from clinical records. The serum tPSA and fPSA were measured by immunofluorescence assay. PV was measured by mpMRI examination using the 3.0-T MRI system (SIEMENS, Germany). The protocol of mpMRI examination complied with the guidelines of the European Society of Urology Radiology, and included T2-weighted Imaging (T2WI), diffusion-weighted imaging (DWI), and dynamic contrast-enhanced imaging (DCE). The prostate mpMRI images were interpreted by two experienced radiologists with at least three years of prostate mpMRI experience. The mpMRI results were divided into three groups: "negative", "equivocal", and "suspicious" for the presence of PCa, according to the mpMRI reports. The "negative", "equivocal", and "suspicious" for MRI-PCa corresponded to the PI-RADS 1 or 2, PI-RADS 3, and PI-RADS 4 or 5 according to the latest Prostate Imaging Reporting and Data System version 2 (PI-RADS v2) guideline (16).

Prostate Biopsy and Histopathological Diagnosis

All patients underwent a transrectal ultrasound (TRUS)-guided systematic 12-point prostate biopsy (15). If there are suspected malignant nodules by mpMRI and/or ultrasound, additional 1–5 needles were performed in regions with cognitive MRI-TRUS fusion and/or abnormal ultrasound echoes. Biopsy cores were analyzed according to the standards of the ISUP (17).

Statistical Analysis

We described the profile of age, PSA derivates (tPSA, fPSA, f/tPSA, PSAD), PV, and prostate biopsy results of the enrolled patients by the category of mpMRI results. The χ^2 test or Fisher's exact test was used to analyze categorical data. The Mann-Whitney U test was used to analyze ranked data. Student's t-test or ANOVA was used to analyze continuous data. Multivariable logistic regression analysis with a stepwise strategy was used to develop models to predict mpMRI results. The area under the ROC curve (AUC) was used to evaluate the diagnostic accuracy of the clinical parameters and multivariable model. Differences between the AUCs were compared using the method of DeLong et al. (18). The calibration plot was used to assess the performance characteristics of the models. Calibration was assessed by grouping men in the validation cohort into delices (each of size 23 or 24), and then comparing the mean of the predicated probabilities and the observed proportions. The sum squares of the residues (SSR) were used to assess the deviation of calibration plots from the 45° line (19). Decision-curve analysis was used to measure the clinical utility. All tests were two sided with significance level set at 0.05. Data cleaning and analyses were conducted using the R statistical software (Version 4.0.2).

RESULTS

A total of 784 patients underwent PSA test, mpMRI scans, and subsequent prostate biopsy enrolled in this study. Of the enrolled patients, 296 (37.8%) were negative for MRI-PCa, 133 (17.0%) were equivocal for MRI-PCa, and 355 (45.2%) were suspicious for MRI-PCa (**Table 1**). The clinical parameters including age, tPSA, fPSA, f/tPSA, PSAD, PV, and prostate biopsy categorized by the mpMRI results are displayed in **Table 1**. The training and validation cohorts consisted of 548 (70%) and 236 (30%) patients. The clinical parameters were similar between the training cohorts and validation cohorts (each $P > 0.05$, **Supplementary Table 1**). Of the validation cohorts, 91 (39%) were negative for MRI-PCa, 38 (16%) were equivocal for MRI-PCa, 107 (45%) were suspicious for MRI-PCa; 138 (58%) were benign biopsy, 12 (5%) were PCa (GS = 3 + 3), and 86 (36%) were CSPCa (**Supplementary Table 1**).

Univariate Analysis of Clinical Parameters for Suspicious MRI-PCa

In the univariate analysis, all clinical parameters except age and f/tPSA were significant predictors for suspicious MRI-PCa (each $P < 0.05$, **Table 2**). The risk of suspicious MRI-PCa increased with tPSA (OR = 1.03, 95% CI: 1.02–1.04), fPSA (OR = 1.14, 95% CI: 1.07–1.21), and PSAD (OR = 3.03, 95% CI: 2.05–4.49), but it was conversely associated with PV (OR = 0.995, 95%CI: 0.990–0.999) (**Table 2**). PSAD (AUC = 0.77) had a higher diagnostic accuracy compared with fPSA (AUC = 0.68, $P = 0.017$) and PV (AUC = 0.62, $P < 0.001$) (**Table 2**), and showed a similar diagnostic accuracy with tPSA (AUC = 0.74, $P = 0.144$) in the prediction of MRI-PCa (**Table 2**).

Development of a Multivariate Model to Predict Suspicious MRI-PCa

In the stepwise multivariate analysis, tPSA ($P < 0.001$), fPSA ($P = 0.038$), and PV ($P < 0.001$) remained in the multivariate model as significant predictors for suspicious MRI-PCa. The multivariate model (AUC = 0.80) outperformed tPSA ($P = 0.024$), and behaved similarly with PSAD ($P = 0.108$) in the prediction of suspicious MRI-PCa (**Table 2** and **Figure 1A**). Additionally, the calibration plot indicated an excellent concordance in the multivariate model (SSR = 0.118), followed by tPSA (SSR = 0.146), and PSAD (SSR = 0.241) (**Figure 1B**). The DCA showed

TABLE 1 | The clinical parameters and biopsy results by category of mpMRI results between April 2016 and March 2020.

Clinical parameters	mpMRI examination			
	Negative (n = 296)	Equivocal (n = 133)	Suspicious (n = 355)	*P*
Age (years)	67 (62–72)	68 (61-75)	68 (63–74)	0.032
tPSA (ng/ml)	11.5 (7.71–18.3)	12.7 (5.98–22.3)	23.2 (9.71–45.3)	<0.001
fPSA	1.65 (0.96–2.58)	1.49 (0.84–3.02)	2.59 (1.21–5.31)	<0.001
f/tPSA	0.14 (0.10–0.20)	0.14 (0.10–0.20)	0.11 (0.07–0.19)	0.002
PSAD (ng/ml^2)	0.21 (0.13–0.34)	0.22 (0.11–0.40)	0.48 (0.21–0.96)	<0.001
PV (ml)	58 (37–84)	51 (34–74)	46 (33–68)	<0.001
Biopsy result, No. (%)				<0.001
No-PCa	254 (86)	99 (74)	104 (29)	
GS = 3 + 3	14 (5)	9 (7)	23 (6)	
GS = 3 + 4	12 (4)	10 (8)	28 (8)	
GS = 4 + 3	9 (3)	4 (3)	75 (21)	
GS ≥ 8	7 (2)	11 (8)	125 (36)	

tPSA, total prostate-specific antigen; fPSA, free PSA; f/tPSA, free PSA/total PSA; PSAD, PSA density; PV, prostate volume; GS, Gleason score.

TABLE 2 | Univariate and multivariate regression analysis of clinical parameters to predict suspicious MRI-PCa in the validation cohort.

Clinicalparameters	Univariate analysis			Multivariate analysis		
	OR (95% CI)	AUC (95% CI)	*P*	Coefficient	OR (95% CI)	*P*
Intercept	NA		NA	-1.537	NA	0.019
Age (yrs)	1.01 (1.00–1.03)	0.59 (0.51–0.66)	0.135	NA	NA	NA
tPSA (ng/ml)	1.03 (1.02–1.04)	0.74 (0.68–0.81)	<0.001	0.031	1.03 (1.02–1.04)	<0.001
fPSA	1.14 (1.07–1.21)	0.68 (0.61–0.75)	<0.001	0.070	1.07 (1.00–1.14)	0.038
f/tPSA	1.52 (0.69–3.37)	0.61 (0.53–0.68)	0.302	NA	NA	NA
PV (ml)	0.995 (0.990–0.999)	0.62 (0.54–0.69)	0.017	-0.012	0.99 (0.98–0.99)	<0.001
PSAD (ng/ml^2)	3.03 (2.05–4.49)	0.77 (0.71–0.83)	<0.001	NA	NA	NA

tPSA, total prostate-specific antigen; fPSA, free PSA; f/tPSA, free PSA/total PSA; PV, prostate volume; PSAD, PSA density; GS, Gleason score; NA, not applicable.

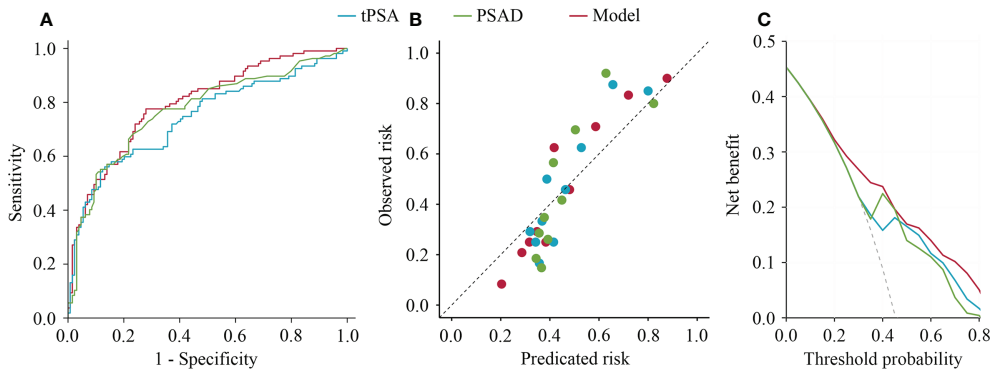

FIGURE 1 | Receiver operating characteristics curves, calibration plot, and decision curve analysis of tPSA, PSAD, and multivariable model for predicting suspicious prostate cancer by mpMRI. **(A)** Receiver operating characteristics curves; **(B)** Calibration plot; **(C)** Decision curve analysis.

that the multivariate model had the highest net clinical benefit across the threshold probabilities above 20% (**Figure 1C**). It was considered that the multivariate model was most helpful to rule out the "Suspicious MRI-PCa".

Impact of the Clinical Parameters and Multivariate Model on mpMRI Scans Reduced and CSPCa Diagnosis Delayed

To further assess the potential clinical benefit of the tPSA, PSAD, and multivariate model, the clinical consequences of using various cut-offs for the tPSA, PSAD, and multivariate model are listed in **Table 3**. Using of a 32% cutoff for the multivariate model would allow for reducing 64/236 (27%) mpMRI scans, while keeping 96/107 (90%) sensitivity in the prediction of suspicious MRI-PCa. At the same level of sensitivity as the multivariate model to predict suspicious MRI-PCa, applying the tPSA and PSAD could reduce 37/236 (16%) and 48/236 (20%) mpMRI scans, respectively. All the 236 patients in the validation cohort obtained clear pathological results of prostate biopsy. Assuming that the indications for subsequent biopsies were only based on the mpMRI findings, biopsies among men who would not have undergone mpMRI scans revealed three CSPCa using the tPSA, three CSPCa using the PSAD, and one CSPCa using the multivariate model in the validation cohort.

DISCUSSION

The added value of mpMRI for the detection and localization of CSPCa has been validated (5, 12, 20). However, it is controversial to perform mpMRI in every man with an elevated serum tPSA level. Our study revealed that tPSA, fPSA, PV, and PSAD were significant predictors for suspicious MRI-PCa, and the number of mpMRI scans could be reduced based on the low cost and readily available clinical parameters. At the same level of sensitivity (90%) in the prediction of suspicious MRI-PCa, the multivariate model could reduce more mpMRI scans (27%) and missed less CSPCa (1%), compared with PSAD (20% and 4%) and tPSA (16% and 4%).

Reported proportions of the total negative MRI (PI-RADS 1-2) ranged from 37% to 58% for individual studies depending on the prevalence of PCa in the study populations (21–23). The ratios of negative MRI-PCa and equivocal MRI-PCa were 38% and 17% in our study. These indicate that the overuse of prostate mpMRI is common in the current healthcare environments, and it is

TABLE 3 | The diagnostic performance of tPSA, PSAD, and multivariate model in prediction of suspicious MRI-PCa in the validation cohort.

Strategies	Sensitivity	Cut-off	mpMRI scans reduced (n = 236), n (%)	Suspicious mpMRI delayed		
				No-PCa (n = 28) n (%)	GS = 3 + 3 (n = 6), n (%)	GS ≥ 3 + 4 (n = 73), n (%)
tPSA	106/107 (99%)	0.90 ng/ml	3 (1)	0 (0)	0 (0)	1 (1)
PSAD	106/107 (99%)	0.03 ng/ml^2	4 (2)	0 (0)	0 (0)	1 (1)
Multivariate	106/107 (99%)	0.25	19 (8)	1 (4)	0 (0)	0 (0)
tPSA	102/107 (95%)	4.50 ng/ml	19 (8)	2 (7)	0 (0)	3 (4)
PSAD	102/107 (95%)	0.10 ng/ml^2	27 (11)	2 (7)	0 (0)	3 (4)
Multivariate	102/107 (95%)	0.29	41 (17)	4 (14)	0 (0)	1 (1)
tPSA	96/107 (90%)	6.70 ng/ml	37 (16)	8 (29)	0 (0)	3 (4)
PSAD	96/107 (90%)	0.13 ng/ml^2	48 (20)	8 (29)	0 (0)	3 (4)
Multivariate	96/107 (90%)	0.32	64 (27)	10 (36)	0 (0)	1 (1)
tPSA	91/107 (85%)	9.10 ng/ml	65 (28)	10 (36)	1 (17)	5 (7)
PSAD	91/107 (85%)	0.18 ng/ml^2	80 (34)	12 (43)	0 (0)	4 (5)
Multivariate	91/107 (85%)	0.35	85 (36)	14 (50)	0 (0)	2 (3)
tPSA	86/107 (80%)	10.7 ng/ml	89 (38)	11 (39)	1 (17)	9 (12%)
PSAD	87/107 (81%)	0.21 ng/ml^2	92 (39)	15 (54)	0 (0)	5 (7)
Multivariate	86/107 (80%)	0.37	100 (42)	17 (61)	0 (0)	4 (5)

PCa, prostate cancer; CSPCa, clinically significant prostate cancer; GS, Gleason score; tPSA, total prostate-specific antigen; PV, prostate volume; SVI, seminal vesicle invasion; LNI, lymph node invasion.

essential to identify men who will benefit from mpMRI in the current MRI era. In this study, we assessed the inexpensive and readily available parameters as the predictor for suspicious MRI-PCa, and found that PSAD and tPSA had a higher diagnostic accuracy than other single parameters. However, the PV, which was used to calculate the PSAD and develop a multivariate model, were estimated by the mpMRI examination. However, the PV could be reliably measured by TRUS, which was a routine and low-cost procedure (24). Hence, an accurate PSAD could be obtained using TRUS before mpMRI without changing the clinical workflow.

To date, multivariate models or machine learning models for the detection of CSPCa have been developed in a growing body of literatures (8–12, 25). Studies demonstrated that a risk-based triage strategy could reduce more unnecessary biopsy and the overdiagnosis in comparison with single parameters (8, 11, 25). However, the study about developing a multivariate model to predict the results of prostate mpMRI and selecting patients who could benefit from mpMRI is limited (13, 14). The study by Alberts et al. introduced the concept of a patient triage strategy to avoid prostate mpMRI, and assessed the rate of potentially avoidable mpMRI by applying the risk calculators for detecting PCa (Rotterdam Prostate Cancer Risk Calculator, RPCRC) in a small cohort with one or more previously negative random TRUS-guided biopsies (14). The RPCRC (57/83, 69%) incorporating a multitude of variables spared less unnecessary mpMRI scans than our simple model (106/138, 77%) at the same level of sensitivity for the detection of CSPCa. These may indicate that commonly risk models for detecting PCa and/or CSPCa do not address the appropriate use of mpMRI. It is essential to establish risk models and decision thresholds for the prediction of mpMRI results.

In this study, our developed multivariate model including tPSA, fPSA, and PV has a similar diagnostic accuracy with the PSAD in the prediction of suspicious MRI-PCa ($P = 0.108$). This was consistent with the study by Dominik Deniffel (13). Although cross-study comparisons are challenging, our multivariate model (AUC = 0.80) performed similarly with the model developed by Dominik Deniffel (AUC = 0.75) in the prediction of mpMRI results (13). Using the two simple multivariate model could reduce above a quarter of mpMRI scans at a high sensitivity for the detection of CSPCa. It substantiates that the mpMRI scans could be reduced based on the readily available clinical parameters. The strength of our study was able to establish the definite link between mpMRI omission and the rate of CSPCa delayed. Some studies showed that a high-resolution micro-ultrasound had a comparable or higher sensitivity for the detection of CSPCa compared to mpMRI (26, 27), and was an independent parameter to predict the results of biopsy (28). In the further study, we will evaluate more convenient, low-cost, clinical parameters as predictors for the results of mpMRI, and to strengthen our multivariate model.

Our study was subject to several limitations. First, this study is a single center study based on a Chinese population, and limited by the inherent drawbacks of its retrospective design. The study results should be cautiously applied to other populations, and further prospective multicenter validation is required. Second, the PV used to calculate PSAD and build a multivariate model was estimated by mpMRI in our study. However, a study showed that PV could be reliably measured by TRUS (24), and a low-cost micro-ultrasound had a high sensitivity for the detection CSPCa (26, 27). Third, our model only included clinical parameters such as age, PSA test, and volume. The race, family history, and micro-ultrasound (26–28) will be considered in future studies to augment our multivariate model.

CONCLUSIONS

Our study demonstrated that tPSA, fPSA, PV, and PSAD were significant predictors for the mpMRI results. The multivariate model based on the inexpensive and readily available clinical parameters could be used as an aid to select patients who could

benefit from mpMRI and to reduce the unnecessary mpMRI scans without compromising the ability to diagnose CSPCa. Further prospective validation is required.

DATA AVAILABILITY STATEMENT

The raw data supporting the conclusions of this article will be made available by the authors, without undue reservation.

AUTHOR CONTRIBUTIONS

XZ, JL, and SY conceptualized, designed, and supervised the study. JL, SY, BD, and GH coordinated and participated in the data collection. SY and JL carried out the statistical analysis and drafted the manuscript. XZ, SY, JT, and FY provided guidance on the data analysis. JL, SY, ZZ, ZW, and XZ revised the manuscript. All authors contributed to the article and approved the submitted version.

FUNDING

The research was supported by the Henan Medical Science and Technology Project [grant no. LHGJ20190181 (XZ) and LHGJ20200334 (SY)].

SUPPLEMENTARY MATERIAL

The Supplementary Material for this article can be found online at: https://www.frontiersin.org/articles/10.3389/fonc.2021.732027/full#supplementary-material

REFERENCES

1. International Agency for Research on Cancer. *Global Cancer Observatory* (2020). Available at: http://gco.iarc.fr/.
2. EAU Guidelines on Prostate Cancer. *European Association of Urology* (2020). Available at: https://uroweb.org/guideline/prostate-cancer/.
3. Naji L, Randhawa H, Sohani Z, Dennis B, Lautenbach D, Kavanagh O, et al. Digital Rectal Examination for Prostate Cancer Screening in Primary Care: A Systematic Review and Meta-Analysis. *Ann Family Med* (2018) 16(2):149–54. doi: 10.1370/afm.2205
4. Catalona WJ, Richie JP, Ahmann FR, Hudson MA, Scardino PT, Flanigan RC, et al. Comparison of Digital Rectal Examination and Serum Prostate Specific Antigen in the Early Detection of Prostate Cancer: Results of a Multicenter Clinical Trial of 6,630 Men. *J Urol* (2017) 197(2s):S200–s7. doi: 10.1016/j.juro.2016.10.073
5. Bratan F, Niaf E, Melodelima C, Chesnais AL, Souchon R, Mege-Lechevallier F, et al. Influence of Imaging and Histological Factors on Prostate Cancer Detection and Localisation on Multiparametric MRI: A Prospective Study. *Eur Radiol* (2013) 23(7):2019–29. doi: 10.1007/s00330-013-2795-0
6. Johnson DC, Raman SS, Mirak SA, Kwan L, Bajgiran AM, Hsu W, et al. Detection of Individual Prostate Cancer Foci *via* Multiparametric Magnetic Resonance Imaging. *Eur Urol* (2019) 75(5):712–20. doi: 10.1016/j.eururo.2018.11.031
7. Osses DF, Roobol MJ, Schoots IG. Prediction Medicine: Biomarkers, Risk Calculators and Magnetic Resonance Imaging as Risk Stratification Tools in Prostate Cancer Diagnosis. *Int J Mol Sci* (2019) 20(7):1637. doi: 10.3390/ijms20071637
8. Yu S, Hong G, Tao J, Shen Y, Liu J, Dong B, et al. Multivariable Models Incorporating Multiparametric Magnetic Resonance Imaging Efficiently Predict Results of Prostate Biopsy and Reduce Unnecessary Biopsy. *Front Oncol* (2020) 10:57261. doi: 10.3389/fonc.2020.575261
9. Hansen J, Auprich M, Ahyai SA, de la Taille A, van Poppel H, Marberger M, et al. Initial Prostate Biopsy: Development and Internal Validation of a Biopsy-Specific Nomogram Based on the Prostate Cancer Antigen 3 Assay. *Eur Urol* (2013) 63(2):201–9. doi: 10.1016/j.eururo.2012.07.030
10. Verbeek JFM, Bangma CH, Kweldam CF, van der Kwast TH, Kümmerlin IP, van Leenders G, et al. Reducing Unnecessary Biopsies While Detecting Clinically Significant Prostate Cancer Including Cribriform Growth With the ERSPC Rotterdam Risk Calculator and 4Kscore. *Urol Oncol* (2019) 37(2):138–44. doi: 10.1016/j.urolonc.2018.11.021
11. Tomlins SA, Day JR, Lonigro RJ, Hovelson DH, Siddiqui J, Kunju LP, et al. Urine TMPRSS2:ERG Plus PCA3 for Individualized Prostate Cancer Risk Assessment. *Eur Urol* (2016) 70(1):45–53. doi: 10.1016/j.eururo.2015.04.039
12. Alberts AR, Roobol MJ, Verbeek JFM, Schoots IG, Chiu PK, Osses DF, et al. Prediction of High-Grade Prostate Cancer Following Multiparametric Magnetic Resonance Imaging: Improving the Rotterdam European Randomized Study of Screening for Prostate Cancer Risk Calculators. *Eur Urol* (2019) 75(2):310–8. doi: 10.1016/j.eururo.2018.07.031
13. Deniffel D, Zhang Y, Salinas E, Satkunasivam R, Khalvati F, Haider MA. Reducing Unnecessary Prostate Multiparametric Magnetic Resonance Imaging by Using Clinical Parameters to Predict Negative and Indeterminate Findings. *J Urol* (2020) 203(2):292–8. doi: 10.1097/JU.0000000000000518
14. Alberts AR, Schoots IG, Bokhorst LP, van Leenders GJ, Bangma CH, Roobol MJ. Risk-Based Patient Selection for Magnetic Resonance Imaging-Targeted Prostate Biopsy After Negative Transrectal Ultrasound-Guided Random Biopsy Avoids Unnecessary Magnetic Resonance Imaging Scans. *Eur Urol* (2016) 69(6):1129–34. doi: 10.1016/j.eururo.2015.11.018
15. Liu J, Dong B, Qu W, Wang J, Xu Y, Yu S, et al. Using Clinical Parameters to Predict Prostate Cancer and Reduce the Unnecessary Biopsy Among Patients With PSA in the Gray Zone. *Sci Rep* (2020) 10(1):5157. doi: 10.1038/s41598-020-62015-w
16. Kasel-Seibert M, Lehmann T, Aschenbach R, Guettler FV, Abubrig M, Grimm MO, et al. Assessment of PI-RADS V2 for the Detection of Prostate Cancer. *Eur J Radiol* (2016) 85(4):726–31. doi: 10.1016/j.ejrad.2016.01.011
17. Egevad L, Delahunt B, Evans AJ, Grignon DJ, Kench JG, Kristiansen G, et al. International Society of Urological Pathology (ISUP) Grading of Prostate Cancer. *Am J Surg Pathol* (2016) 40(6):858–61. doi: 10.1097/PAS.0000000000000642
18. DeLong ER, DeLong DM, Clarke-Pearson DL. Comparing the Areas Under Two or More Correlated Receiver Operating Characteristic Curves: A Nonparametric Approach. *Biometrics* (1988) 44(3):837–45. doi: 10.2307/2531595
19. Poulakis V, Witzsch U, de Vries R, Emmerlich V, Meves M, Altmannsberger H-M, et al. Preoperative Neural Network Using Combined Magnetic Resonance Imaging Variables, Prostate Specific Antigen, and Gleason Score to Predict Prostate Cancer Recurrence After Radical Prostatectomy. *Eur Urol* (2004) 46(5):571–8. doi: 10.1016/j.eururo.2004.07.010
20. Falagario U, Jambor I, Taimen P, Syvänen KT, Kähkönen E, Merisaari H, et al. Added Value of Systematic Biopsy in Men With a Clinical Suspicion of Prostate Cancer Undergoing Biparametric MRI-Targeted Biopsy: Multi-Institutional External Validation Study. *World J Urol* (2020) 39:1879–87. doi: 10.1007/s00345-020-03393-8
21. Boesen L, Nørgaard N, Løgager V, Balslev I, Bisbjerg R, Thestrup KC, et al. Prebiopsy Biparametric Magnetic Resonance Imaging Combined With Prostate-Specific Antigen Density in Detecting and Ruling Out Gleason 7-10 Prostate Cancer in Biopsy-Naïve Men. *Eur Urol Oncol* (2019) 2(3):311–9. doi: 10.1016/j.euo.2018.09.001
22. Lobo N, Petrides N, Stanowski M, Morrison I, Thomas M, Kommu S, et al. Can We Rely on a Negative Multiparametric MRI to Exclude Significant Prostate Cancer at Biopsy? Results From a Regional Cancer Centre. *Eur Urol Suppl* (2019) 18:e1876. doi: 10.1016/S1569-9056(19)31359-4
23. Barrett T, Slough R, Sushentsev N, Shaida N, Koo BC, Caglic I, et al. Three-Year Experience of a Dedicated Prostate mpMRI Pre-Biopsy Programme and

Effect on Timed Cancer Diagnostic Pathways. *Clin Radiol* (2019) 74 (11):894.e1–.e9. doi: 10.1016/j.crad.2019.06.004
24. Christie DRH, Sharpley CF. How Accurately Can Prostate Gland Imaging Measure the Prostate Gland Volume? Results of a Systematic Review. *Prostate Cancer* (2019) 2019:6932572. doi: 10.1155/2019/6932572
25. Gronberg H, Adolfsson J, Aly M, Nordstrom T, Wiklund P, Brandberg Y, et al. Prostate Cancer Screening in Men Aged 50-69 Years (STHLM3): A Prospective Population-Based Diagnostic Study. *Lancet Oncol* (2015) 16 (16):1667–76. doi: 10.1016/S1470-2045(15)00361-7
26. Klotz L, Lughezzani G, Maffei D, Sánchez A, Pereira JG, Staerman F, et al. Comparison of Micro-Ultrasound and Multiparametric Magnetic Resonance Imaging for Prostate Cancer: A Multicenter, Prospective Analysis. *Can Urol Assoc J* (2021) 15(1):E11–6. doi: 10.5489/cuaj.6712
27. Lughezzani G, Maffei D, Saita A, Paciotti M, Diana P, Buffi NM, et al. Diagnostic Accuracy of Microultrasound in Patients With a Suspicion of Prostate Cancer at Magnetic Resonance Imaging: A Single-Institutional Prospective Study. *Eur Urol Focus* (2020) 20:30272–8. doi: 10.1016/j.euf.2020.09.013
28. Avolio PP, Lughezzani G, Paciotti M, Maffei D, Uleri A, Frego N, et al. The Use of 29 MHz Transrectal Micro-Ultrasound to Stratify the Prostate Cancer Risk in Patients With PI-RADS III Lesions at Multiparametric MRI: A Single Institutional Analysis. *Urol Oncol* (2021). doi: 10.1016/j.urolonc.2021.05.030

Conflict of Interest: The authors declare that the research was conducted in the absence of any commercial or financial relationships that could be construed as a potential conflict of interest.

Publisher's Note: All claims expressed in this article are solely those of the authors and do not necessarily represent those of their affiliated organizations, or those of the publisher, the editors and the reviewers. Any product that may be evaluated in this article, or claim that may be made by its manufacturer, is not guaranteed or endorsed by the publisher.

frontiers | Frontiers in Oncology

TYPE Original Research
PUBLISHED 30 August 2022
DOI 10.3389/fonc.2022.974257

OPEN ACCESS

EDITED BY
Matteo Ferro,
European Institute of Oncology (IEO), Italy

REVIEWED BY
Achille Aveta,
University of Naples Federico II, Italy
Francesco Del Giudice,
Sapienza University of Rome, Italy

*CORRESPONDENCE
Hui Wu
terrywuhui@sina.com
Aishi Liu
liuaishi@sina.com

SPECIALTY SECTION
This article was submitted to Genitourinary Oncology, a section of the journal Frontiers in Oncology

RECEIVED 21 June 2022
ACCEPTED 02 August 2022
PUBLISHED 30 August 2022

CITATION
Jia Y, Quan S, Ren J, Wu H, Liu A, Gao Y, Hao F, Yang Z, Zhang T and Hu H (2022) MRI radiomics predicts progression-free survival in prostate cancer.
Front. Oncol. 12:974257.
doi: 10.3389/fonc.2022.974257

MRI radiomics predicts progression-free survival in prostate cancer

Yushan Jia[1], Shuai Quan[2], Jialiang Ren[2], Hui Wu[3]*, Aishi Liu[3]*, Yang Gao[3], Fene Hao[3], Zhenxing Yang[3], Tong Zhang[1] and He Hu[1]

[1]Affiliated Hospital, Inner Mongolia Medical University, Hohhot, China, [2]Department of Pharmaceuticals Diagnosis, GE Healthcare (China), Shanghai, China, [3]Department of Radiology, Affiliated Hospital of Inner Mongolia Medical University, Hohhot, China

Objective: To assess the predictive value of magnetic resonance imaging (MRI) radiomics for progression-free survival (PFS) in patients with prostate cancer (PCa).

Methods: 191 patients with prostate cancer confirmed by puncture biopsy or surgical pathology were included in this retrospective study, including 133 in the training group and 58 in the validation group. All patients underwent T2WI and DWI serial scans. Three radiomics models were constructed using univariate logistic regression and Gradient Boosting Decision Tree(GBDT) for feature screening, followed by Cox risk regression to construct a mixed model combining radiomics features and clinicopathological risk factors and to draw a nomogram. The performance of the models was evaluated by receiver operating characteristic curve (ROC), calibration curve and decision curve analysis. The Kaplan-Meier method was applied for survival analysis.

Results: Compared with the radiomics model, the hybrid model consisting of a combination of radiomics features and clinical data performed the best in predicting PFS in PCa patients, with AUCs of 0.926 and 0.917 in the training and validation groups, respectively. Decision curve analysis showed that the radiomics nomogram had good clinical application and the calibration curve proved to have good stability. Survival curves showed that PFS was shorter in the high-risk group than in the low-risk group.

Conclusion: The hybrid model constructed from radiomics and clinical data showed excellent performance in predicting PFS in prostate cancer patients. The nomogram provides a non-invasive diagnostic tool for risk stratification of clinical patients.

KEYWORDS

prostate cancer, radiomics, progression-free survival, magnetic resonance imaging, predictions

Introduction

Prostate cancer is the most common malignancy of the male reproductive system, the fourth most common cancer worldwide, and the fifth leading cause of cancer death in men (1, 2). There are significant geographical differences in its incidence. With economic development and increased life expectancy, the incidence and mortality of PCa are on the rise in Asian countries, with an increasing disease burden (3). According to the US Surveillance, Epidemiology and End Results (SEER) Database 2010-2016 data, the 5-year survival rate for metastatic PCa is only 30% (4). The onset of PCa is insidious, and most patients are already at intermediate to the advanced risk of PCa at the time of initial diagnosis, with a high rate of recurrence and risk of metastasis (5). Therefore, it is particularly important to find a suitable way to predict the progression of prostate cancer patients and intervene early to prolong their survival.

Artificial intelligence (AI), the ability of machines to perform cognitive tasks to achieve specific goals based on the data provided, is transforming our healthcare system. Machine learning (ML) is a subfield of AI, meaning that algorithms are created and deployed to analyze data and its properties, and are not specifically given tasks based on certain predefined inputs in the environment. In order to improve the probability of survival of prostate cancer patients, it is necessary to develop appropriate predictive models for PCa. Jović S et al. (6) applied and compared several machine learning techniques in their study for analytical discussion and concluded that machine learning techniques can be used for prediction related to prostate cancer. The use of computer-based learning models has become a major area of research in PCa. Conventional imaging is usually used for diagnosis, staging and treatment guidance of tumors and the information obtained from the images is subjective. Dutch scholar Lambin (7) first introduced the concept of radiomics in 2012, which promises to visualize heterogeneity within tumors and reveal the prognostic information behind the images. It builds on imaging techniques such as magnetic resonance imaging (MRI), computed tomography and positron emission tomography to convert medical images into high-dimensional, mineable data through high-throughput extraction of quantitative features, thereby providing decision support for oncology at low cost and non-invasively (8). Ferro M et al. (9) summarize the latest studies using different imaging modalities, following a predefined methodology, looking for studies with validated protocols, but also looking at how AI can improve radiomics and translate these results into clinical practice, and about the advantages and limitations of the different algorithms used in PCa radiomics. In addition, many studies in recent years have shown that radiomic features are related to molecular features of cancer tissue, genomics, proteomics and metabolomics (10). This new area of research in PCa is an extension of radiomics, whose main focus is on tailored approaches to diagnose aggressive PCa (11), predict prognosis (12), progression (13) and response to treatment (11). MRI with its high soft tissue resolution and multidirectional imaging capabilities can clearly show the different locations of lesions in prostate cancer, and in combination with functional imaging plays an important role in assessing the presence of extra capsular extension (ECE), seminal vesicle invasion, in prostate cancer detection (14), staging (15) and aggressiveness assessment (16) and is the most commonly used imaging modality in prostate cancer screening. A number of published findings support mp-MRI (17, 18) as the most sensitive and specific imaging modality.

Progression-free survival is important for the prognostic assessment of tumor patients, and studies have demonstrated that radiomics can be used to predict progression-free survival in glioma (19), breast cancer (20), lung cancer (21) and ovarian cancer (22), but to date, no personalized imaging prediction models have been developed for progression-free survival in prostate cancer patients. Therefore, this study evaluates the value of MRI radiomics in predicting progression-free survival in PCa patients to develop a hybrid clinical-imaging histology model to help improve decision-making and guide individualized treatment.

Material and methods

Patient selection

This study was approved by the Ethics Committee of the Affiliated Hospital of Inner Mongolia Medical University, and informed consent was obtained from patients. A retrospective collection of 373 patients with PCa retrieved from our hospital's image archiving and communication system (PACS, GE) from January 2016 to December 2018 was conducted. Patient groupings are shown in Figure 1. Inclusion criteria: 1. Patients with histologically confirmed T1-4N0M0 prostate cancer confirmed by puncture biopsy or surgical pathology; 2. Undergoing MRI one week prior to treatment. Exclusion criteria: 1. previous endocrine, radiotherapy or chemotherapy; 2. clear signs of metastasis on MRI; 3. incomplete clinical profile. The final 191 patients were included in the study, (aged 45-89 years, median age 74 years) and were randomised in a 7:3 ratio into a training group (n=133) and a validation group (n=58). Clinical information on all patients included age, pre-treatment PSA levels, number of lesions, clinical T-stage and Gleason score.

All patients are followed up at 3 months for 2 years, every 6 months after 2 years and once a year after 5 years. The follow-up deadline is December 2021. Follow-up visits include PSA levels, CT of the chest, abdomen and pelvis or MRI of the pelvis, and

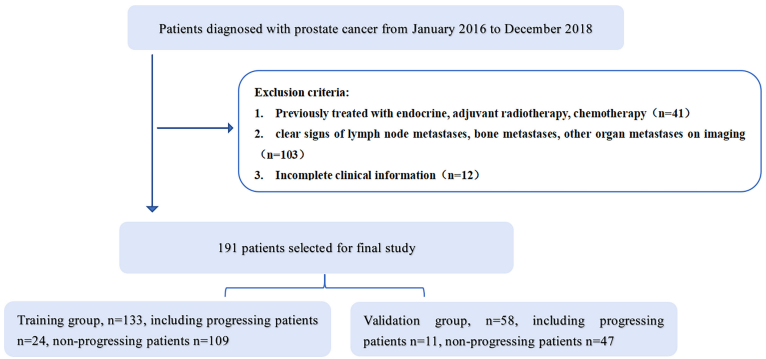

FIGURE 1
Patient selection flow chart. Includes exclusion criteria and grouping.

bone scans. The endpoint is progression-free survival, defined as the time from the first day of treatment until disease progression (biochemical recurrence, distant metastases, including bone metastases, lymph node metastases and other distant organ metastases) or death from any cause, or the last follow-up visit.

MRI acquisition

All scans were performed using a GE Discovery MR 750 3.0T superconducting MRI machine with an abdominal coil in all patients. The acquisition parameters were as follows: axial T2-weighted spin-echo images (repetition time/echo time [TR/TE]: 3,480/85 ms, field of view[FOV] = 24 cm, matrixs = 320x320, lice thickness = 4 mm, spacing = 1.0 mm), axial T1-weighted spin-echo images (TR/TE: 811/10 ms, FOV = 24 cm, matrixs = 320x224, slice thickness = 4 mm, spacing = 1.0 mm), and axial DWI SE-EPI images (TR/TE: 2,900/61, FOV = 28 cm, matrixs = 512x512, slice thickness = 4 mm, spacing = 1.0 mm, b = 0, 1,000 s/mm$^{2)}$. ADC maps were obtained in GE AW 4.6 Functool workstation post-processing.

Image segmentation

We used the open-source software ITK-SNAP software for lesion segmentation. Radiologists with 5 years of experience in male pelvic MRI imaging were used to outline ROIs along the edges of the lesion at the largest level of the lesion on T2WI and ADC images, respectively, avoiding fat, calcifications and hemorrhagic foci. To select robust features for intra-rater and inter-rater description variation, intra-rater test datasets and intra-rater test datasets were obtained for 50 patients (**blind** with 15 years of experience in urological imaging) by the same radiologist and another radiologist, respectively (Figure 2).

Extraction and selection of radiomics features

From each Roi, radiomic features were extracted from DWI, ADC images using the open-source tool pyradiomics. These features include: 1. Shape features: used to describe the geometric properties of the ROI, including size elements that describe the volume and surface area of the ROI. 2. First-order features, which are features describing the intensity distribution of voxels within the ROI, calculated by histogram analysis. 3.Texture features that describe the intensity level of the spatial distribution of voxels. Includes Grey Level Co-occurrence Matrix (GLCM) features, Grey Level Travel Length Matrix (GLRLM) features and Grey Level Size Zone Matrix (GLSZM) features.4. Algorithmically transformed features: first-order and higher-order texture features obtained by transforming the original image with Wavelet and Laplacian-of-Gaussian (LOG). 1307 radiomic features were extracted from each ROI.

Construction of radiomics signatures

First, features with low repeatability were excluded from the subsequent analysis. Here the intra-rater and inter-rater repeatability for each feature was quantified by intraclass correlation coefficient (ICC) calculated on the intra-rater test data set and inter-rater test data set respectively. Features with ICC > 0.8 are retained. All features were normalized using the Z-Score transform. Single-factor logistic regression and GBDT were then used to further filter the histological features to ensure reproducibility of the model and reduce overfitting or selection bias in the radiomics model. The screened radiomics features were analyzed using Cox risk regression to create a radiomics model. Significant clinical variables were screened using univariate Cox risk regression. ROC curves, calibration

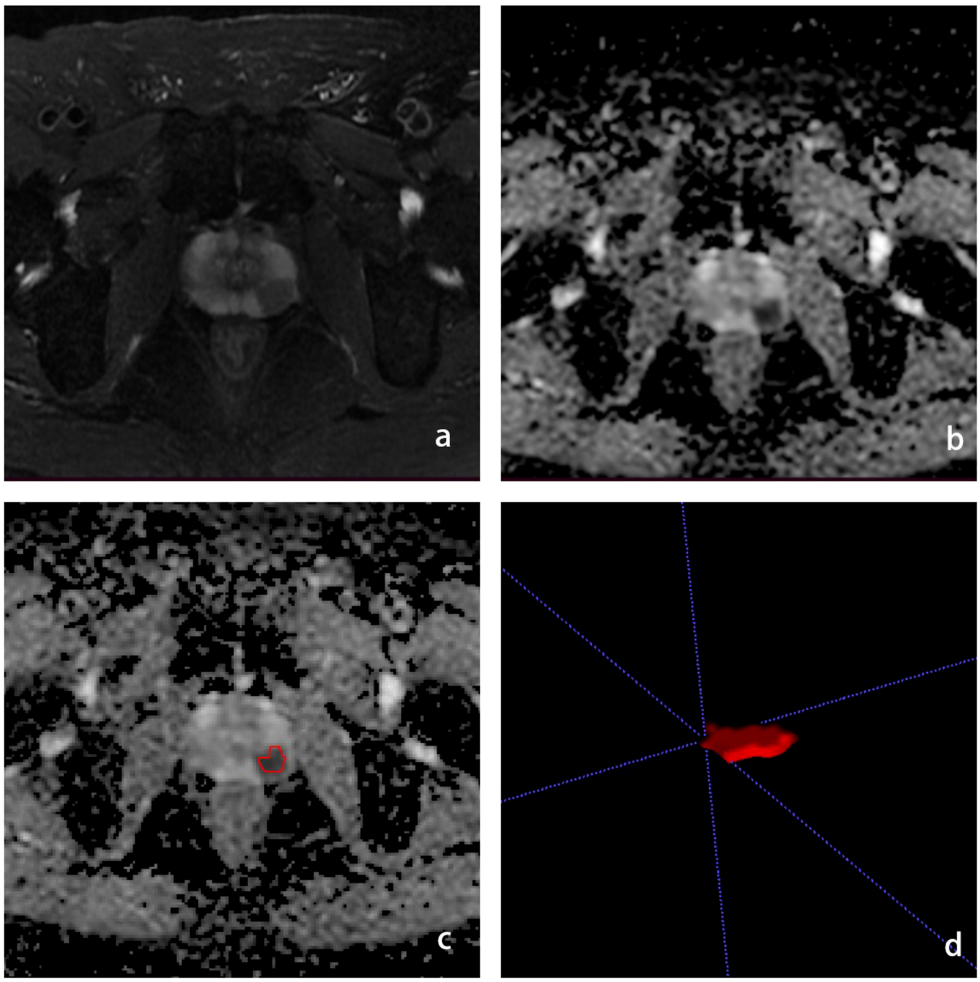

FIGURE 2
Schematic diagram of the ROI outline. **(A)** is the T2WI sequence with PCa in the left peripheral band, **(B)** is the ADC sequence with the cancer foci showing low signal, **(C)** is the ROI outline, **(D)** is the generated ROI.

curves, and decision curve analysis were applied to assess model performance.

Validation of radiomics signatures

Kaplan-Meier survival analysis was used in the training group to assess the potential association of radiomic features with PFS, which was then validated in the validation group. Classification of patients into high and low risk groups based on cut-off values based on radiomic signatures as determined by optimal cut-off analysis using X-title software. The truncation values are estimated on the training group and validated on the validation group. A weighted log-rank test was used to assess the difference in survival curves between the high and low risk groups. To demonstrate the value of radiomic features for individualized assessment of PFS, separate radiomic column line plots were constructed. Radiomics scores (Rad scores) and clinical data were combined to create a mixed model of radiomics and clinical data to plot nomograms and provide a visual tool for predicting progression-free survival in PCa. The Rad score is calculated by adding selected imaging histology features that are weighted by their respective coefficients. Significant clinical variables were screened using univariate Cox risk regression.

Statistical analysis

All statistical analyses for this study were performed using R software (Version 3.6.3, Statistical Computing Basis). A two-

sided P < 0.05 was considered statistically significant. The Kolmogorov-Smimov test was used to verify that the histological characteristics conformed to a normal distribution, using the two independent samples t-test for normal distribution and the Mann-Whitney U test for non-normal distribution. The ability of the model was assessed by the ROC, calculating the AUC and 95% confidence intervals. The diagnostic sensitivity, specificity, accuracy, positive predictive value and negative predictive value of the models were also calculated. Calibration curves were used to assess the predictive performance of each model. Decision curves were used to assess the net benefit of each model at different threshold probabilities and to evaluate the clinical applicability of each model.

Results

Clinical data

Clinical data for patients in the training and validation groups are shown in Table 1. Patients were aged 45-89 years, with a median age of 74 years. The median progression-free survival time was 42 months (range 10-72 months). There was no statistically significant difference between the training and validation groups in terms of patient age (p > 0.05) and statistically significant differences in Gleason score, clinical T-stage, number of lesions and pre-treatment PSA levels (p < 0.05).

Radiomic signature building

1037 radiomic features were extracted from the ROI, and after t-test or Mann-WhitneyU test screening to remove the meaningless features, 5 optimal features were finally obtained from T2W1 and 4 optimal features from ADC using single factor logistic regression and the GBDT method, and the feature screening results are shown in Table 2. The results show that the hybrid model has better predictive ability, and the ROC curves of the four models in the training and validation groups are shown in Figures 3A, B. The AUCs of the T2WI, ADC, T2WI-ADC models and the hybrid model in the training group are 0.876 (0.815, 0.931), 0.722 (0.562, 0.856), 0.904 (0.833, 0.965), 0.904 (0.833, 0.965), and 0.926 (0.882, 0.962), and the AUCs in the validation group were 0.843 (0.673, 0.965), 0.713 (0.444, 0.945), 0.870 (0.75, 0.972), and 0.917 (0.808, 1.0), respectively (shown in Table 3). The four model decision curves and calibration curves are shown in Figures 3C–F.

Radiomics scoring and normogram creation

The Rad score was obtained by weighting the nine optimal features by their respective coefficients, calculated as = -1.6371 +

TABLE 1 Comparison of clinical characteristics between the training and validation groups.

Clinical data	Training group n=133	Validation group n=58	*P*
Age (mean ± SD, years)	72.12 ± 8.82	73.31 ± 8.40	0.765
T stage			0.001
T1	47	15	
T2	53	32	
T3	15	6	
T4	18	5	
Pre-treatment PSA levels(n/ml)			0.001
<100	67	30	
>100	66	28	
Gleason Score			0.001
5	12	2	
6	23	11	
7	43	22	
8	29	13	
9	16	6	
10	10	4	
Number of tumors			0.013
=1	86	31	
>1	47	27	

SD, standard deviation; PSA, prostate specific antigen.

10.3389/fonc.2022.974257

TABLE 2 Radiomic feature selection result.

Classification of results	T2WI	ADC	T2WI-ADC
Number of features	5	4	9
Radiomics Features	log-sigma-5-0-mm-3D_firstorder_10Percentile	wavelet-LLL_firstorder_InterquartileRange	log-sigma-5-0-mm-3D_firstorder_10Percentile
	Wavelet-LHL_gldm_SmallDependenceHighGrayLevelEmphasis	wavelet-LLL_glszm_SmallAreaHighGrayLevelEmphasis	wavelet-LHL_gldm_SmallDependenceHighGrayLevelEmphasis
	wavelet-HLL_glcm_Correlation	original_glrlm_GrayLevelNonUniformityNormalized	wavelet-HLL_glcm_Correlation
	Wavelet-LHL_glcm_MaximumProbability	wavelet-LHH_glrlm_RunEntropy	wavelet-LHL_glcm_MaximumProbability
	log-sigma-3-0-mm-3D_firstorder_Minimum		log-sigma-3-0-mm-3D_firstorder_Minimum
			wavelet-LLL_firstorder_InterquartileRange
			wavelet-LLL_glszm_SmallAreaHighGrayLevelEmphasis
			original_glrlm_GrayLevelNonUniformityNormalized
			wavelet-LHH_glrlm_RunEntropy

T2WI, T2- weightedimagine; ADC, apparent diffusion coefficient.

0.3323 × " log-sigma-5-0-mm-3D_firstorder_10Percentile "-0.1502 ×"wavelet-LHL_gldm_SmallDependenceHighGrayLevel Emphasis "+ 0.1918 ×" wavelet-HLL_glcm_Correlation"+ 0.3284" wavelet-LHL_glcm_MaximumProbability"+ 0.5209 × "log-sigma-3-0-mm-3D_firstorder_Minimum "- 0.5178 × " wavelet-LLL_firstorder_InterquartileRange "+ 0.0487 ×" wavelet-LLL_glszm_SmallAreaHighGrayLevelEmphasis "- 0.4251 ×" original_glrlm_GrayLevelNonUniformityNormalized "- 0.3291 ×" wavelet-LHH_glrlm_RunEntropy". The Rad score plots for the training and validation groups are shown in Figure 4. Independent clinical predictors combined with Rad scores make up the Nomogram, as shown in Figure 5.

Survival analysis

Patients were divided into high-risk and low-risk groups based on radiomics scores. PFS survival curves were plotted using the Kaplan-Meier method. Using the log-rank chi-square test, there was a statistically significant difference in survival rates between the different risk groups in the training and validation groups ($p<0.001$) (Figure 6).

Discussion

PCa is a common malignancy in elderly men, and its incidence and mortality are on the rise in some countries, especially in Asia. The insidious onset of PCa and the fact that it is mostly mid-to late-stage when first diagnosed has led to a decline in patient survival. Prognostic models associated with PFS have been developed in other tumor types with promising applications; however, according to our literature search, prognostic survival models for PFS imaging of PCa have not been studied. Imaging is an important clinical examination tool for diagnosis, staging and treatment decisions for tumors but relies heavily on the physician's visual assessment of the images, which is subjectively biased and produces limited information. With the increased digitization of clinical information and the application of artificial intelligence research, radiomics has become a hot research topic. Solid tumors are spatially and temporally heterogeneous, and imaging histology can capture this heterogeneity noninvasively and express it in terms of pixel density and spatial distribution, which may correlate with tumor aggressiveness, pathological grading, posttreatment response and prognosis (7, 23, 24). In contrast, PCa is characterized by its remarkable heterogeneity and the variability of tumor prognosis. Most prostate cancers are inert, while the remaining proportion can be very aggressive and even life-threatening, so stratified management of patients with prostate cancer, early detection and effective intervention in high-risk patients to reduce recurrence and metastasis are important goals of current clinical research. Reliable and accurate predictors and prognostic models can help guide clinical decision-making to the

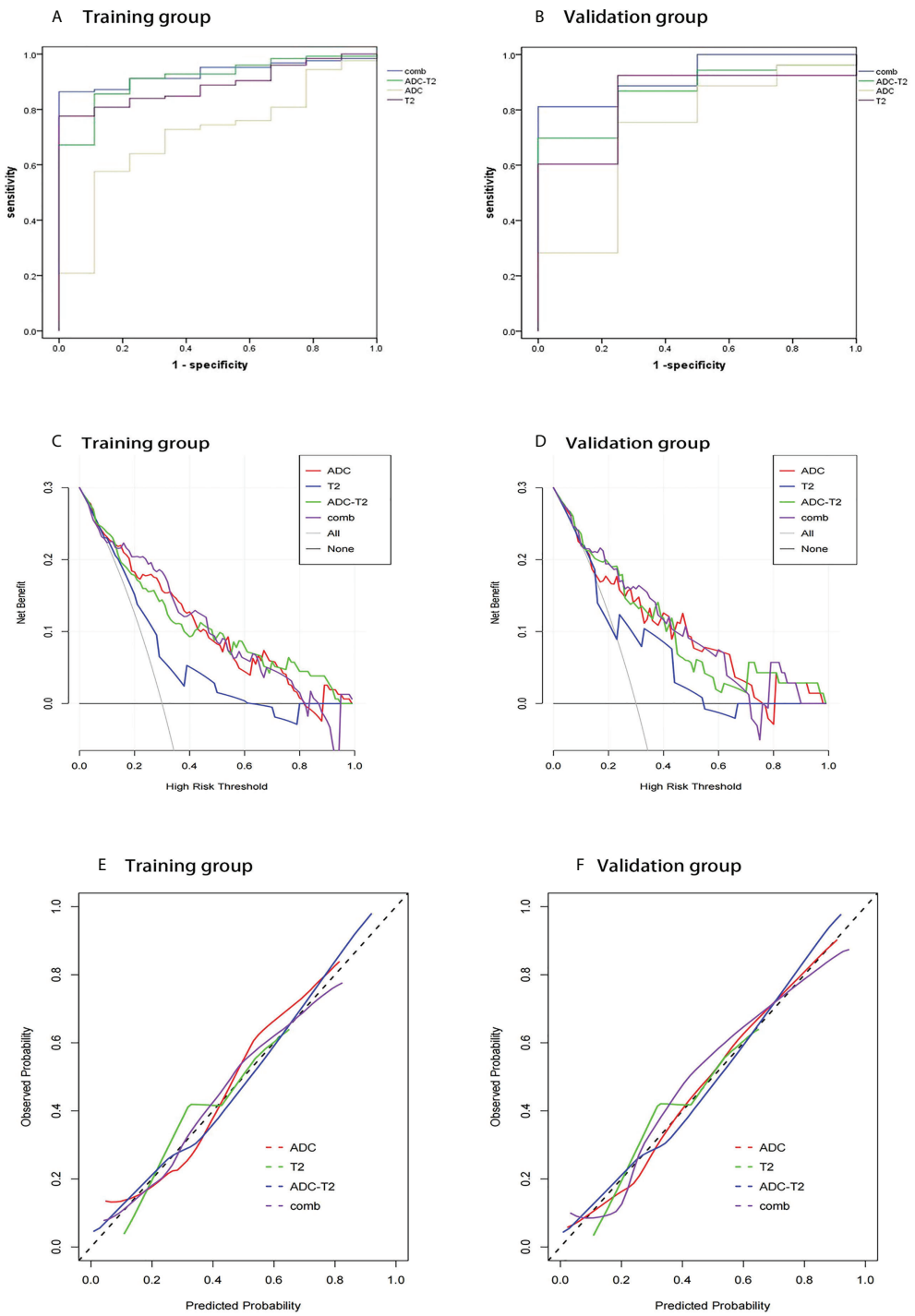

FIGURE 3
ROC curves, decision curve analysis, calibration curves for different models in the training and validation groups. The ROC curves for the four models in the training and validation groups are shown in **(A, B)**. The decision curves for the four models in the training and validation groups are shown in **(C, D)**. The calibration curves for the four models are shown in **(E, F)**.

10.3389/fonc.2022.974257

TABLE 3 Predictive performance of T2WI, ADC, T2WI-ADC and hybrid models.

Cohort	Model	AUC(95%CI)	ACC	SEN	SPE	PPV	NPV
Training	ADC	0.722(0.562,0.850)	0.729	0.728	0.750	0.978	0.150
	T2WI	0.876(0.815,0.930)	0.782	0.768	1.000	1.000	0.216
	T2WI-ADC	0.904(0.833,0.960)	0.850	0.848	0.875	0.991	0.269
	Hybrid models	0.926(0.882,0.960)	0.865	0.856	1.000	1.000	0.308
Validation组	ADC	0.713(0.444,0.940)	0.741	0.741	0.750	0.976	0.176
	T2WI	0.843(0.673,0.960)	0.707	0.704	0.750	0.974	0.158
	T2WI-ADC	0.870(0.750,0.972)	0.810	0.815	0.750	0.978	0.231
	Hybrid models	0.917(0.808, 1.000)	0.793	0.778	1.000	1.000	0.250

T2WI, T2- weightedimagine; ADC, apparent diffusion coeffificient; AUC, area under curve; SEN, sensitivity; SPE, specificity; ACC, accuracy; PPV, positive predictive value; NPV, negative predictive.

clinical benefit of patients. In this context, we extracted features from MRI, constructed models and combined them with clinical factors to create nomograms for the further risk assessment of prostate cancer patients.

MRI-based radiomics have been extensively used in the diagnosis of prostate cancer, the Gleason score and other areas with satisfactory results (25–28). Recently, MRI radiomics has also been used to predict the risk of biochemical recurrence (BCR) after radical prostate cancer surgery and radiotherapy. BCR is considered a marker of local recurrence, distant metastasis and prostate cancer-specific death. Studies have reported (29) that the 10-year BCR rate after radical prostatectomy is as high as 50%. Gnep et al. (30) previously demonstrated in that Haralick features from T2WI were associated with BCR occurrence, suggesting that radiomics analysis may be able to capture the difference between BCR-positive and BCR-negative lesions on MRI. However, the role of MRI-based radiomics in assessing PFS in PCa has not yet been reported, so we have undertaken a study to investigate this. We used T2WI and ADC sequences to extract features because T2WI can clearly show the anatomical features of the tumor and the presence of perineural involvement and seminal gland involvement in prostate cancer patients, and the images contain more valuable textural features. ADC values objectively reflect the degree of diffusion of water molecules in biological tissue and correlate with the malignancy of the tumor, avoiding the penetration effect of DWI due to the very long T2 decay time of the tissue. The combination of T2WI and ADC allows for more accurate and comprehensive tumor information to be obtained. In our study, the combined sequence of T2WI and ADC showed better performance in predicting 3-year PFS in PCa patients than the model with the sequence alone, with the highest AUC in both the training and validation groups.

Age, pretreatment PSA levels, TNM stage and Gleason score all have an impact on the prognosis of PCa. In this study, using univariate Cox risk regression analysis, the clinical T stage, pretreatment PSA level and Gleason score were found to have a statistically significant impact on the prognosis of PCa; age was not. Some scholars (31) conducted an epidemiological survey and analysis on the effect of age on survival, comparing the effect

FIGURE 4
Rad score chart for training and validation groups. **(A, B)** show the distribution of radiomics scores for the training and validation groups respectively. The pink bars represent the radiomics scores of patients who did not experience disease progression, while the blue bars represent the radiomics scores of patients who experienced disease progression.

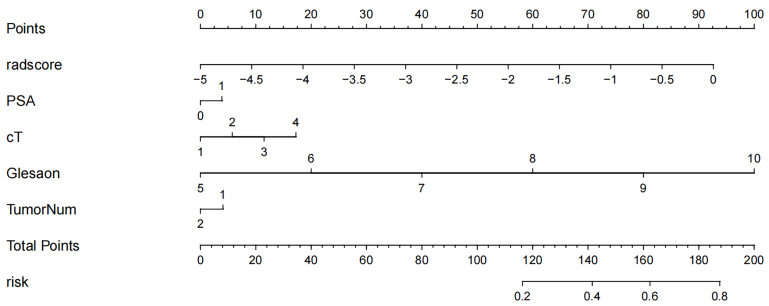

FIGURE 5
Radiology nomogram. The radiology nomogram prediction model predicts the probability of progression in patients with PCa. How to use: (1) locate the patient's radiomic score, PSA level, clinical T-stage, Gleason score, number of tumor and then draw a straight line on the top dot axis to obtain the corresponding score; (2) sum the scores obtained (3) find the final sum on the total point axis and draw a straight line down to assess the risk of progression in patients with prostate cancer.

of different age segments on survival. The results showed that patients in the younger group survived longer, and the difference was statistically significant, but it has also been shown (32) that age is not an influential factor in the prognosis of prostate cancer. Our findings do not support age as an independent influential factor in the prognosis of patient survival. We also did a simple Kendall correlation analysis of the effect of T-stage, Gleason score and number of lesions on the patient's PSA levels and found that the three clinical factors were positively correlated with PSA levels and that the Gleason score correlated more significantly with them. This suggests that the PSA level is also increased with an increase in Gleason score. The PIRADS v2 score is currently the most widely used and internationally recognized MRI reporting system for the prostate. de Cobelli O et al. (33) found a significant association between PIRADS score and GS escalation, ECE, unfavorable prognosis and large tumor volume: increasing with increasing PIRADS score. We will also include PI-RADS in a follow-up study to discuss its relevance to the prognosis of prostate cancer.

The concept of adequate mutual agreement between genitourinary radiologists has been a key point of discussion. mpMRI has changed the paradigm of prostate cancer detection, characterization and management, refining treatment planning and patient selection for active surveillance, and assessing post-treatment outcomes, but the interpretation of mpMRI remains difficult and has substantial inter-reader variability, leading to the development of the original (v.1) and updated (v.2 and 2.1) versions of the PI-RADS development. Del Giudice et al. (34) demonstrated that Vesical Imaging-Reporting and Data System (VI-RADS) provides a standard method for radiologists in the acquisition, interpretation and reporting of MRI of bladder cancer. Despite the existence of two very independent

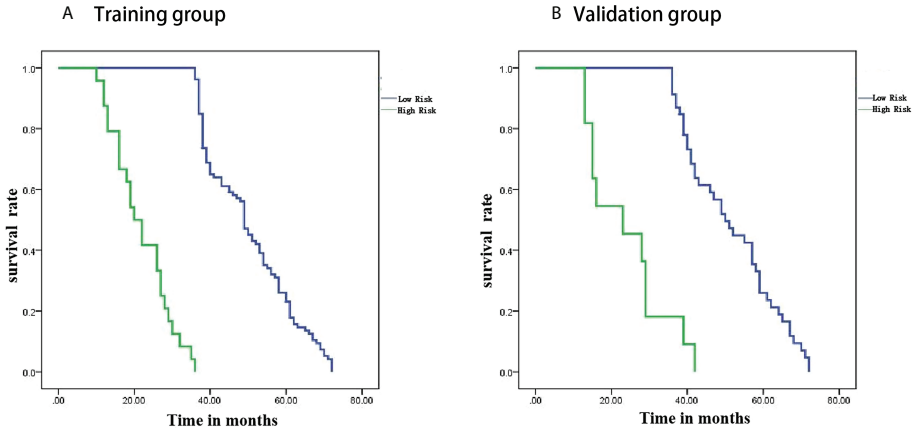

FIGURE 6
Kaplan-Meier analysis. **(A)** is the training group and **(B)** is the validation group.

diagnostic goals between PI-RADS and VI-RADS, these standard certainties share the common goal of pursuing a higher reliability of diagnostic findings in the reader than a purely subjective interpretation of MRI sequences, which also provides ample evidence of the importance of rigorous monitoring for a high degree of inter-reader agreement between different AI and radiomic features.

Many studies have attempted to combine imaging histology with clinical parameters to improve the predictive power of the model. The nomogram was developed by Yu et al. (35) With the combination of radiomics features and clinical parameters was able to predict peritoneal metastases in ovarian cancer preoperatively well, and its efficacy was superior to that of a single model with radiomics and the clinic. We also developed a hybrid model to plot a nomogram combining Rad scores and important clinical features for the assessment of 3-year PFS in PCa patients. The hybrid model showed superior predictive performance for 3-year PFS prediction compared to the radiomics model alone. The ROC curve analysis also validates this result. Our study also found that the Rad score could be used as a marker to distinguish between low- and high-risk patients. Patients with higher Rad scores are at greater risk of progression and have shorter PFS. These results provide new insights into future treatment options for patients with PCa. For example, patients at high risk of progression may consider a combination of early multiple treatments; conversely, patients at low risk of progression may opt directly for surgery, local radiotherapy or even monitoring, thus avoiding ineffective or excessive treatment and disease progression due to delays in effective treatment. Therefore, the Rad score can be used as a valid biomarker to improve the prognosis of patients with PCa.

There are some limitations to our study. First, this is a single-center, retrospective study with some possible bias in the selection of patients, which will be validated in future research through multicenter, prospective studies to provide more reliable evidence for clinical application. Second, the follow-up period was relatively short, and longer follow-up is needed to predict 5-year and 10-year progression-free survival, which can be used as part of our follow-up study. Third, radiomics seeks to find the most valuable features in a variety of data, and we only analyzed T2WI and ADC images without adding dynamic enhancement images to the analysis. Multiparametric data analysis may help improve the quality of the model. Fourth, some important protein and gene biomarkers associated with PCa progression were not considered for the features we extracted from the MRI. Finally, our ROIs were obtained by manual segmentation by radiologists, with subjective observer bias, and a reliable and robust automated segmentation method should be further developed to address this issue.

Conclusion

In summary, in this study, we retrospectively analyzed the relationship between MRI radiomics features and progression-free survival in patients with prostate cancer confirmed by biopsy puncture or surgical pathology and analyzed the feasibility of imaging histology for the assessment of progression-free survival. The radiomics features extracted by MRI provide a highly accurate, noninvasive, easy-to-perform, real-time method for preoperatively predicting progression-free survival in prostate cancer patients. Multiple sequence combination models are superior to single sequence models. We developed a nomogram to provide a noninvasive, individualized tool for the stratified management of prostate cancer patients to support clinical decision-making. Although there are some limitations to our study, we have provided a means of assessing the preoperative prediction of tumor progression in prostate cancer patients, compensating for the shortcomings of conventional imaging.

Data availability statement

The raw data supporting the conclusions of this article will be made available by the authors, without undue reservation.

Ethics statement

The studies involving human participants were reviewed and approved by Ethics Committee of the Affiliated Hospital of Inner Mongolia Medical University. The patients/participants provided their written informed consent to participate in this study.

Author contributions

YJ and SQ substantial contributions to the conception or design of the work; or the acquisition, analysis or interpretation of data for the work. HW and AL drafting the work or revising it critically for important intellectual content. TZ, HH, JR and ZY provide approval for publication of the content. YG and FH agree to be accountable for all aspects of the work in ensuring that questions related to the accuracy or integrity of any part of the work are appropriately investigated and resolved. All authors contributed to the article and approved the submitted version.

Funding

This article was funded by the Inner Mongolia Autonomous Region Fund of Natural Science (2021MS08026); the General Program of Inner Mongolia Medical University (YKD2021MS045); Inner Mongolia Medical University College Students Science and Technology Innovation "Talent Cultivation"(YCPY2021088); Inner Mongolia Autonomous Region Fund of Natural Science(2022SHZR2186).

Conflict of interest

Author SQ and JR were employed by GE Healthcare.

The remaining authors declare that the research was conducted in the absence of any commercial or financial relationships that could be construed as a potential conflict of interest.

Publisher's note

All claims expressed in this article are solely those of the authors and do not necessarily represent those of their affiliated organizations, or those of the publisher, the editors and the reviewers. Any product that may be evaluated in this article, or claim that may be made by its manufacturer, is not guaranteed or endorsed by the publisher.

References

1. Sung H, Ferlay J, Siegel RL, Laversanne M, Soerjomataram I, Jemal A, et al. Global cancer statistics 2020: GLOBOCAN estimates of incidence and mortality worldwide for 36 cancers in 185 countries. *CA Cancer J Clin* (2021) 71(3):209–49. doi: 10.3322/caac.21660

2. Dy GW, Gore JL, Forouzanfar MH, Naghavi M, Fitzmaurice C. Global burden of urologic cancers, 1990-2013. *Eur Urol* (2017) 71(3):437–46. doi: 10.1016/j.eururo.2016.10.008

3. Chen W, Zheng R, Baade PD, Zhang S, Zeng H, Bray F, et al. Cancer statistics in China, 2015. *CA Cancer J Clin* (2016) 66(2):115–32. doi: 10.3322/caac.21338

4. Liu Z, Jiang Y, Fang Q, Yuan H, Cai N, Suo C, et al. Future of cancer incidence in Shanghai, China: Predicting the burden upon the ageing population. *Cancer Epidemiol* (2019) 60:8–15. doi: 10.1016/j.canep.2019.03.004

5. Shin S, Saito E, Sawada N, Ishihara J, Takachi R, Nanri A, et al. Dietary patterns and prostate cancer risk in Japanese: The Japan public health center-based prospective study (JPHC study). *Cancer Causes Control* (2018) 29(6):589–600. doi: 10.1007/s10552-018-1030-3

6. Jović S, Miljković M, Ivanović M, Šaranović M, Arsić M. Prostate cancer probability prediction by machine learning technique. *Cancer Investig* (2017) 35:647–51. doi: 10.1080/07357907.2017.1406496

7. Lambin P, Rios-Velazquez E, Leijenaar R, Carvalho S, van Stiphout RG, Granton P, et al. Radiomics: Extracting more information from medical images using advanced feature analysis. *Eur J Cancer* (2012) 48(4):441–6. doi: 10.1016/j.ejca.2011.11.036

8. Gillies RJ, Kinahan PE, Hricak H. Radiomics: Images are more than pictures, they are data. *Radiology* (2016) 278(2):563–77. doi: 10.1148/radiol.2015151169

9. Ferro M, de Cobelli O, Musi G, Del Giudice F, Carrieri G, Busetto GM, et al. Radiomics in prostate cancer: An up-to-date review. *Ther Adv Urol* (2022) 4 (14):17562872221109020. doi: 10.1177/17562872221109020

10. Ferro M, de Cobelli O, Vartolomei MD, Lucarelli G, Crocetto F, Barone B, et al. Prostate cancer radiogenomics-from imaging to molecular characterization. *Int J Mol Sci* (2021) 22(18):9971. doi: 10.3390/ijms22189971

11. Norris JM, Simpson BS, Parry MA, Allen C, Ball R, Freeman A, et al. Genetic landscape of prostate cancer conspicuity on multiparametric magnetic resonance imaging: A systematic review and bioinformatic analysis. *Eur Urol Open Sci* (2020) 20:37–47. doi: 10.1016/j.euros.2020.06.006

12. Bodalal Z, Trebeschi S, Nguyen-Kim TDL, Schats W, Beets-Tan R. Radiogenomics: Bridging imaging and genomics. *Abdom Radiol* (2019) 44 (6):1960–84. doi: 10.1007/s00261-019-02028-w

13. Fischer S, Tahoun M, Klaan B, Thierfelder KM, Weber A, Krause BJ, et al. A radiogenomic approach for decoding molecular mechanisms underlying tumor progression in prostate cancer. *Cancers* (2019) 11(9):1293. doi: 10.3390/cancers11091293

14. Tan CH, Hobbs BP, Wei W, Kundra V. Dynamic con-trast-Enhanced MRI for the detection of prostate cancer: Meta-analysis. *Am J Roentgenol* (2015) 204:439–48. doi: 10.2214/AJR.14.13373

15. Augustin H, Fritz GA, Ehammer T, Auprich M, Pummer K. Accuracy of 3-Tesla magnetic resonance imaging for the staging of prostate cancer in comparison to the partin tables. *Acta Radiol* (2009) 50(5):562–9. doi: 10.1080/02841850902889846

16. Kobus T, Vos PC, Hambrock T, De Rooij M, Hulsbergen-Van de Kaa CA, Barentsz JO, et al. Prostate cancer aggressiveness: *In vivo* assessment of mr spectroscopy and diffusion-weighted imaging at 3 T. *Radiology* (2012) 265 (2):457–67. doi: 10.1148/radiol.12111744

17. Barentsz JO, Richenberg J, Clements R, Choyke P, Verma S, Villeirs G, et al. ESUR prostate MR guidelines 2012. *Eur Radiol* (2012) 22(4):746–57. doi: 10.1007/s00330-011-2377-y

18. Turkbey B, Merino MJ, Gallardo EC, Shah V, Aras O, Bernardo M, et al. Comparison of endorectal coil and nonendorectal coil T2W and diffusion-weighted MRI at 3 Tesla for localizing prostate cancer: Correlation with whole-mount histopathology. *J Magn Reson Imaging* (2014) 39(6):1443–8. doi: 10.1002/jmri.24317

19. Ammari S, Sallé de Chou R, Balleyguier C, Chouzenoux E, Touat M, Quillent A, et al. A predictive clinical-radiomics nomogram for survival prediction of glioblastoma using MRI. *Diagnostics (Basel)* (2021) 11(11):2043. doi: 10.3390/diagnostics11112043

20. Yu Y, Tan Y, Xie C, Hu Q, Ouyang J, Chen Y, et al. Development and validation of a preoperative magnetic resonance imaging radiomics-based signature to predict axillary lymph node metastasis and disease-free survival in patients with early-stage breast cancer. *JAMA Netw Open* (2020) 3(12):e2028086. doi: 10.1001/jamanetworkopen

21. He L, Li Z, Chen X, Huang Y, Yan L, Liang C, et al. A radiomics prognostic scoring system for predicting progression-free survival in patients with stage IV non-small cell lung cancer treated with platinum-based chemotherapy. *Chin J Cancer Res* (2021) 33:592–605. doi: 10.21147/j.issn.1000-9604.2021.05.06

22. Yao F, Ding J, Hu Z, Cai M, Liu J, Huang X, et al. Ultrasound-based radiomics score: A potential biomarker for the prediction of progression-free survival in ovarian epithelial cancer. *Abdom Radiol (NY)* (2021) 46(10):4936–45. doi: 10.1007/s00261-021-03163-z

23. Goh V, Sanghera B, Wellsted DM, Sundin J, Halligan S. Assessment of the spatial pattern of colorectal tumour perfusion estimated at perfusion CT using two-dimensional fractal analysis. *Eur Radiol* (2009) 19(6):1358–65. doi: 10.1007/s00330-009-1304-y

24. Skogen K, Ganeshan B, Good C, Critchley G, Miles K. Measurements of heterogeneity in gliomas on computed tomography relationship to tumour grade. *J Neurooncol* (2013) 111(2):213–9. doi: 10.1007/s11060-012-1010-5

25. Wibmer A, Hricak H, Gondo T, Matsumoto K, Veeraraghavan H, Fehr D, et al. Haralick texture analysis of prostate MRI: Utility for differentiating non-cancerous prostate from prostate cancer and differentiating prostate cancers with different Gleason scores. *Eur Radiol* (2015) 25(10):2840–50. doi: 10.1007/s00330-015-3701-8

26. Li M, Chen T, Zhao W, Wei C, Li X, Duan S, et al. Radiomics prediction model for the improved diagnosis of clinically significant prostate cancer on biparametric MRI. *Quant Imaging Med Surg* (2020) 10(2):368–79. doi: 10.21037/qims.2019.12.06

27. Toivonen J, Montoya Perez I, Movahedi P, Merisaari H, Pesola M, Taimen P, et al. Radiomics and machine learning of multisequence multiparametric prostate MRI: Towards improved non-invasive prostate cancer characterization. *PLoS One* (2019) 14(7):e0217702. doi: 10.1371/journal.pone.0217702

28. Chaddad A, Niazi T, Probst S, Bladou F, Anidjar M, Bahoric B. Predicting Gleason score of prostate cancer patients using radiomic analysis. *Front Oncol* (2018) 8:630. doi: 10.3389/fonc.2018.00630

29. Diaz M, Peabody JO, Kapoor V, Sammon J, Rogers CG, Stricker H, et al. Oncologic outcomes at 10 years following robotic radical prostatectomy. *Eur Urol* (2015) 67(6):1168–76. doi: 10.1016/j.eururo.2014.06.025

30. Gnep K, Fargeas A, Gutiérrez-Carvajal RE, Commandeur F, Mathieu R, Ospina JD, et al. Haralick textural features on T2 -weighted MRI are associated with biochemical recurrence following radiotherapy for peripheral zone prostate cancer. *J Magn Reson Imagin* (2017) 45(1):103–17. doi: 10.1002/jmri.25335

31. Freedland SJ, Presti JCJr, Kane CJ, Aronson WJ, Terris MK, Dorey F, et al. Do younger men have better biochemical outcomes after radical prostatectomy? *Urology* (2004) 63(3):518–22. doi: 10.1016/j.urology.2003.10.045

32. de Camargo Cancela M, Comber H, Sharp L. Age remains the major predictor of curative treatment non-receipt for localised prostate cancer: A population-based study. *Br J Cancer* (2013) 109(1):272–9. doi: 10.1038/bjc.2013.268

33. de Cobelli O, Terracciano D, Tagliabue E, Raimondi S, Bottero D, Cioffi A, et al. Predicting pathological features at radical prostatectomy in patients with prostate cancer eligible for active surveillance by multiparametric magnetic resonance imaging. *PLoS One* (2015) 10(10):e0139696. doi: 10.1371/journal.pone.0139696

34. Del Giudice F, Pecoraro M, Vargas HA, Cipollari S, De Berardinis E, Bicchetti M, et al. Systematic review and meta-analysis of vesical imaging-reporting and data system (VI-RADS) inter-observer reliability: An added value for muscle invasive bladder cancer detection. *Cancers (Basel)* (2020) 12(10):2994. doi: 10.3390/cancers12102994

35. Yu XY, Ren J, Jia Y, Wu H, Niu G, Liu A, et al. Multiparameter MRI radiomics model predicts preoperative peritoneal carcinomatosis in ovarian cancer. *Front Oncol* (2021) 21:765652(11). doi: 10.3389/fonc.2021.765652

frontiers | Frontiers in Oncology

TYPE Technology and Code
PUBLISHED 23 September 2022
DOI 10.3389/fonc.2022.992032

OPEN ACCESS

EDITED BY
Rulon Mayer,
University of Pennsylvania,
United States

REVIEWED BY
Biagio Barone,
University of Naples Federico II, Italy
Bogdan Geavlete,
St. John Hospital Emergency Clinic,
Romania

*CORRESPONDENCE
Xiao-Dong Liu
xdliu005@foxmail.com
Juan Hu
hujuan_1111@163.com

†These authors have contributed equally to this work and share first authorship

SPECIALTY SECTION
This article was submitted to Genitourinary Oncology, a section of the journal Frontiers in Oncology

RECEIVED 12 July 2022
ACCEPTED 15 August 2022
PUBLISHED 23 September 2022

CITATION
Lei Y, Li T-J, Gu P, Yang Y-k, Zhao L, Gao C, Hu J and Liu X-D (2022) Combining prostate-specific antigen density with prostate imaging reporting and data system score version 2.1 to improve detection of clinically significant prostate cancer: A retrospective study.
Front. Oncol. 12:992032.
doi: 10.3389/fonc.2022.992032

Combining prostate-specific antigen density with prostate imaging reporting and data system score version 2.1 to improve detection of clinically significant prostate cancer: A retrospective study

Yin Lei[1†], Tian Jie Li[2†], Peng Gu[3†], Yu kun Yang[4], Lei Zhao[5], Chao Gao[5], Juan Hu[5*] and Xiao Dong Liu[3*]

[1]Department of Urology, The First People's Hospital of Shuangliu District, Chengdu, China, [2]School of Clinical Medicine, Tsinghua University, Beijing, China, [3]Department of Urology, The First Affiliated Hospital of Kunming Medical University, Kunming, China, [4]Medical school, University of Electronic Science and Technology of China, Chengdu, China, [5]Medical Imaging Department, The First Affiliated Hospital of Kunming Medical University, Kunming, China

Globally, Prostate cancer (PCa) is the second most common cancer in the male population worldwide, but clinically significant prostate cancer (CSPCa) is more aggressive and causes to more deaths. The authors aimed to construct the risk category based on Prostate Imaging Reporting and Data System score version 2.1 (PI-RADS v2.1) in combination with Prostate-Specific Antigen Density (PSAD) to improve CSPCa detection and avoid unnecessary biopsy. Univariate and multivariate logistic regression and receiver-operating characteristic (ROC) curves were performed to compare the efficacy of the different predictors. The results revealed that PI-RADS v2.1 score and PSAD were independent predictors for CSPCa. Moreover, the combined factor shows a significantly higher predictive value than each single variable for the diagnosis of CSPCa. According to the risk stratification model constructed based on PI-RADS v2.1 score and PSAD, patients with PI-RADS v2.1 score of ≤2, or PI-RADS V2.1 score of 3 and PSA density of <0.15 ng/mL^2, can avoid unnecessary of prostate biopsy and does not miss clinically significant prostate cancer.

KEYWORDS

prostate biopsy, prostate cancer, prostate imaging reporting and data system score, prostate-specific antigen density (PSAD), clinically significant prostate cancer (csPCa)

Introduction

Prostate cancer (PCa) accounts for 13.5% of all cancer cases and 6.7% of all cancer deaths among males worldwide, ranking second and sixth for cancer incidence and mortality among men respectively (1). Most prostate cancers are not aggressive and represent little or no damage to the patient's health or life expectancy, despite the disease's high occurrence. Many will not be diagnosed with prostate cancer until an autopsy or screening is performed. Although there is no standardized definition of clinically significant prostate cancer, the disease has become more aggressive. However, clinically significant prostate cancer is an aggressive, fatal disease that causes death in some men; definite treatment is required. Prostate-specific antigen (PSA) testing is crucial for the diagnosis of prostate cancer, which has led to a decrease in disease-specific mortality and advanced disease during the previous two decades (2). Regrettably, PSA testing alone increased the detection of many clinically insignificant prostate cancer, which usually progress indolently and does not need any clinical intervention (3). Therefore, It is imperative to establish a non-invasive method to prevent over-diagnosis and eliminate unnecessary biopsies, while simultaneously identifying clinically significant prostate cancer as early as possible.

Multiparametric Magnetic Resonance Imaging (mpMRI) that combines T2-weighted imaging (T2WI) with functional pulse sequences such as dynamic contrast-enhanced (DCE) and/or diffusion-weighted imaging (DWI) imaging has demonstrated high application value in PCa diagnosis, local staging, and active surveillance. PI-RADS v2.1 was recommended to assess the likelihood of a clinically significant cancer of any lesion based on mpMRI in the prostate using a 5-level subjective score (4). A meta-analysis found that the median mpMRI negative predictive value (NPV) was 82.4% (IQR, 69.0–92.4%) for overall cancer and 88.1% (IQR, 85.7–92.3) for CSPCa (5). PRECISION trial (6) and PROMIS trial (7) demonstrated that the use of mpMRI to triage men prior to prostate biopsy could allow a quarter of men to avoid a primary biopsy and reduce the number of clinically insignificant cancer missed. The significance of PI-RADS point 3 for the diagnosis of PCa and CSPCa has, however, varied considerably between investigations (8, 9). The suspicious lesion concerns the presence of clinically relevant cancer was assigned PI-RADS point 3 per the standards. As a result, managing unclear or ambiguous PI-RADS 3 lesions has become difficult for doctors. To overcome these shortcomings and increase the consistency of physician assessments, the PI-RADS Steering Committee has revised PI-RADS v2 based on consensus (PI-RADS v2.1).Previous studies have validated the diagnostic performance of PI-RADS v2.0 score combined with PSAD in the detection of CSPCa. However, due to inconsistent methodology across different studies, heterogeneous outcomes were observed. In some studies, PI-RADS v2.0 scores were assessed based on 1.5T MRI machine, while the others were based on 3.0T machine (10), In addition, some studies apply MR protocol that only consists of T2WI and DWI, which is called bi-parametric MRI(bpMRI) does not precisely meet the requirements of PI-RADS v2.0 system (10). In contrast, the majority of studies lack follow-up information for patients whose biopsies were negative (11, 12). Consequently, the purpose of the current study is to further validate the performance of PI-RADS v2.1 score combined with PSAD in the detection of CSPCa, using a more accurate PI-RADS v2.1 score based on a 3.0T machine that includes T2WI, DWI, and DCE.

Materials and methods

Patients selection

We retrospectively reviewed a cohort including 422 patients who underwent mpMRI prior prostate biopsy and underwent their first prostate biopsy between January 2016 and January 2019 at the First Affiliated Hospital of Kunming Medical University. Inclusion criteria: 1. Patients with suspected prostate cancer found by a rectal exam, PSA, TRUS, MRI; 2. Patients willing to undergo prostate puncture biopsy. The exclusive criteria were as follows: 1) lack of any T2WI, DWI and DCE; 2) lack of histopathological results or clinical information, including age, PSA, fPSA and MRI-measured prostate volume; 3) the previous history of prostate surgery; 4) received 5α reductase inhibitors; 5) lost to follow-up.

MRI

All mpMRI scans of the prostate were performed with 3.0T MR scanner (Achieva, Philips/Discovery MR W750, GE), which involved axial T2WI, DWI, and DCE. The Apparent Diffusion Coefficient (ADC) map was automatically calculated. And the locations of these axial sequences were exactly matched. PI-RADS score of each case was graded separately according to the PI-RADS v2.1 criteria by two independent radiologists (R1, R2) blinded to the clinical information and pathological outcomes. If scores were inconsistent, the final PI-RADS scores were determined through a discussion between two radiologists. The volume of the prostate was measured according to the PI-RADS v2.1 criteria based on mpMRI: ([maximum anteroposterior {AP} diameter] X [maximum transverse diameter] X [maximum longitudinal diameter] X 0.52), the maximum AP and longitudinal diameters are placed on the midsagittal T2W image, while the maximum transverse diameter is placed on the axial T2W image. And the TNM

staging of prostate cancer was determined mainly based on mpMRI by the radiologist(R2).

Prostate biopsy and pathological analysis

The indications of prostate biopsy and repeated biopsy were performed in accordance with the Chinese Urology Association Guidelines and European Association of Urology Guidelines. In all patients, 12-core systematic transrectal ultrasound-guided prostate biopsies were performed by urinary specialists with more than 10 years of experience, and two cognitive fusion-targeted biopsy cores were added for each lesion based on mpMRI findings.

The final pathological results of this study are subject to biopsy and follow-up results. Patients who received negative results in their initial biopsies were followed up on, which included repeat biopsy results, surgical therapy results, MRI results, and PSA results. Clinically significant prostate cancer was defined as Gleason score≥3+4 or ≥T3 staging (extracapsular extension). Clinically insignificant prostate cancer was defined as Gleason score<3+4 or ≤T2 staging.

Statistical analysis

For normally and non-normally distributed data, the mean (standard deviation [SD]) and the median (interquartile range [IQR]) will be used. To assess between-group differences in normally and non-normally distributed data, the Student t-test and Mann-Whitney U-test were used. Categorical variables were represented as percentages, and chi-square test was used to assess between-group differences. The area under the curve (AUC) was used to assess the accuracy of the receiver operating curves (ROC) for factors evaluated for the risk of PCa and CSPCa. PSAD was divided into four subgroups based on the appropriate PSAD cut-off points for detecting PCa and CSPCa and recognizing outliers, and the risk category for CSPCa was constructed using PI-RADS V2.1 scores and PSA subgroups.

P value less than 0.05 was considered to indicate a statistically significant. SPSS software was used to conduct all analyses (Version 20.0. IBM).

Results

Patients data

The Profiles of 422 patients were analyzed. As stated in Table 1, the mean age was 68.50 ± 7.44 years. The median values for [interquartile range (IQR)] tPSA, f/tPSA, PV and PSAD were, 14.20(8.24~37.18) ng/mL, 0.15(0.11~0.22), 56.69 (37.70~77.08) ml, and 0.27(0.15~0.76) ng/ml^2, respectively.

TABLE 1 Patients' characteristics.

Variables	Value
Median (IQR)	
tPSA(ng/ml)	14.21(8.25~37.90)
f/tPSA	0.15(0.11~0.21)
PV (ml)	54.66(37.31~74.98)
PSAD (ng/ml^2)	0.27(0.15~0.77)
Mean ± SD	
Age (years)	68.49 ± 7.47
N (%)	
PI-RADS v2 score	
1-2	167(39.6%)
3	**53(12.6%)**
4	**67(15.8%)**
5	**135(32.0%)**

The number of PI-RADS V2.1 score 1-2, 3, 4, 5 were 167, 53, 67, 135, respectively.

Pathological outcomes

The flow chart of pathological outcomes is depicted in Figure 1. 194 patients were confirmed with positive outcomes from the initial biopsy, of which 149 patients were diagnosed with CSPCa. In the meantime, 228 patients were diagnosed with BPH in their initial biopsy and would be followed up; of which 29 patients underwent a repeat biopsy and 2 of them were diagnosed with PCa, including 1 CSPCa; 123 patients underwent TURP or HOLEP, and 2 patients of them were diagnosed with CISPCa; and 11 patients who underwent both biopsy and TURP were diagnosed with BPH. Regular monitoring of PSA, MRI, and transrectal ultrasound, if needed, demonstrated the absence of disease development for 85 patients. Finally, the pathological results for benign prostate hyperplasia (BPH), PCa, and CSPCa were 221(53.1%), 201 (46.9%), and 150(35.5%), respectively.

Group analysis

First of all, we divide all patients into groups based on the following criteria, 1) BPH group and PCa group according to their pathological results, 2) CSPCa group and non-CSPCa group (including CISPCa and BPH patients) according to whether the pathological outcome is CSPCa. Then we analyzed the differences of risk factors by groups described above, 1) BPH group and PCa group, 2) CSPCa group and non-CSPCa group.

As shown in Table 2, the BPH group and the PCa group contained 224 and 198 patients respectively. While the CSPCa group and non-CSPCa group contained 150 and 272 patients

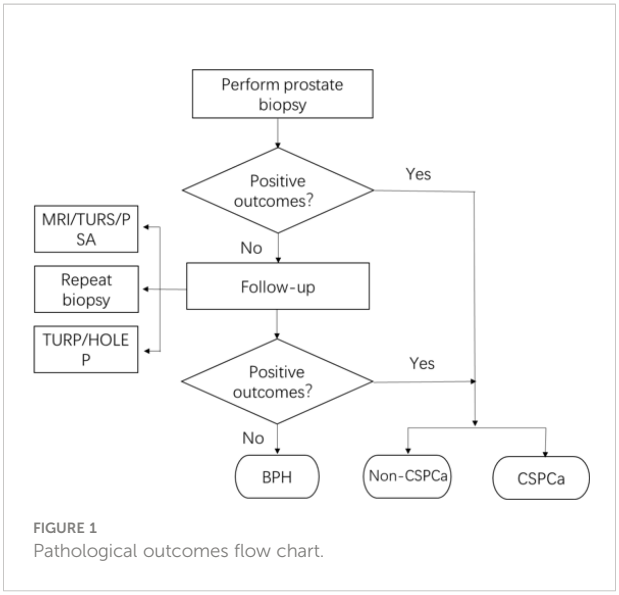

FIGURE 1
Pathological outcomes flow chart.

respectively. Intriguingly, we discovered that biopsy results were significantly correlated with age, PSA, PV, PSAD, and MRI findings (all $p < 0.05$, Table 2) between CSPCa and non-CSPCa group, as well as BPH and PCa group.

Efficiency of risk factors in the diagnosis of PCa and CSPCa

Then, we aimed to identify PCa and CSPCa-associated risk variables. As shown in Table 3, the AUC values of PI-RADS v2.1 score and PSAD were 0.91 and 0.84, 0.95 and 0.89 for PCa and CSPCa, respectively, which was greater than all other factors (P<0.05). Then we determined that PI-RADS v2.1 score 4 as the cut-off point for distinguishing PCa and CSPCa, and 0.38 and 0.65 as the cut-off of PSAD for diagnosing PCa and CSPCa, respectively. Finally, the cutoff for PI-RADS v2.1 score and PSAD were selected for the prediction models, which were constructed for discriminating PCa and CSPCa. Consequently, the AUC of the prediction model consists of PI-RADS v2.1 score and PSAD was higher for PCa and CSPCa in comparison to PI-RADS v2.1 score and PSAD alone (Table 3).

Construction of a multivariate risk category to predict CSPCa

For further analysis, we divided PSAD into four subgroups based on the study-confirmed cutoff point(0.38, 0.65) and widely accepted threshold (0.15) (Table 6). The examination of multivariate logistic regression indicated that PI-RADS v2 score and PSAD were independent predictors of CSPCa. Further analysis revealed no significant difference was observed for CSPCa for PI-RADS v2.1 score 2 and 3 (Table 4).

Next, we attempted to validate our findings about CSPCa prediction. As indicated in Table 5, patients with a PI-RADS v2.1 score of 2 were negative for CSPCa, while 53 patients with a PI-RADS v2.1 score of 3 were diagnosed with CSPCa. Moreover, only 2 out of 108 individuals with a PSAD of 0.15 ng/mL2 were proven to have CSPCa. Therefore, we developed a risk category for CSPCa based on the combined PI-RADS v2.1 score of PSAD subgroups.

As demonstrated in Table 6, we confirmed that PI-RADS v2 score of ≥4, or a PI-RADS v2 score of 3, and a PSAD≥0.65 ng/mL^2 (red zones) as the high-risk group, with the highest CSPCa detection rate (72.1%). In contrast, a PI-RADS v2 score of 2, or a PI-RADS v2 score of 3 with PSAD of ≤0.15 ng/mL^2 (green zones), were assigned as the low-risk group in which no CSPCa was detected. Others (blue zones) with a 10.3% detection rate for CSPCa were assigned as the moderate-risk group. The detection rates for PCa in patients assigned with low-, moderate-, and high-risk prostate cancer were 9.0%, 37.9%, and 83.3%, respectively.

TABLE 2 Univariate analysis of the Clinical Characteristics in the different groups.

Variables	Group 1			Group 2		*P* value
	PCa	BPH	*P* value	CSPCa	Non-CSPCa	
patients	198(46.9%)	224(53.1%)	–	150(35.5%)	172(64.5%)	–
Age	69.85 ± 7.35	67.29 ± 7.38	*P*<0.001[1)]	69.45 ± 7.36	67.69 ± 7.49	*P*<0.001[1)]
tPSA (ng/ml)	34.85(12.37~100.00)	10.36(6.85~16.07)	*P*<0.001[2)]	71.85(17.88~100.00)	10.76(7.18~16.72)	*P*<0.001[2)]
f/tPSA	0.15(0.10~0.24)	0.15(0.11~0.19)	*P*=0.54[2)]	0.16(0.09~0.26)	0.15(0.11~0.20)	*P*=0.527[2)]
PV (ml)	48.40(32.31~66.97)	60.52(44.03~85.85)	*P*=0.003[1)]	49.29(32.31~66.97)	57.74(42.56~85.55)	*P*=0.036[1)]
PSAD (ng/ml2)	0.76(0.29~1.46)	0.17(0.12~0.28)	*P*<0.001[2)]	1.01(0.43~1.71)	0.18(0.12~0.29)	*P*<0.001[2)]
MRI (%)			*P*<0.001[3)]			*P*<0.0013)
positive	187	68		150	14	
negative	11	156		0	34	

PCa, prostate cancer; CSPCa, clinically significant prostate cancer; PSA, prostate-specific antigen; f/tPSA, the ratio of free to total prostate specific antigen; PV, prostate volume; PSAD PSA density.

TABLE 3 Diagnostic performance of risk factors for PCa and CSPCa.

Variable	PCa						CSPCa					
	AUC	SEN	SPE	PPV	NPV	Cut-off	AUC	SEN	SPE	PPV	NPV	Cut-off
PI-RADS v2 score	0.91	85.4	85.3	83.7	86.8	4	0.95	97.3	79.4	72.3	98.2	4
PSAD	0.84	68.2	87.5	56.4	80.6	0.38	0.89	70.0	94.9	88.2	85.1	0.65
PSA	0.79	57.1	89.3	82.5	70.2	24.0	0.85	68.0	91.5	91.6	83.8	31.2
f/tPSA	0.52	16.7	98.7	91.7	57.3	0.33	0.52	20.0	97.8	83.3	68.9	0.33
PV	0.62	54.0	65.6	58.1	61.8	50.1	0.59	42.7	73.2	46.7	69.8	43.4
age	0.59	48.0	66.5	55.9	59.1	70	0.55	47.3	63.6	41.8	68.6	70
PI-RADS +PSAD	0.93	90.4	80.8	80.6	90.5	–	0.97	92.7	87.9	80.8	95.6	–

PCa, prostate cancer; CSPCa, clinically significant prostate cancer; CISPCa, clinically insignificant prostate cancer; PSA, prostate-specific antigen; f/tPSA, the ratio of free to total prostate specific antigen; PV, prostate volume; PSAD, PSA density; AUC, area under of curve; SEN, sensitivity; SPE, specificity; PPV, positive predictive value; NPV, negative predictive value.

Discussion

The previous report in China (44%, 6123/13904), as published by 33 member hospitals of the Chinese Prostate Cancer Consortium (CPCC) (13). We enrolled 422 patients in our trial for a minimum of 14 months follow-up, and we discovered the same outcome. 53.1 percent (224/422) of patients were diagnosed with benign lesions (prostatic hyperplasia, prostatitis, etc.), while 46.9 percent (198/422) were diagnosed with PCa.

Since the release of PI-RADS V2 based on mpMRI, PI-RADS v2.0 has been widely recognized in radiology and urology, as well as clinical practice. Its clinical value and practicability have been extensively validated. Current studies have also shown that PI-RADS V2.1 has excellent performance in predicting PCa, particularly for CSPCa (14–17), with an even higher accuracy over systematic TRUS biopsies for PCa diagnosis (6, 7, 18). In this study, PI-RADS v2.1 score was an independent predictor for PCa with excellent diagnostic performance, the AUC was 0.9108 with PI-RADS v2.1 score 4 as the cut-off. The sensitivity, specificity, PPV and NPV were 85.4%, 85.3%, 83.7% and 86.8%, respectively.

For CSPCa, We defined clinically significant prostate cancer as Gleason score≥3+4 or ≥T3 staging (extracapsular extension). PI-RADS v2.1 has improved diagnostic accuracy. The AUC was 0.95 with PI-RADS v2.1 score 4 as the cut-off, and NPV was up to 98.2%. A high NPV can help minimize unnecessary prostate biopsies and their associated problems.

Although the PI-RADS score had an advantage in predicting CsPCa in this study, PI-RADS V2.1 of 4 score has s NPV up to 98.2% for CSPCa, If the biopsy was carried on a PI-RADS score = 3, 7.5% (4/53) of CsPCa patients would be omitted; however, if set at a PI-RADS score≥3, 19.2% (49/255) of patients would receive an unnecessary biopsy. Overtreatment of inactive prostate cancer diminishes the quality of life, but the delayed treatment of more aggressive CSPCa increases the incidence of metastatic illness and mortality. Therefore, a decision to puncture the prostate based exclusively on PI-RADS V2.1 is not recommended.

In this study, prostate volume was measured using 3T MRI, and PSAD was then calculated. PSAD demonstrated outstanding diagnostic performance for PCa and CSPCa when utilizing the cut-off values of 0.38 and 0.65, with AUC values of 0.84 and 0.89, respectively. This study's PSAD cutoff value was much higher than 0.15, which may be a result of the population's generally high PSA levels (median 14.21 ng/ml). The PI-RADS v2.1score and PSAD were independent predictors of CSPCa, according to

TABLE 4 The multivariate logistic regression analysis of PI-RADS v2 score and PSAD for CSPCa.

Variables	OR	95%CI	*P* value
PSAD (ng/ml^2)			–
<0.15	–	–	P<0.001
~0.38	0.060	0.016~0.223	P<0.001
~0.65	0.126	0.050~0.321	P<0.001
≥0.65	0.320	0.104~0.983	P<0.001
PI-RADS V2 score			
2	–	–	–
3	0	0	P=0.994
4	0.029	0.009~0.100	P<0.001
5	0.148	0.065~0.336	P<0.001

PIRADS v2 prostate imaging-reporting and data system version 2; PSAD, PSA density; OR, odds ratio; CI, confidence interval.

TABLE 5 Detection of PSAD subgroups and PI-RADS v2 score for PCa and CSPCa.

Outcomes	PSAD subgroups				PI-RADS v2 score			
	<0.15	~0.38	~0.65	≥0.65	1-2	3	4	5
patients	108	150	44	120	167	53	67	135
PCa(n, %)	21(20.9)	42(28.0)	26(59.1)	109(90.8)	11(6.6)	18(34.0)	44(65.7)	125(92.6)
CSPCa(n, %)	7(3.6)	25(16.7)	13(29.5)	105(87.5)	0(0)	4(7.5)	26(38.8)	120(88.9)

PCa, prostate cancer; CSPCa, clinically significant prostate cancer; PIRADS v2, prostate imaging-reporting and data system version 2; PSAD, PSA density.

multivariate logistic regression analysis. According to a prior study, PSAD not only predicts the results of prostate biopsy but also is a predictor for CSPCa. Kosaka et al. reported that PSAD could become a useful predictor of significant PCa in men aged ≤ 50 (19). According to a number of studies, higher PSAD is an important independent predictor of pathological upgrade between prostate biopsy and radical prostatectomy (20–23), and PSAD derived from MRI shows a more significant correlation with CSPCa compared with using TRUS (24). So, PI-RADS v2.1 score and PSAD were applied as risk factors in the prediction models for CSPCa. We reported that the diagnostic performance of the model was significantly better than each single variable ($p < 0.05$). Despite the paucity of studies employing PI-RADS v2.1 score combined PSAD, outcomes from studies employing PI-RADS v2.0 score combined PSAD have been inconsistent. Several studies have shown that PI-RADS v2.0 score combined with PSAD as a screening tool had a higher predictive value for CSPCa (11, 12, 21, 25). Using the PI-RADS v2.1 score combined with PSAD as a screening tool for CSPCa, our study demonstrated a better predictive effect. However, Cuocolo et al. found that PSAD combined PI-RADS v2.0 score did not show a significant improvement in the diagnostic performance (26).

In this study, if the PI-RADS v2.1 score of 3 was the recommended threshold for biopsy, 19.2% of patients would have received an unnecessary biopsy. The specificity was fair low. Although the calculators reported were useful for predicting CSPCa (27), they are not convenient and practical for clinicians. As a result, we divided PSAD into four subgroups based on the cut-off points for PCa and CSPCa identified in this study (0.38, 0.65) and accepted threshold (0.15), and then combined them with PI-RADS v2.1 scores to constructed the risk category of CSPCa. The absence of CSPCa in the low-risk group suggests that 44.8 percent (189/422) of patients might have avoided unnecessary biopsies, and CSPCa would not have been missed. Furthermore, for high-risk patients who got negative results in the first biopsy, risk stratification could help to formulate a follow-up strategy.

Washino's research (10) had confirmed that a combination of PI-RADS v2 score and PSA density can assist with prostate biopsy decision-making. The most significant difference between our study and theirs was the replacement of PI-RADS 2.0 with PI-RADS V2.1. Correspondingly, the calculation method of prostate volume has also changed. As an improved version, PI-RADS V2.1 is more accurate than PI-RADS V2.0 in diagnosing CSPCa, according to our research. Moreover, there were less PI-RADS scores of 3 in our study than in Washino's (42.0%, 122/20 vs. 12.0%, 53/422), which was regarded as the probability of CSPCa being uncertain, making its diagnosis extremely difficult. Second, compared to Washino's research10, which merely classified PSAD subgroups based on a simple multiple relationship of 0.15ng/ml2, our study is more detailed. Our research established more subgroups and performed more thorough risk classification. Thirdly, our analysis comprised a bigger sample size and tracked individuals with a negative first biopsy for up to two years. Overall, our study was one of the few to evaluate the effectiveness of the combined PI-RADS V2.1 and PSAD scores in predicting biopsy outcomes. Our research not only supports prior findings but also serves as a foundation for future studies.

Additionally, certain studies are useful as clinical references. In patients with PSA levels between 4 and 10 ng/mL, the combination of PI-RADS v2.0 and PSAD has been demonstrated to improve the

TABLE 6 Risk category of CSPCa.

		PI-RADS v2 score			
		1-2	3	4	5
PSAD	<0.15	0 (0/72)	0 (0/22)	28.6% (2/7)	71.4% (5/7)
	~0.38	0 (0/77)	15% (3/20)	30.3% (10/33)	60.0% (12/20)
	~0.65	0 (0/10)	0 (0/9)	25.0% (3/12)	76.9% (10/13)
	≥0.65	0 (0/8)	50.0% (1/2)	73.3% (11/15)	97.9% (93/95)

Red, green and blue zones indicate high-, moderate- and low-risk groups, respectively. The detection rates for PCa in patients assigned with low-, moderate-, and high-risk prostate cancer were 9.0%, 37.9% and 83.3%, respectively.

predictive value of CSPCa and reduce the number of unnecessary biopsies (28, 29). In addition, the combination also improves predictive value of CSPCa in targeted prostate biopsy and reduce unnecessary biopsies (12, 30, 31).

We did not include multiple CSPCa definitions in the meta-analysis due to the substantial variability in NPV that was caused by the various definitions. Consequently, this would have brought unacceptable clinical heterogeneity into the data, possibly leading to erroneous and biased estimations. Last but not least, various factors, such as racial differences radiologists' experience (32), etc., influence the outcomes of different studies.

There are several limitations in this study that need to be noted. First of all, it is a retrospective single-center study, and prospective validation is lacking because of insufficient follow-up time. Second, although the previous study has shown that MRI/US cognitive fusion-targeted biopsies(COG-TB) are superior to systemic biopsies in detecting PCa (33), MRI/US COG-TB also exists false negative, which may result in possible bias (34, 35). Third, our outcomes were assigned according to biopsy-proven Gleason score and mpMRI-proven T staging, which deviates from the pathology results after radical prostatectomy.

Conclusion

In the present study, PSAD and PI-RADS v2.1 scores demonstrated more predictive value than tPSA, f/tPSA, PV, and age. We utilized the PI-RADS v2.1 score and PSAD as jointed factors to diagnose PCa and CSPCa, which displayed significantly greater predictive value. In the risk category we constructed, patients with PI-RADS v2.1 score of ≤2, or PI-RADS v2.1 score of 3 and PSA density of <0.15 ng/mL^2, could avoid unnecessary prostate biopsy without missing clinically significant prostate cancer. In conclusion, our study offers a novel predictive risk category to improve the diagnosis of CSPCa while preventing unnecessary biopsies for clinicians.

Data availability statement

The original contributions presented in the study are included in the article/supplementary material. Further inquiries can be directed to the corresponding authors.

Authors contributions

X-DL and JH designed the study and provided funding acquisition. YL, T-JL, and PG conducted the initial retrospective analysis, participated in the study, analyzed the data, and prepared the initial manuscript, collected clinical data and performed patients followed-up. Y-KY, CG, and LZ measured the prostate volume and calculated the PI-RADS v2.1 score. All authors contributed to the article and approved the submitted version.

Funding

This study was supported by the National Natural Science Foundation of China (Grant No. 81802548, 81860451), Yunnan Health Training Project of High Level Talents (for Peng Gu, Grant No. H2018070), Provincial Natural Science Foundation of Yunnan-Kunming Medical University Joint Foundation (Grant No. 2019FE001-136), and Scientific Research Project of Yunnan Provincial Educational Department (Grant No. 2018JS208). Funding for young doctors (for Peng Gu), from the 1st Affiliated Hospital of Kunming Medical University (Grant No. 2017BS016). Supported by Priority Union Foundation of Yunnan Provincial Science and Technology Department and Kunming Medical University 2017FE467 (-136).

Conflict of interest

The authors declare that the research was conducted in the absence of any commercial or financial relationships that could be construed as a potential conflict of interest.

Publisher's note

References

1. Bray F, Ferlay J, Soerjomataram I, Siegel RL, Torre LA, Jemal A. Cancer statistics 2018: GLOBOCAN estimates of incidence and mortality worldwide for 36 cancers in 185 countries. *CA Cancer J Clin* (2018) 68(6):394–424. doi: 10.3322/caac.21492

2. From the American Association of Neurological Surgeons (AANS), American Society of Neuroradiology (ASNR), Cardiovascular and Interventional Radiology Society of Europe (CIRSE), Canadian Interventional Radiology Association (CIRA), Congress of Neurological Surgeons (CNS) and European Society of Minimally Invasive Neurological Therapy (ESMINT), et al. Multisociety consensus quality improvement revised consensus statement for endovascular therapy of acute ischemic stroke. *Int J Stroke* (2018) 13(6):612–32. doi: 10.1177/1747493018778713

3. Loeb S, Bjurlin MA, Nicholson J, Tammela TL, Penson DF, Carter HB, et al. Overdiagnosis and overtreatment of prostate cancer. *Eur Urol* (2014) 65(6):1046–55. doi: 10.1016/j.eururo.2013.12.062

4. Weinreb JC, Barentsz JO, Choyke PL, Cornud F, Haider MA, Macura KJ, et al. PI-RADS prostate imaging–reporting and data system: 2015, version 2. *Eur Urol* (2016) 69(1):16–40. doi: 10.1016/j.eururo.2015.08.052

5. Moldovan PC, Van den Broeck T, Sylvester R, Marconi L, Bellmunt J, van den Bergh RCN, et al. What is the negative predictive value of multiparametric magnetic resonance imaging in excluding prostate cancer at biopsy? A systematic review and meta-analysis from the European association of urology prostate cancer guidelines panel. *Eur Urol* (2017) 72(2):250–66. doi: 10.1016/j.eururo.2017.02.026

6. Kasivisvanathan V, Rannikko AS, Borghi M, Panebianco V, Mynderse LA, Vaarala MH, et al. MRI-Targeted or standard biopsy for prostate-cancer diagnosis. *New Engl J Med* (2018) 378(19):1767–77. doi: 10.1056/NEJMoa1801993

7. Ahmed HU, Bosaily AE-S, Brown LC, Gabe R, Kaplan R, Parmar MK, et al. Diagnostic accuracy of multi-parametric MRI and TRUS biopsy in prostate cancer (PROMIS): A paired validating confirmatory study. *Lancet* (2017) 389(10071):815–22. doi: 10.1016/S0140-6736(16)32401-1

8. Washino S, Okochi T, Saito K, Konishi T, Hirai M, Kobayashi Y, et al. Combination of prostate imaging reporting and data system (PI-RADS) score and prostate-specific antigen (PSA) density predicts biopsy outcome in prostate biopsy naïve patients. *BJU Int* (2017) 119(2):225–33. doi: 10.1111/bju.13465

9. Zhang Y, Zeng N, Zhu YC, Huang YXR, Guo Q, Tian Y. Development and internal validation of PI-RADs v2-based model for clinically significant prostate cancer. *World J Surg Oncol* (2018) 16(1):102. doi: 10.1186/s12957-018-1367-9

10. Jordan EJ, Fiske C, Zagoria RJ, Westphalen AC. Evaluating the performance of PI-RADS v2 in the non-academic setting. *Abdominal Radiol* (2017) 42:2725–31. doi: 10.1007/s00261-017-1169-5

11. Chen R, Xie L-P, Zhou L-Q, Huang Y-R, Fu Q, He D, et al. Current status of prostate biopsy in Chinese prostate cancer consortium member hospitals. *Chin J Urol* (2015) 36:342–5.

12. van der Leest M, Cornel E, Israel B, Hendriks R, Padhani AR, Hoogenboom M, et al. Head-to-head comparison of transrectal ultrasound-guided prostate biopsy versus multiparametric prostate resonance imaging with subsequent magnetic resonance-guided biopsy in biopsy-naïve men with elevated prostate-specific antigen: A large prospective multicenter clinical study. *Eur Urol* (2019) 75(4):570–8. doi: 10.1016/j.eururo.2018.11.023

13. Cash H, Maxeiner A, Stephan C, Fischer T, Durmus T, Holzmann J, et al. The detection of significant prostate cancer is correlated with the prostate imaging reporting and data system (PI-RADS) in MRI/transrectal ultrasound fusion biopsy. *World J Urol* (2016) 34(4):525–32. doi: 10.1007/s00345-015-1671-8

14. Zhang L, Tang M, Chen S, Lei X, Zhang X, Huan Y. A meta-analysis of use of prostate imaging reporting and data system version 2 (PI-RADS V2) with multiparametric MR imaging for the detection of prostate cancer. *Eur Radiol* (2017) 27(12):5204–14. doi: 10.1007/s00330-017-4843-7

15. Kasel-Seibert M, Lehmann T, Aschenbach R, Guettler FV, Abubrig M, Grimm MO, et al. Assessment of PI-RADS v2 for the detection of prostate cancer. *Eur J Radiol* (2016) 85(4):726–31. doi: 10.1016/j.ejrad.2016.01.011

16. Padhani AR, Weinreb J, Rosenkrantz AB, Villeirs G, Turkbey B, Barentsz J. Prostate imaging-reporting and data system steering committee: PI-RADS v2 status update and future directions. *Eur Urol* (2019) 75(3):385–96. doi: 10.1016/j.eururo.2018.05.035

17. Kosaka T, Mizuno R, Shinojima T, Miyajima A, Kikuchi E, Tanaka N, et al. The implications of prostate-specific antigen density to predict clinically significant prostate cancer in men≤ 50 years. *Am J Clin Exp Urol* (2014) 2(4):332–6.

18. Corcoran NM, Casey RG, Hong MK, Pedersen J, Connolly S, Peters J, et al. The ability of prostate-specific antigen (PSA) density to predict an upgrade in Gleason score between initial prostate biopsy and prostatectomy diminishes with increasing tumour grade due to reduced PSA secretion per unit tumour volume. *Bju Int* (2012) 110(1):36–42. doi: 10.1111/j.1464-410X.2011.10681.x

19. Tsang CF, Lai TCT, Lam W, Ho BSH, Ng ATL, Ma WK, et al. Is prostate specific antigen (PSA) density necessary in selecting prostate cancer patients for active surveillance and what should be the cutoff in the Asian population? *Prostate Int* (2019) 7(2):73–7. doi: 10.1016/j.prnil.2018.03.002

20. Oh JJ, Hong SK, Lee JK, Lee BK, Lee S, Kwon OS, et al. Prostate-specific antigen vs prostate-specific antigen density as a predictor of upgrading in men diagnosed with Gleason 6 prostate cancer by contemporary multicore prostate biopsy. *BJU Int* (2012) 110(11 Pt B):E494–E9. doi: 10.1111/j.1464-410X.2012.11182.x

21. Ha Y-S, Yu J, Salmasi AH, Patel N, Parihar J, Singer EA, et al. Prostate-specific antigen density toward a better cutoff to identify better candidates for active surveillance. *Urology* (2014) 84(2):365–72. doi: 10.1016/j.urology.2014.02.038

22. Karademir I, Shen D, Peng Y, Liao S, Jiang Y, Yousuf A, et al. Prostate volumes derived from MRI and volume-adjusted serum prostate-specific antigen: Correlation with Gleason score of prostate cancer. *Am J Roentgenol* (2013) 201(5):1041–8. doi: 10.2214/AJR.13.10591

23. Wang H, Tai S, Zhang L, Zhou J, Liang C. A calculator based on prostate imaging reporting and data system version 2 (PI-RADS V2) is a promising prostate cancer predictor. *Sci Rep* (2019) 9:1–8. doi: 10.1038/s41598-019-43427-9

24. Cuocolo R, Stanzione A, Rusconi G, Petretta M, Ponsiglione A, Fusco F, et al. PSA-density does not improve bi-parametric prostate MR detection of prostate cancer in a biopsy naïve patient population. *Eur J Radiol* (2018) 104:64–70. doi: 10.1016/j.ejrad.2018.05.004

25. Roobol MJ, Steyerberg EW, Kranse R, Wolters T, van den Bergh RC, Bangma CH, et al. A risk-based strategy improves prostate-specific antigen–driven detection of prostate cancer. *Eur Urol* (2010) 57:79–85. doi: 10.1016/j.eururo.2009.08.025

26. Liu C, Liu S-L, Wang Z-X, Yu K, Feng C-X, Ke Z, et al. Using the prostate imaging reporting and data system version 2 (PI-RIDS v2) to detect prostate cancer can prevent unnecessary biopsies and invasive treatment. *Asian J androl* (2018) 20(5):459–64. doi: 10.4103/aja.aja_19_18

27. Qi Y, Zhang S, Wei J, Zhang G, Lei J, Yan W, et al. Multiparametric MRI-based radiomics for prostate cancer screening with PSA in 4–10 ng/mL to reduce unnecessary biopsies. *J Magnetic Resonance Imaging* (2020) 51(6):1890–9. doi: 10.1002/jmri.27008

28. Liu J, Dong B, Qu W, Wang J, Xu Y, Yu S, et al. Using clinical parameters to predict prostate cancer and reduce the unnecessary biopsy among patients with pSA in the gray zone. *Sci Rep* (2020) 10(1):5157. doi: 10.1038/s41598-020-62015-w

29. Distler FA, Radtke JP, Bonekamp D, Kesch C, Schlemmer H-P, Wieczorek K, et al. The value of PSA density in combination with PI-RADS™ for the accuracy of prostate cancer prediction. *J Urol* (2017) 198(3):575–82. doi: 10.1016/j.juro.2017.03.130

30. Glazer DI, Mayo-Smith WW, Sainani NI, Sadow CA, Vangel MG, Tempany CM, et al. Interreader agreement of prostate imaging reporting and data system version 2 using an in-bore MRI-guided prostate biopsy cohort: A single institution's initial experience. *Am J Roentgenol* (2017) 209(3):W145–W51. doi: 10.2214/AJR.16.17551

31. Puech P, Rouvière O, Renard-Penna R, Villers A, Devos P, Colombel M, et al. Prostate cancer diagnosis: multiparametric MR-targeted biopsy with cognitive and transrectal US–MR fusion guidance versus systematic biopsy–prospective multicenter study. *Radiology* (2013) 268(2):461–9. doi: 10.1148/radiol.13121501

32. Nafie S, Wanis M, Khan M. The efficacy of transrectal ultrasound guided biopsy versus transperineal template biopsy of the prostate in diagnosing prostate cancer in men with previous negative transrectal ultrasound guided biopsy. *Urol J* (2017) 14(2):3008–12.

33. Moore CM, Robertson NL, Arsanious N, Middleton T, Villers A, Klotz L, et al. Image-guided prostate biopsy using magnetic resonance imaging–derived targets: a systematic review. *Eur Urol* (2013) 63(1):125–40. doi: 10.1016/j.eururo.2012.06.004

34. Schoots IG. MRI In early prostate cancer detection: how to manage indeterminate or equivocal PI-RADS 3 lesions? *Trans androl Urol* (2018) 7:70. doi: 10.21037/tau.2017.12.31

35. Mertan FV, Greer MD, Shih JH, George AK, Kongnyuy M, Muthigi A, et al. Prospective evaluation of the prostate imaging reporting and data system version 2 for prostate cancer detection. *J Urol* (2016) 196(3):690–6. doi: 10.1016/j.juro.2016.04.057

frontiers | Frontiers in Oncology

TYPE Original Research
PUBLISHED 16 November 2022
DOI 10.3389/fonc.2022.1024204

OPEN ACCESS

EDITED BY
Rulon Mayer,
University of Pennsylvania,
United States

REVIEWED BY
Angelo Porreca,
Veneto Institute of Oncology (IRCCS),
Italy
Jianbo Li,
Case Western Reserve University,
United States

*CORRESPONDENCE
Jun Xiao
anhuiurology@126.com
Tao Tao
taotao_urology@ustc.edu.cn

SPECIALTY SECTION
This article was submitted to Genitourinary Oncology, a section of the journal Frontiers in Oncology

RECEIVED 21 August 2022
ACCEPTED 20 October 2022
PUBLISHED 16 November 2022

CITATION
Wang C, Yuan L, Shen D, Zhang B, Wu B, Zhang P, Xiao J and Tao T (2022) Combination of PI-RADS score and PSAD can improve the diagnostic accuracy of prostate cancer and reduce unnecessary prostate biopsies. *Front. Oncol.* 12:1024204. doi: 10.3389/fonc.2022.1024204

Combination of PI-RADS score and PSAD can improve the diagnostic accuracy of prostate cancer and reduce unnecessary prostate biopsies

Changming Wang[1], Lei Yuan[2], Deyun Shen[1], Bin Zhang[3], Baorui Wu[1], Panrui Zhang[4], Jun Xiao[1,3]* and Tao Tao[1]*

[1]Department of Urology, The First Affiliated Hospital of USTC of China, Division of Life Sciences and Medicine, University of Science and Technology of China, Hefei, China, [2]Department of Radiology, The First Affiliated Hospital of USTC, Division of Life Sciences and Medicine, University of Science and Technology of China, Hefei, China, [3]Department of Urology, Affiliated Anhui Provincial Hospital of Anhui Medical University, Hefei, China, [4]Hefei National Laboratory for Physical Sciences at Microscale, The CAS Key Laboratory of Innate Immunity and Chronic Disease, School of Basic Medical Sciences, Division of Life Sciences and Medicine, University of Science and Technology of China, Hefei, China

Objectives: The purpose of this study is to evaluate the diagnostic accuracy of the clinical variables of patients with prostate cancer (PCa) and to provide a strategy to reduce unnecessary biopsies.

Patients and methods: A Chinese cohort that consists of 833 consecutive patients who underwent prostate biopsies from January 2018 to April 2022 was collected in this retrospective study. Diagnostic ability for total PCa and clinically significant PCa (csPCa) was evaluated by prostate imaging–reporting and data system (PI-RADS) score and other clinical variables. Univariate and multivariable logistic regression analyses were performed to figure out the independent predictors. Diagnostic accuracy was estimated by plotting receiver operating characteristic curves.

Results: The results of univariate and multivariable analyses demonstrated that the PI-RADS score ($P < 0.001$, OR: 5.724, 95% CI: 4.517–7.253)/($P < 0.001$, OR: 5.199, 95% CI: 4.039–6.488) and prostate-specific antigen density (PSAD) ($P < 0.001$, OR: 2.756, 95% CI: 1.560–4.870)/($P < 0.001$, OR: 4.726, 95% CI: 2.661–8.396) were the independent clinical factors for predicting total PCa/csPCa. The combination of the PI-RADS score and PSAD presented the best diagnostic performance for the detection of PCa and csPCa. For the diagnostic criterion of "PI-RADS score ≥ 3 or PSAD ≥ 0.3", the sensitivity and negative predictive values were 94.0% and 93.1% for the diagnosis of total PCa and 99.2% and 99.3% for the diagnosis of csPCa, respectively. For the diagnostic criterion "PI-RADS score >3 and PSAD ≥ 0.3", the specificity and positive predictive values were 96.8% and 92.6% for the diagnosis of total PCa and 93.5% and 82.4% for the diagnosis of csPCa, respectively.

Conclusions: The combination of the PI-RADS score and PSAD can implement the extraordinary diagnostic performance of PCa. Many patients may safely execute active surveillance or take systematic treatment without prostate biopsies by stratification according to the PI-RADS score and the value of PSAD.

KEYWORDS

prostate cancer, prostate biopsy, multiparameter magnetic resonance imaging, prostate imaging-reporting and data system score, prostate-specific antigen density

Introduction

Prostate cancer (PCa) is the most common malignancy of the male genitourinary system. According to the latest data, there will be 268,490 new diagnosed cases and 34,500 deaths in the United States in 2022 (1). In China, with the rapid development of economy and wide adoption of early detection techniques, the incidence of PCa is gradually increasing year by year (2). The incidence of PCa is closely related to the age of the patients; a study has shown that PCa is extremely rare in men under 50 years of age, but more than 85% of the patients are over 60 years of age (3). Therefore, the increasing aging of the Chinese population will inevitably lead to a fast increase in the number of patients with PCa. In the face of the rapidly growing patient population, early screening, diagnosis, and treatment of PCa have great clinical significance to improve prognosis, reduce the proportion of advanced cases, and prolong life span (4).

To date, the main methods recommended by the guidelines for the early detection of PCa include digital rectal examination (DRE), serum total prostate-specific antigen (tPSA), transrectal ultrasound, and genetic tests for inherited PCa (5). Results of DRE by different operators were inconsistent, and both the pooled sensitivity and specificity are less than 60% (6). Serum tPSA has satisfactory sensitivity for the diagnosis of PCa, but elevated PSA is not specific for PCa; some PSA derivatives, such as PSA density (PSAD), PSA velocity, PSA doubling time, and free/total PSA ratio, also have a fairly diagnostic value for PCa, but their clinical value is still controversial, and more high-quality studies are still necessary before clinical practice (7, 8). Multiparameter magnetic resonance imaging (mpMRI) has been widely used in the diagnosis of PCa in recent years. The results of mpMRI can be quantitatively evaluated by prostate imaging–reporting and data system (PI-RADS) (9). A study found that the addition of PSAD can improve the predictive performance of PI-RADS for the identification of PCa (10). However, mpMRI has poor identification of small masses, inflammatory lesions, and low-grade PCa (11).

Ultimately, prostate biopsies are required to confirm the diagnosis of suspected patients. Although prostate biopsy is the current gold standard for diagnosing PCa, it still has some deficiencies such as unpredictable complications, and most important is that the detection rate of PCa by prostate biopsy is less than 50% in light of the previous studies (12, 13). The purpose of this study was to evaluate the diagnostic accuracy of mpMRI and clinical parameters and to propose a strategy to reduce unnecessary prostate biopsies.

Patients and methods

Patients and selection criteria

This study was approved by the ethics committee of The First Affiliated Hospital of USTC (No. 2022-RE-125). In total, the information of 833 consecutive patients who accepted prostate biopsies from January 2018 to April 2022 was collected from the Department of Urology at The First Affiliated Hospital of USTC to accomplish this retrospective analysis. The baseline clinicopathologic features of all the patients were obtained by the methods that we described previously (14). Only patients with naïve prostate biopsy and complete clinicopathologic characteristics could be included in this study; meanwhile, patients were still excluded for any of the following conditions: a history of other malignancies, more than 2 weeks from laboratory tests to operations, have taken 5a-reductase inhibitors before biopsy, and serum tPSA ≥100 or <4 ng/ml. Each participant signed an informed consent prior to biopsy.

MRI image acquisition and PI-RADS score

All enrolled patients underwent mpMRI examinations with a 3.0T scanner with an external six-channel body array coil (Trio Tim, Siemens Healthineers, Erlangen, Germany). Patients were placed in the supine position, and endorectal coils were not used. The imaging protocol included transverse T1-weighted imaging (T1WI), multiplanar (transverse, sagittal, and coronal) T2-weighted imaging (T2WI), and transverse diffusion-weighted

imaging (DWI) with a quantitative apparent diffusion coefficient (ADC) (*b* values were 0, 800, and 1,400 s/mm^2). All the images required within 2 months before prostate biopsy. Then, the interpretation was performed by two professional radiologists with more than 3 years of experience in prostate mpMRI. They first reviewed the images separately and discussed the controversial results together subsequently. They were blinded to the pathological results throughout the process. Ultimately, a definite PI-RADS score (version 2.1) from 1 to 5 was obtained for every incorporated participant (15). Figure S1 shows the representative images of mpMRI.

Biopsy protocol and histopathological results

In our hospital, prostate biopsies were performed by specialized urologists; all patients underwent transperineal procedures with the help of a transrectal ultrasound-guided system (biplane imaging scan). Systematic biopsy with a 12-core protocol was performed for each patient at first, and patients who had regions of interest in mpMRI (PI-RADS score ≥ 3) would receive cognitive fusion–targeted biopsy with additional one to six cores. All samples were sent to the pathology department for standard histological examinations, which was also regarded as the "gold standard" in this study. Histopathological grade was recorded according to the International Society of Urological Pathology 2014 updated Gleason score grading system (16). The primary endpoint of our study was the detection rate of clinically significant PCa (csPCa) defined as high-grade PCa with Gleason score ≥ 3 + 4, and clinically insignificant PCa (cisPCa) refers to low-grade PCa with Gleason score = 3 + 3.

Statistical analyses

Non-normal distributed continuous variables were presented as median [interquartile ranges (IQRs)] and compared by the Kruskal–Wallis test. Descriptive statistic counts (proportions) and chi-square test were used to describe the categorical variables. The correlation coefficients were evaluated using Spearman's rank correlation analysis. Univariate and multivariable logistic regression analyses were applied to screen the independent predictors of PCa or csPCa, and the odds ratio (OR) and 95% confidence interval (95% CI) were also recorded. Diagnostic performance was evaluated by plotting receiver operating characteristic (ROC) curves and their values of area under the curve (AUC). Sensitivity and specificity were calculated for clinical variables and the probability of combined PI-RADS score with PSAD at the optimal cutoff value. The accuracy of diagnostic tests was evaluated by sensitivity, specificity, positive predictive values (PPVs), and negative predictive values (NPVs) for different diagnostic criteria. Statistical analysis was performed using IBM SPSS (version 25.0) and R software (version 4.2.0) (http://www.R-project.org), and ROC curves were plotted and compared using MedCalc (version 18.9.1). $P < 0.05$ was considered statistically significant.

Results

Demographic characteristics of the enrolled patients

The original information of all the patients was summarized in Table S1. In total, 833 patients were incorporated in the retrospective analysis; there were 336/833 (40.3%) PCa cases and 497/833 (59.7%) cases with a non-cancerous outcome. Within these patients with PCa, 248/336 (73.8%) were diagnosed with csPCa, and 88/336 (26.2%) were diagnosed with cisPCa. The median value (IQR) of age, body mass index (BMI), PSA, prostate volume (PV), and PSAD were 69 (63–75) years, 23.77 (21.80–25.50) kg/m^2, 13.83 (9.36–21.61) ng/ml, 47.62 (32.18–67.78) ml, and 0.30 (0.16–0.52) ng/ml^2 of all the patients, respectively. Comparisons of these clinical variables among the non-cancer, csPCa, and cisPCa patients revealed that PSA and PSAD levels were significantly higher in the csPCa group ($P < 0.001$) (Figures 1A, C). The PV of the non-cancer group was the biggest followed by the cisPCa and csPCa groups ($P < 0.01$) (Figure 1B). After stratifying patients by the PI-RADS score and PSAD subgroups, the detection rate of csPCa increased dramatically with an elevated PSAD level and PI-RADS score ($P < 0.001$) (Figures 1D, E). These data discovered that the PI-RADS score and PSAD have potential discriminative ability for prostate biopsy results.

PI-RADS score and PSAD were independent predictors of the prostate biopsy results

First, correlation analysis indicated that the PI-RADS score and PSAD were two main factors related to PCa and csPCa detection (Figure S2). Then, the results of univariate analysis revealed that age, PSA, PV, PSAD, and PI-RADS score were associated factors for both PCa and csPCa. Because PSAD had strong correlations with PSA and PV (Figure S2), PSA and PV were excluded from the multivariable analysis to avoid confounding. The results of multivariable analysis demonstrated that the PI-RADS score ($P < 0.001$, OR: 5.724, 95% CI: 4.517–7.253; $P < 0.001$, OR: 5.199, 95% CI: 4.039–6.488) and PSAD ($P < 0.001$, OR: 2.756, 95% CI: 1.560–4.870; $P < 0.001$, OR: 4.726, 95% CI: 2.661–8.396) were independent clinical factors to predict PCa and csPCa, respectively. The detailed data of univariate and multivariable analyses were concluded in Table 1.

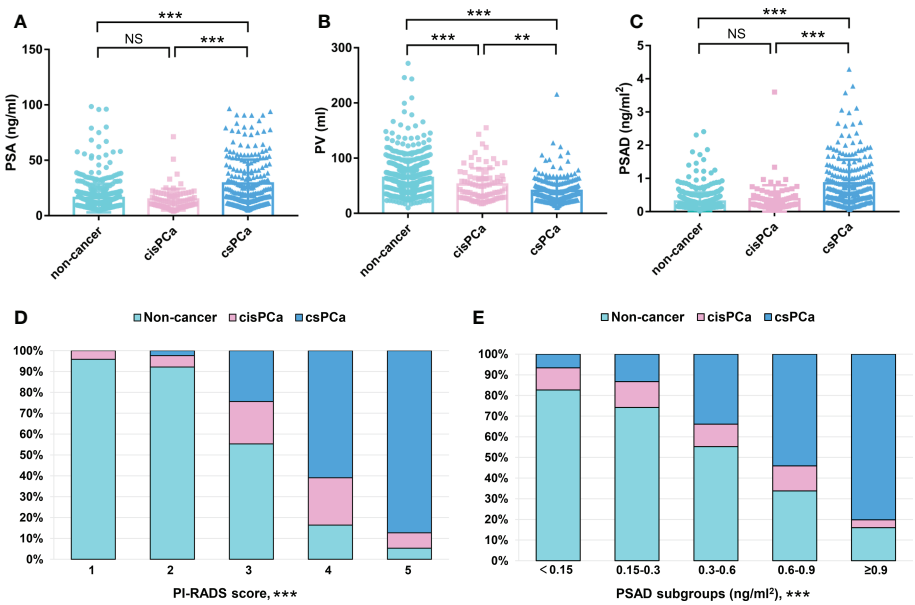

FIGURE 1
Comparisons of the clinical variables among the non-cancer, csPCa, and cisPCa patients: **(A)** total PSA; **(B)** PV; **(C)** PSAD; **(D)** PI-RADS score; **(E)** PSAD subgroups. **P < 0.01; ***P < 0.001; NS, not significant.

Diagnostic performance of the clinical variables and combined PI-RADS score with PSAD

First, the PI-RADS score and PSAD were combined according to the results of multivariable analysis. By plotting ROC curves, the combination of the PI-RADS score and PSAD presented with the best diagnostic accuracy for PCa (Figure 2A) and csPCa (Figure 2B) in prostate biopsy compared with any single clinical variable. Regarding the diagnosis of PCa, the AUC, sensitivity, and specificity were 0.915 (95% CI: 0.894–0.933), 85.71%, and 87.12%, respectively, for the combined PI-RADS

TABLE 1 Univariate and multivariable analysis for screening out the independent factors of total PCa and csPCa.

Parameters	Univariate analysis			Multivariable analysis			
	OR	95% CI	P-value	B	OR	95% CI	P-value
For total PCa							
Age (years)	1.059	1.041–1.078	<0.001	0.024	1.024	0.999-1.051	0.064
BMI (kg/m^2)	1.000	0.954–1.049	0.991				
PSA (ng/ml)	1.037	1.026–1.047	<0.001				
PV (ml)	0.973	0.967–0.979	<0.001				
PSAD (ng/ml^2)	12.154	7.303–20.227	<0.001	1.014	2.756	1.560–4.870	<0.001
PI-RADS score	6.551	5.214–8.231	<0.001	1.745	5.724	4.517–7.253	<0.001
For csPCa							
Age (years)	1.063	1.043–1.084	<0.001	0.028	1.028	0.999–1.058	0.055
BMI (kg/m^2)	0.977	0.928–1.028	0.375				
PSA (ng/ml)	1.049	1.038–1.060	<0.001				
PV (ml)	0.967	0.959–0.974	<0.001				
PSAD (ng/ml^2)	15.438	9.329–25.545	<0.001	1.553	4.726	2.661–8.396	<0.001
PI-RADS score	6.199	4.940–7.779	<0.001	1.633	5.199	4.039–6.488	<0.001

PCa, prostate cancer; csPCa, clinically significant prostate cancer; BMI, body mass index; PSA, prostate-specific antigen; PV, prostate volume; PSAD, prostate-specific antigen density; PI-RADS, prostate imaging-reporting and data system; OR, odds ratio; 95% CI, 95% confidence interval.

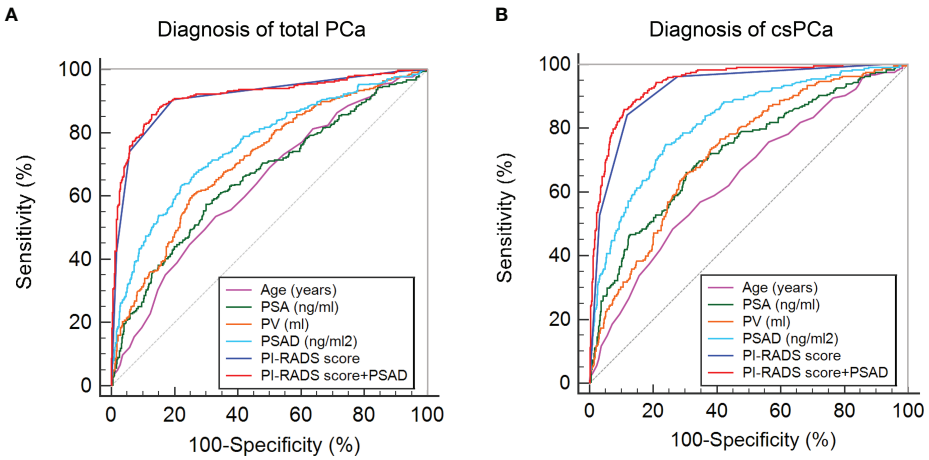

FIGURE 2
ROC curves of clinical variables and combined PI-RADS score with PSAD for the diagnosis of PCa: **(A)** ROC curves for the diagnosis of total PCa; **(B)** ROC curves for the diagnosis of csPCa.

score with PSAD, which was obviously higher than age, PSA, PV, and PSAD ($P < 0.001$), but no statistical difference was observed compared with the PI-RADS score ($P = 0.148$) (Table 2). In terms of the csPCa diagnosis, the AUC, sensitivity, and specificity were 0.942 (95% CI: 0.924–0.957), 85.89%, and 89.06%, respectively, for the combined PI-RADS score with PSAD; the diagnostic accuracy significantly outperformed any single clinical variable including the PI-RADS score ($P < 0.001$) (Table 2). Above all, the combination of the PI-RADS score and PSAD received the best diagnostic performance for the detection of PCa and csPCa in prostate biopsy.

PCa and csPCa detection rate in patients stratified by PI-RADS score and PSAD

To counsel patients for reducing unnecessary prostate biopsies, an exact diagnostic threshold value of the PI-RADS score and PSAD is needed. Then, all patients were divided into different groups according to the separated PI-RADS score and PSAD subgroups. Subsequently, we calculated the detection rates of total PCa and csPCa in these groups, which are exhibited in Tables S2 and S3, respectively. After careful consideration, 291 patients with "PI-RADS score < 3 and PSAD < 0.3" were categorized into group 1; 326 patients with "PI-RADS score ≥ 3 and PSAD < 0.3" or "PI-RADS score < 3 and PSAD ≥

TABLE 2 Diagnostic accuracy of the clinical parameters for total PCa and csPCa.

Parameters	AUC	95% CI	Sensitivity	Specificity	P-value
For total PCa					
Age (years)	0.637	0.603-0.670	53.47%	67.00%	<0.001
PSA (ng/ml)	0.660	0.627-0.692	57.44%	70.02%	<0.001
PV (ml)	0.713	0.681-0.744	60.12%	74.45%	<0.001
PSAD (ng/ml^2)	0.760	0.729-0.788	63.69%	77.46%	<0.001
PI-RADS score	0.909	0.887-0.928	90.48%	80.48%	0.148
PI-RADS score + PSAD	0.915	0.894-0.933	85.71%	87.12%	Reference
For csPCa					
Age (years)	0.645	0.612-0.678	48.39%	73.85%	<0.001
PSA (ng/ml)	0.723	0.692-0.753	66.13%	69.57%	<0.001
PV (ml)	0.726	0.694-0.756	76.61%	58.97%	<0.001
PSAD (ng/ml^2)	0.820	0.792-0.845	75.00%	76.07%	<0.001
PI-RADS score	0.922	0.902-0.939	84.27%	88.21%	<0.001
PI-RADS score + PSAD	0.942	0.924-0.957	85.89%	89.06%	Reference

PCa, prostate cancer; PSA, prostate-specific antigen; PV, prostate volume; PSAD, prostate-specific antigen density; PI-RADS, prostate imaging-reporting and data system; csPCa, clinically significant prostate cancer; AUC, area under curve; 95% CI, 95% confidence interval.

0.3" were regarded as group 2; and 216 patients with "PI-RADS score > 3 and PSAD ≥ 0.3" were defined as group 3 (Figure 3A). The distribution and frequencies of the patients in each group are summarized in Table S4. We found only 2/291 (0.7%) patients diagnosed with csPCa in group 1 and only 16/216 (7.4%) patients diagnosed with non-PCa by prostate biopsy in group 3 (Figure 3B). Therefore, we established two diagnostic criteria: criterion 1 is "PI-RADS scored ≥ 3 or PSAD ≥ 0.3", and the sensitivity, specificity, PPV, and NPV of criterion 1 were 94.0%, 54.5%, 58.3%, and 93.1% for the diagnosis of total PCa and 99.2%, 49.4%, 45.4%, and 99.3% for the diagnosis of csPCa, respectively; criterion 2 is "PI-RADS score > 3 and PSAD ≥ 0.3", and the sensitivity, specificity, PPV, and NPV of criterion 2 were 59.5%, 96.8%, 92.6%, and 78.0% for the diagnosis of total PCa and 71.8%, 93.5%, 82.4%, and 88.7% for the diagnosis of csPCa, respectively (Table 3). These data suggest that patients with negative results by diagnostic criterion 1 can almost rule out the possibility of PCa and, inversely, a high probability of PCa for patients with positive results by diagnostic criterion 2.

External validation of our results by other Chinese datasets

Our results were also externally validated in two other Chinese datasets from the recent report by Tao et al. (14). As we expected, after the patients were categorized into three groups by the PI-RADS score and PSAD with the method mentioned in Figure 3A, the frequency distribution histograms indicated significant discrepancies of patients' composition (Figures 3C, D). In the external validation dataset 1, only 7/104 (6.7%) patients were diagnosed with csPCa in group 1, and just 8/92 (8.7%) patients were excluded from diagnosis of PCa in group 3. Similarly, in the second external validation dataset, only 4/101 (3.9%) patients were diagnosed with csPCa in group 1, and just 7/98 (9.1%) patients were diagnosed with non-cancerous diseases in group 3 (Table S4). These data illustrated a pretty good performance of multicenter verifications.

Strategy for avoiding unnecessary prostate biopsy

Finally, a strategy was established to avoid unnecessary prostate biopsies (Figure 4). Outpatients with suspicion of PCa can be stratified by the combination of the PI-RADS score and PSAD, and patients categorized into group 2 should accept routine prostate biopsies; patients divided into group 1 can safely avoid biopsies and carry out active surveillance on account of only 2/291 (0.7%) csPCa cases that received missed diagnoses in the current observation. In addition, patients in

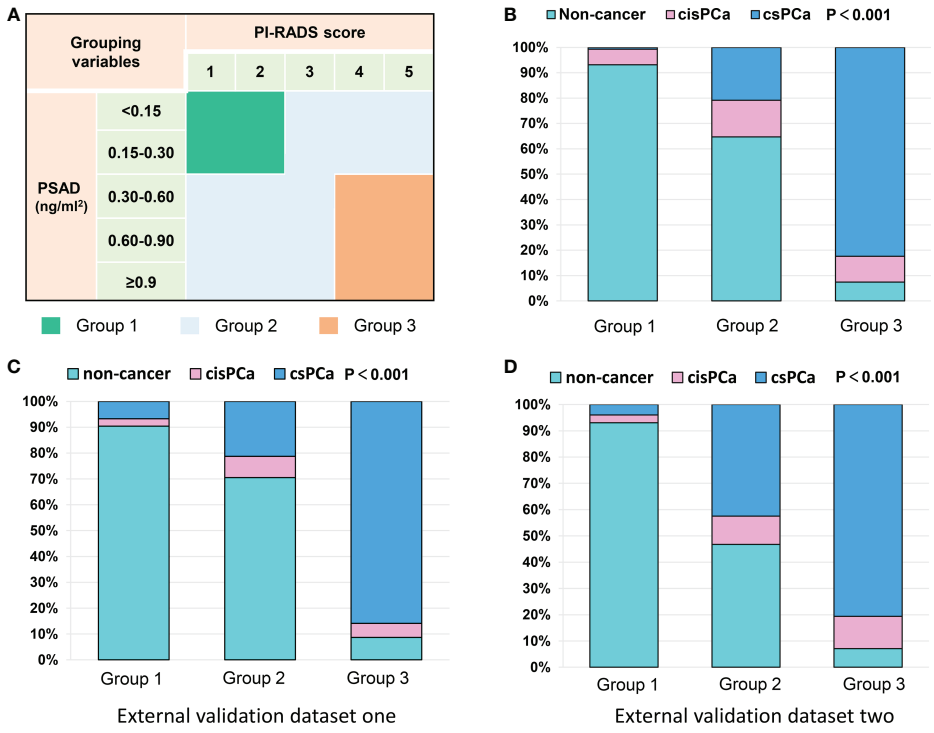

FIGURE 3
Grouping scheme of patients and frequency distribution in each group: **(A)** grouping scheme of patients by PI-RADS score and PSAD subgroups; **(B)** frequency distribution of the patients in different groups; **(C, D)** frequency distribution histograms of two external datasets.

TABLE 3 Diagnostic accuracy of total PCa and csPCa by different diagnostic threshold.

Diagnostic threshold	Sensitivity	Specificity	PPV	NPV	Accuracy
For total PCa					
PI-RADS scored ≥ 3 or PSAD ≥ 0.3	94.0%	54.5%	58.3%	93.1%	70.5%
PI-RADS score >3 and PSAD ≥ 0.3	59.5%	96.8%	92.6%	78.0%	81.8%
For csPCa					
PI-RADS scored ≥ 3 or PSAD ≥ 0.3	99.2%	49.4%	45.4%	99.3%	64.2%
PI-RADS score >3 and PSAD ≥ 0.3	71.8%	93.5%	82.4%	88.7%	87.0%

PCa, prostate cancer; csPCa, clinically significant prostate cancer; PI-RADS, prostate imaging-reporting and data system; PSAD, prostate-specific antigen density; PPV, positive predictive value; NPV, negative predictive value.

group 3 can also take radical or systemic therapy without prostate biopsies into consideration because only 16/216 (7.4%) patients with non-PCa were observed in group 3 of this study. However, this may still be full of challenges because of the irretrievable destruction by radical prostatectomy for patients without PCa even if they are in group 3.

Discussion

In recent decades, prostate biopsy has been the most commonly recommended method for the early diagnosis of PCa, but it has some unavoidable shortcomings. First of all, prostate biopsy is invasive and can cause postoperative complications such as sepsis and bleeding (17). Second, the operation will result in a certain degree of psychological and financial burden to patients. Then, for the patients diagnosed with csPCa by biopsies, they need to wait a period of time before radical prostatectomy, and this will increase the probability of cancer dissemination. Furthermore, because of the possibility of false-negative biopsy results, some patients have to undergo repeated biopsies (18). At last, in many studies, the detection rate of PCa or csPCa is less than 50%, which means a general phenomenon that lots of patients accepted undue biopsies (19). Our purpose in this retrospective study is to propose a strategy for clinicians to obviate needless prostate biopsies.

Serum tPSA examination is the most commonly used tool for PCa screening. Abnormal non-specific escalation of tPSA is the primary reason of the unnecessary prostate biopsies (20). To make a triage test of patients prior to biopsy, some risk calculators that incorporated tPSA have been established, such as Prostate Cancer Prevention Trial Risk Calculator (21) and European Randomized

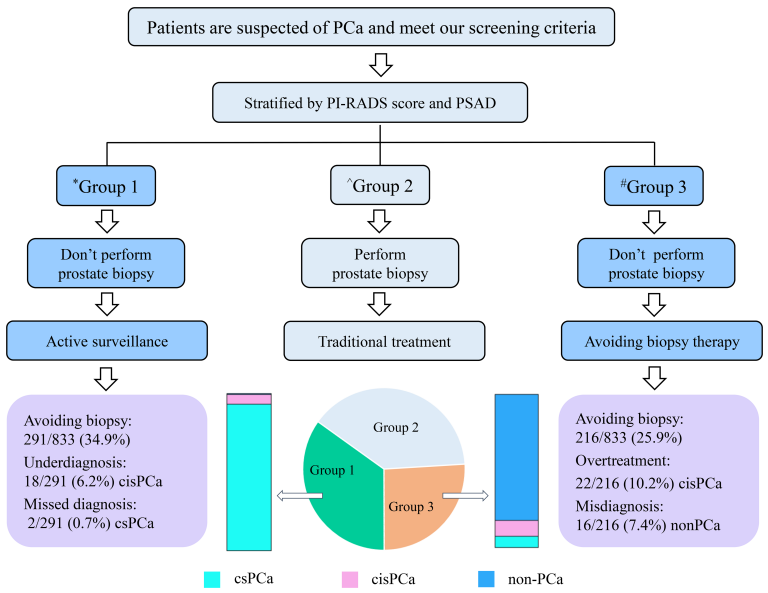

FIGURE 4
Flowchart of the strategy for avoiding unnecessary prostate biopsy. *Group 1 patients with PI-RADS score < 3 and PSAD < 0.3; ^Group 2 patients with "PI-RADS score ≥ 3 and PSAD < 0.3" or "PI-RADS score < 3 and PSAD ≥ 0.3"; #Group 3 patients with PI-RADS score > 3 and PSAD ≥ 0.3.

Study of Screening for Prostate Cancer Risk Calculator (22); however, studies have proved that it will lead to overdiagnosis and overtreatment when these calculators are applied in the Chinese populations, and, as a result, the median or average level of tPSA is usually higher in Chinese patients compared with that in Western cohorts (23, 24). Importantly, the value of mpMRI was not estimated in these studies. mpMRI is a routine examination recommended prior to biopsy nowadays, and latest meta-analyses indicated that the pooled NPV of mpMRI using the definition of negative MRI (PI-RADS score 1–2) and csPCa (Gleason score ≥ 3 + 4 = 7) was 90.8% (95% CI: 88.1–93.1%) for biopsy-naïve men (25). However, the pooled PPV of suspicious mpMRI for csPCa was only 42% (95% CI: 38–45%) in the biopsy-naïve group (26). MRI-guided targeted biopsy can enhance the detection of csPCa and detect significantly fewer cisPCa than systematic biopsy (27). PSAD is the value of serum tPSA divided by the PV, and previous studies have demonstrated that mpMRI combined with PSAD < 0.15 ng/ml^2 can improve the NPV to predict PCa (28, 29). However, these studies were based on Western populations with a small sample size, and there is still a paucity in the data from Chinese patients.

In the present study, we observed the diagnostic value of patients' clinical variables and found that PSAD and the PI-RADS score can independently predict PCa and csPCa of prostate biopsies. The combination of PSAD and the PI-RADS score achieved the best diagnostic performance relative to using a single variable. By setting different diagnostic criteria, we discovered that patients with "PI-RADS score < 3 and PSAD < 0.3" can safely rule out the diagnosis of csPCa, and we make a definitive diagnosis of PCa for patients with "PI-RADS score > 3 and PSAD ≥ 0.3". To reduce unnecessary prostate biopsies, most of the previous studies discussed the diagnostic threshold with a high NPV, just like the diagnostic criterion 1 that we described above. However, we also discussed a diagnostic criterion with a high PPV. Radical prostatectomy without biopsy is a viable option despite 16/216 (7.4%) patients with PI-RADS score > 3 and PSAD ≥ 0.3 diagnosed with non-cancerous diseases in this study. On the one hand, prostate biopsies could produce false-negative results. In addition, ^{68}Ga prostate-specific membrane antigen positron emission tomography/computed tomography (^{68}Ga PSMA PET/CT) is a novel diagnostic modality with excellent performance for both primary and metastatic lesions of PCa (30). A recent study has reported that men with PI-RADS of 4 or 5 combined with a maximum standardized uptake value (SUVmax) ≥ 9 can denote csPCa with 100% specificity (31). In addition, the initial successful experience has been released for 25 patients who received radical prostatectomy without prior biopsy; all these patients got PI-RADS score ≥ 4 in mpMRI and SUVmax ≥ 4.0 in ^{68}Ga PSMA PET/CT (32). In the future, for patients with high suspicion of PCa, prostate biopsy may no longer be the only way for diagnosis before active therapies.

Our study also has some limitations. First, the suspicious regions in the mpMRI with a PI-RADS score of 4 or 5 were detected by cognitive fusion–targeted biopsies, which can produce inevitable deviation without a real-time intraoperative MRI-guided system. Second, some important clinical parameters like DRE and free/total PSA were not analyzed because of too many irretrievable missing values. Third, although mpMRI images were independently reviewed by two radiologists, inter-observer reliability was not assessed. Next, this study was only validated in few tertiary medical centers, and it should be validated in other Chinese high-volume hospitals in the future. Last, selection bias cannot be avoided due to the retrospective nature.

Conclusions

Prostate biopsy is the most commonly used approach for the initial diagnosis of PCa with several inherent shortcomings. In this retrospective study, we found that the combination of the PI-RADS score and PSAD can achieve outstanding diagnostic performance of PCa. Patients with "PI-RADS score < 3 and PSAD < 0.3" may safely avoid biopsies and execute active surveillance, and patients with "PI-RADS score > 3 and PSAD ≥ 0.3" can also take a radical or systematic therapy without prostate biopsies into consideration. However, a study with prospective design is still needed to further confirm our findings in the future.

Data availability statement

The raw data supporting the conclusions of this article will be made available by the authors, without undue reservation.

Ethics statement

This study involving human participants was reviewed and approved by Ethics committee of The First Affiliated Hospital of USTC. The patients/participants provided their written informed consent to participate in this study.

Author contributions

Study concept and design: JX and TT. Acquisition of data: CW, LY, and BZ. Analysis and interpretation of data: LY, DS, and BZ. Statistical analysis: CW, BW, and PZ. Drafting of the manuscript: CW. Review and supervision: JX and TT. All authors contributed to the article and approved the submitted version.

Funding

The current study was partly supported by the Key Researchand Development Program of Anhui Province (No.1804h08020253 and 202004j07020022).

Conflict of interest

The authors declare that the research was conducted in the absence of any commercial or financial relationships that could be construed as a potential conflict of interest.

Publisher's note

Supplementary material

The Supplementary Material for this article can be found online at: https://www.frontiersin.org/articles/10.3389/fonc.2022.1024204/full#supplementary-material

SUPPLEMENTARY FIGURE 1

The representative images of mpMRI of six patients: **(A)** PI-RADS score 1: Normal peripheral zone, axial T2WI shows uniformly hyperintensive signal intensity, high *b*-value DWI and ADC also show no abnormality (white arrow); **(B)** PI-RADS score 2: Axial T2WI shows diffuse hypointensity with indistinct margin, high *b*-value DWI exhibits slightly hyperintense and indistinct hypointense on ADC (white arrow); **(C)** PI-RADS score 3: Axial T2WI exhibits non-circumscribed moderate hypointensity in left peripheral zone, DWI shows mildly hyperintense on high *b*-value and hypointense on ADC (white arrow); **(D)** PI-RADS score 4: Axial T2WI shows circumscribed, homogenous moderate hypointense focus confined in right peripheral zone with greatest dimension <1.5cm, DWI sees focal obviously hyperintense on high *b*-value and hypointense on ADC (white arrow); **(E)** PI-RADS score 5: Axial T2WI shows non-circumscribed, homogenous moderate hypointense focus confined with greatest dimension >1.5cm in left transition zone and peripheral zone. high *b*-value DWI shows focal markedly hyperintense and apparent hypointense on ADC (white arrow); **(F)** Measurement of prostate maximum diameters, green line: anteroposterior diameter, pink line: longitudinal diameter, brown line: transverse diameter.

SUPPLEMENTARY FIGURE 2

Spearman correlation analysis between clinical variables and biopsy results indicated PI-RADS score and PSAD were closely related to the detection of PCa and csPCa. *, P < 0.05; **, P <0.01; ***, P <0.001.

References

1. Siegel RL, Miller KD, Fuchs HE, Jemal A. Cancer statistics, 2022. *CA Cancer J Clin* (2022) 72(1):7–33. doi: 10.3322/caac.21708

2. Xia C, Dong X, Li H, Cao M, Sun D, He S, et al. Cancer statistics in China and united states, 2022: profiles, trends, and determinants. *Chin Med J (Engl)* (2022) 135(5):584–90. doi: 10.1097/cm9.0000000000002108

3. Rebello RJ, Oing C, Knudsen KE, Loeb S, Johnson DC, Reiter RE, et al. Prostate cancer. *Nat Rev Dis Primers* (2021) 7(1):9. doi: 10.1038/s41572-020-00243-0

4. Ilic D, Djulbegovic M, Jung JH, Hwang EC, Zhou Q, Cleves A, et al. Prostate cancer screening with prostate-specific antigen (PSA) test: a systematic review and meta-analysis. *Bmj* (2018) 362:k3519. doi: 10.1136/bmj.k3519

5. Mottet N, van den Bergh RCN, Briers E, Van den Broeck T, Cumberbatch MG, De Santis M, et al. EAU-EANM-ESTRO-ESUR-SIOG guidelines on prostate cancer-2020 update. part 1: Screening, diagnosis, and local treatment with curative intent. *Eur Urol* (2021) 79(2):243–62. doi: 10.1016/j.eururo.2020.09.042

6. Naji L, Randhawa H, Sohani Z, Dennis B, Lautenbach D, Kavanagh O, et al. Digital rectal examination for prostate cancer screening in primary care: A systematic review and meta-analysis. *Ann Fam Med* (2018) 16(2):149–54. doi: 10.1370/afm.2205

7. Welch HG, Albertsen PC. Reconsidering prostate cancer mortality - the future of PSA screening. *N Engl J Med* (2020) 382(16):1557–63. doi: 10.1056/NEJMms1914228

8. Duffy MJ. Biomarkers for prostate cancer: prostate-specific antigen and beyond. *Clin Chem Lab Med* (2020) 58(3):326–39. doi: 10.1515/cclm-2019-0693

9. Dutruel SP, Jeph S, Margolis DJA, Wehrli N. PI-RADS: what is new and how to use it. *Abdom Radiol (NY)* (2020) 45(12):3951–60. doi: 10.1007/s00261-020-02482-x

10. Stevens E, Truong M, Bullen JA, Ward RD, Purysko AS, Klein EA. Clinical utility of PSAD combined with PI-RADS category for the detection of clinically significant prostate cancer. *Urol Oncol* (2020) 38(11):846.e9–e16. doi: 10.1016/j.urolonc.2020.05.024

11. Borofsky S, George AK, Gaur S, Bernardo M, Greer MD, Mertan FV, et al. What are we missing? false-negative cancers at multiparametric MR imaging of the prostate. *Radiology* (2018) 286(1):186–95. doi: 10.1148/radiol.2017152877

12. Berry B, Parry MG, Sujenthiran A, Nossiter J, Cowling TE, Aggarwal A, et al. Comparison of complications after transrectal and transperineal prostate biopsy: a national population-based study. *BJU Int* (2020) 126(1):97–103. doi: 10.1111/bju.15039

13. Raman AG, Sarma KV, Raman SS, Priester AM, Mirak SA, Riskin-Jones HH, et al. Optimizing spatial biopsy sampling for the detection of prostate cancer. *J Urol* (2021) 206(3):595–603. doi: 10.1097/ju.0000000000001832

14. Tao T, Wang C, Liu W, Yuan L, Ge Q, Zhang L, et al. Construction and validation of a clinical predictive nomogram for improving the cancer detection of prostate naive biopsy based on Chinese multicenter clinical data. *Front Oncol* (2021) 11:811866. doi: 10.3389/fonc.2021.811866

15. Turkbey B, Rosenkrantz AB, Haider MA, Padhani AR, Villeirs G, Macura KJ, et al. Prostate imaging reporting and data system version 2.1: 2019 update of prostate imaging reporting and data system version 2. *Eur Urol* (2019) 76(3):340–51. doi: 10.1016/j.eururo.2019.02.033

16. Epstein JI, Egevad L, Amin MB, Delahunt B, Srigley JR, Humphrey PA. The 2014 international society of urological pathology (ISUP) consensus conference on Gleason grading of prostatic carcinoma: Definition of grading patterns and proposal for a new grading system. *Am J Surg Pathol* (2016) 40(2):244–52. doi: 10.1097/pas.0000000000000530

17. Xiang J, Yan H, Li J, Wang X, Chen H, Zheng X. Transperineal versus transrectal prostate biopsy in the diagnosis of prostate cancer: a systematic review and meta-analysis. *World J Surg Oncol* (2019) 17(1):31. doi: 10.1186/s12957-019-1573-0

18. Capitanio U, Pfister D, Emberton M. Repeat prostate biopsy: Rationale, indications, and strategies. *Eur Urol Focus* (2015) 1(2):127–36. doi: 10.1016/j.euf.2015.05.002

19. Ahdoot M, Wilbur AR, Reese SE, Lebastchi AH, Mehralivand S, Gomella PT, et al. MRI-Targeted, systematic, and combined biopsy for prostate cancer diagnosis. *N Engl J Med* (2020) 382(10):917–28. doi: 10.1056/NEJMoa1910038

20. Hamdy FC, Donovan JL, Lane JA, Mason M, Metcalfe C, Holding P, et al. 10-year outcomes after monitoring, surgery, or radiotherapy for localized prostate cancer. *N Engl J Med* (2016) 375(15):1415–24. doi: 10.1056/NEJMoa1606220

21. Ankerst DP, Hoefler J, Bock S, Goodman PJ, Vickers A, Hernandez J, et al. Prostate cancer prevention trial risk calculator 2.0 for the prediction of low- vs high-grade prostate cancer. *Urology* (2014) 83(6):1362–7. doi: 10.1016/j.urology.2014.02.035

22. Roobol MJ, Steyerberg EW, Kranse R, Wolters T, van den Bergh RC, Bangma CH, et al. A risk-based strategy improves prostate-specific antigen-driven detection of prostate cancer. *Eur Urol* (2010) 57(1):79–85. doi: 10.1016/j.eururo.2009.08.025

23. Zhu Y, Wang JY, Shen YJ, Dai B, Ma CG, Xiao WJ, et al. External validation of the prostate cancer prevention trial and the European randomized study of screening for prostate cancer risk calculators in a Chinese cohort. *Asian J Androl* (2012) 14(5):738–44. doi: 10.1038/aja.2012.28

24. He BM, Chen R, Sun TQ, Yang Y, Zhang CL, Ren SC, et al. Prostate cancer risk prediction models in Eastern Asian populations: current status, racial difference, and future directions. *Asian J Androl* (2020) 22(2):158–61. doi: 10.4103/aja.aja_55_19

25. Sathianathen NJ, Omer A, Harriss E, Davies L, Kasivisvanathan V, Punwani S, et al. Negative predictive value of multiparametric magnetic resonance imaging in the detection of clinically significant prostate cancer in the prostate imaging reporting and data system era: A systematic review and meta-analysis. *Eur Urol* (2020) 78(3):402–14. doi: 10.1016/j.eururo.2020.03.048

26. Mazzone E, Stabile A, Pellegrino F, Basile G, Cignoli D, Cirulli GO, et al. Positive predictive value of prostate imaging reporting and data system version 2 for the detection of clinically significant prostate cancer: A systematic review and meta-analysis. *Eur Urol Oncol* (2021) 4(5):697–713. doi: 10.1016/j.euo.2020.12.004

27. Rouvière O, Puech P, Renard-Penna R, Claudon M, Roy C, Mège-Lechevallier F, et al. Use of prostate systematic and targeted biopsy on the basis of multiparametric MRI in biopsy-naive patients (MRI-FIRST): a prospective, multicentre, paired diagnostic study. *Lancet Oncol* (2019) 20(1):100–9. doi: 10.1016/s1470-2045(18)30569-2

28. Washino S, Okochi T, Saito K, Konishi T, Hirai M, Kobayashi Y, et al. Combination of prostate imaging reporting and data system (PI-RADS) score and prostate-specific antigen (PSA) density predicts biopsy outcome in prostate biopsy naïve patients. *BJU Int* (2017) 119(2):225–33. doi: 10.1111/bju.13465

29. Oishi M, Shin T, Ohe C, Nassiri N, Palmer SL, Aron M, et al. Which patients with negative magnetic resonance imaging can safely avoid biopsy for prostate cancer? *J Urol* (2019) 201(2):268–76. doi: 10.1016/j.juro.2018.08.046

30. Hofman MS, Lawrentschuk N, Francis RJ, Tang C, Vela I, Thomas P, et al. Prostate-specific membrane antigen PET-CT in patients with high-risk prostate cancer before curative-intent surgery or radiotherapy (proPSMA): a prospective, randomised, multicentre study. *Lancet* (2020) 395(10231):1208–16. doi: 10.1016/s0140-6736(20)30314-7

31. Emmett L, Buteau J, Papa N, Moon D, Thompson J, Roberts MJ, et al. The additive diagnostic value of prostate-specific membrane antigen positron emission tomography computed tomography to multiparametric magnetic resonance imaging triage in the diagnosis of prostate cancer (PRIMARY): A prospective multicentre study. *Eur Urol* (2021) 80(6):682–9. doi: 10.1016/j.eururo.2021.08.002

32. Meissner VH, Rauscher I, Schwamborn K, Neumann J, Miller G, Weber W, et al. Radical prostatectomy without prior biopsy following multiparametric magnetic resonance imaging and prostate-specific membrane antigen positron emission tomography. *Eur Urol* (2021). doi: 10.1016/j.eururo.2021.11.019

frontiers | Frontiers in Oncology

TYPE Original Research
PUBLISHED 29 November 2022
DOI 10.3389/fonc.2022.1068893

OPEN ACCESS

EDITED BY
Angelo Naselli,
MultiMedica Holding SpA (IRCCS), Italy

REVIEWED BY
Daniele Castellani,
Polytechnic University of Le Marche, Italy
Octavian Sabin Tataru,
Sciences and Technology of Târgu Mures, Romania

*CORRESPONDENCE
Jia-Jia Wang
wangjj6604@enzemed.com
Lin Zheng
y215180575@zju.edu.cn
Zhi-Rui Zhou
zzr3711@163.com

SPECIALTY SECTION
This article was submitted to Genitourinary Oncology, a section of the journal Frontiers in Oncology

RECEIVED 13 October 2022
ACCEPTED 11 November 2022
PUBLISHED 29 November 2022

CITATION
Mo L-C, Zhang X-J, Zheng H-H, Huang X-P, Zheng L, Zhou Z-R and Wang J-J (2022) Development of a novel nomogram for predicting clinically significant prostate cancer with the prostate health index and multiparametric MRI.
Front. Oncol. 12:1068893.
doi: 10.3389/fonc.2022.1068893

Development of a novel nomogram for predicting clinically significant prostate cancer with the prostate health index and multiparametric MRI

Li-Cai Mo[1], Xian-Jun Zhang[1], Hai-Hong Zheng[2], Xiao-peng Huang[3], Lin Zheng[4]*, Zhi-Rui Zhou[5]* and Jia-Jia Wang[6]*

[1]Department of Urology, Taizhou Hospital of Zhejiang Province affiliated with Wenzhou Medical University, Linhai, Taizhou, Zhejiang, China, [2]Department of Pathology, Taizhou Hospital of Zhejiang Province affiliated with Wenzhou Medical University, Linhai, Taizhou, Zhejiang, China, [3]Department of Urology, Taizhou Cancer Hospital, Wenling, Taizhou, Zhejiang, China, [4]Department of Radiation Oncology Center, Taizhou Cancer Hospital, Wenling, Taizhou, Zhejiang, China, [5]Department of Radiation Oncology Center, Huashan Hospital, Shanghai Medical College, Fudan University, Shanghai, China, [6]Department of Traditional Chinese Medicine, Taizhou Hospital of Zhejiang Province affiliated with Wenzhou Medical University, Linhai, Taizhou, Zhejiang, China

Introduction: On prostate biopsy, multiparametric magnetic resonance imaging (mpMRI) and the Prostate Health Index (PHI) have allowed prediction of clinically significant prostate cancer (csPCa).

Methods: To predict the likelihood of csPCa, we created a nomogram based on a multivariate model that included PHI and mpMRI. We assessed 315 males who were scheduled for prostate biopsies.

Results: We used the Prostate Imaging Reporting and Data System version 2 (PI-RADS V2) to assess mpMRI and optimize PHI testing prior to biopsy. Univariate analysis showed that csPCa may be identified by PHI with a cut-off value of 77.77, PHID with 2.36, and PI-RADS with 3 as the best threshold. Multivariable logistic models for predicting csPCa were developed using PI-RADS, free PSA (fPSA), PHI, and prostate volume. A multivariate model that included PI-RADS, fPSA, PHI, and prostate volume had the best accuracy (AUC: 0.882). Decision curve analysis (DCA), which was carried out to verify the nomogram's clinical applicability, showed an ideal advantage (13.35% higher than the model that include PI-RADS only).

Discussion: In conclusion, the nomogram based on PHI and mpMRI is a valuable tool for predicting csPCa while avoiding unnecessary biopsy as much as possible.

KEYWORDS

prostate cancer, nomogram, multiparametric magnetic resonance imaging (mpMRI), prostate health index, predicting

Introduction

Prostate cancer (PCa) is the most frequent cancer among men for more than half of the globe, and it was the sixth major cause of death among men in 2020 (1). Although the frequency of PCa in China is lower than in European and American countries, it is rising at an alarming pace, which may have a negative impact on survival rate (2). Possible explanations include the rising incidence of PSA screening and the widespread use of multiparametric magnetic resonance imaging (mpMRI) in the clinic (3). PSA has been the most significant molecular biomarker for prostate cancer screening and postoperative follow-up since its discovery in the 1980s (4). However, the low specificity of PSA inevitably results in many needless biopsies, and detecting clinically insignificant prostate cancer is not desirable (5). Moreover, PSA testing mostly reveals indolent cancers that are unlikely to develop throughout a patient's lifetime and that benefit from surgery or radiation only very infrequently (6).

In recent years, it has been shown that the Prostate Health Index (PHI), a mathematical formula that integrates total PSA (tPSA), free PSA (fPSA), and [-2] ProSA (p2PSA), is more effective than tPSA in the diagnosis of csPCa (7–9). The PHI blood test was authorized by the US Food and Drug Administration (FDA) in 2012 to detect PCa with elevated PSA (10). Prostate MRI is useful in diagnosing suspected prostate cancer and has a high negative predictive value (NPV) for csPCa (11). The Prostate Imaging Reporting and Data System, version 2 (PI-RADS v2), which was introduced recently, is a powerful tool to identify csPCa needing biopsy and help locate the lesions of the target (12). If the MRI is positive (PI-RADS score ≥3), biopsies should be conducted (13). However, PI-RADS 3 only identified csPCa in ≤20% of patients (14). In a meta-analysis, the positive predictive value (PPV) of mpMRI for csPCa was 40%, and the PPV in PI-RADS 4 and 5 lesions was still suboptimal (15). It is not advisable to use mpMRI alone to screen patients for biopsy (16). To the best of our knowledge, only a few studies have examined the predictive power of combining mpMRI with PHI in men with csPCa (17–19).

Therefore, we performed this study to conduct a novel nomogram incorporating PHI, mpMRI, and other variables to predict csPCa in a Chinese population.

Materials and methods

Patients

We performed a single-center study of patients with abnormal digital rectal examination (DRE) and/or increased blood tPSA who had biopsies between January 2020 and June 2022. Subjects with acute bacterial prostatitis, urinary tract infections, a history of PCa or a prostate biopsy, or who had taken any dose of 5-alpha reductase inhibitors were excluded. Figure 1 illustrates the screening procedure.

Biomarker measurement

The fPSA, tPSA, and p2PSA levels were determined prior to biopsy using the fully automated immunoassay equipment Access 2 analyzer (Beckman Coulter, Brea, CA, USA). PHI was calculated using the formula p2PSA/fPSA×√tPSA. The percentage of fPSA (%fPSA) was calculated as fPSA/PSA×100, while the percentage of p2PSA (%p2PSA) was defined as p2PSA/fPSA × 100. Moreover, PSA density (PSAD) and PHI density (PHID) were determined as the ratios of PSA/prostate volume and PHI/prostate volume, respectively.

Multiparametric MRI

Without an intrarectal coil, mpMRI of the prostate was performed on a 3.0 T GE Signa HDx MR scanner (GE Healthcare, Milwaukee, USA) prior to biopsy. A senior abdominal radiologist with more than 8 years of expertise in prostate MRI and >300 scans yearly reviewed the mpMRI, which includes T2-weighted imaging (T2WI), diffusion-weighted imaging (DWI), b values of 0 and 800-1200 s/mm^2, and apparent diffusion coefficient (ADC). The 2015 scoring rules

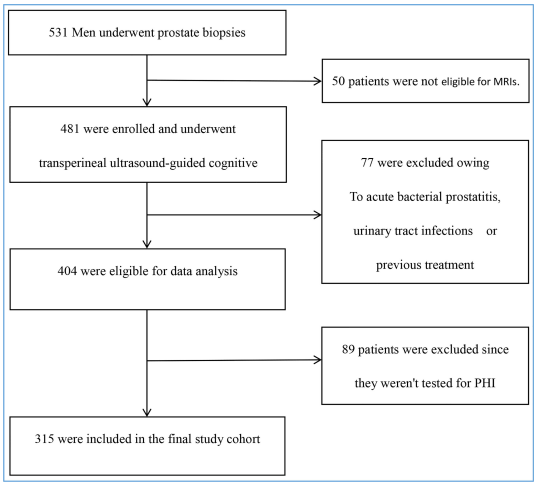

FIGURE 1
Enrollment and outcomes. The primary analysis included all 531 men. Those who were ineligible for MRIs or PHI, as well as those with acute bacterial prostatitis, urinary tract infections, or a history of treatment, were excluded. The final study cohort consisted of 315 people.

for the PI-RADS V2 were used and a score between 1 and 5 was assigned (12).

Biopsy protocol

Patients who had 3.0T mpMRI prior to biopsy received transperineal ultrasound-guided cognitive targeted biopsies for 2-3 cores based on lesions with PI-RADS(≥3) revealed on mpMRI as well as systematic biopsies for at least 12 cores using a biplane TRUS probe (Esaote, Transducer TRT33) and an 18-G disposable needle. Prostate volume was measured using TRUS during a monitoring biopsy. The ellipsoid formula (width × height × length × 0.52) was applied to calculate prostate volume.

Histology

Tissue biopsies were examined by a single dedicated uropathologist. According to the 2014 consensus criteria from the International Society of Urological Pathology, PCa was evaluated as follows: grade group (GG) 1 (Gleason score ≤6), GG 2 (Gleason score 3 + 4 = 7), GG 3 (Gleason score 4 + 3 = 7), GG 4 (Gleason score 8), and GG 5 (Gleason score ≥9) (20). Clinically significant PCa was characterized in prostate biopsy pathology as GG2 ≥2, which is known to be more prevalent in the most recent definitions (21, 22).

Ethics approval

The 1964 Declaration of Helsinki and its later amendments served as the ethical framework for this retrospective investigation. The local ethics commission decided not to require participants to provide their informed consent (Medical Ethics Committee of Taizhou Hospital, Zhejiang Province, China, K20220838).

Statistical analysis

In the case of numerical variables, descriptive statistics (median (25th percentile; 75th percentile)) were utilized to define the entire sample. Percentages and absolute frequencies were used to represent categorical variables. We used Kolmogorov-Smirnov test to test the normal distribution of the continuity variables. For comparisons of continuous variables, the Mann-Whitney U test was utilized. To compare qualitative variables, a chi-squared test was used. We performed ROC analysis to compare the diagnostic accuracy of mpMRI, individual PSA-derived blood indicators, and a combination of the two, and we determined the area under the curve (AUC) and its 95% confidence interval. The DeLong test was employed to evaluate the AUCs of the various prediction models (23). The baseline characteristics of patients (prostate volume), laboratory data (PHI, fPSA), and PI-RADS category were used to develop multivariable logistic models for predicting csPCa. Using a nomogram, the best prediction model was presented for clinical use. Bootstrap resampling (1000 repeats) was utilized to examine both discrimination and calibration for internal model validation. To assess predictive accuracy, a bootstrap method was utilized to obtain bootstrap-corrected estimates of the C-Statistics. Visual and statistical calibration were examined using the Hosmer-Lemeshow test. The Youden index was maximized to obtain an ideal threshold (sensitivity + specificity - 1). IBM SPSS 25.0 (IBM Corp., Armonk, NY, USA) was used for statistical analyses. The results were judged to be statistically significant when the *p*-value was <0.05. Using R and the rms and rmda packages, we were able to visualize nomograms, decision curves, and calibration curves (version. 4.2.1, R Foundation for Statistical Computing, Vienna, Austria).

Results

Clinical characteristics of the study cohort

The clinical characteristics of the patients and the results of auxiliary examination are shown in Table 1. Overall, in the diagnostic setting, 194 patients (61.6%) had a positive biopsy. Patients with negative biopsy and those with PCa on biopsy were compared in terms of age, PI-RADS score, and all PSA-derived serum indicators. The median fPSA concentration was comparable between groups (P = 0.915). Moreover, %fPSA was lower (12.04 vs. 15.90; P <0.001), while p2PSA, %p2PSA, PHI, PSAD and PHID were higher (42.68 vs. 24.76; 2.91 vs. 1.01; 28.23 vs. 17.33; 96.99 vs. 53.22; 0.29 vs. 0.17; 2.91 vs. 1.01, P < 0.001) in patients with PCa.

Of these, 158 (50.2%) had csPCa on biopsy (Table 2). To evaluate csPCa's capacity to distinguish between patients, ROC analyses were carried out. Both the PI-RADS score and PSA-derived biomarkers were substantially associated with the likelihood of csPCa in univariable logistic analysis, with an AUC ranging from 0.52 (95% CI: 0.46 to 0.59) for free PSA to 0.83 (95% CI: 0.79 to 0.88) for PHID. As demonstrated in Table 2, PHID surpassed both the PI-RADS score (AUC: 0.75 (95% CI: 0.70 to 0.81)) and the tPSA (AUC: 0.63 (95% CI: 0.57 to 0.69)) in terms of diagnostic accuracy. In terms of PHI, the optimal cutoff was 77.77, with a corresponding sensitivity of 0.76 (95% CI: 0.68 to 0.82) and specificity of 0.73 (95% CI: 0.65 to 0.80). With a sensitivity of 0.70 (95% CI: 0.62 to 0.77) and specificity of 0.83 (95% CI: 0.76 to 0.89), the optimum threshold for PHID was found to be 2.36. The best cut-off value was established to be a PI-RADS score of 3, with a sensitivity of 0.85

TABLE 1 Demographic and clinical characteristics of the study population.

Parameter	Overall (n = 315)	Negative biopsy (n = 121)	PCa (n = 194)	*P* value
Age (median [IQR]), years	69.00 [64.00, 73.00]	68.00 [61.00, 73.00]	69.00 [65.00, 73.00]	0.118
MRI PI-RADS (%)				<0.001
1	10 (3.2)	8 (6.6)	2 (1.0)	
2	94 (29.8)	57 (47.1)	37 (19.1)	
3	97 (30.8)	36 (29.8)	61 (31.4)	
4	77 (24.4)	17 (14.0)	60 (30.9)	
5	37 (11.7)	3 (2.5)	34 (17.5)	
Prostate volume (median [IQR]), mL	36.04 [26.63, 56.58]	50.40 [32.55, 73.63]	32.94 [24.36, 43.08]	<0.001
tPSA (median [IQR]), ng/mL	9.97 [6.09, 16.54]	8.66 [5.03, 14.26]	10.71 [7.04, 18.97]	0.001
fPSA (median [IQR]), ng/mL	1.42 [0.85, 2.31]	1.43 [0.89, 2.13]	1.39 [0.84, 2.43]	0.915
p2PSA (median [IQR]), pg/mL	36.06 [21.31, 57.14]	24.76 [13.04, 40.80]	42.68 [26.66, 67.74]	<0.001
%fPSA (median [IQR])	13.36 [9.62, 19.22]	15.90 [10.75, 22.72]	12.04 [9.04, 16.73]	<0.001
%p2PSA (median [IQR])	25.02 [16.54, 35.80]	17.33 [12.31, 26.14]	28.23 [20.98, 39.05]	<0.001
PHI (median [IQR])	78.40 [52.33, 118.11]	53.22 [35.86, 76.63]	96.99 [70.12, 150.43]	<0.001
PSAD (median [IQR]), ng/mL/mL	0.24 [0.15, 0.51]	0.17 [0.10, 0.28]	0.29 [0.19, 0.66]	<0.001
PHID (median [IQR])	2.09 [1.03, 3.63]	1.01 [0.70, 1.79]	2.91 [1.85, 4.80]	<0.001

PI-RADS, Prostate Imaging Reporting and Data System; tPSA, total prostate specific antigen; p2PSA, [−2]proPSA; %fPSA,free PSA/total PSA;%p2PSA, p2PSA/free PSA; PHI, prostate health index; PSAD, PSA density, PSA/Prostate volume; PHID, PHI density, PHI/Prostate volume.

TABLE 2 AUC comparing patients with clinically significant prostate cancer (csPCa) versus patients with negative biopsy or clinically insignificant PCa (No csPCa).

Studied Variables	No csPCa (n = 157)	csPCa (n = 158)	*P* value	AUC (95% CI)	Cut-off	Sensitivity	Specificity
Age (median [IQR]), years	68.00 [63.00, 73.00]	70.00 [65.00, 73.00]	0.147	0.55 (0.48-0.61)	69.5	0.51	0.60
MRI PI-RADS (%)			<0.001	0.75 (0.70-0.81)	3	0.85	0.52
1	9 (5.7)	1 (0.6)					
2	72 (45.9)	22 (13.9)					
3	47 (29.9)	50 (31.6)					
4	25 (15.9)	52 (32.9)					
5	4 (2.5)	33 (20.9)					
Prostate volume (median [IQR]), mL	45.11 [30.28, 71.98]	32.64 [23.71, 40.46]	<0.001	0.69 (0.63-0.75)	17.66	0.98	0.03
tPSA (median [IQR]), ng/mL	8.70 [5.19, 14.06]	10.91 [7.28, 21.22]	<0.001	0.63 (0.57-0.69)	17.57	0.32	0.87
fPSA (median [IQR]), ng/mL	1.42 [0.87, 2.13]	1.42 [0.84, 2.52]	0.521	0.52 (0.46-0.59)	2.02	0.37	0.75
p2PSA (median [IQR]), pg/mL	26.81 [14.55, 42.68]	46.16 [29.27, 70.82]	<0.001	0.71 (0.66-0.77)	35.26	0.68	0.66
%fPSA (median [IQR])	15.85 [10.75, 22.16]	11.66 [8.72, 15.21]	<0.001	0.67 (0.61-0.73)	50.03	0.02	1
%p2PSA (median [IQR])	19.58 [12.69, 28.67]	29.72 [22.43, 41.09]	<0.001	0.71 (0.65-0.77)	22.29	0.76	0.62
PHI (median [IQR])	55.79 [38.29, 80.16]	100.20 [78.23, 156.05]	<0.001	0.81 (0.75-0.85)	77.77	0.76	0.73
PSAD (median [IQR]), ng/mL/mL	0.18 [0.11, 0.29]	0.34 [0.21, 0.75]	<0.001	0.74 (0.68-0.79)	0.26	0.65	0.71
PHID (median [IQR])	1.13 [0.77, 2.10]	3.36 [2.09, 5.25]	<0.001	0.83 (0.79-0.88)	2.36	0.70	0.83
PI-RADS + volume			<0.001	0.80 (0.75-0.85)		0.81	0.71
PI-RADS+ PHI			<0.001	0.85 (0.81-0.89)		0.79	0.81
PI-RADS + volume+PHI			<0.001	0.87 (0.84-0.91)		0.81	0.82
PI-RADS+volume +PHI+ fPSA			<0.001	0.88 (0.85-0.92)		0.83	0.83

The AUC of the matching ROC curve with the 95% confidence interval (CI) is provided for each variable. According to the Youden index maximization, the best threshold for the diagnosis of PCa is provided with the achieved sensitivity and specificity. Cases are defined as individuals with values equal to or more than the threshold, with the exception of prostate volume, which is the inverse. PI-RADS, Prostate Imaging Reporting and Data System; tPSA, total prostate specific antigen; p2PSA, [−2]proPSA; %fPSA,free PSA/total PSA;%p2PSA, p2PSA/free PSA; PHI, prostate health index; PSAD, PSA density, PSA/Prostate volume; PHID, PHI density, PHI/Prostate volume; AUC, area under curve; ROC, receiver operating characteristic.

(95% CI: 0.79 to 0.90) and a specificity of 0.52 (95% CI: 0.44 to 0.60) (Table 2).

Correlation between PHID and PI-RADS score

The distribution of PHID and prostate biopsy pathology findings classified by PI-RADS score grade is shown in Figure 2. Patients with PI-RADS 4 presented an increased likelihood of harboring csPCa compared with those with PI-RADS 1 (OR 18.72 (95% CI: 2.25-156.01); P = 0.0068), PI-RADS 2 (OR 6.81 (95% CI: 3.47-13.37); $P < 0.0001$), and PI-RADS 3 (OR 1.96 (95% CI: 1.05-3.64); P = 0.0344). Patients with PI-RADS 5 presented an increased likelihood of harboring csPCa compared with those with PI-RADS 1 (OR 74.25 (95% CI: 7.36-749.46); P = 0.0003), PI-RADS 2 (OR 27.00 (95% CI: 8.62-84.61); $P < 0.0001$), and PI-RADS 3 (OR 7.75 (95% CI: 2.55-23.57); P = 0.0003).

Nomogram development and internal validation for predicting csPCa

Multivariable logistic analysis using PI-RADS, fPSA, PHI, and prostate volume yielded an AUC of 0.882 (95% CI: 0.845 to 0.920), and a nomogram was created to display these findings visually (Table 2, Table 3, and Figure 3). The PHI and mpMRI nomograms were internally tested using a 1000 bootstrap resampled dataset. The computed bootstrap-corrected C-index of 0.877 demonstrates excellent discriminative power. According to the calibration plot, there was a high degree of agreement between the calculated and observed probabilities (Figure 4). As measured by the Hosmer-Lemeshow goodness-of-fit test, the model was calibrated well (P = 0.829). Decision curve analysis (DCA) was carried out to verify the nomogram's clinical applicability, and the results showed a maximum advantage (13.35% higher than the model that include PI-RADS only) (Figure 5). Furthermore, as shown in Figure 5, the net clinical benefit was 0.3206 based on the 50% likelihood threshold of what was expected.

Discussion

To our knowledge, this is a novel viable prediction nomogram model based on PHI and mpMRI that may enhance csPCa detection, greatly lowering PCa overdiagnosis prior to prostate biopsy in an Asian population. The net clinical benefit in this research was 0.3206, indicating that the nomogram would increase the identification of csPCa by 32.06%, leading to fewer needless biopsies when compared to a threshold possibility of 50%.

A change in cancer diagnostic priorities from detecting all cancers to focusing on the identification of potentially aggressive but curable cancers and minimizing the detection and treatment of indolent disease has resulted from the recognition of PCa overdiagnosis and overtreatment (24). In recent years, numerous novel biomarkers, including PHI, have shown promise in distinguishing clinically significant from inconsequential PCa more reliably than PSA (25–27). Extensive multicenter research has shown that employing a PHI threshold of 24, could have prevented 36%–41% of needless biopsies and 17%-24% of overdiagnosed indolent cancers (28). Additionally, the PHI has been verified in Asian populations. According to the results of a multicenter study conducted in China, Na et al. revealed that using a PHI of ≤35 as the threshold would have resulted in the missed diagnosis of 8% of PCa in prostate biopsies and 4% of high-grade lesions (29). The efficacy of PHI was analyzed across

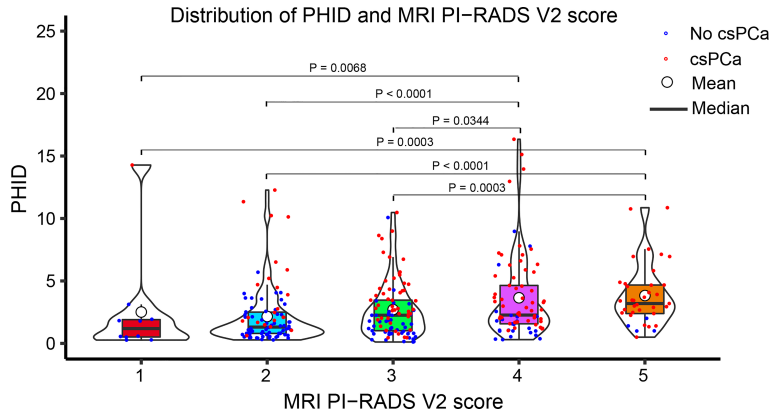

FIGURE 2
Violin plot showing the distribution of PHID according to the PI-RADS v2 score. Data are shown as the median (bold horizontal line in the box) and Q1 and Q3 (borders of the box). *Q1 = 25th percentile; Q3 = 75th percentile; IQR (interquartile range) = Q3-Q1.*.

TABLE 3 Multivariate logistic regression analysis of predictors in the prediction of csPCa.

Predictor	Odds Ratio	95% CI.	coefficient	*P* value
MRI PI-RADS	6.50	3.43-12.33	1.87	<0.0001
Prostate volume	0.42	0.27-0.63	-0.88	<0.0001
PHI	4.59	2.83-7.44	1.52	<0.0001
fPSA	1.23	1.04-1.46	0.21	0.0164

PI-RADS, Prostate Imaging Reporting and Data System; csPCa, clinically significant prostate cancer; PHI, prostate health index.

many Asian populations in a multicenter study. Using PHI criteria of 25, 25-35, 35-55, and >55, higher-grade PCa (Gleason 7) was found to be diagnosed in 1.0%, 1.9%, 13%, and 30% of Asian males, respectively (30).

The success of PSAD encouraged several authors to assess the use of PHID, which was originally reported in 2014 by Mearini et al. (31). The comparison between PHID and PHI showed equivocal findings. In a large cohort of naïve biopsy patients in whom PHI and PHID were compared, PHI seemed to perform better than PHID, especially in those with small prostates (under 40 cc) (32). Additionally, Garrido et al., in a cohort of patients with tPSA less than 10 ng/ml, revealed that PHID had a better diagnostic performance than PHI for overall PCa detection, not specifically for csPCa (33). However, in contrast to these findings, Tosoian et al. observed a considerably higher AUC for PHID (0.84 vs. 0.76 for PHI) in csPCa, leading to future research investigating its value (34). More recently, Druskin et al. reported a higher AUC for PHID (0.82) versus PHI (0.79) in the diagnosis of csPCa on biopsy (35). Our results also showed that PHID performed better than

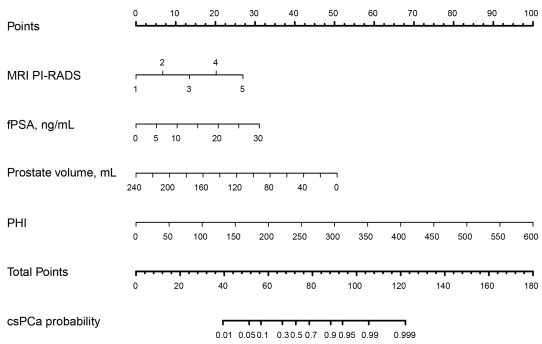

FIGURE 3
The nomogram was employed by determining the patient's location on each factor axis. The scores for each element are summed to obtain a total score, which is depicted on the lower axis and corresponds to the likelihood of csPCa. *PI-RADS, Prostate Imaging Reporting and Data System; fPSA: free PSA; PHI: prostate health index; tPSA: total PSA; csPCa: clinically significant prostate cancer.*.

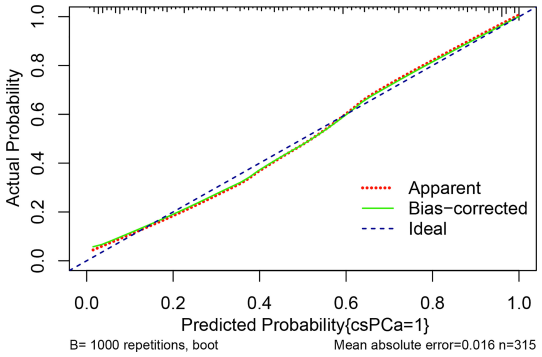

FIGURE 4
The calibration curve compares the accuracy of the original prediction model ("apparent") (light dashed red line) to the bootstrap model ("bias corrected") (solid green line) in predicting the likelihood of csPCa. The ideal calibration is shown by the diagonal blue dot line, which serves as the reference line. The abscissa indicates the anticipated value determined from the nomogram, whereas the ordinate reflects the observed actual probability value. Small vertical lines at the top of the graph represent the distribution of the expected probability. Overprediction occurs when an estimate falls below the reference line, while underprediction occurs when an estimate rises above the reference line. In an ideal situation, these two lines should be close to the diagonally dashed blue line.

PHI, with AUCs of 0.83 and 0.81, respectively. Finally, Chiu et al. found that combining PHI and prostate volume (as PHID) is an excellent indicator of csPCa with an AUC of 0.82. For csPCa, PHID was most effective in preventing unnecessary biopsies (43.7%), achieving 90% sensitivity, and missing the fewest cases (8.5%) when PHID was ≥0.67 (25).

However, these studies did not include prostate MRI, a crucial technology that is increasingly being used in PCa diagnosis. The American Urological Association (AUA) concurs that lesions discovered on prostate mpMRI with PI-RADS ≥3 should be biopsied immediately and that biopsy of PI-RADS 3 lesions should not typically be postponed (36). The PPV of prostate mpMRI, however, is not optimal. Vendrink et al. discovered that 17%, 34%, and 67% of patients with PI-RADS 3, 4, and 5 lesions were diagnosed with csPCa, respectively (37). Together, PHI and MRI have been shown to improve diagnostic performance, allowing doctors to forego needle biopsies while still detecting the presence of advanced PCa. Hsieh et al. demonstrated in a prospective Asian cohort study that if prostate biopsies were only conducted in individuals with PI-RADS ≥3 and PHI ≥30 and just 1 patient with csPCa was excluded, roughly half of these biopsies could be avoided (22). Druskin et al. showed in a study of 104 men that the PI-RADS scores were complimentary to PHID and that the great majority of csPCa patients were diagnosed with a PI-RADS score of 1 or 2, a PHID ≥0.44 or, if a PI-RADS score of 3, 4, or 5 (35). These data confirm our hypothesis that a unique nomogram based on

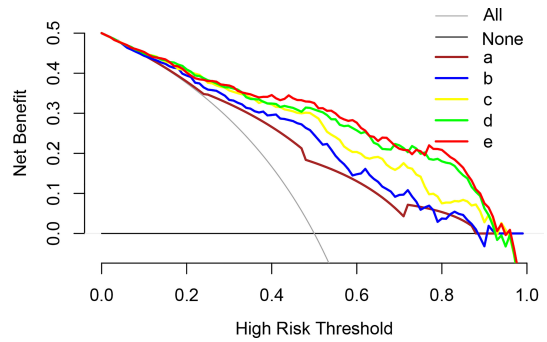

FIGURE 5
Analysis of the decision curves of several basic models and nomogram models. a: MRI PI-RADS; b: MRI PI-RADS + volume; c: MRI PI-RADS + PHI; d: MRI PI-RADS + volume + PHI; e: MRI PI-RADS + volume + PHI + fPSA (Nomogram model). *PI-RADS, Prostate Imaging Reporting and Data System; tPSA, total prostate-specific antigen; PHI, prostate health index.*.

PHID/PHI and multiparametric MRI might be a valuable tool for predicting csPCa.

To our knowledge, this is a novel feasible predictive nomogram model based on PHI and mpMRI for assessing the PHI and PI-RADS scoring systems as a method of avoiding needless needle biopsies and combating overdiagnosis. As a result, the integration of PHI and mpMRI shows potential for csPCa assessment prior to prostate biopsy, which might improve patient quality of life and save healthcare costs. In the current study, we created and internally verified a novel nomogram based on PHI and MRI, achieving excellent csPCa detection accuracy (AUC 0.882). In addition, when compared to the other examined models, the highest net advantage for csPCa detection was achieved with a substantial cutoff possibility. In addition, the net clinical benefit was 0.3206 based on the 50% likelihood threshold of what was projected to happen, indicating that the nomogram would increase the detection of csPCa by 32.06%, hence lowering the number of needless biopsies.

Our results must be evaluated against some constraints. First, over the past few years, csPCa has been defined in a variety of different ways, and there is still no universally agreed upon definition. Overall, the most recent criteria seem to favor a Gleason score of >6 (ISUP >1); hence, we utilized that to designate csPCa in our analysis (38). Second, the analysis was based on prostate biopsy pathology, which is a drawback of this study. Because some individuals in this group who were diagnosed with prostate cancer selected brachytherapy or radiotherapy, the postoperative pathology of prostate cancer could not be collected, and csPCa may have been underestimated. The pathological upgrading rates of systematic biopsy alone, targeted biopsy alone, and targeted biopsy paired with systematic biopsy were 16.8%, 8.2%, and 3.5%, respectively (39, 40). Furthermore, in our investigation, targeted biopsy was performed using cognitive registration, which may be less accurate than MR/US fusion systems.

In conclusion, our PHI- and mpMRI-based nomograms are good prediction tools that may enhance the identification of patients with csPCa while avoiding unnecessary biopsies as much as possible. However, further research is required to externally confirm this nomogram and enhance csPCa detection.

Data availability statement

The original contributions presented in the study are included in the article/Supplementary Material. Further inquiries can be directed to the corresponding authors.

Ethics statement

The studies involving human participants were reviewed and approved by Medical Ethics Committee of Taizhou Hospital, Zhejiang Province, China, K20220838. Written informed consent for participation was not required for this study in accordance with the national legislation and the institutional requirements.

Author contributions

LZ, Z-RZ, J-JW, and L-CM conceived and designed the study and drafted the manuscript. L-CM, X-JZ, H-HZ, and X-PH collected, analyzed, and interpreted the data. LZ, Z-RZ, and J-JW participated in revising the manuscript.

Funding

This work was supported by the National Natural Science Foundation of China (grant 82003231 to Dr. ZRZ), the Traditional Chinese Medicine Science and Technology Plan Project of Zhejiang Province (No. 2022ZB388), Scientific Research Fund of Taizhou Enze Medical Center (Group) (No. 15EZD36), and the Wenling Science and Technology Program (No. 2020S0040001, 2021S00081, and 2021S00088).

Conflict of interest

The authors declare that the research was conducted in the absence of any commercial or financial relationships that could be construed as a potential conflict of interest.

Publisher's note

References

1. Sung H, Ferlay J, Siegel RL, Laversanne M, Soerjomataram I, Jemal A, et al. Global cancer statistics 2020: GLOBOCAN estimates of incidence and mortality worldwide for 36 cancers in 185 countries. *CA Cancer J Clin* (2021) 71:209–49. doi: 10.3322/caac.21660

2. Liu X, Yu C, Bi Y, Zhang ZJ. Trends and age-period-cohort effect on incidence and mortality of prostate cancer from 1990 to 2017 in China. *Public Health* (2019) 172:70–80. doi: 10.1016/j.puhe.2019.04.016

3. Litwin MS, Tan HJ. The diagnosis and treatment of prostate cancer: A review. *JAMA* (2017) 317:2532–42. doi: 10.1001/jama.2017.7248

4. Stamey TA, Yang N, Hay AR, McNeal JE, Freiha FS, Redwine E. Prostate-specific antigen as a serum marker for adenocarcinoma of the prostate. *N Engl J Med* (1987) 317:909–16. doi: 10.1056/NEJM198710083171501

5. Van Poppel H, Hogenhout R, Albers P, van den Bergh R, Barentsz JO, Roobol MJ. Early detection of prostate cancer in 2020 and beyond: Facts and recommendations for the European union and the European commission. *Eur Urol* (2021) 79:327–9. doi: 10.1016/j.eururo.2020.12.010

6. Heijnsdijk EA, Wever EM, Auvinen A, Hugosson J, Ciatto S, Nelen V, et al. Quality-of-life effects of prostate-specific antigen screening. *N Engl J Med* (2012) 367:595–605. doi: 10.1056/NEJMoa1201637

7. Chen H, Qian Y, Wu Y, Shi B, Zhou J, Qu F, et al. Modified prostate health index density significantly improves clinically significant prostate cancer (csPCa) detection. *Front Oncol* (2022) 12:864111. doi: 10.3389/fonc.2022.864111

8. Foley RW, Gorman L, Sharifi N, Murphy K, Moore H, Tuzova AV, et al. Improving multivariable prostate cancer risk assessment using the prostate health index. *BJU Int* (2016) 117:409–17. doi: 10.1111/bju.13143

9. White J, Shenoy BV, Tutrone RF, Karsh LI, Saltzstein DR, Harmon WJ, et al. Clinical utility of the prostate health index (phi) for biopsy decision management in a large group urology practice setting. *Prostate Cancer Prostatic Dis* (2018) 21:78–84. doi: 10.1038/s41391-017-0008-7

10. Hendriks RJ, van Oort IM, Schalken JA. Blood-based and urinary prostate cancer biomarkers: a review and comparison of novel biomarkers for detection and treatment decisions. *Prostate Cancer Prostatic Dis* (2017) 20:12–9. doi: 10.1038/pcan.2016.59

11. Schoots IG, Petrides N, Giganti F, Bokhorst LP, Rannikko A, Klotz L, et al. Magnetic resonance imaging in active surveillance of prostate cancer: a systematic review. *Eur Urol* (2015) 67:627–36. doi: 10.1016/j.eururo.2014.10.050

12. Weinreb JC, Barentsz JO, Choyke PL, Cornud F, Haider MA, Macura KJ, et al. PI-RADS prostate imaging - reporting and data system: 2015, version 2. *Eur Urol* (2016) 69:16–40. doi: 10.1016/j.eururo.2015.08.052

13. Kum F, Elhage O, Maliyil J, Wong K, Faure Walker N, Kulkarni M, et al. Initial outcomes of local anaesthetic freehand transperineal prostate biopsies in the outpatient setting. *BJU Int* (2020) 125:244–52. doi: 10.1111/bju.14620

14. Kasivisvanathan V, Rannikko AS, Borghi M, Panebianco V, Mynderse LA, Vaarala MH, et al. MRI-Targeted or standard biopsy for prostate-cancer diagnosis. *N Engl J Med* (2018) 378:1767–77. doi: 10.1056/NEJMoa1801993

15. Mazzone E, Stabile A, Pellegrino F, Basile G, Cignoli D, Cirulli GO, et al. Positive predictive value of prostate imaging reporting and data system version 2 for the detection of clinically significant prostate cancer: A systematic review and meta-analysis. *Eur Urol Oncol* (2021) 4:697–713. doi: 10.1016/j.euo.2020.12.004

16. Ferro M, Crocetto F, Bruzzese D, Imbriaco M, Fusco F, Longo N, et al. Prostate health index and multiparametric MRI: Partners in crime fighting overdiagnosis and overtreatment in prostate cancer. *Cancers (Basel)* (2021) 13:4723. doi: 10.3390/cancers13184723

17. Stejskal J, Adamcová V, Záleský M, Novák V, Čapoun O, Fiala V, et al. The predictive value of the prostate health index vs. multiparametric magnetic resonance imaging for prostate cancer diagnosis in prostate biopsy. *World J Urol* (2021) 39:1889–95. doi: 10.1007/s00345-020-03397-4

18. Fan YH, Pan PH, Cheng WM, Wang HK, Shen SH, Liu HT, et al. The prostate health index aids multi-parametric MRI in diagnosing significant prostate cancer. *Sci Rep* (2021) 11:1286. doi: 10.1038/s41598-020-78428-6

19. Schwen ZR, Mamawala M, Tosoian JJ, Druskin SC, Ross AE, Sokoll LJ, et al. Prostate health index and multiparametric magnetic resonance imaging to predict prostate cancer grade reclassification in active surveillance. *BJU Int* (2020) 126:373–8. doi: 10.1111/bju.15101

20. Epstein JI, Egevad L, Amin MB, Delahunt B, Srigley JR, Humphrey PA. The 2014 international society of urological pathology (ISUP) consensus conference on Gleason grading of prostatic carcinoma: Definition of grading patterns and proposal for a new grading system. *Am J Surg Pathol* (2016) 40:244–52. doi: 10.1097/PAS.0000000000000530

21. Mohler JL, Antonarakis ES, Armstrong AJ, D'Amico AV, Davis BJ, Dorff T, et al. Prostate cancer, version 2.2019, NCCN clinical practice guidelines in oncology. *J Natl Compr Canc Netw* (2019) 17:479–505. doi: 10.6004/jnccn.2019.0023

22. Hsieh PF, Li WJ, Lin WC, Chang H, Chang CH, Huang CP, et al. Combining prostate health index and multiparametric magnetic resonance imaging in the diagnosis of clinically significant prostate cancer in an Asian population. *World J Urol* (2020) 38:1207–14. doi: 10.1007/s00345-019-02889-2

23. DeLong ER, DeLong DM, Clarke-Pearson DL. Comparing the areas under two or more correlated receiver operating characteristic curves: a nonparametric approach. *Biometrics* (1988) 44:837–45. doi: 10.2307/2531595

24. McDonald ML, Parsons JK. The case for tailored prostate cancer screening: An NCCN perspective. *J Natl Compr Canc Netw* (2015) 13:1576–83. doi: 10.6004/jnccn.2015.0183

25. Chiu ST, Cheng YT, Pu YS, Lu YC, Hong JH, Chung SD, et al. Prostate health index density outperforms prostate health index in clinically significant prostate cancer detection. *Front Oncol* (2021) 11:772182. doi: 10.3389/fonc.2021.772182

26. Foj L, Filella X. Development and internal validation of a novel PHI-nomogram to identify aggressive prostate cancer. *Clin Chim Acta* (2020) 501:174–8. doi: 10.1016/j.cca.2019.10.039

27. Catalona WJ, Partin AW, Sanda MG, Wei JT, Klee GG, Bangma CH, et al. A multicenter study of [-2]pro-prostate specific antigen combined with prostate specific antigen and free prostate specific antigen for prostate cancer detection in the 2.0 to 10.0 ng/ml prostate specific antigen range. *J Urol* (2011) 185:1650–5. doi: 10.1016/j.juro.2010.12.032

28. de la Calle C, Patil D, Wei JT, Scherr DS, Sokoll L, Chan DW, et al. Multicenter evaluation of the prostate health index to detect aggressive prostate cancer in biopsy naïve men. *J Urol* (2015) 194:65–72. doi: 10.1016/j.juro.2015.01.091

29. Na R, Ye D, Qi J, Liu F, Helfand BT, Brendler CB, et al. Prostate health index significantly reduced unnecessary prostate biopsies in patients with PSA 2-10 ng/mL and PSA >10 ng/mL: Results from a multicenter study in China. *Prostate* (2017) 77:1221–9. doi: 10.1002/pros.23382

30. Chiu PK, Ng CF, Semjonow A, Zhu Y, Vincendeau S, Houlgatte A, et al. A multicentre evaluation of the role of the prostate health index (PHI) in regions with differing prevalence of prostate cancer: Adjustment of PHI reference ranges is needed for European and Asian settings. *Eur Urol* (2019) 75:558–61. doi: 10.1016/j.eururo.2018.10.047

31. Mearini L, Ferri C, Lazzeri M, Bini V, Nunzi E, Fiorini D, et al. Evaluation of prostate-specific antigen isoform p2PSA and its derivates, %p2PSA, prostate health index and prostate dimension-adjusted related index in the detection of prostate cancer at first biopsy: an exploratory, prospective study. *Urol Int* (2014) 93:135–45. doi: 10.1159/000356240

32. Peters R, Stephan C, Jung K, Lein M, Friedersdorff F, Maxeiner A. Comparison of PHI and PHI density for prostate cancer detection in a Large retrospective Caucasian cohort. *Urol Int* (2022) 106:878–83. doi: 10.1159/000517891

33. Garrido MM, Ribeiro RM, Pinheiro LC, Holdenrieder S, Guimarães JT. The prostate health index (PHI) density: Are there advantages over PHI or over the prostate-specific antigen density. *Clin Chim Acta* (2021) 520:133–8. doi: 10.1016/j.cca.2021.06.006

34. Tosoian JJ, Druskin SC, Andreas D, Mullane P, Chappidi M, Joo S, et al. Prostate health index density improves detection of clinically significant prostate cancer. *BJU Int* (2017) 120:793–8. doi: 10.1111/bju.13762

35. Druskin SC, Tosoian JJ, Young A, Collica S, Srivastava A, Ghabili K, et al. Combining prostate health index density, magnetic resonance imaging and prior negative biopsy status to improve the detection of clinically significant prostate cancer. *BJU Int* (2018) 121:619–26. doi: 10.1111/bju.14098

36. Rosenkrantz AB, Verma S, Choyke P, Eberhardt SC, Eggener SE, Gaitonde K, et al. Prostate magnetic resonance imaging and magnetic resonance imaging targeted biopsy in patients with a prior negative biopsy: A consensus statement by AUA and SAR. *J Urol* (2016) 196:1613–8. doi: 10.1016/j.juro.2016.06.079

37. Heidegger I, Klocker H, Pichler R, Pircher A, Prokop W, Steiner E, et al. ProPSA and the prostate health index as predictive markers for aggressiveness in low-risk prostate cancer-results from an international multicenter study. *Prostate Cancer Prostatic Dis* (2017) 20:271–5. doi: 10.1038/pcan.2017.3

38. Matoso A, Epstein JI. Defining clinically significant prostate cancer on the basis of pathological findings. *Histopathology* (2019) 74:135–45. doi: 10.1111/his.13712

39. Bittner N, Merrick G, Taira A, Bennett A, Schattel A, Butler W, et al. Location and grade of prostate cancer diagnosed by transperineal template-guided mapping biopsy after negative transrectal ultrasound-guided biopsy. *Am J Clin Oncol* (2018) 41:723–9. doi: 10.1097/COC.0000000000000352

40. Ahdoot M, Wilbur AR, Reese SE, Lebastchi AH, Mehralivand S, Gomella PT, et al. MRI-Targeted, systematic, and combined biopsy for prostate cancer diagnosis. *N Engl J Med* (2020) 382:917–28. doi: 10.1056/NEJMoa1910038

frontiers | Frontiers in Oncology

TYPE Original Research
PUBLISHED 05 January 2023
DOI 10.3389/fonc.2022.1033323

OPEN ACCESS

EDITED BY
Radka Stoyanova,
University of Miami, United States

REVIEWED BY
Evangelia Zacharaki,
University of Miami, United States
Jeffrey Tuan,
National Cancer Centre Singapore, Singapore
Francesco Del Giudice,
Sapienza University of Rome, Italy

*CORRESPONDENCE
Rulon Mayer
mayerru@yahoo.com

SPECIALTY SECTION
This article was submitted to Genitourinary Oncology, a section of the journal Frontiers in Oncology

RECEIVED 31 August 2022
ACCEPTED 30 November 2022
PUBLISHED 05 January 2023

CITATION
Mayer R, Turkbey B, Choyke P and Simone CB II (2023) Assessing and testing anomaly detection for finding prostate cancer in spatially registered multi-parametric MRI.
Front. Oncol. 12:1033323.
doi: 10.3389/fonc.2022.1033323

Assessing and testing anomaly detection for finding prostate cancer in spatially registered multi-parametric MRI

Rulon Mayer[1,2*], Baris Turkbey[3], Peter Choyke[3] and Charles B. Simone II[4,5]

[1]Department of Radiation Oncology, Perelman School of Medicine, University of Pennsylvania, Philadelphia, PA, United States, [2]OncoScore, Garrett Park, MD, United States, [3]Molecular Imaging Branch, National Institutes of Health (NIH), Bethesda, MD, United States, [4]Department of Radiation Oncology, New York Proton Center, New York, NY, United States, [5]Memorial Sloan Kettering Cancer Center, New York, NY, United States

Background: Evaluating and displaying prostate cancer through non-invasive imagery such as Multi-Parametric MRI (MP-MRI) bolsters management of patients. Recent research quantitatively applied supervised target algorithms using vectoral tumor signatures to spatially registered T1, T2, Diffusion, and Dynamic Contrast Enhancement images. This is the first study to apply the Reed-Xiaoli (RX) multi-spectral anomaly detector (unsupervised target detector) to prostate cancer, which searches for voxels that depart from the background normal tissue, and detects aberrant voxels, presumably tumors.

Methods: MP-MRI (T1, T2, diffusion, dynamic contrast-enhanced images, or seven components) were prospectively collected from 26 patients and then resized, translated, and stitched to form spatially registered multi-parametric cubes. The covariance matrix (CM) and mean μ were computed from background normal tissue. For RX, noise was reduced for the CM by filtering out principal components (PC), regularization, and elliptical envelope minimization. The RX images were compared to images derived from the threshold Adaptive Cosine Estimator (ACE) and quantitative color analysis. Receiver Operator Characteristic (ROC) curves were used for RX and reference images. To quantitatively assess algorithm performance, the Area Under the Curve (AUC) and the Youden Index (YI) points for the ROC curves were computed.

Results: The patient average for the AUC and [YI] from ROC curves for RX from filtering 3 and 4 PC was 0.734[0.706] and 0.727[0.703], respectively, relative to the ACE images. The AUC[YI] for RX from modified Regularization was 0.638 [0.639], Regularization 0.716[0.690], elliptical envelope minimization 0.544 [0.597], and unprocessed CM 0.581[0.608] using the ACE images as Reference Image. The AUC[YI] for RX from filtering 3 and 4 PC was 0.742 [0.711] and 0.740[0.708], respectively, relative to the quantitative color images. The AUC[YI] for RX from modified Regularization was 0.643[0.648], Regularization 0.722[0.695], elliptical envelope minimization 0.508[0.605],

and unprocessed CM 0.569[0.615] using the color images as Reference Image. All standard errors were less than 0.020.

Conclusions: This first study of spatially registered MP-MRI applied anomaly detection using RX, an unsupervised target detection algorithm for prostate cancer. For RX, filtering out PC and applying Regularization achieved higher AUC and YI using ACE and color images as references than unprocessed CM, modified Regularization, and elliptical envelope minimization.

KEYWORDS

anomaly and outlier detection, multi-parametric MRI, prostate cancer, tumor detection, regularization, principal component analysis, image analysis, color analysis

Introduction

Optimal prostate cancer (PCa) management requires an accurate evaluation of potential tumor aggressiveness (1–3). Several clinical indicators (4–17), such as prostate specific antigen (PSA) (7–9), seminal vesicle involvement (10, 11), tumor volume (12–16), extraprostatic extension and other MRI features (17–21), and the Gleason score (22) predict clinical outcomes such as biochemical recurrence after treatment (4–6) and cancer metastasis (10, 11, 14). However, some data, such as PSA (8), are not consistently predictive of outcome. By interpreting multi-parametric MRI using the Prostate Imaging Reporting and Data System (PI-RADS) protocol (17–20), radiologists apply a series of rules to generate a PI-RADS score for the lesion. Visual inspection and assessment of imaging or histology slices rely on the experience and judgment of radiologists and pathologists (17–20), possibly creating inconsistent evaluations due to inter-reader variability. A more objective and quantitative approach could reduce such variability.

To achieve this, there is interest in quantitatively applying and assessing supervised target algorithms to spatially registered T1, T2, diffusion, and dynamic contrast enhancement images at the voxel level (23–28). Previous research examined tumors using vectoral tumor signatures that were inserted into supervised target algorithms applied to spatially registered MRI hypercubes. The supervised target detection algorithms applied to (23–28) assessing prostate cancer were adapted from remote sensing applications designed to analyze hyperspectral images generated from airborne platforms. The spectral signature helps discriminate tumors (or targets in the case of remote sensing) from normal tissue (or backgrounds). Instead of exploiting the unique spectral content of a target, remote sensing can also peruse an image for candidate targets by examining and finding pixels (or voxels) that statistically depart from the background, also known as anomaly detection. Although less specific than supervised target detection, anomaly detection (29–31) can find unsuspected targets but is also subject to detecting additional false positives. For multispectral or hyperspectral images, the commonly used algorithm is called Reed-Xiaoli (RX) (32) and computes the magnitude of a voxel's vector distance (in whitened space) from the background or normal prostate. The larger the RX value, the more the voxel departs from normal tissue. A hypersphere decision surface surrounding the background provides a criterion for whether a voxel is normal (inside the hypersphere) or anomalous (outside the hypersphere).

Anomaly detection has also been applied to medical images (33–38). However, this study significantly differs from previous efforts. The background (normal prostate) is characterized by second-order statistics such as a multi-dimensional covariance matrix and mean, not features derived through spatial processing. Specifically, most of the other studies extracted features from images derived in a single modality, unlike the work described in this manuscript. Previously, extra dimensions were added (37, 38) through spatial processing from a single modality. In another study, anomaly detection followed the temporal evolution (35) of a contrast agent from a single modality and considered time to be the "fourth dimension." In this study, voxels from structural (T1, T2), dynamic contrast enhancement, and diffusion images composed the "fourth dimension." The RX algorithm is purely spectral and does not require spatial processing. In addition, other studies employed deep learning and artificial intelligence approaches, unlike the present work, which used a faster, simpler algorithm (RX). The present work, unlike deep learning approaches that require retraining, can more easily be adapted to clinics that employ different magnetic fields and pulse sequences (23) by using whitening –dewhitening transforms.

This study of spatially registered multi-parametric MRI is the first to apply an unsupervised target detection for prostate

cancer, specifically the RX algorithm, that does not use a tumor signature. The covariance matrix (CM) and mean background vector proscribes the decision surface for RX, an anomaly detector. The anomaly detector searches for voxels that depart from the normal tissue, or background. Such an anomaly detector may be sensitive to both higher and lesser vascularized regions of the tumor and provide a more complete assessment of the lesion.

Method and materials

Overall summary

Figure 1 shows schematically the procedures for computing anomaly detection and generating the receiver operator characteristic (ROC) curve. First, the MRI images are collected, resized, translated, resampled, and stitched together to assemble spatially registered hyperspectral image cubes. The normal prostate is outlined to help form a mask that is applied to the hyperspectral image cubes to aid calculations for RX (red outline, arrow) and Adaptive Cosine Estimator (31) or ACE (blue outline, arrow), a supervised target detection algorithm. The normal prostate mask aids the hyperspectral statistics computation for the normal prostate and delineates the normal prostate reference mask (orange arrow) for the ROC calculations. The color (green outline) scheme, specifically the RGB (red, green, and blue channels), is assigned to the washout from the dynamic contrast enhancement and the high B from the diffusion weighted images, respectively. The colors are quantified using CIELAB computations (24). Color/CIELAB is used to display tumors, to generate a Reference Mask. Thresholds applied to the ACE (blue outline) and CIELAB color (green outline, arrow) calculations help form two independent tumor reference image masks that are used for the ROC calculation (yellow outline). A signature of the tumor is taken from the hyperspectral image cube and inserted into the ACE calculation. Four options were examined for reducing noise in the covariance matrix for the RX calculation (red outline): principal component filtering, regularization, modified regularization, and the unprocessed covariance matrix (red outline).

The *Methods and materials* section qualitatively describes the individual components, namely the spatial registered hypercube assembly, reference mask, anomaly detector generator, and assessment. The Appendix summarizes the mathematics used to generate the components. More details can be found in the cited references.

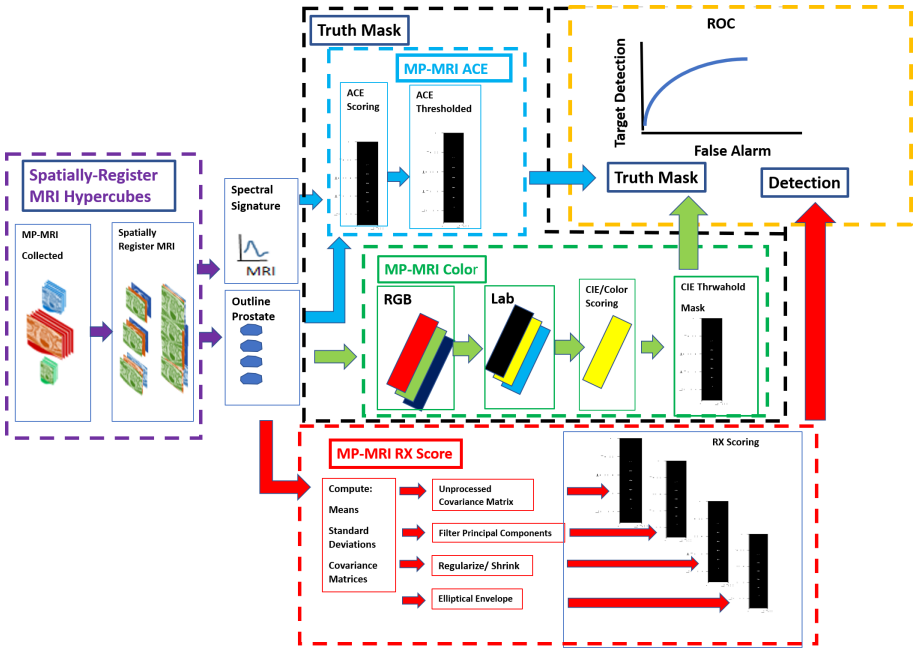

FIGURE 1
Schematic overview of processes that need to generate ROC curve (yellow outline). A spatially registered hypercube (purple outline, arrow) is composed of MRI modalities. Reference mask options include ACE (blue outline) and CIELAB (green outline). Detection map from the RX computation (red outline, arrow).

Spatial registered hypercube assembly: Study cohort

The Cancer Imaging Archive (TCIA) (39, 40), affiliated with the National Institutes of Health (NIH), collected and stored patient data from prostate tumor MRI and histology from whole-mount prostatectomy specimens. This study followed the Declaration of Helsinki (as revised in 2013). Since the images were anonymized, this investigation was determined to be IRB-exempt. This study followed the Health Insurance Portability and Accountability Act guidelines. A total of 26 patients were included. All patients had biopsy-proven adenocarcinoma of the prostate, with a median patient age of 60 years (range, 49 to 75 years), a median PSA of 5.8 ng/ml (range, 2.3 to 23.7 ng/ml), and a median GS of 7 (range, 6 to 9). Eighteen of the 26 patients had tumors larger than 1 cc. This study placed no restrictions on tumor location within the prostate. Robotic-assisted radical prostatectomy was performed at a median time of 60 days (minimum 3 days, maximum 180 days) following MRI without any intervening treatment.

Spatial registered hypercube assembly: Whole mount prostatectomy and histology

The whole mount prostatectomy histology has previously been described in detail and is very briefly summarized (41–43). Following radical prostatectomy, the specimen was fixed at room temperature in formalin for 2 to 24 h and then placed in a customized 3D mold that is based on MRI and sliced in sections with a separation of 6 mm in the axial direction, corresponding to the MRI axial plane section. The individual tumor foci, dimensions, and Gleason scores from the histology slides were independently determined by two experienced pathologists who were blinded to the MRI results.

Spatial registered hypercube assembly: Magnetic resonance imaging

The MRI collection was composed of structural (T1, T2) images, diffusion-weighted images (DWIs), and dynamic contrast-enhanced (DCE) images. The pulse sequences were described in earlier studies (41–43). This MRI protocol included triplanar T2W turbo spin echo, DW MRI, and axial pre-contrast T1-weighted axial 3D fast field echo DCE MRI sequences. A prior study (26) described their detailed sequence parameters.

Spatial registered hypercube assembly: Image processing, pre-analysis

DCE images consist of a time series at fixed locations in the prostate, encompassing the entire prostate. These images display the evolution in time of contrast material over several hundred seconds following injection. The DCE shows contrast uptake in the tissues. By analyzing the DCE and exploiting the unique tumor physiology, a portion of tumors may be identified. The tracer concentration in the tissue that supplies and empties through the tumor vasculature is described by a simple two compartment model (23, 44, 45). For times greater than the time to reach the peak uptake of the contrast material in a tumor (>50 s), every voxel was fitted with an exponentially decaying function to form the washout (k_{ep}) images and the probability likelihood (prob) images.

All MRI images were digitally resized (23–28) to 1 mm resolution in the transverse direction. Using the known location of the patient's position on the table, all slices were resized to 6 mm spacing and aligned using resampling. The Dynamic Contrast Enhancement images were treated as the reference for spatial registration. Due to the short time intervals between scan types (<20 min), small rigid adjustments (minor transverse translation) were applied to the structural, diffusion, and DCE images. A "cube" is composed of stacked individual slices that were scaled, translated, and resliced to be spatially registered at the pixel level. These " three-dimensional" (two transverse directions plus a spectral dimension composed of MP-MRI sequences) cubes were "stitched" together into a narrow three-dimensional hypercube to depict the entire prostate and other tissues in the field of view of the MRI scan. This stitching, or mosaicking, follows the approach used in remote sensing, in which large areas are stitched together. Mosaicking or stitching cubes greatly increases the processing speed for handling high-dimensional data. The spectral content of the hypercube had seven components (23–28): T1 (pre-contrast), T1 (maximum contrast), T2, ADC, DWI-high B (B = 1,000 s/mm^2), Washout or k_{ep} from DCE.

Anomaly detector generator: Anomaly detector (RX)

An anomaly detector (29–31) examines and computes statistics, such as mean value and covariance matrix, that characterize a background (the normal prostate organ) and identifies targets (tumor, benign prostatic hyperplasia) by noting voxels that quantitatively depart from the background. In contrast, supervised target detection uses a target signature to help distinguish a target from the background. This study, like many that examine multi- and hyperspectral images, applies the RX (32) algorithm to detect anomalous voxels. The RX algorithm queries each voxel and computes the voxel value and background statistics for all components, specifically the covariance matrix and mean. A voxel's RX value (32) is the voxel's Mahalanobis distance (Euclidean distance in whitened space) from the background (normal prostate) mean. A voxel's large RX value shows a large deviation from the background. The

RX decision surface is a hypersphere with background residing inside a sphere and anomalies outside. The covariance matrix corrects and accounts for correlations among the different components (for example, the correlation between ADC and DWI) to get a true measure of the aggregate contribution of each component to the deviation of the voxel from the background. Actual data fails to follow the ideal RX probability distribution, namely a chi-square distribution (32) requiring *ad-hoc* anomaly cutoff thresholds or employing acceptable false alarm rates. The Appendix summarizes some of the mathematics behind the RX algorithm. For more details, see references (29–32).

Anomaly detector generator: Filtering noise

Computing the RX covariance matrix generates principal components (46). Principal components are linear combinations of all MRI components but are orthogonal or totally decorrelated from each other. The principal components are ordered based on their eigenvalues or statistical variation. Well-resolved images have large eigenvalues and high variation. In contrast, noisy principal components have small eigenvalues. Noise is reduced by filtering and eliminating the noisy (low eigenvalue) principal components, resulting in a more accurate RX calculation. The Appendix summarizes some of the mathematics behind the filtering of principal components. For more details, see references (27, 28, 47).

Anomaly detector generator: Regularization and shrinkage

Regularization is another way to correct for the imperfections of the computed covariance matrix. The statistics describing the background (normal prostate) should follow a normal distribution. However, the analytical formula for the covariance matrix results in only an approximation. The goal of shrinkage regularization (27, 28, 48) is to perturb the original covariance matrix CM(γ) by mixing in a diagonal matrix with a mixing parameter γ to generate a regularized or modified regularized covariance matrix. The appropriate γ is chosen to maximize the normal distribution. Regularized or modified regularized covariance matrix generation follows the same procedure but differs in the mixing diagonal matrix. The Appendix summarizes some of the mathematics behind regularization. For more details, see references (27, 28, 48).

Anomaly detector generator: Elliptical volume minimization

Elliptical volume minimization (EVM) (49) provides another approach for reducing the effects of noise in the covariance matrix calculation. EVM does not use an analytical solution. Instead, EVM sequentially removes 10% of randomly chosen pixel searches and computes and records the hypervolume elliptical volume for the remaining 90% of the prostate pixels. The minimum elliptical volume after the search is chosen, presumably reducing the effects of the 10% aberrant voxels.

Reference mask: Color quantification: CIELAB

Perceiving color is a neuro-psychological phenomenon that depends on the observer and display (50–52). Objectively quantifying color to assess images is, therefore, fraught with challenges. However, considerable empirical research and effort have allowed for the conversion of color perception into quantitative metrics, specifically by using the CIELAB color space, also referred to the as $L^*a^*b^*$ color space (50–52). CIELAB is designed to relate to the CIE standard observer. The CIE standard observer is generated from color matching experiments conducted under laboratory conditions. The CIELAB is designed to be independent of any device, such as a computer monitor or a printer. It is based on the opponent color model of human vision, where red and green form an opponent pair, and blue and yellow form an opponent pair. Color is described by three values: L^* for perceptual lightness and a^* and b^* for the four unique colors of human vision: red, green, blue, and yellow. The L^* defines black at 0 and white at 100. The a^* axis follows the green–red opponent colors, with negative values toward green and positive values toward red. The b^* axis represents blue–yellow opponents, with negative numbers toward blue and positive toward yellow. Yellow for this study is related to tumor in this study and is of most interest. The Appendix summarizes some of the mathematics behind coloring. For more details, see references (50–52).

Reference mask: ACE

A target, such as a tumor, can be characterized by its spectral signature. The spectral signature is a vector whose components are values from each of the MRI modalities. The tumor signature differs from the background (normal prostate) vector. The difference between the tumor and normal prostate vectors is exploited by supervised target algorithms. The adaptive cosine estimator (ACE) is one example of supervised target detection. The Appendix summarizes some of the mathematics behind ACE. For more details, see references (22–28, 31).

Assessment: Receiver operator characteristic

The receiver operator characteristic (ROC) curve (53) evaluates the performance of a binary target detection

algorithm, specifically the RX anomaly detector and its variants (filtering, regularization). In this study, for a given RX anomaly detector threshold, each voxel in normal tissue is classified as either a target (above the RX threshold) or a normal prostate (below the RX threshold). This study uses two types of reference images, namely ACE (threshold = 0.65) and CIELAB (threshold = 0.35), to depict the targets. The ROC curve displays the sensitivity (how well RX characterizes targets) and the 1-Specificity (how well RX characterizes background) for all RX thresholds. The area under the curve (AUC) from the ROC curve and the Youden Index (YI) or maximum accuracy summarize RX performance. The Appendix summarizes some of the mathematics behind the ROC curve. For more details, see reference (53).

Reference mask and assessment: Reference masks/threshold cutoffs

Ideally, a " ground truth" image mask depicts the actual locations, sizes, and shapes of the tumors. Current practice attributes " ground truth" to the pathologist's assessment and markings on the histology slides derived from a whole-mount prostatectomy. Pathology evaluation is acceptable for Gleason score and tumor volume determinations. However, pathology assessment of the histology for tumor location and position for MRI suffers from a few limitations. The histology preparations can result in distortions, shrinkage, and tearing. Tissues imaged by MRI are supported by muscles and other soft tissues and subject to gravity, further complicating their registration to histology slides. Due to the absence of any registration points, it is impossible to precisely register the histology slides to the axial MRI images in both the axial and transverse directions.

The radiologist's delineation of tumors on the multi-parametric MRI might have served as candidate "ground truth" but it was not available. Instead, the images derived from ACE and Color/CIELABS applied to the spatially registered MRI marked the tumors at the voxel level for the ROC curve computations. In-scene signatures were inserted into the ACE calculations. The thresholds from the ACE or Color/CIELABS were taken from a previous study (24) that computed the correlation coefficients of tumor volumes derived from the ACE and Color/CIELABS using varying thresholds with the tumor volume generated from the pathologist's evaluation of the slides taken from wholemount prostatectomy. The highest correlation was achieved with 0.65 and 0.35 for ACE and color/CIELABS, respectively, and was therefore chosen for this study. In practice (31, 32), RX applied to data does not follow the expected Chi-Square distribution. In practice, *ad hoc* or acceptable false alarm rates set the cutoff threshold values.

Results

The patient average (± standard error) for the AUC and YI for the ROC curves for RX for all 26 patients are shown in Tables 1, 2, respectively. For both calculations, the covariance matrix was filtered by eliminating 3 and 4 principal components. This was followed by applying modified regularization and regularization, as well as searching for the minimum elliptical volume. In addition, RX was generated, and ROC curves were computed using an unprocessed covariance matrix. The best performance in terms of highest AUC and YI was from the filtered covariance matrix approach and from applying the regularization to the covariance matrix. Elliptical volume minimization performed even worse than using an unprocessed covariance matrix.

Unlike processing using ACE and CIELAB (24), anomaly detection failed to achieve high correlation with histology-derived tumor volume or those derived from manual coloring.

Discussion

This is the first spatially registered multi-parametric MRI study to apply an unsupervised target detection algorithm,

TABLE 1 Average Area Under the Curve (AUC) and [standard error].

	Delete three PC	Delete four PC	Modified Regularization	Regularization	Elliptical Envelope	Unprocessed
ACE	0.734[0.022]	0.727[0.022]	0.638[0.017]	0.716[0.017]	0.544[0.025]	0.581[0.018]
CIELAB B	0.742[0.025]	0.740[0.022]	0.643[0.023]	0.722[0.022]	0.508[0.024]	0.569[0.020]

The covariance matrix corrections are denoted as gray. ACE (threshold=0.65, denoted as blue) and CIELAB (threshold 0.35) are the Reference images.

TABLE 2 Youden Index and [Standard Error].

	Delete three PC	Delete four PC	Modified Regularization	Regularization	Elliptical Envelope	Unprocessed
ACE	0.706[0.017]	0.727[0.016]	0.639[0.012]	0.690[0.013]	0.597[0.017]	0.608[0.012]
CIELAB B	0.711[0.020]	0.708[0.018]	0.648[0.016]	0.695[0.018]	0.605[0.014]	0.615[0.012]

The covariance matrix corrections are denoted as gray. ACE (threshold=0.65, denoted as blue) and CIELAB (threshold 0.35) are the Reference images.

namely the RX algorithm for prostate cancer. The best performance in terms of highest AUC and YI were the filtered covariance matrix approach, and from applying regularization to the covariance matrix. Elliptical volume minimization performed even worse than using an unprocessed covariance matrix. The anomaly detection attained high AUC and YI from ROC when using ACE and CIELAB color images as reference images. However, unlike supervised target detection, anomaly detection failed to achieve high correlation with histology derived tumor volume or those derived from manual coloring.

Imaging is only one way to non-invasively evaluate a patient for the possible presence of prostate cancer. Recent research (54) evaluated biomarkers residing in urine or blood (beyond prostate serum antigen tests) to determine whether a patient has prostate cancer, its stage, and its potential aggressiveness. Using metrics derived from imaging does not preclude using biomarkers. Greater accuracy might be achieved by combining the new biomarkers with predictors derived from algorithms applied to spatially registered hypercubes. Each patient can be individually evaluated by determining the presence of biomarkers and computing imaging metrics to generate a patient-specific probability for the presence of prostate cancer and its likelihood to metastasize and extend beyond the prostate.

It is important to note that the " reference image" for the prostate tumors in this ROC curve study for anomaly detection was taken from ACE and CIELAB images. Tumor delineation from pathologists ' histology images is available but is not a good reference for this study. The histology images suffer from distortion and shrinkage during the slicing, staining and preservation processes and are not subject to stresses from connections to muscles and other soft tissues as well as gravity. Using ACE and CIELAB images can also be problematic due to their unverified connection to pathology assessed histology slides. However, ACE and CIELAB are perfectly spatially registered to the RX detection images. The ACE and CIELAB images also describe classic tumor behavior, i.e., ones that exhibit low diffusion but high vasculature. Future investigation is warranted to use " reference image" masks generated with multiple signatures for ACE and/or some green (low vasculature, low diffusion) CIELAB images.

Anomaly detection is sensitive to volumes within the prostate that do not necessarily display the spectral characteristics of an archetypal tumor, namely one that shows low diffusion but high vascularization. Malignant tumors can show limited vascularization but limited diffusion and, therefore, can be sufficiently spectrally anomalous to be detected by RX but not by supervised target detection. However, anomaly detectors may also detect hyperplasia, or swelling, within the prostate. In addition, anomaly detection is sensitive to image artifacts such as misregistration in multi-parametric MRI.

Previous work (27) on Signal to Clutter Ratio and Gleason score found that the covariance matrix was more optimally handled by deleting three principal components, not four principal components. Earlier work also found that a better-performing RX used a covariance matrix treated with a modified regularization procedure, not the more standard regularization procedure. In contrast, the more optimal covariance matrix for anomaly detectors was generated by filtering four principal components, not three. The standard regularization performed better than the modified regularization for generating a more optimal covariance matrix and likelihood and a better performing RX.

The large ROC AUC and large Youden Index relating the RX to the supervised target algorithm ACE and quantitative CIELAB coloring scheme suggest a strong relationship between anomalies and regions sharing typical tumor characteristics. However, the thresholds associated with the Youden Index vary considerably and unpredictably from patient to patient. ROC curves sample all classifier gray levels or thresholds. However, employ ing RX for tumor volume determination or prediction requires a single threshold. Previous studies and the present work find that RX do not obey expected the chi-squared distribution (31), complicating efforts to set detection thresholds. Employing RX to reliably predict tumor volume requires an appropriate threshold. Further work is needed to identify an appropriate RX threshold for determining tumor volume.

This study has some limitations. Future work should employ radiologist-delineated tumors on the MRI as the " ground truth." The threshold parameters for ACE, CIELABS, and ultimately RX should be checked through cross-validation studies. The patients in this study were prospectively enrolled but were analyzed retrospectively from a single institution (NIH). Clinical implementation variations, therefore, could not be examined, and the effects of variation on this analysis are uncertain. In addition, as with all retrospective analyses, the findings herein may be subject to biases. Lastly, the dataset comprised only 26 patients. Although a limited number of patients were assessed, consecutive patients were analyzed to minimize potential bias, and nevertheless highly statistically significant AUC and YI values were achieved, showing the potential clinical value of this approach.

Data availability statement

The raw data supporting the conclusions of this article will be made available by the authors, without undue reservation.

Ethics statement

Ethical review and approval were not required for the study on human participants in accordance with the local legislation and institutional requirements. Written informed consent for participation was not required for this study in accordance with the national legislation and the institutional requirements.

Author contributions

Conception and design: RM. Administrative support: RM, CS, and PC. Provision of study materials or patients: BT and PC. Collection and assembly of data: RM, BT, and PC. Data analysis and interpretation: RM. All authors listed have made a substantial, direct, and intellectual contribution to the work and approved it for publication.

Conflict of interest

RM works for Oncoscore.

The remaining authors declare that the research was conducted in the absence of any commercial or financial relationships that could be construed as a potential conflict of interest.

Publisher's note

Supplementary material

The Supplementary Material for this article can be found online at: https://www.frontiersin.org/articles/10.3389/fonc.2022.1033323/full#supplementary-material

References

1. Sobin L, Wittekind C. *TNM classification of malignant tumors. 5th ed*. New York: John Wiley and Sons, Inc(1997).

2. Shariat SF, Karakiewicz PI, Roehrborn CG, Kattan MW. An updated catalog of prostate cancer predictive tools. *Cancer*(2008) 113:3075–99. doi: 10.1002/cncr.23908

3. Martin NE, Mucci LA, Loda M, DePinho RA. Prognostic determinants in prostate cancer. *Cancer J*(2011) 17(6):429–37. doi: 10.1097/PPO.0b013e31823b042c

4. Ho R, Siddiqui MM, George AK, Frye T, Kilchevsky A, Fascelli M, et al. Preoperative multiparametric magnetic resonance imaging predicts biochemical recurrence in prostate cancer after radical prostatectomy. *PLos One*(2016) 11(6): e0157313. doi: 10.1371/journal.pone.0157313

5. May M, Siegsmund M, Hammermann F, Loy V, Gunia S. Visual estimation of the tumor volume in prostate cancer: a useful means for predicting biochemical-free survival after radical prostatectomy? *Prostate Cancer Prostatic Dis*(2007) 10:66–71. doi: 10.1038/sj.pcan.4500928

6. Poulakis V, Witzsch U, de Vries R, Emmerlich V, Meves M, Altmannsberger HM, et al. Preoperative neural network using combined magnetic resonance imaging variables, prostate-specific antigen, and Gleason score for predicting prostate cancer biochemical recurrence after radical prostatectomy. *Urology*. (2004) 64:1165–70. doi: 10.1016/j.urology.2004.06.030

7. Gurumurthy D, Maggad R, Patel S. Prostate carcinoma: correlation of histopathology with serum prostate specific antigen. *Sci J Clin Med*(2015) 4(4):1–5. doi: 10.11648/j.sjcm.s.2015040401.11

8. Ngwu PE, Achor GO, Eziefule VU, Orji JI, Alozie FT. Correlation between prostate specific antigen and prostate biopsy Gleason score. *Ann Health Res*(2019) 5(2):243–8. doi: 10.30442/ahr.0502-26-56

9. Zivkovic S. Correlation between prostate-specific antigen and histopathological difference of prostate carcinoma. *Arch Oncol*(2004) 12(3):148–51. doi: 10.2298/AOO0403148Z

10. Wang L, Hricak H, Kattan MW, Chen HN, Kuroiwa K, Eisenberg HF, et al. Prediction of seminal vesicle invasion in prostate cancer: incremental value of adding endorectal MR imaging to the kattan nomogram. *Radiology*.(2007) 242:182–8. doi: 10.1148/radiol.2421051254

11. Villers AA, McNeal JE, Redwine EA, Freiha FS, Stamey TA. Pathogenesis and biological significance of seminal vesicle invasion in prostatic adenocarcinoma. *J Urol*(1990) 143(6):1183–7. doi: 10.1016/S0022-5347(17)40220-5

12. Shukla-Dave A, Hricak H, Kattan MW, Pucar D, Kuroiwa K, Chen HN, Spector J, Koutcher JA, Zakian KL, Scardino PT. Cancer volume and site of origin of adenocarcinoma in the prostate: relationship to local and distant spread. *Hum Pathol*(1992) 23(3):258–66. doi: 10.1016/0046-8177(92)90106-D

13. Friedersdorff F, Groß B, Maxeiner A, Jung K, Miller K, Stephan C, et al. Does the prostate health index depend on tumor volume?–a study on 196 patients after radical prostatectomy. *Int J Mol Sci*(2017) 18(3):488. doi: 10.3390/ijms18030488

14. McNeal JE, Villers AA, Redwine EA, Freiha FS, Stamey TA. Histologic differentiation, cancer volume, and pelvic lymph node metastasis in adenocarcinoma of the prostate. *Cancer*(1990) 66(6):1225–33. doi: 10.1002/1097-0142(19900915)66:6<1225::AID-CNCR2820660624>3.0.CO;2-X

15. Epstein JI, Carmichael M, Partin AW, Walsh PC. Is tumor volume an independent predictor of progression following radical prostatectomy? a multivariate analysis of 185 clinical stage b adenocarcinomas of the prostate with 5 years of followup. *J Urol*(1993) 149(6):1478–81. doi: 10.1016/S0022-5347(17)36421-2

16. Kikuchi E, Scardino PT, Wheeler TM, Slawin KM, Ohori M. Is tumor volume an independent prognostic factor in clinically localized prostate cancer? *J Urol*(2004) 172(2):508–11. doi: 10.1097/01.ju.0000130481.04082.1a

17. Weinreb JC, Barentsz JO, Choyke PL, Cornud F, Haider MA, Macura KJ, et al. PI-RADS prostate imaging-reporting and data System:2015,Version 2. *Eur Urol*(2016) 69:16–40. doi: 10.1016/j.eururo.2015.08.052

18. Bastian-Jordan M. Magnetic resonance imaging of the prostate and targeted biopsy, comparison of PIRADS and Gleason grading. *J Med Imaging Radiat Oncol* (2018) 62(2):183–7. doi: 10.1111/1754-9485.12678

19. Slaoui H, Neuzillet Y, Ghoneim T, Rouanne M, Abdou A, PM L-D, et al. Gleason Score within prostate abnormal areas defined by multiparametric magnetic resonance imaging did not vary according to the PIRADS score. *Urol Int*(2017) 99(2):156–61. doi: 10.1159/000468947

20. Kızılay F, Çelik S, Sozen S, Ozveren B, Eskiçorapçı S, Ozgen M, et al. Correlation of prostate-imaging reporting and data scoring system scoring on multiparametric prostate magnetic resonance imaging with histopathological factors in radical prostatectomy material in Turkish prostate cancer patients: a multicenter study of the urooncology association. *Prostate Int*(2020) 8:10–5. doi: 10.1016/j.prnil.2020.01.001

21. Shukla-Dave A, Hricak H, Kattan MW, Pucar D, Kuroiwa K, Chen HN, et al. The utility of magnetic resonance imaging and spectroscopy for predicting insignificant prostate cancer: an initial analysis. *BJU Int*(2007) 99:786–93. doi: 10.1111/j.1464-410X.2007.06689.x

22. Gleason DF, Mellinger GT. Prediction of prognosis for prostatic adenocarcinoma by combined histological grading and clinical staging. *J Urol* (1974) 111:58–64. doi: 10.1016/S0022-5347(17)59889-4

23. Mayer R, Simone CB2nd, Skinner W, Turkbey B, Choykey P. Pilot study for supervised target detection applied to spatially registered multiparametric MRI in order to non-invasively score prostate cancer. *Comput Biol Med*(2018) 94:65–73. doi: 10.1016/j.compbiomed.2018.01.003

24. Mayer R, Simone CB2nd, Turkbey B, Choyke P. Algorithms applied to spatially registered multi-parametric MRI for prostate tumor volume measurement. *Quant Imaging Med Surg*(2021) 11:119–32. doi: 10.21037/qims-20-137a

25. Mayer R, Simone CB2nd, Turkbey B, Choyke P. Correlation of prostate tumor eccentricity and Gleason scoring from prostatectomy and multi-parametric-magnetic resonance imaging. *Quant Imaging Med Surg*(2021) 11:4235–44. doi: 10.21037/qims-21-24

26. Mayer R, Simone CB2nd, Turkbey B, Choyke P. Prostate tumor eccentricity predicts Gleason score better than prostate tumor volume. *Quant Imaging Med Surg*(2022) 12:1096–108. doi: 10.21037/qims-21-466

27. Mayer R, Simone CB2nd, Turkbey B, Choyke P. Development and testing quantitative metrics from multi-parametric magnetic resonance imaging that predict Gleason score for prostate tumors. *Quant Imaging Med Surg*(2022) 12:1859–70. doi: 10.21037/qims-21-761

28. Mayer R, Turkbey B, Choyke P, Simone CB2nd. Combining and analyzing novel multi-parametric magnetic resonance imaging metrics for predicting Gleason score. *Quant Imaging Med Surg*(2022) 12:3844–59. doi: 10.21037/qims-21-1092

29. Jain AK. *Fundamentals of digital image processing*. Upper Saddle River, NJ: Prentice Hall(1989).

30. Richards JA, Jia X. *Remote sensing digital image analysis*. New York: Springer-Verlag (1999).

31. Manolakis D, Shaw G. Detection algorithms for hyperspectral imaging applications, in: *IEEE Sign. Processing Magazine*, (2002). Vol. 19. pp. 29–43.

32. Reed I, Yu X. Adaptive multiple-band CFAR detection of an optical pattern with unknown spectral distribution, in: *IEEE Transactions on Acoustics, Speech and Signal Processing*, (1990), Vol. 38. pp. 1760–17705.

33. Tschuchnig ME, Gadermayr M. Anomaly detection in medical imaging-a mini review. *Data Science– Analytics Applications* (2022), 33–38. doi: 10.1007/978-3-658-36295-9_5

34. Fernando T, Gammulle H, Denman S, Sridharan S, Fookes C. Deep learning for medical anomaly detection– a survey. *ACM Computing Surveys (CSUR)*(2021) 54(7):1–37. doi: 10.48550/arXiv.2012.02364

35. Rubinstein E, Salhov M, Nidam-Leshem M, White V, Golan S, Baniel J, et al. Unsupervised tumor detection in dynamic PET/CT imaging of the prostate. *Med image analysis*(2019) 55:27–40. doi: 10.1016/j.media.2019.04.001

36. Rampun A, Chen Z, Zwiggelaar R. Detection and localisation of prostate abnormalities, in: *In 3rd International Conference on Computational & Mathematical Biomedical Engineering (CMBE' 13)*, (2013); 204–208.

37. Mejia AF, Nebel MB, Eloyan A, Caffo B, Lindquist MA. Pca leverage: outlier detection for high-dimensional functional magnetic resonance imaging data. *Biostatistics* (2017) 18(3):521–36. doi: 10.1093/biostatistics/kxw050

38. Kim C-M, Hong EJ, Park RC. *Chest X-ray outlier detetion model using dimension reduction and edge detection*. IEEE Access (2021); 9: 86096–86106.

39. Choyke P, Turkbey B, Pinto P, Merino M, Wood B. *Data from PROSTATE-MRI. the cancer imaging archive*. (2016). doi: 10.7937/K9/TCIA.2016.6046GUDv.

40. Clark K, Vendt B, Smith K, Freymann J, Kirby J, Koppel P, et al. The cancer imaging archive (TCIA): maintaining and operating a public information repository. *J Digit Imaging*(2013) 26:1045–57. doi: 10.1007/s10278-013-9622-7

41. Shah V, Pohida T, Turkbey B, Mani H, Merino M, Pinto PA, et al. A method for correlating *in vivo* prostate magnetic resonance imaging and histopathology using individualized magnetic resonance-based molds. *Rev Sci Instrum*(2009) 80:104301. doi: 10.1063/1.3242697

42. Turkbey B, Mani H, Shah V, Rastinehad AR, Bernardo M, Pohida T, et al. Multiparametric 3T prostate magnetic resonance imaging to detect cancer: histopathological correlation using prostatectomy specimens processed in customized magnetic resonance imaging based molds. *J Urol*(2011) 186:1818–24. doi: 10.1016/j.juro.2011.07.013

43. Turkbey B, Pinto PA, Mani H, Bernardo M, Pang Y, McKinney YL, et al. Prostate cancer: value of multiparametric MR imaging at 3 T for detection–histopathologic correlation. *Radiology*(2010) 255:89–99. doi: 10.1148/radiol.09090475

44. Tofts PS, Brix G, Buckley DL, Evelhoch JL, Henderson E, Knopp MV, et al. Estimating kinetic parameters from dynamic contrast-enhanced T(1)-weighted MRI of a diffusable tracer: standardized quantities and symbols. *J Magn Reson Imaging*(1999) 10:223–32. doi: 10.1002/(SICI)1522-2586(199909)10:3<223::AID-JMRI2>3.0.CO;2-S

45. Tofts PS. T1-weighted DCE imaging concepts: Modelling, acquisition and analysis. *Magnetom Flash*(2010) 3:31–9.

46. Strang G. *Linear algebra and its applications. 4th ed.* Belmont, CA, Thomson: Brooks/Cole(2006).

47. Chen G, Qian S. Denoising of hyperspectral imagery using principal component analysis and wavelet shrinkage, in: *IEEE Transactions on Geoscience and Remote Sensing*, (2011) Vol. 49. pp. 973–80.

48. Friedman JH. Regularized discriminant analysis. *J Amer Stat Assoc*(1989) 84:165–75. doi: 10.1080/01621459.1989.10478752

49. Rousseeuw PJ, Van Driessen K. A fast algorithm for the minimum covariance determinant estimator. *Technometrics*(1999) 41(3):212–23. doi: 10.1080/00401706.1999.10485670

50. Fairchild MD. *Color appearance models*. Chichester, West Sussex, PO19 8SQ John Wiley and Sons (2013).

51. Jain AK. *Fundamentals of digital image processing*. New Jersey, United States of America: Prentice Hall(1989).

52. János S. *Colorimetry: understanding the CIE system*. Hoboken, New Jersey, John Wiley & Sons (2007).

53. Fawcett T. An introduction to ROC analysis. *Pattern Recognition Letters* (2006) 27(8):861–74. doi: 10.1016/j.patrec.2005.10.010

54. Salciccia S, Capriotti AL, Laganà A, Fais S, Logozzi M, DeBerardinis E, et al. Biomarkers in prostate cancer diagnosis: From current knowledge to the role of metabolomics and exosomes. *Int J Mol Sci*(2021) 22:4367. doi: 10.3390/ijms22094367

frontiers | Frontiers in Oncology

TYPE Original Research
PUBLISHED 24 January 2023
DOI 10.3389/fonc.2023.1066498

OPEN ACCESS

EDITED BY
Diederik M. Somford,
Canisius Wilhelmina Hospital, Netherlands

REVIEWED BY
Enrico Checcucci,
IRCCS Candiolo Cancer Institute, Italy
Mark Emberton,
University College London,
United Kingdom

*CORRESPONDENCE
Rulon Mayer
mayerru@yahoo.com

SPECIALTY SECTION
This article was submitted to Genitourinary Oncology, a section of the journal Frontiers in Oncology

RECEIVED 10 October 2022
ACCEPTED 04 January 2023
PUBLISHED 24 January 2023

CITATION
Mayer R, Turkbey B, Choyke P and Simone CB II (2023) Pilot study for generating and assessing nomograms and decision curves analysis to predict clinically significant prostate cancer using only spatially registered multi-parametric MRI. *Front. Oncol.* 13:1066498. doi: 10.3389/fonc.2023.1066498

Pilot study for generating and assessing nomograms and decision curves analysis to predict clinically significant prostate cancer using only spatially registered multi-parametric MRI

Rulon Mayer[1,2]*, Baris Turkbey[3], Peter Choyke[3] and Charles B. Simone II[4]

[1]Department of Radiation Oncology, Perelman School of Medicine, University of Pennsylvania, Philadelphia, PA, United States, [2]OncoScore, Garrett Park, MD, United States, [3]Molecular Imaging Branch, National Institutes of Health (NIH), Bethesda, MD, United States, [4]Department of Radiation Oncology, New York Proton Center, New York, NY, United States

Background: Current prostate cancer evaluation can be inaccurate and burdensome. To help non-invasive prostate tumor assessment, recent algorithms applied to spatially registered multi-parametric (SRMP) MRI extracted novel clinically relevant metrics, namely the tumor's eccentricity (shape), signal-to-clutter ratio (SCR), and volume.

Purpose: Conduct a pilot study to predict the risk of developing clinically significant prostate cancer using nomograms and employing Decision Curves Analysis (DCA) from the SRMP MRI-based features to help clinicians non-invasively manage prostate cancer.

Methods: This study retrospectively analyzed 25 prostate cancer patients. MP-MRI (T1, T2, diffusion, dynamic contrast-enhanced) were resized, translated, and stitched to form SRMP MRI. Target detection algorithm [adaptive cosine estimator (ACE)] applied to SRMP MRI determines tumor's eccentricity, noise reduced SCR (by regularizing or eliminating principal components (PC) from the covariance matrix), and volume. Pathology assessed wholemount prostatectomy for Gleason score (GS). Tumors with GS >=4+3 (<=3+4) were judged as "Clinically Significant" ("Insignificant"). Logistic regression combined eccentricity, SCR, volume to generate probability distribution. Nomograms, DCA used all patients plus training (13 patients) and test (12 patients) sets. Area Under the Curves for (AUC) for Receiver Operator Curves (ROC) and p-values evaluated the performance.

Results: Combining eccentricity (0.45 ACE threshold), SCR (3, 4 PCs), SCR (regularized, modified regularization) with tumor volume (0.65 ACE threshold) improved AUC (>0.70) for ROC curves and p-values (<0.05) for logistic fit. DCA

showed greater net benefit from model fit than univariate analysis, treating "all," or "none." Training/test sets achieved comparable AUC but with higher p-values.

Conclusions: Performance of nomograms and DCA based on metrics derived from SRMP-MRI in this pilot study were comparable to those using prostate serum antigen, age, and PI-RADS.

KEYWORDS

prostate cancer, multi-parametric magnetic resonance imaging (MP-MRI), Gleason score (GS), signal-to-clutter ratio (SCR), regularization, nomograms, decision curve analysis, multiple variable regression

Introduction

For prostate cancer, deciding to treat clinically significant disease or to monitor benign lesions or low risk invasive disease (1) requires correct assessment in order to properly manage the disease. A large number of factors, such as Gleason score, prostate serum antigen (PSA) (2–4), metadata (5) such as patient age, family history, tumor size (6), clinical stage and visual inspection of images of the lesion (7–11), etc. contribute to a patient's evaluation, but they vary in their correlation to disease status. The large number and variation of contributing factors among patients can complicate cancer management and confuse the clinician and patient. A nomogram (12–14) is a graphical depiction that quantitatively combines a number of factors to help summarize a patient's status and simplify the assessment. The nomogram produces a probability distribution for the likelihood of serious disease that is tailored for each individual patient. Along with a nomogram, a Decision Curve Analysis (DCA) (15) can refine and enhance the management of the patient by providing a graph to suggest when or if to apply certain procedures.

Further complicating patient management, the factors that contribute to patient evaluation can also potentially discomfort the patient and produce side effects (16). Specifically, a prostate biopsy, currently the standard assessment, can cause hemorrhaging, pain, and infection, and it can possibly miss properly sampling the tumor (17). To elevate patient assessment, imaging, such as MRI, can non-invasively display the entire image and tumor with minimal patient discomfort. Specifically, qualitative assessment of multiple modalities of MRI or Multi-Parametric MRI (MP-MRI) employ trained radiologists who follow the Prostate Imaging Reporting and Data System (PI-RADS) protocol (7). Recently, PI-RADS assessments have been incorporated into nomograms and achieved significant accuracy in predicted disease outcomes (18–23). However, the quality of the PI-RADS assessment can vary depending on the training or experience of the radiologist examining a patient's image (24). A more quantitative, robust approach is desired.

Recently (25–30), algorithms have been applied to spatially registered MP-MRI to assess prostate tumors. These algorithms exploit the vectoral nature of each voxel in the prostate organ, unlike others that process individual modalities. Each voxel is treated as a vector, not a scalar. The recent studies determined the prostate tumor's Gleason score (25–30), tumor volume (26), eccentricity (shape) (27), and Signal-to-Clutter Ratio (SCR) (29).

This study is the first to use spatially registered MP-MRI as input information for a nomogram and for DCA. This study used patient data from The Cancer Imaging Archive (TCIA) (37, 38) that is composed of twenty-six consecutive patients who had biopsy proven adenocarcinoma of the prostate, had undergone MRI scan, and histological examination of wholemount prostatectomy. For this study, clinically significant (insignificant) prostate cancer was defined by the pathology assessment of Gleason scores >=4+3 (<=3+4). The present retrospective work does not use other clinical data (18–23) such as age, PSA nor use PI-RADS as input for the nomogram. Instead, the nomograms use various combinations of eccentricity, filtered and regularized SCR, and tumor volume indicators to find the probability that the prostate tumor is highly aggressive. This study extends and builds upon earlier work (28, 30) that examined multivariable regression fits to Gleason scores in order to generate a clinical tool to aid in the management of prostate cancer. The nomogram and decision curve analysis were quantitatively assessed by computing the Area Under the Curve (AUC) for the Receiver Operator Characteristic (ROC), p-values.

Methods

Overall description

Figure 1 provides an overview of the methodology to generate a nomogram from metrics derived from spatially registered MP-MRI (25–30) along with accompanying performance evaluations. The main components in the summary are described in greater detail below. The independent variable for the multivariable fit originates from spatially registered MP-MRI and the dependent categorical variable Clinically Significant Prostate Cancer derived from Gleason score and pathology exam of histology of the resected prostate.

Sequences of MRI (T1, T2, Dynamic Contrast Enhancement, Diffusion) were collected from each patient. The images were rescaled, cropped, translated, and resampled to form spatially registered multispectral cubes. These cubes were then stitched together to form spatially registered hypercubes. From visual inspection, the normal prostate was digitally outlined using an axial view to form the normal tissue or background. A vector tumor signature was taken from certain voxels identified in the colorized registered hypercube (25–30) and inserted into the Adaptive Cosine Estimator, and a threshold (25–30) was applied to find the tumor volume and eccentricity.

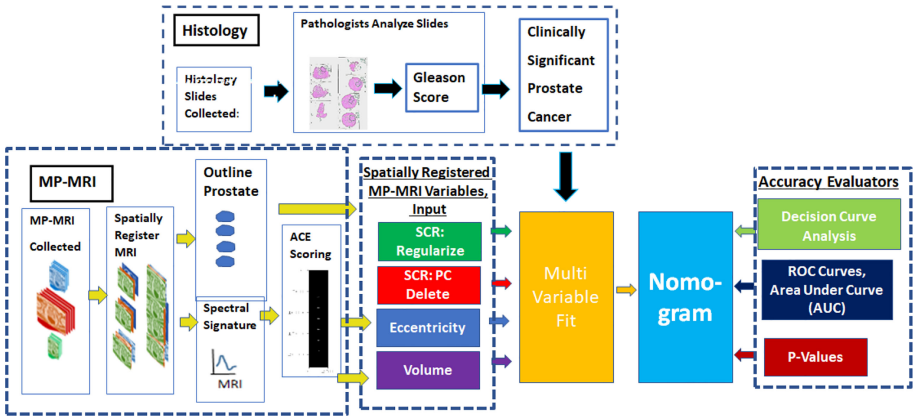

FIGURE 1
provides an overview of the methodology to generate a nomogram from metrics derived from spatially registered MP-MRI (25–30) along with accompanying performance evaluations. The main components in the summary are described in greater detail below. The independent variable for the multivariable fit originates from spatially registered MP-MRI and the dependent categorical variable Clinically Significant Prostate Cancer derived from Gleason score and pathology exam of histology of the resected prostate.

The nomogram (text box colored as baby blue in Figure 1) receives input from a multi-variable fit (yellow text box). Multivariable regression fits independent variables from spatially registered MP-MRI to the independent variable Gleason score. The independent variables are Regularized SCR (green), SCR with principal component filtering (red), tumor eccentricity (blue), tumor volume (purple) and combined in a variety of permutations to achieve an optimal fit. The dependent variable is categorical Clinically Significant Prostate Cancer, related to the Gleason score and is derived from pathology, not MRI. A pathologist determines the Gleason score from microscopic inspection of histology slides of wholemount prostatectomy.

To assess the multivariable regression fit and the nomogram, Receiver Operator Characteristic curves were generated and the Area Under the Curve (AUC) was computed. The coefficient of determination (R2) between the independent and dependent variables was computed along with the probability for the null hypothesis (p-value). To further assess and extend the clinical application of the nomogram, a Decision Curve Analysis was computed to find the net benefit for applying the nomogram.

The Methods qualitatively describes the individual components of anomaly detector generator and assessment. The Appendix summarizes the mathematics used to generate the components. More details can be found in the cited references.

Study design and population

Patient data from prostate tumor MRI and histology from whole mount prostatectomy specimens were collected and stored through The Cancer Imaging Archive (TCIA) (37, 38), affiliated with The National Institutes of Health (NIH). This study followed the Declaration of Helsinki (as revised in 2013). This study is compliant with the Health Insurance Portability and Accountability Act. The NIH Institutional Review Board approved this retrospectively designed single institution study and determined that individual consent for this retrospective analysis was not required. Twenty-six consecutive patients in the TCIA database were assessed. All patients had biopsy proven adenocarcinoma of the prostate, with median patient age of 60 years (range, 49 to 75 years), with a median PSA of 5.8 ng/mL (range, 2.3 to 23.7 ng/mL) and with median GS of 7 (range, 6 to 9). Eighteen of the 26 patients had tumor sizes >1 cc. One patient did not uptake the contrast material used for Dynamic Contrast Enhancement. This study did not place restrictions on tumor location within the prostate. Robotic assisted radical prostatectomy was performed following MRI without any intervening treatment. All cases were anonymized for subsequent analysis.

Whole mount prostatectomy and histology

The whole mount prostatectomy histology has previously been described (39–41). Following radical prostatectomy, the specimen was fixed at room temperature in formalin for 2 to 24 hours, placed in the customized 3D mold, and sliced in sections with a separation of 6 mm. in the axial direction (corresponding to the MRI axial plane section). The individual tumor foci, dimensions, and GSs from the histology slides were independently determined by two experienced pathologists blinded to the MRI results. As in earlier studies (25–30) and to better reflect the patient's status, a patient's GS was a weighted average (based on histology blob size) of the GSs assessed by the pathologists.

Magnetic resonance imaging

The MRI collection was composed of diffusion weighted images (DWIs), dynamic contrast enhanced (DCE), and structural (T1, T2) images. The pulse sequences were described in earlier studies (39–41). Triplanar T2W turbo spin echo, DW MRI, and axial pre-contrast T1-weighted axial 3D fast field echo DCE MRI sequences were part of this MRI protocol. The detailed sequence parameters were described in a prior study (41). The mean interval between MRI and radical prostatectomy was 60 days (range, 3 to 180 days).

Image processing, pre-analysis

The DCE are a time series of images follow contrast material in tissues over several hundred seconds following injection. A portion of tumors may be identified through analysis of DCE and exploiting the unique tumor physiology. The tracer concentration in the tissue that supplies and empties through the tumor vasculature is described by a simple two compartment model (25, 42, 43). For longer times (>50 seconds) than the time to reach the contrast material peak uptake in a tumor, every voxel was fitted with an exponentially decay function to form the washout (k_{ep}).

The MRI images were digitally resized (25–30) to 1 mm resolution in the transverse direction. In the axial direction, the slices were resized to 6 mm spacing and aligned using resampling based on the known location of patient's table position. Due to the short time interval between scans (<20 minutes), only small rigid adjustments (minor transverse translation) were applied to the structural, diffusion, and DCE images. A "cube" was formed from stacked individual slices that were scaled, translated, resliced and were thereby spatially registered at the voxel level. These "three dimensional" (two transverse directions plus spectral composed of MP-MRI modalities) cubes were then "stitched" together into a narrow three-dimensional hypercube in order to depict the entire MRI scan. The spectral content of the hypercube had 7 components (25–30) [T1 (pre-contrast), T1 (maximum contrast), T2, ADC, DWI-high B (B=1,000 s/mm^2), Washout or k_{ep} from DCE].

Eccentricity calculation

Custom software (coded in Python 3) was used to calculate the eccentricity (27, 28) for every labeled blob. The moment of inertia matrix I for the kth blob was computed. From the eigenvalues of the moment of inertia I, the largest eigenvalue was assigned to the large axis l_k and the second eigenvalue was assigned to the transverse moment s_k. The eccentricity E_k for the kth blob is a weighted difference of the major axis and minor axis. Eccentricity values E_k range from 0 (spherical shape) to 1 (line). For more details see References (27, 28).

Overall quantitative metrics description: SCR

Instead of relying on trained radiologists to visually inspect multiple MRI images, the Signal to Clutter Ratio quantitatively assesses tumors departure from normal prostate tissue. The SCR formulation combines all components of the MP-MRI. But in addition, the SCR formulation uses the covariance matrix, to correct and account for correlations among the different components (for example, the correlation between ADC and DWI) to get a true measure of the aggregate contribution of each. The Appendix summarizes some of the mathematics behind the SCR algorithm. For more details see (29, 31, 34–36).

SCR: Filtering noise

Computing the SCR covariance matrix generates principal components (34). Principal component are linear combinations of all MRI components but are orthogonal or totally decorrelated from each other. The principal components are ordered based on their eigenvalue or statistical variation. Well resolved images have eigenvalue and high variation. In contrast, the noisy principal components have small eigenvalues. Noise is reduced by filtering and eliminating the noisy (low eigenvalue) principal components resulting in a more accurate RX calculation. The Appendix summarizes some of the mathematics behind the filtering of principal components. For more details see (29, 31, 35).

Regularization and shrinkage

Regularization is another way to correct for the imperfections of the computed covariance matrix. The statistics describing the background (normal prostate) should follow a normal distribution. However, the analytic formula for the covariance matrix results in only an approximation. The goal of shrinkage regularization (29, 36) is to perturb the original covariance matrix CM(γ) by mixing in a diagonal matrix with a mixing parameter γ to generate a regularized or modified regularized covariance matrix. The appropriate γ is chosen to maximize the normal distribution. Regularized or modified regularized covariance matrix generation follow the same procedure but differ in the mixing diagonal matrix. The Appendix summarizes some of the mathematics behind regularization. For more details see (29, 36).

Tumor volume measurements, supervised target detection

The Supervised target detection algorithm or ACE was applied to the spatially registered MRI (26) and was used to determine the tumor volume. Voxels exceeding a threshold for ACE scores are assigned to tumor and normal tissue are assigned to ACE scores residing below the threshold. The number of voxels exceeding the threshold (tumor) were counted and converted to volume based on the MRI spatial resolution The Appendix summarizes some of the mathematics behind tumor volume computation. For more details see (26).

Logistic regression

A logistic regression fit (44, 45) was applied to the dependent categorial variable CsPCa, using all combinations of the continuous independent variables (eccentricity, SCR, volume). The GS derived from the pathological assessment of histology slides from prostatectomy. The clinically significant PCa (CsPCa) was assigned to Gleason score >=4+3 and the clinically insignificant PCa (CiPCa) is assigned to<=3+4 This study only reports the combination of independent variables that achieved the highest performance in earlier studies (27–30). The eccentricity from the largest blob used ACE threshold 0.45. SCR includes cutoff from three and four principal components, regularized SCR and modified regularization. The volume derived from MP-MRI used ACE threshold 0.65. The coefficient of determination R2 assesses the fit. In addition, the quality of fit was assessed by computing the F-value and affiliated P value (44, 45).

Receiver operator characteristic

The Receiver Operator Characteristic curve summarizes (46) and helps assess a binary classifier by plotting the probability of target detection (or sensitivity) against the false alarm probability (or 1-specificity) for all threshold settings. The classifier's accuracy is assessed by comparing the multivariable logistic regression fitted results with the pathologist's Gleason score determination for each patient.

The ROC vertical axis (Sensitivity) surveys the patients with clinically significant prostate cancer (CsPCa) and determines whether the patient's prostate cancer status is correctly identified by the logistic regression for a given threshold. The horizontal axis (False Alarm probability or 1-Specificity) displays the relative accuracy for determining the status of patients with clinically identified as insignificant prostate cancer (CiPCa) for a given probability threshold. The ROC curve is monotonically increasing. If feasible, the best ROC curve value would be 100% target detection and 0% False Alarm probability (upper left corner for the ROC curve). The Area Under the Curve (AUC) is used to assess classifier and ranges from 0 (poor performance) to 1 (optimal performance).

Nomogram and decision curve analysis

A nomogram (12–14) is a two-dimensional calculating device designed to graphically depict a statistical prognostic model that generates a probability of a clinical event. Nomograms use biologic and clinical variables. In this study, the nomograms employ a logistic regression to model the probability that a prostate tumor is clinically significant. Each variable is listed separately, with a corresponding number of points assigned to a given magnitude of the variable. The individual points are summed from each variable to generate the total number of points for all variables. The total point score is projected onto the scale of outcome. Nomograms can be tailored to an individual patient and potentially reduce biopsies and their morbidity. They are widely used for cancer prediction.

Decision Curve Analysis (15) plots the net benefit associated with a model against the model's threshold probability. Net benefit is a weighted difference combination of True and False identifications of clinically significant prostate cancer, weighted by the threshold probability.

Alternatively, the threshold probability is the minimum probability of an event at which a decision-maker would take a given action, i.e. the probability of cancer at which a doctor would order a SRMP MRI scan. A lower threshold probability means a patient's greater concern about cancer, while a higher threshold reflects greater concern about a patient's aversion to SRMP-MRI. A positive classification is defined by whether predicted probability is at least as great as the threshold probability. As a reference (and by convention), the display includes the results of the default strategies of assuming that all or no observations are positive as a function of threshold probability.

Decision Curve Analysis assesses the clinical value of a predictor, unlike other evaluation statistical methods. Applying decision curve analysis can determine whether using a predictor to make clinical decisions like performing a SRMP MRI scan will provide benefit over alternative decision criteria, given a specified threshold probability

Results

Table 1 summarizes the assessments of 25 consecutive patients with contrast enhanced MRIs. Patients were assessed for the best fitting combinations of metrics derived from spatially registered MP-MRI to the Risk of PCa categorical variable. The independent variables include

TABLE 1 Summary of Logistic Regression fits for All patients.

Independent Variables	# Variables	F Value	p-value	R2	AUC [95% LL, 95% UL]
3PC+Vol	2	16.08	0.0003	0.664	0.912 [0.792, 1.00]
Ecc+3PC	2	14.43	0.0007	0.614	0.882 [0.719, 1.00]
Ecc+Mod Reg+3PC	3	14.47	0.0023	0.615	0.882 [0.719, 1.00]
Ecc+ Reg+3PC	3	14.99	0.0018	0.631	0.882 [0.719, 1.00]
Ecc+3PC+Vol	3	16.87	0.0008	0.687	0.919 [0.799,1.00]
Ecc+ Reg+3PC+Vol	4	17.03	0.0019	0.691	0.919 [0.799,1.00]
Ecc+Mod Reg+3PC+Vol	4	17.02	0.0019	0.691	0.926 [0.804,1.00]

Analyzing all patients, Summary of Best Regression fits of combinations eccentricity, SCR, and Volume to Gleason score. AUC, Area Under Curve; R2, coefficient of determination; LL, Lower Limit Confidence Interval; UL Upper Limit 95% Confidence Interval; ECC, eccentricity(0.45 ACE Threshold); Mod_Reg, Modified Regularization; SCR, Reg, Regularized SCR; Vol, Volume (0.65 ACE threshold).

tumor eccentricity using an ACE threshold of 0.45 (Ecc), SCR using regularization (Reg), SCR using Modified SCR (Mod_Reg), SCR after filtering out 3 PC (3PC), and tumor volume (Vol) using 0.65 for the ACE threshold. The dependent categorical variable (Risk of PCa) was taken from the pathology determined Gleason Scores. The number of variables identified for each fit. Tables 1, 2 lists each fit's F values and associated probability of null hypothesis p-values, coefficient of determination (R2), Area Under the Curve (AUC) for the Receiver Operator curves and the AUC's 95% Confidence intervals Lower Level (LL) and Upper Level (UL). The fits have statistical significance (p-values<0.01), achieve high coefficient of determination (R2>0.60), high AUC (>0.85) but large confidence interval (0.20).

Table 2 replicates Table 1 except using a greater number of independent variables(eccentricity, SCR, volume) and the analysis follows a test set (12 consecutive odd numbered patients) that used the fitted parameters from training 13 consecutive even numbered patient. Like Table 1, high AUC scores (>0.85) are achieved. However, p-values were higher, and the coefficients of determination were lower.

Figure 2A shows a nomogram resulting from logistic regression fits using Eccentricity (0.45 ACE threshold), SCR after regularization, and SCR after filtering by removing 3 principal components. For a given patient, each component's contribution is determined by projecting their values onto the "Points." The total points are computed by summing each of the contributions. "Total points" is projected onto the "Risk of PCa" axis to determine the probability that a given patient suffers from clinically relevant prostate cancer.

Figure 2B shows an example of a ROC curve (shown as a bold black line) that displays the Sensitivity plotted against (1-Specificity) (the Specificity value is decreasing along the axis). The bold black line corresponding to the AUC (0.882) and the vertical lines in the ROC curve correspond to the 95% Confidence interval for the AUC. This particular ROC evaluates the logistic fit to Eccentricity, regularized SCR, and SCR filtered by deleting 3 principal components.

Associated with the nomogram is the Decision Curve Analysis (Figure 2C). Figure 2C shows the net benefit from using each component (eccentricity, regularized SCR, SCR after removing 3 principal components), all components in the regression fit, as a function of Threshold Probability or expected likelihood that the patient has clinically significant prostate cancer. In addition, the net benefit of treating all patient and treating no patients are shown as a standard reference. Applying the regression fit generates the highest net benefit for all threshold probability values relative to applying the individual components (eccentricity, SCR).

Similarly, Figures 3A–C show a nomogram, ROC curve, and a Decision Curve Analysis resulting from fitting Eccentricity (0.45 ACE threshold), SCR after regularization, and SCR after filtering by removing 3 principal components, Volume (0.65 ACE threshold). Again, applying the regression fit generates the highest net benefit for all threshold probability values relative to applying the individual components (eccentricity, SCR, volume).

Discussion

This study is the first to generate a nomogram using features derived from algorithms applied to spatially registered MP-MRI (25–30). Previous studies formed a foundation for the present study, although this study is novel and extended the findings to generate and evaluate the probability for tumor aggressiveness. In addition, the DCA provides an additional tool for guiding application of the nomogram, guiding which input and fits should be employed, and under what conditions. From the high AUC (>0.85), high R2 (>0.70), and low p-values (<0.05), this pilot study found that nomograms can accurately predict the probability of prostate tumor aggressiveness. The nomogram performance as described by AUC from ROC curves is comparable with other studies (18–23) that use metadata such age, clinical data such as PSA, and PI-RADS and that achieve AUC ranging from 0.8 to 0.90.

The transformation of remote sensing-based approaches and algorithms for prostate cancer evaluation discussed in this manuscript forms only a part of the research constellation. There has been considerable progress and research in using biomarkers (47) and multi-parametric MRI (48) to determine the possible presence of prostate cancer and their role in disease management. Companies have translated bench research (47) in biomarkers into clinical tests for their efficacy and offer promising alternatives to the standard prostate serum antigen. Studies investigated the effectiveness of how multi-parametric MRI is employed (49) in the clinic and alternative, simpler configurations and approaches (50) that may eventually make MP-MRI more accommodating for patients and the clinic. Future research may combine the approaches applied to spatially registered hyperspectral hypercubes discussed in this study with biomarkers (47) and may also be modified with the aid of insights gained from MP-MRI implementation (48).

TABLE 2 Summary of Logistic Regression fits for Training, Test Sets.

Independent Variables	# Variables	F Value	p-value	R2	AUC (Train)	AUC (Test) [95% LL, 95%UL]
3PC+Vol, Train-Test	2	5.63	0.0598	0.496	0.861	0.969 [0.882-1.00]
Ecc+ Reg+3PC, Train+Test	3	6.29	0.0984	0.541	0.889	0.906 [0.702-1.00]
Ecc+ Reg+3PC+Vol, Train+Test	4	6.98	0.137	0.586	0.944	0.938 [0.791-1.00]

Analysis of Training and Test Cases, Summary of Best Regression fits of combinations of eccentricity, SCR, and Volume to Gleason score. AUC, Area Under Curve; R2, coefficient of determination; LL, Lower Limit Confidence Interval; UL Upper Limit 95% Confidence Interval; ECC, eccentricity(0.45 ACE Threshold); Mod_Reg, Modified Regularization SCR; Reg, Regularized SCR; Vol, Volume (0.65 ACE threshold).

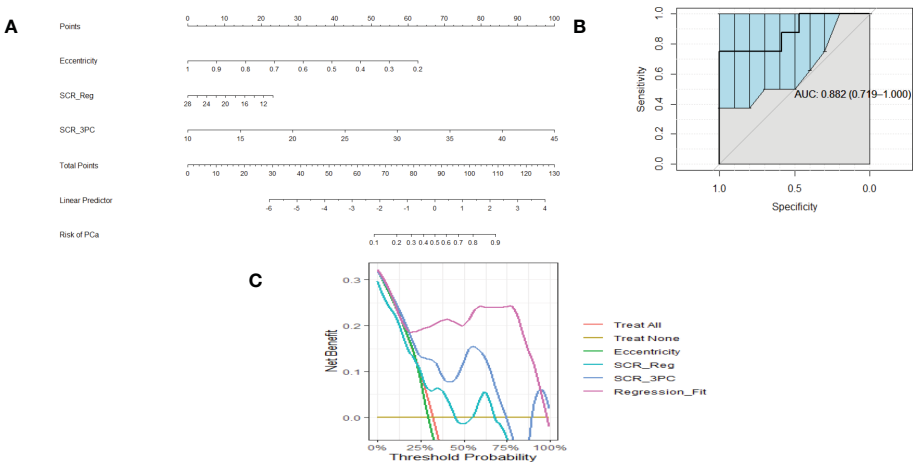

FIGURE 2
(A) is a nomogram resulting from logistic fit to Gleason score with eccentricity, regularized SCR, and SCR with 3 PC removed. **(B)**. ROC curve for fitting eccentricity, regularized SCR and SCR after 3 PC removed, Area Under the Curve (AUC) and 95% Confidence Limits shown as bold and lighter line with vertical bars **(C)**. Decision Curve Analysis for **(A)** nomogram.

The metrics (AUC, p-value) that assess the accuracy of the nomogram for this study were confined to employing features from spatially registered MP-MRIs. The restricted composition of features nevertheless performed as well or better than studies (18–23) that employed more conventional features such as PSA, age, PI-RADS. Adding extra features from the clinic such as age, PSA etc. to the inputs from spatially registered MP-MRI may further increase the accuracy of the prediction for tumor aggressiveness, as in studies that use PI-RADS data.

Logistic Regression fits the input variables to a binary or a categorical variable, in this case the "Risk of PCa," which can only be 0 (non-clinically relevant PCa) or 1 (clinically relevant PCa). Earlier multi-variable fitting studies treated the Gleason score as a continuous variable. Better fits for each of the independent variables ($p<0.03$) were achieved in univariable and multivariable fitting when the Gleason score was treated as continuous. Although the overall fitting (shown in Tables 1, 2) achieves high correlation, assessment of a larger number of samples should improve the univariable fitting using the categorical dependent variable, especially for training/test analysis.

The performance of the multivariable fits diminishes slightly when dividing the patients into training and test sets, as is common in most studies. Due to the limited size of this data set, other combinations of training and testing sets were not feasible. Future analyses using larger patient numbers could reduce confidence intervals and bolster confidence in this study's findings. Nevertheless, the results described in this manuscript merit further studies that employ larger patient sample sizes that may successfully predict prostate tumor aggressiveness.

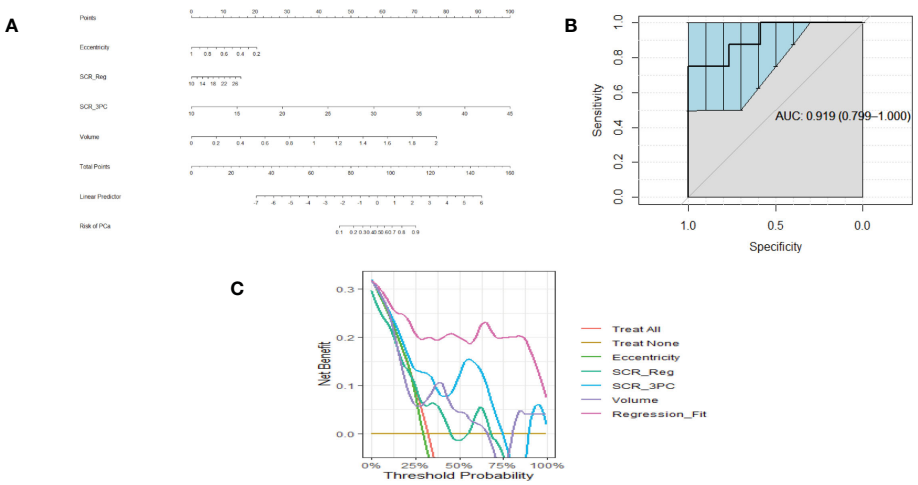

FIGURE 3
(A) is a nomogram resulting from logistic fit to Gleason score with eccentricity, tumor volume, and SCR with 3 PC removed. **(B)** Receiver Operator Curve applied to Logistic Regression for eccentricity, 3 PCs removed from SCR, tumor volume. Area Under the Curve (AUC) and 95% Confidence Limits shown as bold and lighter line with vertical bars. Area Under the Curve (AUC) and 95% Confidence Limits shown as bold and lighter line with vertical bars **(C)**. Decision Curve Analysis for **(A)** nomogram.

There is a question of whether the results are robust or fundamentally unchanged upon using differing target signatures and normal prostate outlines. For a number (but not all) of patients, calculations were rerun with different choice of signatures and different contouring of the normal prostate. The resulting calculations generated virtually the same as those using initial input data. However, a more definitive study is merited.

This study has some limitations. The patients in this study all originated from a single institution (NIH), potentially limiting generalizability. Furthermore, although all patients were prospectively enrolled, this is a retrospective analysis of the data and may be subject to biases. Furthermore, the dataset comprised only 25 patients. Although a small number of patients were assessed, consecutive patients were analyzed to minimize potential bias. Despite this being a pilot analysis with a limited dataset, highly statistically significant P values, high AUC, high coefficient of determination values, and high net benefits in the decision analysis curves were achieved, showing potential clinical value of this approach.

Conclusions

This retrospective pilot study shows that nomograms that only use metrics from spatially registered MP-MRI achieve comparable performance relative to nomograms that use prostate serum antigen, age, PI-RADS. Validation of these finds from larger and multicenter cohorts are needed before clinical implementation.

Data availability statement

The raw data supporting the conclusions of this article will be made available by the authors, without undue reservation.

Ethics statement

Ethical review and approval was not required for the study on human participants in accordance with the local legislation and institutional requirements. The patients/participants provided their written informed consent to participate in this study.

Author contributions

(I) Conception and design: RM. (II) Administrative support: RM, CS, PC. (III) Provision of study materials or patients: BT, PC. (IV) Collection and assembly of data: RM, BT, PC. (V) Data analysis and interpretation: RM. (VI) Manuscript writing: All authors. (VII) Final approval of manuscript: All authors.

Conflict of interest

RM works for Oncoscore.

The remaining authors declare that the research was conducted in the absence of any commercial or financial relationships that could be construed as a potential conflict of interest.

Publisher's note

References

1. Dall'Era MA, Albertsen PC, Bangma C, Carroll PR, Carter HB, Cooperberg MR, et al. Active surveillance for prostate cancer: a systematic review of the literature. *Eur Urol* (2012) 62:976–83. doi: 10.1016/j.eururo.2012.05.072

2. Gurumurthy D, Maggad R, Patel S. Prostate carcinoma: correlation of histopathology with serum prostate specific antigen. *Sci J Clin Med* (2015) 4:1–5. doi: 10.11648/j.sjcm.s.2015040401.11

3. Ngwu PE, Achor GO, Eziefule VU, Orji JI, Alozie FT. Correlation between prostate specific antigen and prostate biopsy Gleason score. *Ann Health Res* (2019) 5(2):243–8. doi: 10.30442/ahr.0502-26-56

4. Zivkovic S. Correlation between prostate-specific antigen and histopathological difference of prostate carcinoma. *Arch Oncol* (2004) 12:148–51. doi: 10.2298/AOO0403148Z

5. Poulakis V, Witzsch U, de Vries R, Emmerlich V, Meves M, Altmannsberger HM, et al. Preoperative neural network using combined magnetic resonance imaging variables, prostate-specific antigen, and gleason score for predicting prostate cancer biochemical recurrence after radical prostatectomy. *Urology* (2004) 64:1165–70. doi: 10.1016/j.urology.2004.06.030

6. Eichelberger LE, Michael Koch MO, Eble JN, Ulbright TM, Juliar BE, Cheng L. Maximum tumor diameter is an independent predictor of prostate-specific antigen recurrence in prostate cancer. *Mod Pathol* (2005) 18:886–90. doi: 10.1038/modpathol.3800405

7. Weinreb JC, Barentsz JO, Choyke PL, Cornud F, Haider MA, Macura KJ, et al. PI-RADS prostate imaging - reporting and data system: 2015, version 2. *Eur Urol* (2016) 69:16–40. doi: 10.1016/j.eururo.2015.08.052

8. Wang L, Hricak H, Kattan MW, Chen HN, Kuroiwa K, Eisenberg HF, et al. Prediction of seminal vesicle invasion in prostate cancer: incremental value of adding endorectal MR imaging to the kattan nomogram. *Radiology* (2007) 242:182–8. doi: 10.1148/radiol.2421051254

9. Kızılay F, Çelik S, Sözen S, Özveren B, Eskiçorapçı S, Özgen M, et al. Correlation of prostate-imaging reporting and data scoring system scoring on multiparametric prostate magnetic resonance imaging with histopathological factors in radical prostatectomy material in Turkish prostate cancer patients: a multicenter study of the urooncology association. *Prost Int* (2020) 8:10–5. doi: 10.1016/j.prnil.2020.01.001

10. Slaoui H, Neuzillet Y, Ghoneim T, Rouanne M, Abdou A, Lugagne-Delpon PM, et al. Gleason Score within prostate abnormal areas defined by multiparametric magnetic resonance imaging did not vary according to the PIRADS score. *Urol Int* (2017) 99:156–61. doi: 10.1159/000468947

11. Bastian-Jordan M. Magnetic resonance imaging of the prostate and targeted biopsy, comparison of PIRADS and Gleason grading. *J Med Imaging Radiat Oncol* (2018) 62:183–7. doi: 10.1111/1754-9485.12678

12. Balachandran VP, Gonen M, J. Smith JJ, DeMatteo RP. Nomograms in oncology – more than meets the eye. *Lancet Oncol* (2015) 16(4):e173–80. doi: 10.1016/S1470-2045(14)71116-7

13. Kattan MW. Nomograms are superior to staging and risk grouping systems for identifying high-risk patients: preoperative application in prostate cancer. *Curr Opin Urol.* (2003) 13(2):111–6. doi: 10.1097/00042307-200303000-00005

14. Kranse R, Roobol M, Schröder FH. A graphical device to represent the outcomes of a logistic regression analysis. *Prostate* (2008) 68(15):1674–80. doi: 10.1002/pros.20840

15. Vickers AJ E, Elkin EB. Decision curve analysis: a novel method for evaluating prediction models. *Med Decis Mak* (2006) 26(6):565–74. doi: 10.1177/0272989X06295361

16. Loeb S, Vellekoop A, Ahmed HU, Catto J, Emberton M, Nam R, et al. Systematic review of complications of prostate biopsy. *Eur Urol.* (2013) 64(6):876–92. doi: 10.1016/j.eururo.2013.05.049

17. Streicher J, Meyerson BL, Karivedu V, Sidana A. A review of optimal prostate biopsy: indications and techniques. *Ther Adv Urol.* (2019) 11:1756287219870074. doi: 10.1177/1756287219870074

18. Zhou Z, Zhen Liang Z, Zuo Y, Zhou Y, Yan W, Wu X, et al. Development of a nomogram combining multiparametric magnetic resonance imaging and PSA-related parameters to enhance the detection of clinically significant cancer across different region. *Prost* (2022) 82:556–65. doi: 10.1002/pros.24302

19. Zhang Y, Chen W, Yue X, Shen J, Gao C, Pang P, et al. Development of a novel, multi-parametric, MRI-based radiomic nomogram for differentiating between clinically significant and insignificant prostate cancer. *Front Oncol* (2020) 10:888. doi: 10.3389/fonc.2020.00888

20. Chau EM, Russell B, Santaolalla A, Van Hemelrijck M, McCracken S, Page T, et al. MRI-Based nomogram for the prediction of prostate cancer diagnosis: A multi-centre validated patient–physician decision tool. *J Clin Urol* (2022) 0(0):1–8. doi: 10.1177/20514158211065949

21. Huang C, Song G, Wang H, Ji G, Li J, Chen Y, et al. MultiParametric magnetic resonance imaging-based nomogram for predicting prostate cancer and clinically significant prostate cancer in men undergoing repeat prostate biopsy. *BioMed Res Int* (2018) 2018:6368309. doi: 10.1155/2018/6368309

22. Niu XL, Li J, Das SK, Xiong Y, Yang CB, Tao Peng T. Developing a nomogram based on multiparametric magnetic resonance imaging for forecasting high-grade prostate cancer to reduce unnecessary biopsies within the prostate-specific antigen gray zone. *BMC Med Imaging* (2017) 17:11. doi: 10.1186/s12880-017-0184-x

23. Lee SM, Liyanage SH, Wulaningsih W, Wolfe K, Carr T, Younis C, et al. Toward an MRI-based nomogram for the prediction of transperineal prostate biopsy outcome: A physician and patient decision tool. *Urol Oncol* (2017) 35(11):664.e11–664.e18. doi: 10.1016/j.urolonc.2017.07.018

24. Westphalen AC, McCulloch CE, Anaokar JM, Arora S, NSi B, JBarentsz JO, et al. Variability of the positive predictive value of PI-RADS for prostate MRI across 26 centers: Experience of the society of abdominal radiology prostate cancer disease-focused panel. *Radiology* (2020) 296:76–84. doi: 10.1148/radiol.2020190646

25. Mayer R, Simone CB2nd, Skinner W, Turkbey B, Choykey P. Pilot study for supervised target detection applied to spatially registered multiparametric MRI in order to non-invasively score prostate cancer. *Comput Biol Med* (2018) 94:65–73. doi: 10.1016/j.compbiomed.2018.01.003

26. Mayer R, Simone CB2nd, Turkbey B, Choyke P. Algorithms applied to spatially registered multi-parametric MRI for prostate tumor volume measurement. *Quant Imaging Med Surg* (2021) 11:119–32. doi: 10.21037/qims-20-137a

27. Mayer R, Simone CB2nd, Turkbey B, Choyke P. Correlation of prostate tumor eccentricity and Gleason scoring from prostatectomy and multi-parametric-magnetic resonance imaging. *Quant Imaging Med Surg* (2021) 11:4235–44. doi: 10.21037/qims-21-24

28. Mayer R, Simone CB2nd, Turkbey B, Choyke P. Prostate tumor eccentricity predicts Gleason score better than prostate tumor volume. *Quant Imaging Med Surg* (2022) 12:1096–108. doi: 10.21037/qims-21-466

29. Mayer R, Simone CB2nd, Turkbey B, Choyke P. Development and testing quantitative metrics from multi-parametric magnetic resonance imaging that predict Gleason score for prostate tumors. *Quant Imaging Med Surg* (2022) 12:1859–70. doi: 10.21037/qims-21-761

30. Mayer R, Turkbey B, Choyke P, Simone CB2nd. Combining and analyzing novel multi-parametric magneticresonance imaging metrics for predicting Gleason score. *Quant Imaging Med Surg* (2022) 12(7):3844–38. doi: 10.21037/qims-21-1092

31. Manolakis D, Shaw G. Detection algorithms for hyperspectral imaging applications. *IEEE Sign. Process Magaz* (2002) 19:29–43. doi: 10.1109/79.974724

32. Jain AK. *Fundamentals of digital image processing*. Upper Saddle River, NJ: Prentice Hall (1989).

33. Richards JA, Jia X. *Remote sensing digital image analysis*. New York: Springer-Verlag (1999).

34. Strang G. *Linear algebra and its applications (Fourth ed)*. CA, Thomson, Brooks/Cole: Belmont (2006).

35. Chen G, Qian S. Denoising of hyperspectral imagery using principal component analysis and wavelet shrinkage. *IEEE Trans Geosci Remote Sens* (2011) 49:973–80. doi: 10.1109/TGRS.2010.2075937

36. Friedman JH. Regularized discriminant analysis. *J Amer Stat Assoc* (1989) 84:165–75. doi: 10.1080/01621459.1989.10478752

37. Choyke P, Turkbey B, Pinto P, Merino M, Wood B. Data from PROSTATE-MRI. *Cancer Imaging Arch* (2016). doi: 10.7937/K9/TCIA.2016.6046GUDv

38. Clark K, Vendt B, Smith K, Freymann J, Kirby J, Koppel P, et al. The cancer imaging archive (TCIA): maintaining and operating a public information repository. *J Digit Imaging* (2013) 26:1045–57. doi: 10.1007/s10278-013-9622-7

39. Shah V, Pohida T, Turkbey B, Mani H, Merino M, Pinto PA, et al. A method for correlating *in vivo* prostate magnetic resonance imaging and histopathology using individualized magnetic resonance-based molds. *Rev Sci Instrum* (2009) 80:104301. doi: 10.1063/1.3242697

40. Turkbey B, Mani H, Shah V, Rastinehad AR, Bernardo M, Pohida T, et al. Multiparametric 3T prostate magnetic resonance imaging to detect cancer: histopathological correlation using prostatectomy specimens processed in customized magnetic resonance imaging based molds. *J Urol* (2011) 186:1818–24. doi: 10.1016/j.juro.2011.07.013

41. Turkbey B, Pinto PA, Mani H, Bernardo M, Pang Y, McKinney YL, et al. Prostate cancer: value of multiparametric MR imaging at 3 T for detection–histopathologic correlation. *Radiology* (2010) 255:89–99. doi: 10.1148/radiol.09090475

42. Tofts PS, Brix G, Buckley DL, Evelhoch JL, Henderson E, Knopp MV, et al. Estimating kinetic parameters from dynamic contrast-enhanced T(1)-weighted MRI of a diffusable tracer: standardized quantities and symbols. *J Magn Reson Imaging* (1999) 10:223–32. doi: 10.1002/(SICI)1522-2586(199909)10:3<223::AID-JMRI2>3.0.CO;2-S

43. Tofts PS. Modeling tracer kinetics in dynamic Gd-DTPA MR imaging. *J Magn Reson Imaging* (1997) 7(1):91–101. doi: 10.1002/jmri.1880070113

44. Hosmer DW, Lemeshow S. *Applied logistic regression (2nd ed.)*. Hoboken, NJ, USA: Wiley (2000), ISBN.

45. The nomogram prediction model was generated by applying the r package rms (version 6.0-1) . Available at: https://CRAN.R-project.org/package=rms.

46. Fawcett T. An introduction to ROC analysis. *Pattern Recognit Lett* (2006) 27(8):861–74. doi: 10.1016/j.patrec.2005.10.010

47. Ferro M, Lucarelli G, de Cobelli O, Del Giudice F, Musi G, Mistretta FA, et al. The emerging landscape of tumor marker panels for the identification of aggressive prostate cancer: the perspective through bibliometric analysis of an Italian translational working group in uro-oncology. *Minerva Urol Nephrol* (2021) 73:442–51. doi: 10.23736/S2724-6051.21.04098-4

48. Manfredi M, De Luca S, Russo F. Multiparametric magnetic resonance imaging-targeted prostate biopsy: present and future of the prostate cancer diagnostic pathway. *Minerva Urol Nephrol* (2021) 73:128–9. doi: 10.23736/S2724-6051.21.04341-1

49. Checcucci E, De Cillis S, Piramide F, Amparore D, Kasivisvanathan V, Giganti F, et al. The role of additional standard biopsy in the MRI-targeted biopsy era. *Minerva Urol Nefrol* (2020) 72:637–9. doi: 10.23736/S0393-2249.20.03958-2

50. Cereser L, Giannarini G, Bonato F, Pizzolitto S, Como G, Valotto C, et al. Comparison of multiple abbreviated multiparametric MRI-derived protocols for the detection of clinically significant prostate cancer. *Minerva Urol Nephrol* (2022) 74:29–37. doi: 10.23736/S2724-6051.20.03952-1

Appendix

Overall quantitative metrics description: SCR

The SCR (30–33) is given by

$$SCR = (S-\mu)^T CM^{-1}(S-\mu) \qquad (1)$$

that is a matrix multiplication over MP-MRI modalities. The superscript T denotes a vector transpose operation, CM is the covariance matrix, and the superscript -1 denotes a matrix inverse operation, where S is the vector tumor signature or mean over the identified tumor voxels. Vector μ is the mean value for normal prostate or background.

SCR: Filtering noise

The filtered $SCR_{Filtered}$ is given by

$$SCR_{Filtered} = (S-\mu)^T CM^{-1}_{Filtered}(S-\mu) \qquad (2)$$

where the inverse covariance matrix $CM^{-1}_{Filtered}$is a square symmetrical matrix and decomposes into three parts (34),

$$CM^{-1}_{Filtered} = \Lambda^T \lambda^{-1}_{Filtered} \Lambda \qquad (3)$$

$$\lambda^{-1}_{Filtered} = \begin{bmatrix} \frac{1}{\lambda_1^2} & 0 & & 0 & 0 \\ 0 & \frac{1}{\lambda_2^2} & & & 0 \\ \dots & & \dots & & \dots \\ 0 & & & 0 & 0 \\ 0 & 0 & \dots & 0 & 0 \end{bmatrix} \qquad (4)$$

The eigenvalues are ordered according to size ranging from the largest Λ_1 to the smallest Λ_M. For unfiltered processing, the images corresponding to the eigenvalues and eigenvectors range from high signal and variation (1, 2) to low variation and very noisy (M-1, M. Filtering out the noisy eigenvectors (29, 31, 35) means removing or deleting the lowest valued eigenvalues (3 or 4 in this study) (Eq 3,4) from the inverse matrix (see Eq 4).

Regularization and shrinkage

Shrinkage and regularization (29, 36) perturbs the covariance matrix CM(γ) to maximize the normal distribution, or equivalently minimize the discriminant function d(γ) [=-ln(normal distribution)] by adding a diagonal component that is controlled by the parameter γ. This study examines two types of regularization: regularization and modified regularization. Both follow the same procedure but differ in the mixture component. Specifically, the modified regularized SCR_{Mod_reg}

$$SCR_{mod\_Reg}(\gamma = \gamma_{min}) = (S-\mu)^T CM^{-1}_{mod\_Reg}(\gamma = \gamma_{min})(S-\mu) \qquad (5)$$

where $CM_{mod\_Reg}(\gamma)$ is

$$CM_{mod\_Reg}(\gamma) = (1-\gamma)CM + \gamma V \qquad (6)$$

and V is a diagonal matrix filled up with the square of the standard deviations from M modalities and is given by

$$V = \begin{bmatrix} \sigma_1^2 & 0 & & 0 & 0 \\ 0 & \sigma_2^2 & & & 0 \\ \dots & & \dots & & \dots \\ 0 & & & \sigma^2_{M-1} & 0 \\ 0 & 0 & \dots & 0 & \sigma^2_M \end{bmatrix} \qquad (7)$$

Using Eqs. [6,7] the modified discriminant function d_{mod_Reg} (γ)

$$d_{mod\_Reg}(\gamma) = \sum_{i=1}^{N}(x_i-\mu)^T CM^{-1}_{mod\_Reg}(\gamma)(x_i-\mu) + \ln\left(\det\left(CM_{mod\_Reg}(\gamma)\right)\right) \qquad (8)$$

is computed for 0<γ<1 and a minimum $d_{mod}(\gamma_{min})$ is found at γ_{min} resulting in a SCR_{Mod_Reg} (Eq. [5]) using a modified regularization procedure (using Eqs. [6,7]).

For SCR_{Reg}, the CM_{Reg} uses a matrix containing identical components (proportional to the identity matrix and is simply the average standard deviation σ.

$$CM_{Reg}(\gamma) = (1-\gamma)CM + \frac{\gamma Tra(CM)}{M} I \qquad (9)$$

by control value γ where Tra denotes the trace operator and I is the identity matrix. γ ranges from γ=0.0 or no CM modification to γ=1.0 or CM is proportional to the identity matrix. Again, the covariance matrix $CM_{Reg}(\gamma)$ is perturbed to maximize the normal distribution, or equivalently minimize the discriminant function d(γ) (=-ln(normal distribution)) by using CM_{Reg} (Eq 9) i.e.

$$d_{Reg}(\gamma) = \sum_{i}^{N}(x_i-\mu)^T CM_{Reg}(\gamma)^{-1}(x_i-\mu) + \ln\left(\det\left(CM_{Reg}(\gamma)\right)\right) \qquad (11)$$

The SC_{Reg} is given by

$$SCR_{Reg}(\gamma = \gamma_{min}) = (S-\mu)^T CM^{-1}_{Reg}(\gamma = \gamma_{min})(S-\mu) \qquad (9)$$

Tumor volume measurements, supervised target detection

The procedure for estimating the tumor volume using the supervised target detection algorithm or ACE has been previously described (26). For spatially-registered MP-MRI, threshold is applied to the ACE map. Voxels exceeding a threshold for ACE scores are assigned to tumor and normal tissue are assigned to ACE scores residing below the threshold. Earlier study (26) examined thresholds 0.40 to 0.85 assessed in 0.05 increments and found that 0.65 was optimal. The number of tumor voxels are converted to volume based on the MRI spatial resolution (1 mm × 1 mm) and slice separation (6 mm) resulting in a voxel volume (r=0.006 cm^3). Each blob's volume V_k is

10.3389/fonc.2023.1066498

given by a total number of pixels within each blob and corrected by the voxel volume r (assuming density of unity for each voxel),

$$V_k = rN = r\sum_{i=1}^{N} \frac{x_i}{abs(x_i)} \quad (12)$$

Frontiers in Oncology

Advances knowledge of carcinogenesis and tumor progression for better treatment and management

The third most-cited oncology journal, which highlights research in carcinogenesis and tumor progression, bridging the gap between basic research and applications to imrpove diagnosis, therapeutics and management strategies.

Discover the latest Research Topics

See more →

Frontiers

Avenue du Tribunal-Fédéral 34
1005 Lausanne, Switzerland
frontiersin.org

Contact us

+41 (0)21 510 17 00
frontiersin.org/about/contact